PHOTOSPHERIC PARAMETERS OF EARLY-TYPE STARS

Gordon C. Stewart

A Thesis Submitted for the Degree of PhD
at the
University of St Andrews

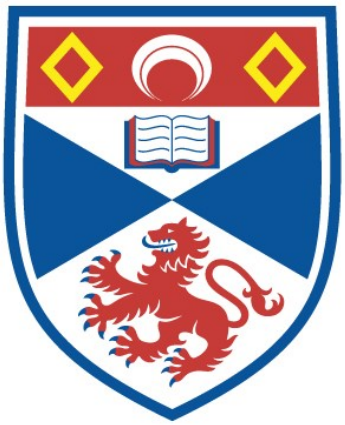

1984

PHOTOSPHERIC PARAMETERS OF EARLY-TYPE STARS

Gordon C. Stewart

A dissertation submitted in partial fulfillment of the requirements of the degree of Ph.D.

University of St. Andrews

1983

Abstract

The development of an interactive data reduction and analysis system for astronomical spectra written in the FORTH computing language and operated on the Nova 820 minicomputer at the University Observatory, St. Andrews is discussed.

Spectra of a number of B stars, many of which were obtained by the author at the South African Astronomical Observatory, were measured and reduced using this system. Equivalent widths of metal absorption lines are used to deduce the stars' fundamental photospheric parameters and abundances by comparison with the predictions of both non-LTE and line-blanketed LTE models.

It is shown that effective temperatures derived with the line-blanketed LTE models are in good agreement with those found by other authors for near main sequence B stars using measurements of the integrated flux of the stars. Unblanketed non-LTE models give effective temperatures which are systematically high by approximately 7%, similar to the difference between blanketed and unblanketed LTE models.

The major differences between the predictions for absorption lines using LTE and non-LTE models are due to the different level populations predicted and not to the different photospheric structures. The use of non-LTE models is found to reduce the microturbulence required to bring element abundances derived from strong lines into agreement with those found for weak lines but not to remove the need for the inclusion of microturbulence in the solutions for most B stars.

An investigation of the suitability of the analysis of high resolution Michelson interferometry using fourier decomposition techniques as a means of determining the broadening mechanisms and velocity fields in the photospheres of early A stars is made.

I, Gordon C. Stewart, hereby certify that this thesis which is approximately 40000 words in length has been written by me, that it is the record of work carried out by me, and that it has not been submitted in any previous application for a higher degree.

I was admitted as a research student under Ordinance No. 12 on 1st October, 1976 and as a candidate for the degree of Ph.D. on 1st October, 1977; the higher study for which this is a record was carried out in the University of St. Andrews between 1976 and 1979.

10th Sept 1983

I certify that G. C. Stewart has fulfilled the conditions of the Resolution and Regulations appropriate to the degree of Ph.D. of the University of St. Andrews and that he is qualified to submit this thesis in application for that degree.

Date: 13/9/83 Signature

Contents

OVERVIEW

Stars with a Morgan-Keenan (MK) spectral classification of type B play an important role in many areas of astrophysical research because of their intrinsic properties and position in the Hertzsprung-Russell (HR) diagram. Previous studies have indicated that these stars have effective temperatures of between 10000K and 30000K and masses of between $\approx$ twice and twenty-five times that of the sun. Models of stellar evolution suggest that the evolutionary timescales of such stars are relatively short. Important input to studies of recent star formation can thus be gained from studies of the B stars. While O stars have shorter timescales, $\approx 10^6$ years, the greater number of B stars implies that star formation over the last 10^8 years can be studied better by using B stars.

The visual spectrum of *normal* B stars is dominated by absorption lines of hydrogen and helium. Lines of ionised carbon, nitrogen and oxygen, together with those of silicon and magnesium, are also prominent. As carbon, nitrogen and oxygen are products of hydrogen and helium nuclear burning, knowledge of the absolute and relative abundances of these elements is important. The composition of main sequence B stars places constraints on nucleosynthesis models. Additional information is gained about models of the enrichment of the interstellar medium and the recycling of heavy elements.

Unfortunately the very position of the B stars in the HR diagram renders many of the assumptions of the classical model atmosphere doubtful. Without a detailed understanding of the structure of the stellar atmospheres of B stars and the physical processes which shape their spectra accurate abundance determinations are impossible.

Observations suggest that many early-type stars are losing mass via a stellar wind (e.g. Snow and Morton, 1976). Changes in the line profiles of some B stars (e.g. Smith, 1977) and the β-Cepheid phenomenon (e.g. Lesh and Aizenman, 1978) have been attributed to pulsations in the stars. Some doubt is therefore cast on the total validity of the assumption of hydrostatic equilibrium.

The detection of X-rays from early-type stars and the probable existence of stellar coronae above the photospheres of B stars (e.g. Stewart and Fabian, 1981) clearly indicate the presence of non-thermal activity in the upper atmospheres of these stars.

Two approximations were introduced at an early stage in the calculation of model photospheres, principally for ease of computation, which may introduce large errors for early-type stars. Only recently has it been possible to calculate model photospheres and absorption line strengths with the removal of either of these approximations.

The first of these approximations was the neglect of the effect on the photospheric structure of *line−blanketing*, that is the contribution of line absorption to the opacity of the photosphere. The second approximation of the classical model photosphere which may be of doubtful validity for B stars is the assumption of local thermodynamic equilibrium (LTE). The assumption of LTE requires that matter and radiation in the photosphere are everywhere in equilibrium and that the distribution of the atoms amongst their ionisation stages and excitation levels is determined by the Saha and Boltzmann equations.

No calculations are available as yet which remove both these approximations simultaneously. In this study the predictions of models which remove one or other of the two approximations are critically compared with observations of the spectra of B stars. Particular importance is placed on investigating the values found for the microturbulent velocity parameter, ξ_t. This parameter, originally introduced by Struve and Elvey, 1934, has been commonly used as a fitting parameter in abundance determinations. Values of the same order as the sound speed or thermal velocities in the stellar photospheres are sometimes found to be necessary to bring the abundances found from strong absorption lines into agreement with those found from weak lines of the same ion, even within the same multiplet. Hardorp and Scholz, 1970, in their analysis of the B0 V star, τ Sco, found a value of $\approx 3 kms^{-1}$ for ξ_t from the above method. In contradiction, however, they also found that the half-widths of the line profiles were too small to permit any broadening mechanism other than thermal Doppler broadening. To reconcile these observations they suggested that the computed lines were too shallow due to the neglect of the effects of departure from LTE (or non-LTE effects).

Kamp, 1978, has shown in a series of calculations for silicon absorption lines that the

differences between lines calculated using LTE and non-LTE models mimic the inclusion of microturbulence - that is the stronger the line the more it is enhanced when the assumption of LTE is relaxed. This effect is particularly evident for lines in the visible and near-infrared portions of the spectrum, the regions from which most abundances are derived.

Kurucz, 1979, has constructed a computer program which calculates model stellar photospheres in LTE but which allows for the inclusion of $\approx 1,000,000$ absorption lines to the stellar opacity. He claims that the effect of the inclusion of line-blanketing on the derived line profiles is also such as to reduce the amount of microturbulence required to bring abundances derived from different lines into agreement.

No analysis has yet been made of a large number of B stars with homogeneous observational material in which values of effective temperature, surface gravity, microturbulent velocity and chemical abundances are determined from the absorption line spectrum using both line-blanketed LTE and non-LTE models. No comparison of the merits of either type of model for the analysis of B stars has thus been made. This problem is addressed in this project.

The observational material used in the present study consists principally of photographic spectra. While a number of plates were provided by Drs. P. W. Hill and R. W. Hilditch many were obtained by the author for the purposes of this project. These latter spectra were recorded on IIIaJ emulsion which has improved noise and resolution properties as compared to the emulsions which have been used in the majority of previous studies of the spectra of early-type stars.

An interactive package of computer programs was developed by the author for the measurement, reduction and analysis of the plate material. As part of the project an investigation was made of the accuracy of photographic spectral analysis using high quality emulsions and computerised reduction techniques to determine whether the photographic plate is still a competetive detector compared to modern electronic devices.

In addition to the photographic spectra a number of observations were made of the silicon II doublet at 5056Å using a high resolution Michelson interferometer. These were useful as a comparison with, and control for, the photographic data. Further, Gray and his

co-workers (e.g. Gray, 1976) have suggested that the various mechanisms which contribute to the broadening of spectral lines may be more easily distinguished by examining the power spectra of the lines. The properties of the Michelson interferometer make it a very useful instrument for such a study and the possibility of such an investigation of early-type stars is investigated.

In the first chapter of this thesis a brief review of the theory of stellar atmospheres and of previous analyses of B stars is given. The physical processes which influence the observed spectrum and the techniques used to parameterise these processes are discussed, as are the computer programs used to generate the model photospheres utilised in the analysis.

The photographic observations used in the analysis and in particular those made by the author are described in chapter 2, while the interactive computer package develeped for the measurement and reduction of the plates is the subject of chapter 3. The overall accuracy of the system is examined in chapter 4 using both internal comparisons and comparisons with the results of other authors. Chapter 5 contains the results derived from the analysis of the stellar spectra and a discussion on the validity of the model photospheres used.

A description of the observations made with the Michelson interferometer and their subsequent analysis is given in chapter 6. In chapter 7 some general conclusions are drawn about the present capability of interpreting observations of stellar spectra and some suggestions are made as to which future developments may be the most fruitful.

CHAPTER ONE

STELLAR PHOTOSPHERES: THEORY AND MODELS

1.i *Introduction*

Since Huggins, (e.g. Huggins and Miller,1863), first demonstrated that the absorption lines studied by Fraunhofer, 1815, in the spectra of stars could be attributed to different chemical elements one of the major goals of astrophysics has been the determination of the chemical composition and physical state of the region from which the observed radiation comes. This region has become known as the *stellar atmosphere*. Only the properties of the stellar atmosphere can be derived directly from the stellar spectrum. The shielding of the radiation from the interior of the star by the outer layers means that the properties of the interior must be inferred from knowledge of the atmospheric properties.

Some sub-divisions of the stellar atmosphere have been delimited according to the overall nature of the particular region. The deeper portion of the atmosphere from where most of the light in the visual spectrum originates is known as the *photosphere*. Above the photosphere are regions known as the *chromosphere* and *corona* which are hotter and more tenuous than the photosphere. There is also evidence for the existence of a gas flow escaping from many stars. This gas flow is known as a *stellar wind*. Underhill (e.g. Underhill and Doazan, 1982) has coined the term *mantle* to collectively describe the regions above the photosphere.

This study involves the use of models to investigate the photospheric properties of stars in the spectral range O8 to B8. As was discussed in the overview to this thesis an understanding of the properties of these stars is important for a number of reasons. Previous studies, however, have shown that the photospheric parameters are in a region where some of the approximations adopted in the past to ease the computational problems involved in generating a model photosphere may not be fully justified.

More complete reviews of previous work in this field can be found in the works of Underhill, 1966, Underhill and Doazan, 1982, and Scholz, 1972, which concentrate on the analysis of observational data, and the works of Mihalas, 1970, 1978, and Gray, 1976, where the theory and techniques required for the construction of a model photosphere are discussed in detail. For completeness, however, a resumé of the theory and techniques involved is also given here and is followed by a short history of the analysis of early-type stars.

1.ii *Definitions*

In this section definitions of some of the parameters and terms used in the study of stellar photospheres will be given.

To completely specify a stellar photosphere the variations of temperature, pressure, chemical abundances, velocity and radiation with depth in the photosphere would be necesssary. However, if the physics and assumptions which have been input to the model are known, it is possible to reduce this parameter set and still be able to reconstruct the model. The most widely used parameters are the effective temperature and surface gravity of the photosphere, the latter being most frequently expressed in terms of its logarithm.

The effective temperature, T_{eff}, in units of K is defined by the expression

$$\sigma_R T_{eff}^4 = \int_0^\infty f_\nu d\nu$$

where σ_R is the Stefan-Boltzmann constant, and f_ν is the monochromatic flux in $ergs\,cm^{-2}\,s^{-1}$ emitted at the stellar surface. T_{eff} is the temperature of a blackbody with the same power output as the star.

Log g, the logarithm of the surface gravity is given by

$$\log g = \log\left(\frac{GM_*}{R_*^2}\right)$$

where M_* is the stellar mass in grammes, R_* is the stellar radius in centimetres, G is the gravitational constant and g is in units of $cm\,s^{-2}$.

For stars for which the stellar disc cannot be resolved, the flux average from integration over the disc, F_ν, is observed. To most completetely characterise an absorption

line the line profile must be specified, that is the observed distribution of flux with frequency. This can be done in terms of the residual flux, R_ν, which is the ratio of the flux in the line, F_ν, to the flux in the continuum, F_c, which would have been observed in the absence of the line:-

$$R_\nu = \frac{F_\nu}{F_c}$$

or in terms of the absorption depth, A_ν, where

$$A_\nu = 1 - R_\nu$$

Where it is not possible to measure the line profile in detail, a measure of the integrated line strength known as the equivalent width, W, of the line is useful.

$$W = \int_0^\infty (1 - R_\nu) d\lambda = \int_0^\infty A_\nu d\lambda$$

W is the width of a perfectly black line which removes the same total energy from the continuum as the line under study.

As line profiles contain more information than equivalent widths they should be used wherever possible to compare with the predictions of models. For a given equivalent width there exists an infinite number of possible line profiles, all having different implications about the structure of the photosphere.

Any interpretation based solely on equivalent widths may be misleading. Techniques which simultaneously utilise measurements of many equivalent widths are more useful. One such technique is the use of the *curve of growth* (COG) which has been frequently applied to studies of stellar spectra. Care must be taken to select the appropriate theoretical curve to fit the observations.

The Models

After the development of the simple one temperature, one pressure 'reversing layer' model photosphere came the development of the 'classical' model photosphere. The classical model satisfied four criteria :-

a) homogeneity

b) plane-parallel stratification

c) hydrostatic and radiative equilibrium

d) LTE

In general the equations

$$\frac{dP}{d\tau_\nu} = \frac{g}{\kappa_\nu}$$

$$\sigma_R T_r^4(\tau_\nu) = \sigma_R T_{eff}^4$$

where P is the total gas and radiation pressure, τ_ν is the optical depth and κ_ν is the opacity at frequency ν are solved in an iterative fashion. The approximation of LTE is used to find

$$P = P(T, P_e, composition)$$

and

$$\kappa_\nu = \kappa_\nu(T, P_e, composition)$$

Once the temperature and pressure stratification for the photosphere has been determined the next stage in the procedure is the calculation of parameters to be compared directly with the observations.

Absorption Line Formation

As the radiation in a line originates from a range of depths in the photosphere, to calculate the flux emergent at the stellar surface requires the solution of a radiative transfer problem.

To formulate and solve this problem the line and continuum optical depth scales, τ_ν and τ_c, and the respective source functions, S_ν and S_c, must be known.

Where the continuous aborption and scattering coefficients, κ_ν and σ_ν, are known as a function of depth in the photosphere, z, together with the line absorption coefficient, l_ν, then

$$\tau_\nu = \int_z^{z_{max}} (\kappa_\nu + \sigma_\nu + l_\nu) dz$$

and

$$\tau_c = \int_z^{z_{max}} (\kappa_\nu + \sigma_\nu) dz$$

When coupled with the source functions these allow the calculation of both

$$F_\nu = 2 \int_0^\infty S_\nu(\tau_\nu) E_2(\tau_\nu) d\tau_\nu$$

and

$$F_c = 2\int_0^\infty S_c(\tau_c)E_2(\tau_c)d\tau_c$$

where E_2 is the second order exponential integral. Only in the case of strict LTE is the source function known *a priori*. (In this case the source function is the Planck function $(S_\nu(\tau_\nu) \equiv B_\nu(\tau_\nu))$.

The line absorption coefficient can be considered to be composed of two components, the line profile, which determines the line shape, and the line strength.

The spectral lines of an isolated atom with levels of almost infinite lifetimes would be virtually perfectly sharp and could be represented by delta functions.

Many mechanisms, however, exist in real stars which cause the broadening of spectral lines by introducing a diffuseness to the energy levels of the atom or by causing, through the Doppler shift, a difference between the observer's and the atom's energy frames.

The most important broadening mechanisms in the photospheres of early-type stars are

a) Natural broadening

b) Pressure broadening

c) Thermal Doppler broadening

d) Mass Motion broadening

Other mechanisms such as magnetic (Zeeman) broadening and the existence of hyperfine structure are not of much importance in the spectra of normal B stars.

Thermal Doppler broadening has a profile which is Gaussian in shape while both natural broadening, and, where the impact approximation is valid, pressure broadening yield Lorentz or dispersion profiles. (Derivations of these properties can be found in many text books.) The convolution of the Lorentz and the Gaussian profiles gives a resultant Voigt profile, $H(a,\nu)$. The absorption profile per atom, ϕ_ν, is then given by

$$\phi_\nu d\nu = \pi^{-\frac{1}{2}}\Delta\nu_D^{-1}H(a,\nu)d\nu$$

where $\Delta\nu_D$ is the Doppler width.

A parameter, f, known as the oscillator strength, has been defined such that the line absorption coefficient per atom is given by

$$a_\nu = \frac{\pi e^2}{mc} f \phi_\nu$$

The derivation of accurate oscillator strengths is still a major problem in the interpretation os stellar spectra. Some oscillator strengths are determined experimentally (e.g. Corliss and Bozmann, 1962, Blackwell and Shallis, 1979) while others are determined theoretically using the Coulomb approximation or some other technique (e.g. Wiese *et al*, 1969, Treffitz and Zare, 1969, Dufton and Hibbert, 1981). Uncertainties in published f-values are high. For the best studied lines an error of 10% is usual while errors of $\approx$ 50% are often quoted.

The influence of mass motions on the emergent line profile is dependent on the scale length over which the motion takes place. Three types of mass motion can be identified:-

a) microturbulence

b) macroturbulence

c) rotation

Microrturbulence

Where the size of the moving element is small compared to the mean free path of a photon then the motion may be described as microturbulence. The influence on the line profile is similar to that of the thermal motion of the atoms or ions. Where only thermal motion exists the Doppler width is given by

$$\Delta\nu_D = \frac{\nu_0}{c}\left[\frac{2kT}{m}\right]^{\frac{1}{2}}$$

If the microturbulent velocities are also distributed as a Maxwellian distribution then, where the most probable value of the microturbulent velocity is ξ_t,

$$\Delta'\nu_D = \frac{\nu_0}{c}\left[\frac{2kT}{m} + \xi_t^2\right]^{\frac{1}{2}}$$

The concept of microturbulence was first documented by Struve and Elvey, 1934. It was introduced, not on a physical basis, but as a fitting parameter to explain why

strong lines of a given ion in some stars required systematically higher abundances of that element than weaker lines.

Conceptually the effect of microturbulence can best be seen by considering absorption by a uniform slab of thickness L with radiation incident on one side. Assuming the slab contains atoms which produce line absorption but has no source of emission, the reversing-layer approximation, then the emergent intensity, I_ν, is

$$I_\nu = I_0 e^{-\tau_\nu}$$

where I_0 is the incident intensity. Now

$$\tau_\nu = NLa_\nu = NL\frac{\pi e^2}{mc} f\phi_\nu$$

where N is the number of absorbing atoms per unit volume. The equivalent width of the line is

$$W = \int_0^\infty (1 - e^{-NL\frac{\pi e^2}{mc} f\phi_\nu}) d\nu$$

For weak lines, those with $NL\pi e^2 f\phi_\nu/mc \ll 1$, then

$$W \approx \int_0^\infty NL\frac{\pi e^2}{mc} f\phi_\nu d_\nu$$

$$= NL\frac{\pi e^2}{mc} f \int_0^\infty \phi_\nu d\nu$$

$$= NL\frac{\pi e^2}{mc} f$$

For lines of moderate strength where absorption in the Doppler core is strong but absorption in the line wings is still weak it can be shown that

$$W \approx 2\Delta\nu_D \left[\ln\left(\frac{NL\pi^{\frac{1}{2}} e^2}{mc\Delta\nu_D}\right)\right]^{\frac{1}{2}}$$

while for the very strong lines

$$W = \left(\frac{NLe^2}{\pi mc} f\gamma\right)^{\frac{1}{2}}$$

where γ is a constant depending on the magnitude of the pressure and natural broadening for that line.

Figure 1.1 shows a schematic plot of the way in which the equivalent width increases with increasing abundance. The three phases, linear, saturation and damping correspond to the three cases discussed above respectively. The dashed line illustrates the effect of increasing the the Doppler width of the line by introducing microturbulence. This diagram is a curve of growth.

A rather worrying aspect of the the analyses of early-type stars is that the value of ξ_t deduced often approaches the value of the sound speed in the stellar photospheres and is often higher than the thermal velocity of the heavier ions. At 30000K the thermal velocities of hydrogen, carbon and silicon are $\approx$ 13, 4 and 2 $km\ s^{-1}$ respectively while the sound speed is $\approx$ 11 $km\ s^{-1}$.

Conventional models for stellar interiors suggest that convection is likely to be limited in B stars and hence unable to generate turbulence. Nelson, 1980, has modelled a stellar photosphere with $T_{eff} = 30000K$ and $\log g = 4.0$ and shown that radiative cooling rapidly damps out fluctuations. This limits convection velocities to only a few $m\ s^{-1}$ rather than the few $km\ s^{-1}$ attributed to microturbulence in early-type stars.

Macroturbulence

Broadening from macroturbulence occurs when the individual spectra of mass elements moving with different velocities are viewed simultaneously. The mass elements must be large enough such that the photons remain within the element within which they are created until they escape from the star. The effect of macroturbulence is to alter the line profile without altering the equivalent width of the line.

If the velocity spectrum is defined generally by

$$\Theta'(v)dv \equiv \Theta(\Delta\lambda)d\lambda$$

then for each mass element the emergent spectrum is given by (e.g. Gray, 1976)

$$I_\nu = I_\nu^0 \otimes \Theta(\Delta\lambda)$$

where I_ν^0 is the emergent spectrum without macroturbulence and $\otimes$ represents a convolution.

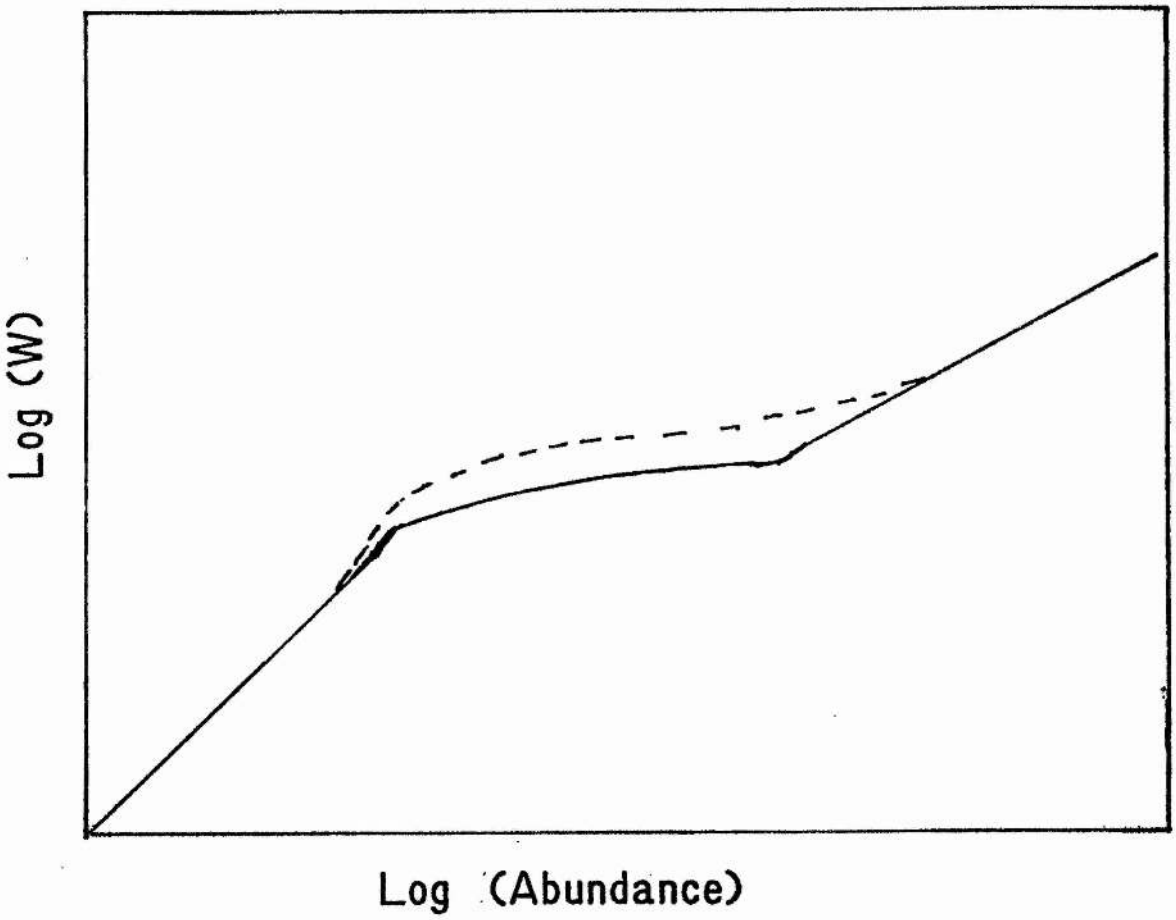

Fig. 1.1 :- Schematic curve of growth. Dashed line illustrates the effect of including microturbulence in the calculation.

The emergent flux is then

$$F_\nu = \oint I_\nu \otimes \Theta(\Delta\lambda) \cos\theta d\omega$$

If $\Theta(\Delta\lambda)$ is isotropic this reduces to

$$F_\nu = \Theta(\Delta\lambda) \otimes \oint I_\nu^0 \cos\theta d\omega$$

where the integral term is simply the line profile in the absence of macroturbulence.

Gray, 1976, and Huang and Struve, 1953, have investigated velocity distributions other than isotropic, and again shown that the equivalent width is invariant.

The convolution technique has its limitations in the calculation of emergent line profiles. Implicit assumptions are made that $\Theta(\Delta\lambda)$ and I_ν are constant over the stellar disc, an approximation which is poor for early-type stars.

A more exact approach is to divide the stellar surface into a number of cells, explicitly calculate and Doppler shift the emergent line profile from each cell and then integrate over the stellar surface.

In the case of macroturbulence this technique is rather cumbersome as the number of cells, N, required is of the order of

$$N \approx \left(\frac{R}{H}\right)^2$$

where R is the stellar radius,

$$H = 800\left(\frac{T}{\mu_m g}\right) km$$

is the pressure scale height and μ_m is the mean atomic weight (Karp and Fillmore, 1980). For a typical main sequence B star $N \approx 10^8$.

Smith, 1976, has approximated this method by using a Monte-Carlo technique to assign random radial and tangential velocities to 2500 cells. This is computationally expensive but still only achieves results which vary by $\approx \frac{1}{2}\%$ in intensity at each point in the line profile from run to run.

Rotation

The broadening of spectral lines by rotation of the star is, in some respects, similar to macroturbulence. Again the first order effect is to alter the line profile without changing the equivalent width of the line.

Similarly, to completely specify the effects of rotational broadening it is necessary to compute line profiles at each point on the stellar disc, Doppler shift these profiles by the line-of-sight velocity component and then integrate to determine the emergent flux profile.

This approach has been used by Stoeckly and Mihalas, 1973, who calculated intensity profiles as a function of limb-darkening angle for four helium I lines and the magnesium II line blend at 4481Å and rotationally broadened line profiles over a grid of effective temperatures, surface gravities and rotational velocities. Slettebak *et al*, 1975, calculated flux profiles for He I 4471Å, Fe I 4476Å and Mg II 4481Å in a similar fashion.

With the assumption that the line profiles are constant over the disc and that only continuum limb-darkening is important then an analytic approach is possible. It can be shown (e.g. Gray, 1976) that in this case

$$R_v = H(\lambda) \otimes C(\lambda)$$

where $H(\lambda)$ is the flux profile for a non-rotating star and $C(\lambda)$ is the rotational profile. For a linear limb-darkening law of the form

$$I_c = I_c^0[(1-\epsilon) + \epsilon \cos\theta]$$

then

$$C(\Delta\lambda) = \frac{2(1-\epsilon)[1-(\Delta\lambda c/v_{rot}\sin i)^2]^{\frac{1}{2}} + \frac{1}{2}\pi\epsilon[1-(\Delta\lambda c/v_{rot}\sin i)^2]}{(1-\epsilon/3)\quad \pi\lambda v_{rot}\sin i/c} \quad ; A = \frac{\Delta\lambda}{\lambda}$$

where v_{rot} is the star's rotational velocity and i is the inclination to the line of sight.

Carroll, 1933, derived an analytic expression for $C(\sigma)$ the fourier transform of $C(\lambda)$ for $\epsilon = 0.6$. This can be generalised to

$$C(\sigma) = \frac{aJ_1(u\sigma)}{u\sigma} + 4b\left[\frac{\sin(u\sigma)}{(u\sigma)^3} - \frac{\cos(u\sigma)}{(u\sigma)^2}\right] \qquad 1A$$

where J_1 is the first order Bessell function, $a = 2(1-\epsilon)/(1-\epsilon/3)$, $b = \epsilon/2(1-\epsilon/3)$ and $u = v_{rot}\sin i\,\lambda/c$.

Values for ϵ depend on the observational wavelength and the temperature structure of the stellar photosphere. Values must therefore be calculated for a particular model. For a main-sequence early-type star $\epsilon \approx 0.3$ at visual wavelengths.

The analytic approximation is most accurate when $C(\lambda)$ dominates $H(\lambda)$. From the tables of Stoeckly and Mihalas, 1973, the variation in the line profile for $v_{rot} \sin i = 10\,km\,s^{-1}$ is larger than the variation in the intensity profile from centre to limb for the Mg II line at 4481Å and values of T_{eff} and log g typical of mid B stars.

(Another source of broadening which must be taken into account when comparing predicted line profiles with those observed is instrumental broadening. This varies in importance according to to the observational equipment used and is discussed in a later section of this thesis.)

1.iii *Historical Review*

The first spectroscopic analysis of a B star was carried out by Unsöld, 1941. He utilised the method known as *coarse analysis* in which it is assumed that the lines are formed in a region of the stellar photosphere to which unique mean values of temperature and pressure can be assigned. Unsöld found abundances for 8 elements in the photosphere of τ Sco making the additional assumption of LTE.

Coarse analysis methods were improved upon by the technique of *fine analysis*. In this method the variations of temperature and pressure with photospheric depth are included in the model. Again the first early-type star to be analysed was τ Sco. Traving, 1955 found results which were little different from those of Unsöld.

A number of analyses of early-type stars have subsequently been made using this technique, with varying degrees of sophistication in the calculation of the model. The total number, however, of B stars analysed in detail prior to the commencement of this project was relatively small, particularly for stars of mid to late B classification.

Table 1.i summarises the principal analyses of the absorption line spectra of early-type stars made with the assumption of LTE up to 1977. While the results are in general in reasonable agreement several aspects of the analyses cast doubt on the overall validity of the models used.

Observers found that the observed line profile cores were deeper than those predicted.

Table 1.1

Analyses Previous to 1977

Star	*MK*	T_{eff}	log *g*	ξ_t	*Ref.*	*He*	*C*	*N*	*O*	*Mg*	*Si*	*S*
10 *Lac*	*O9 V*	37450	4.45	0	*A*	11.2	8.4	8.4	8.8	8.2	7.8	–
τ Sco	*B0 V*	35000	4.3	0	*B*	11.1	7.7	8.3	8.6	8.3	7.6	–
		32800	4.45	0	*A*	11.2	8.4	8.6	9.1	7.7	8.0	–
		32800	4.2	5	*C*	11.1	8.2	8.5	8.8	7.7	7.7	7.3
		32000	4.1	4.5	*D*	11.0	8.1	8.3	8.7	7.5	7.6	7.2
		34000	4.8	5	*E*	11.0	7.9	8.2	8.9	7.7	7.7	8.0
δ CMa	*B0.5 IV*	31300	4.2	0	*F*	–	8.0	8.2	9.0	7.3	7.8	7.1
λ *Lep*	*B0.5 IV*	30900	4.05	4.5	*D*	11.0	8.5	8.0	8.8	7.7	7.8	7.4
β Cru	*B0.5 IV*	24500	3.85	4	*G*							
ζ Per	*B1 Ib*	27200	3.6	–	*H*	11.3	8.3	8.3	9.0	7.8	8.0	7.5
β CMa	*B1 II*	23700	3.74	4	*G*							
σ Sco	*B1 III*	22800	3.81	4	*G*							
α Lup	*B1 III*	20700	3.56	4	*G*							
ζ CMa	*B1 IV*	23900	3.73	4	*G*							
HD 36959	*B1 V*	28900	4.2	0	*F*	11.0	8.0	7.6	8.6	7.5	7.3	7.3
ν Eri	*B2 III*	21500	3.78	4	*G*							
15 *CMa*	*B2 III*	23300	3.80	4	*G*							
η Peg	*B2 IV*	24000	3.8	0	*F*	11.2	8.6	8.0	8.6	8.0	7.0	7.8
		20700	3.84	4	*G*							
δ Cet	*B2 IV*	20700	3.81	4	*G*							
τ Lup	*B2 IV*	19800	3.89	4	*G*							
θ Oph	*B2 IV*	20500	4.01	4	*G*							
η Hya	*B3 V*	21900	4.0	5	*I*	10.8	7.8	–	8.5	7.4	7.3	–
ι Her	*B3 V*	20200	3.75	5	*I*	10.8	8.1	7.7	8.4	7.3	7.2	7.1
τ Her	*B5 IV*	15500	3.75	5	*J*	10.8	8.5	–	–	7.8	7.5	7.3
ζ Dra	*B6 III*	13400	4.0	–	*K*							
β Sex	*B6 V*	15000	–	–	*K*							
α Leo	*B7 V*	12900	–	–	*K*							

References:

A: Traving, 1957

B: Aller, Elste and Jugaku, 1957

C: Scholz,1967

D: Hardorp and Scholz, 1970

E: Dufton, 1972

F: Aller and Jugaku, 1959

G: Watson,1971

H: Cayrel, 1958

I: Kodaira and Scholz, 1971

J: Adelman, 1977

K: Underhill, 1973

The abundances found for neon and magnesium, particularly in O stars, were much higher than the solar values, often by a factor of $\approx$ 10. Discrepancies between the values of effective temperature derived from continua criteria, such as the Balmer jump, and from the ionisation equilibria of different elements were often found. Silicon lines, in particular, caused a problem. Lines of Si II, Si III and Si IV are observed simultaneously in the spectra of some B stars. It was often found (e.g. Aller, 1960) that a self-consistent solution for all three ionisation states could not be obtained.

Several possibilities were suggested as to the source of model inadequacies. Primary amongst these were the use of the LTE approximation, the omission of absorption lines from the calculation of the opacity of the photosphere and the lack of inclusion of chromospheric or coronal regions in the models.

The Princeton group calculated model photospheres including the effects of strong ultra-violet lines (e.g. Morton and Adams, 1968, Bradley and Morton, 1969). The stratification of the model photospheres was found to be such that they predicted similar visual observables as un-blanketed models with higher effective temperatures.

Simultaneously work was being carried out on models which relaxed the assumption of LTE. The fact that radiation escapes from a star is sufficient to make the hypothesis of LTE inaccurate. Without the approximation of LTE it is necesssary to solve simultaneously the equations of statistical equilibrium, radiative equilibrium and hydrostatic equilibrium in a self-consistent manner. While the physics of the problem were well understood the advent of powerful computers and the development of sophisticated numerical techniques were required before the problem could be tackled. The development of the techniques required is described in Mihalas, 1978.

Early successes of these non-LTE models occurred in the predictions for O stars. The anomalous abundances previously found for neon and magnesium were shown to be artefacts of the LTE approximation (Auer and Mihalas, 1973, Mihalas, 1972). The variation of the equivalent widths of the hydrogen lines with spectral type was also more successfully predicted using non-LTE models (Auer and Mihalas, 1972) and the deeper line cores were also in better agreement with the observations. Similar improvements in predictions of He I and He II lines were also noted, particularly for lines in the red to

infrared region of the spectrum. Calculations for a number of silicon lines were made by Kamp, 1973, for non-LTE models with $T_{eff} > 25000K$. He showed that the predicted equivalent widths were larger by up to a factor of 2 than if LTE populations had been used, although the same non-LTE model photospheres were used in both cases.

Most of the comparisons of the non-LTE predictions with observations were made for O stars. This was because the LTE approximation is better justified where collisional rates dominate radiative rates. This criterion is only strongly violated for the highest temperatures and luminosities. The comparisons for metallic lines were, in general, only made between predicted and observed equivalent widths, little use being made of line profile information.

Kamp, 1976, calculated a more extensive grid of silicon line profiles. These suggested that abundances derived for silicon using LTE models could be in error by between 50% and 300% even at temperatures of 15000K. In an analysis of equivalent widths of varying quality and determined by a number of different authors, Kamp, 1978, used these predictions to suggest that some of the problems previously noted were partially resolved and that lower values of ξ_t compared to those found using LTE models were necessary.

1.iv *The Model Photospheres Used*

The models used are based on two important computer programs for the calculation of model photospheres - the non-LTE code written by Mihalas and the line-blanketed LTE code of Kurucz. These programs are discussed in detail in Mihalas, Heasley and Auer, 1975, and Kurucz, 1979, respectively but a brief description of the major features of each will be given here.

LTE Models

The LTE models used in this project were calculated using a version of the ATLAS program written by Kurucz. This version was implemented on the CRAY-1 computer at the SERC Daresbury laboratory. (At an earlier stage of the project use was made of the modified ATLAS program - SAM1 - implemented at University College, London by Dr. S. Wright (Wright, 1975, Wright and Argyros, 1975) and subsequently implemented on the IBM 370 computer at Cambridge by Dr. A. E. Lynas-Gray. Access to this version

was by computer link from the IBM 360 at St. Andrews.)

Two actual programs were used. The first, known as ATLAS6, generates the structure of the model photosphere and the second, WIDTH6, calculates various parameters for specified input absorption lines using the model photosphere generated by ATLAS6 as input.

ATLAS6 includes the effects of almost one million absorption lines as sources of opacity in its calculation of a model. Individual line opacities, however, are not included explicitly. The spectrum is divided instead into a number of wavelength ranges and opacity distribution functions calculated for each of these ranges. This technique makes the assumptions that the absorption coefficient spectrum has the same shape at all photospheric depths and that, either lines of different strengths are uniformly distributed throughout the interval or the continuum source function or opacity do not vary radically over the frequency interval.

Gustaffson *et al*, 1975, have shown that the first of these approximations is not a serious source of error in their models. Suitable choices of the wavelength intervals to avoid strong opacity discontinuities reduces the possibility of the introduction of errors due to the second approximation.

The other assumptions of the classical model photosphere are included in the calculations, i.e.

a) plane parallel geometry

b) hydrostatic equilibrium

c) LTE

d) energy transport is either radiative or convective.

The use of the ATLAS programme is described in Kurucz, 1970 and in Wright and Argyros, 1975. For this project the following parameters were selected. The calculations were made over 40 depth points covering a range in the *mass* cm^{-2} of $\approx 10^{-4} - 10^{2}\ g\,cm^{-2}$, or in terms of the Rosseland optical depth, $\approx 10^{-5} - 10^{2}$. The frequency points used were identical to those of Kurucz, 1980.

A typical iteration of the calculation took $\approx 3s$ of computer time and, generally, 8 iterations were used per model. This number of iterations was sufficient to obtain flux

errors of $< 0.5\%$ and flux derivatives accurate to $\approx 1\%$ except for the uppermost depth points where the flux derivatives were about ten times higher than this.

During the running of the program the opacity switches were set so as to include the effects of the bound-free and free-free opacities of hydrogen, helium I and helium II. Eight bound levels of hydrogen, eleven of He I and nine of He II are explicitly included. Rayleigh scattering from hydrogen and helium as well as isotropic electron scattering were also used. Opacities from the 'COOL', 'LUKE' and 'HOT' sources together with the line opacities were used for all computations. Solar abundances were assumed.

The companion program written by Kurucz, WIDTH6, was also used. This program takes the structure of the model photosphere calculated by the ATLAS6 program and calculates equivalent widths of absorption lines input by the user. The user must supply log gf values, damping constants and energy levels for each transition. The program will then calculate equivalent widths for each line over a grid of abundances and microturbulent velocites supplied by the user. For a grid of eight abundances and 3 microturbulent velocities the computation time per line was $\approx \frac{1}{4}s$. In another mode the program can be set to output the line profiles at twenty wavelengths.

Non – LTE Models

No new non-LTE calculations were made for this project. Instead predictions made without the constraint of LTE were taken from the literature. Most use was made of calculations based on model photospheres calculated using the non-LTE code of Mihalas. A grid of these calculations and a description of the methods used in their construction is given in Mihalas, 1972b. They use the complete linearisation technique modified to include variable Eddington factors (Auer and Mihalas, 1969, 1970). Non-LTE effects are allowed in five levels of hydrogen and two levels of each of He I and He II. A mean light element equivalent to a weighted mixture of carbon, nitrogen and oxygen is included in LTE. Predictions for the line profiles of H_α, H_β, and H_γ are given.

Use of these models has also been made in the calculation of the spectral lines of some light elements. In this project the predictions for helium and magnesium (Stoeckley and Mihalas, 1973) and the predictions of Kamp, 1976 for silicon have been used. Particular emphasis has been placed on the latter for two reasons, the silicon anomaly discussed

earlier and the larger atomic weight of silicon. This latter factor means that silicon lines are more useful as a measure of non-thermal effects in stellar photospheres. The accessibilty of a reasonable number of lines of different ionisation stages in the visible range of the spectrum is also important.

Calculations for several nitrogen lines using an updated version of the Auer, Heasley and Mikey, 1972, code have also been made (Dufton *et al*, 1981, Dufton and Hibbert, 1981). An alternative series of calculations for magnesium lines has been made by Snijders and Lamers, 1975.

The general procedure in all these calculations is the same. The model photosphere is calculated first. The level populations are then calculated in an iterative manner, frequently using the LTE populations as an initial estimate and then finally the line profiles are calculated. Usually only a subset of the possible levels are calculated with non-LTE and the others are assumed to have LTE populations.

It is possible, therefore, to distinguish two different effects on the resultant line profiles. The first is the effect of the non-LTE calculations on the structure of the stellar photosphere and the other is the effect of the use of non-LTE on the level populations themselves.

To illustrate the magnitude and sense of these effects the results for a number of lines of calculations using different methods are compared here. Both Kamp, 1976, and Dufton and Hibbert, 1981, present results for lines in a photosphere calculated in non-LTE for level populations both with and without the assumption of LTE. These are compared with the results obtained with the WIDTH6 and ATLAS6 programs during the course of this project. Identical values of oscillator strengths and damping constants to those used in the non-LTE calculations were chosen.

Calculations were made over a range of effective temperatures, $15000K < T_{eff} < 30000K$ and at two surface gravities, log g = 3.0 and log g = 4.0. (N.b. No line-blanketed models with effective temperatures greater than $\approx 25000K$ could be calculated for log g = 3.0 as the models became unstable due to the radiation pressure exceeding the surface gravity.)

Comparisons

(a) Silicon Lines

Figures 1.2, 1.3 and 1.4 illustrate the equivalent widths found for the Si II 4128Å line, the Si III 4567Å line and the Si IV 4088Å line respectively. The results are coded with the following symbols :-

+ line-blanketed LTE (A)

× non-LTE photosphere, LTE populations (B)

• non-LTE photosphere, non-LTE populations (C)

At first glance there appears to be a systematic trend for the Si II 4128Å line with the equivalent widths increasing from A through B to C. The difference between B and C diminishes at higher temperatures. However, a constant shift in the temperature scale of $\approx$ 1600K would be sufficient to make the results of A almost indistinguishable from those of B. This is similar to the size of shift between the temperature scales of line-blanketed and unblanketed LTE model photospheres found from earlier studies of the continuum predictions. Indeed, figures 41 and 42 of Kurucz, 1980, show that the difference between such models at Rosseland optical depths $\leq 10^{-2}$ in terms of their temperature distribution is simply approximated by a temperature shift of between 800K and 1000K.

Similar differences between results A and B can be seen for the 4567Å and 4088Å lines where temperature shifts of between 1500K and 2000K would superimpose the results. It is particularly apparent from the results for the 4567Å line that the same maximum equivalent width is attained. Clearly, then, in this temperature regime the "photospheric non-LTE" effects could be represented reasonably accurately by a simple temperature shift.

A comparison with results from type C models, however, illustrates, the importance of "line non-LTE" effects. The maximum equivalent widths obtained are up to a factor of 2 larger than using models of type A or B.

The magnitude of the enhancement of the line strength is not a simple function of temperature. The magnitude of the effect is greatest at the individual lines' position of maximum strength. This has been noted by Kamp, 1978. As the stronger lines are, in general, the easiest to observe and consequently most frequently used in the determination

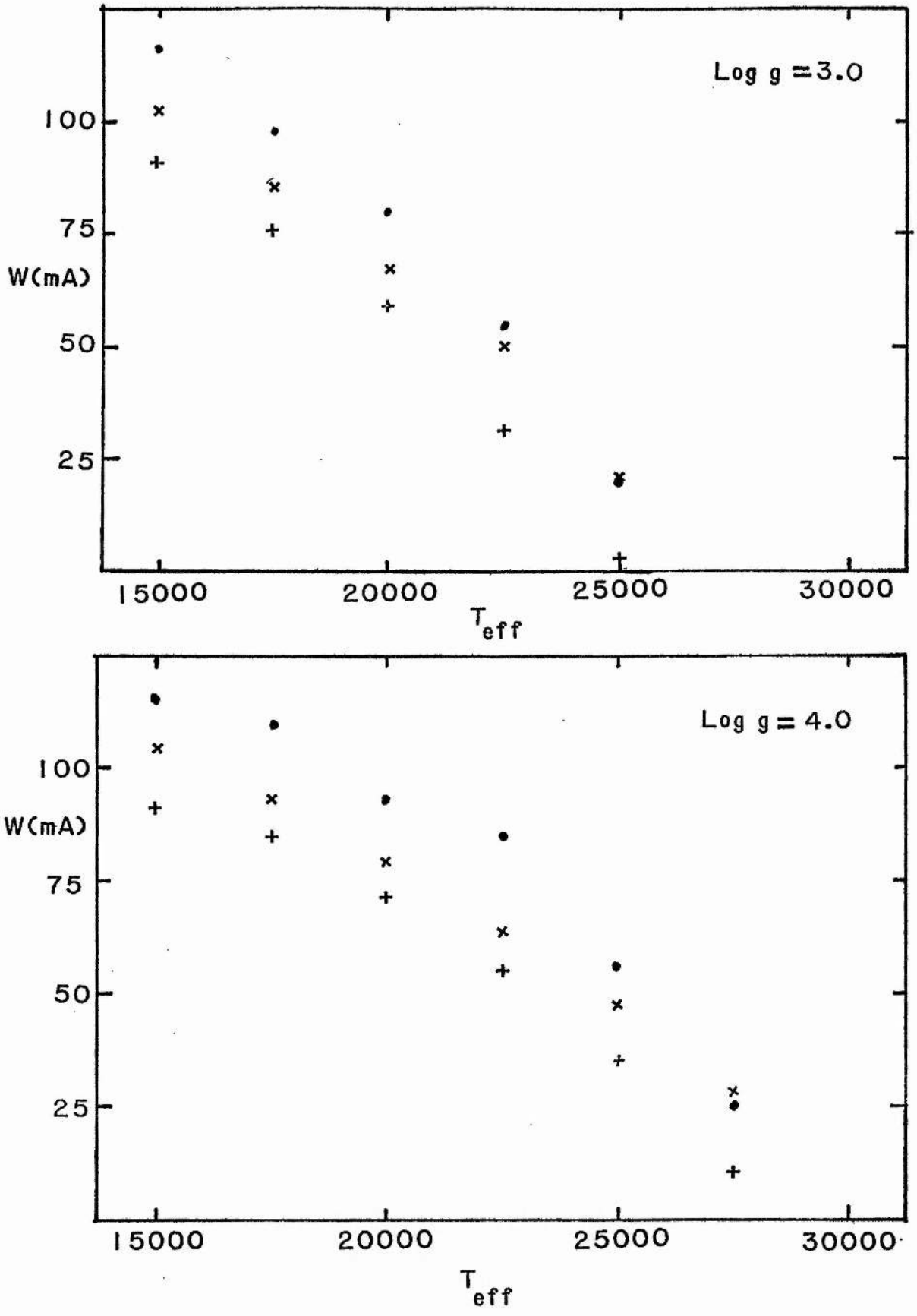

Fig. 1.2 :- **Comparison of equivalent widths of Si II 4128Å predicted by ---(+) LTE line-blanketed model photosphere, (×) non-LTE model photosphere with LTE populations and (⊙) non-LTE model photosphere with non-LTE populations.**

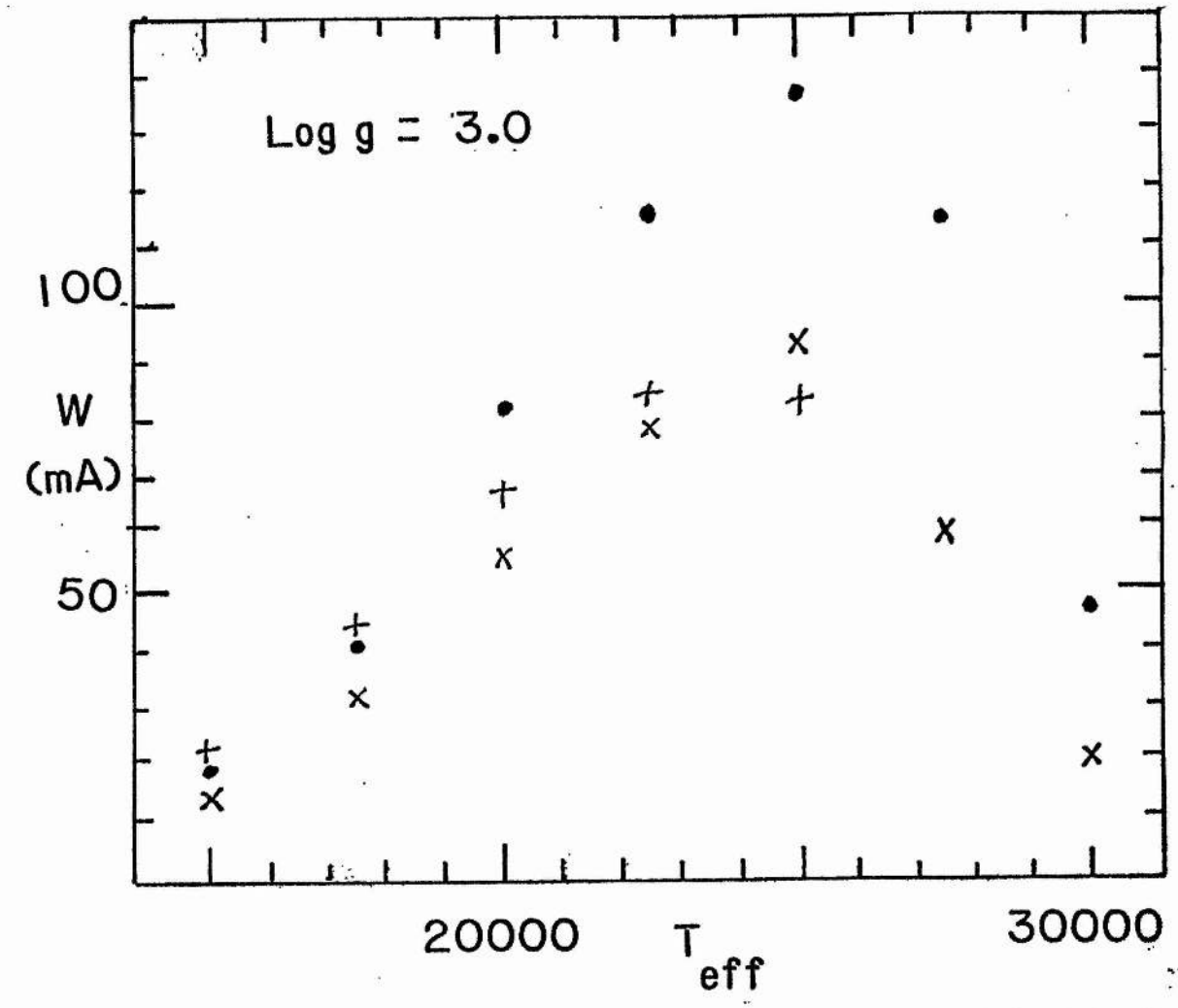

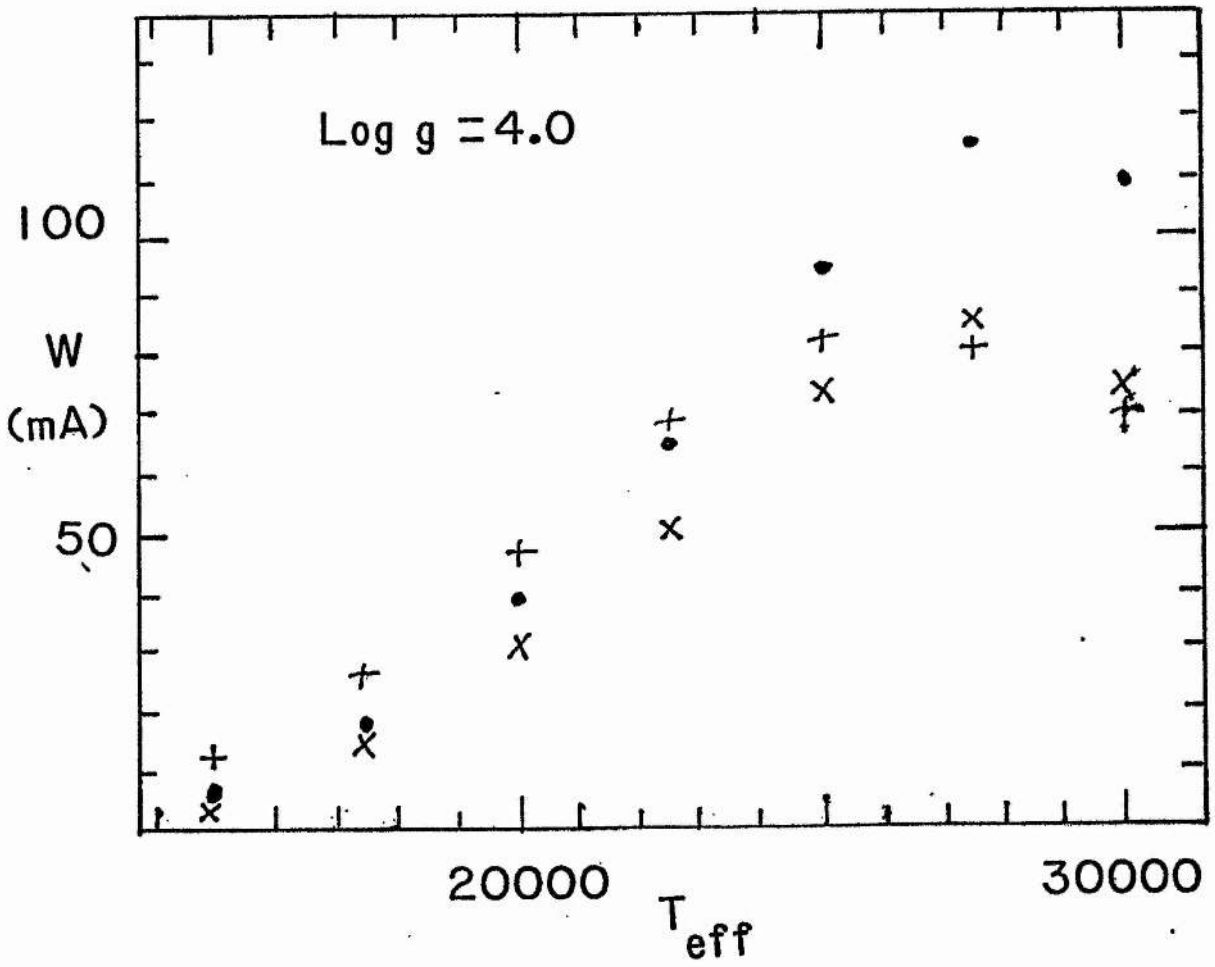

Fig. 1.3 :- As figure 1.2 for Si III 4567Å.

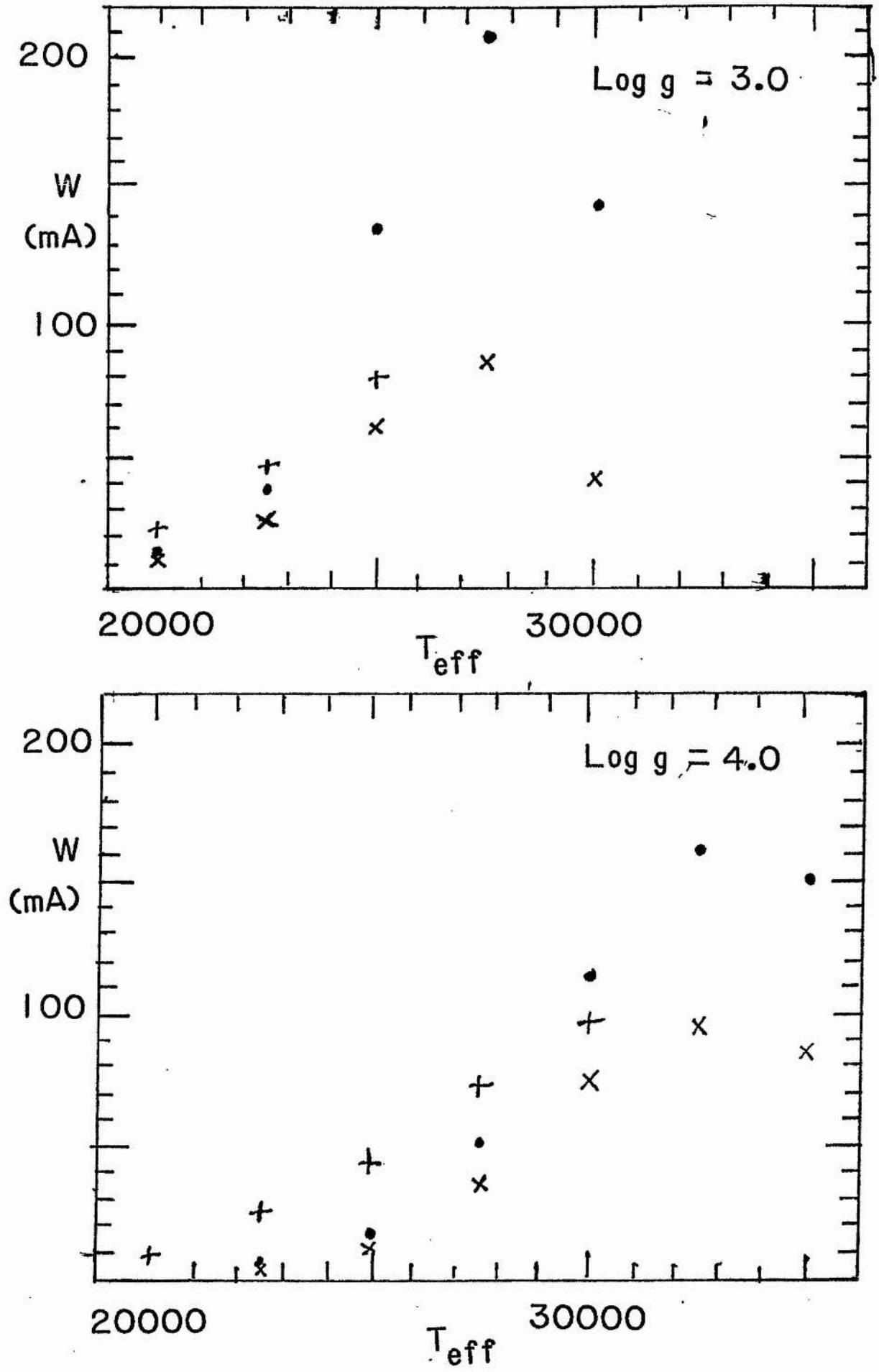

Fig. 1.4 :- As figure 1.2 for Si IV 4088Å.

of abundances such an effect may be of considerable importance. It should be stressed that the effects persist to the lower end of the temperature range investigated and also that the effects will mimic microturbulence in that the stronger lines are more affected than the weaker lines.

Equivalent widths are not the only diagnostic. Differences in the line profiles can also be expected. In his calculations for the silicon lines Kamp quotes values of the central residual intensity, R_o, for each line. This parameter can also be determined from the results of the WIDTH6 program. Figures 1.5, 1.6 and 1.7 show the results obtained for the same models and using the same legend as the equivalent width calculations.

Differences between all three models are apparent. The most consistent trend is that the deepest line cores are attained by models of type C with the shallowest being formed by models of type B. Unlike the equivalent widths, residual intensities from models of type A and B cannot be brought into agreement by the expediency of a simple temperature shift.

(*b*) *Nitrogen Lines*

Dufton and Hibbert, 1981, present equivalent widths for models of type B and C discussed above. They make predictions for a number of N II lines for model photospheres with log=4.0 and over the temperature range$20000K < T_{eff} < 32500K$. A comparison of their results with those obtained in this project using the WIDTH6 program is shown for the 3995Å line in figure 1.8.

A similar result to that obtained for the silicon lines is evident. Again results from models of types A and B can be made consistent by the introduction of a temperature shift. Roughly similar maximum equivalent widths are derived for both types. The equivalent widths obtained with the use of non-LTE populations, however, are again larger than in either of the other cases. Here the enhancement is only $\approx$ 50% at maximum. This is still equivalent to an abundance difference of $\approx$ 2.

Unfortunately, Dufton and Hibbert do not give any information about the line profiles so a comparison cannot be made. The influence of pressure differences is also uncertain as they present results for only one value of the surface gravity. (The line-blanketed results show that the nitrogen lines are not particularly sensitive to variations

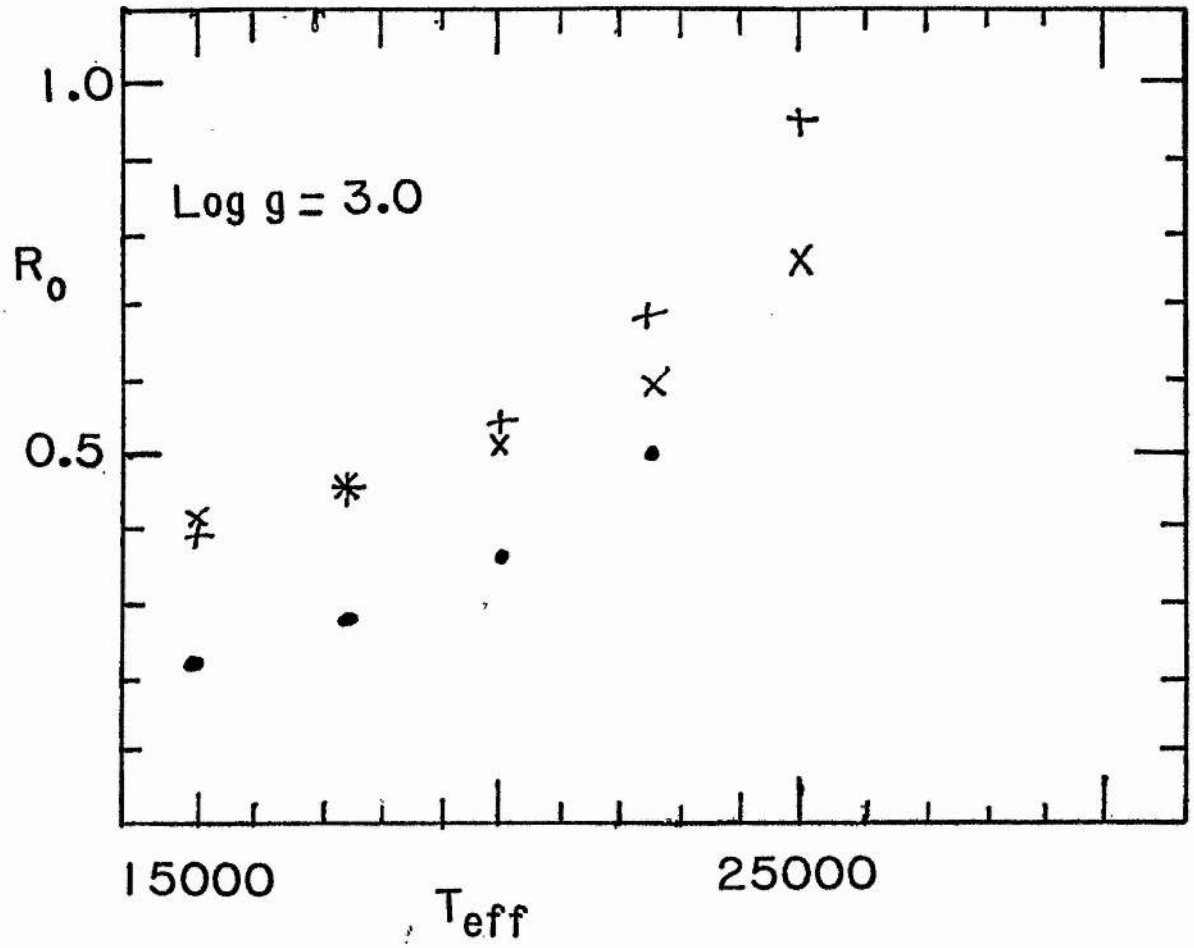

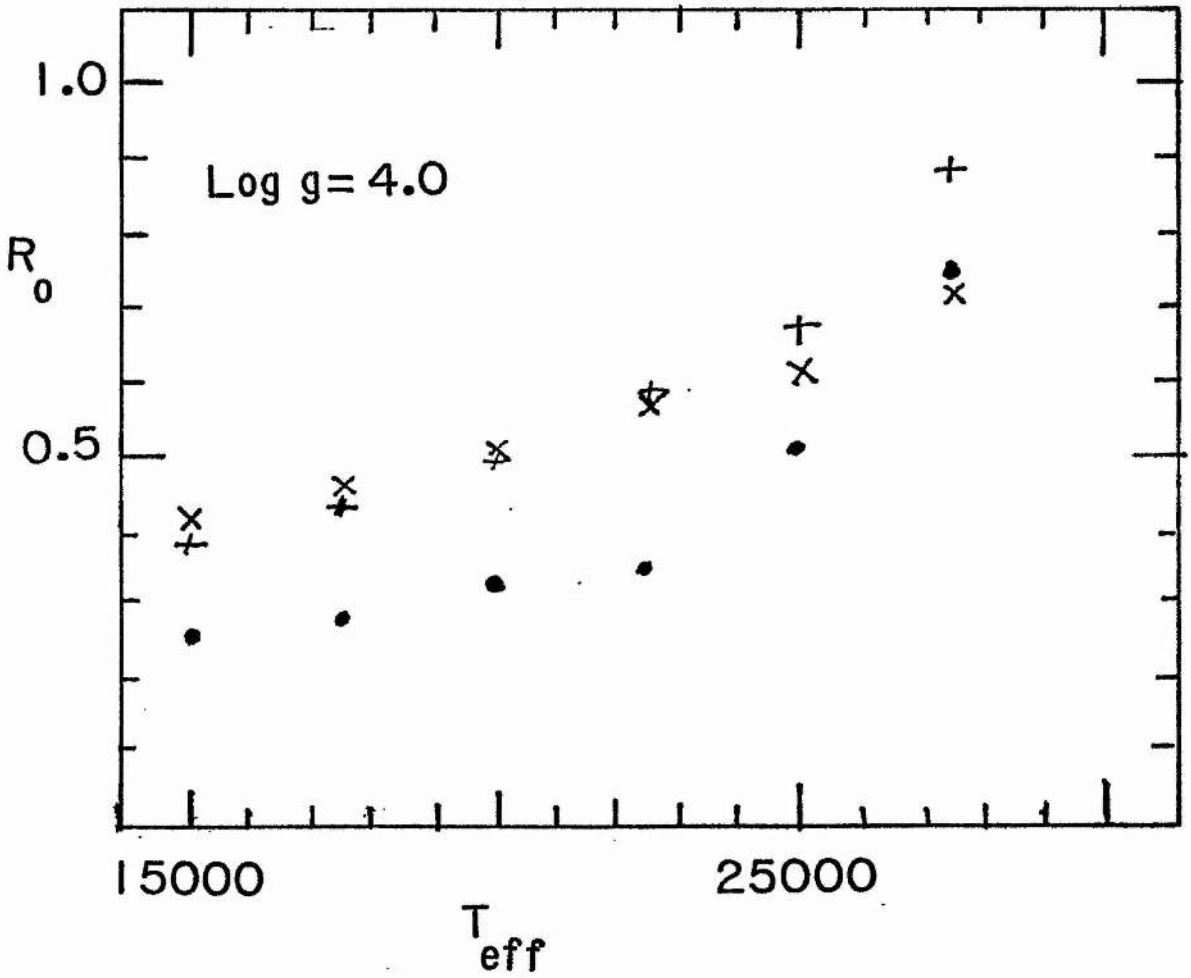

Fig. 1.5 :- Predicted central depths for Si II 4128Å from models as in figure 1.2.

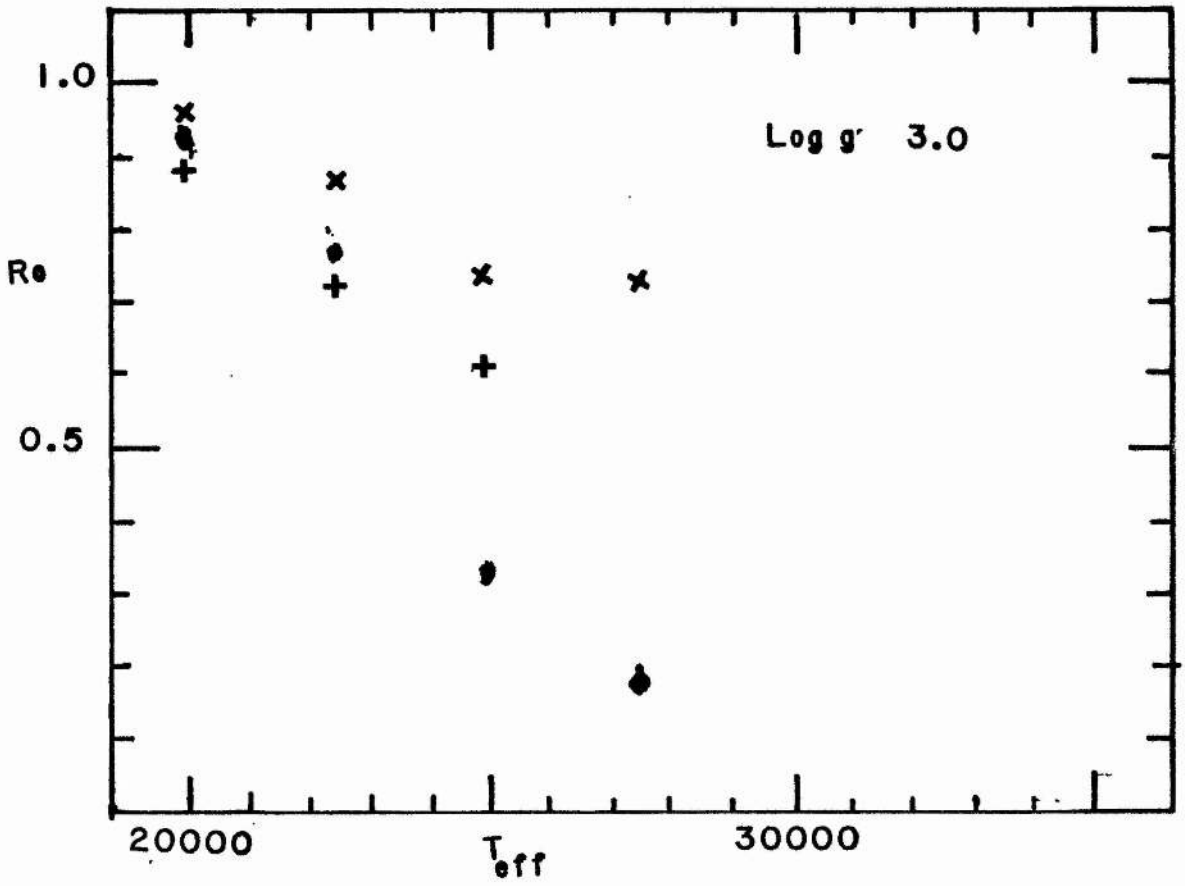

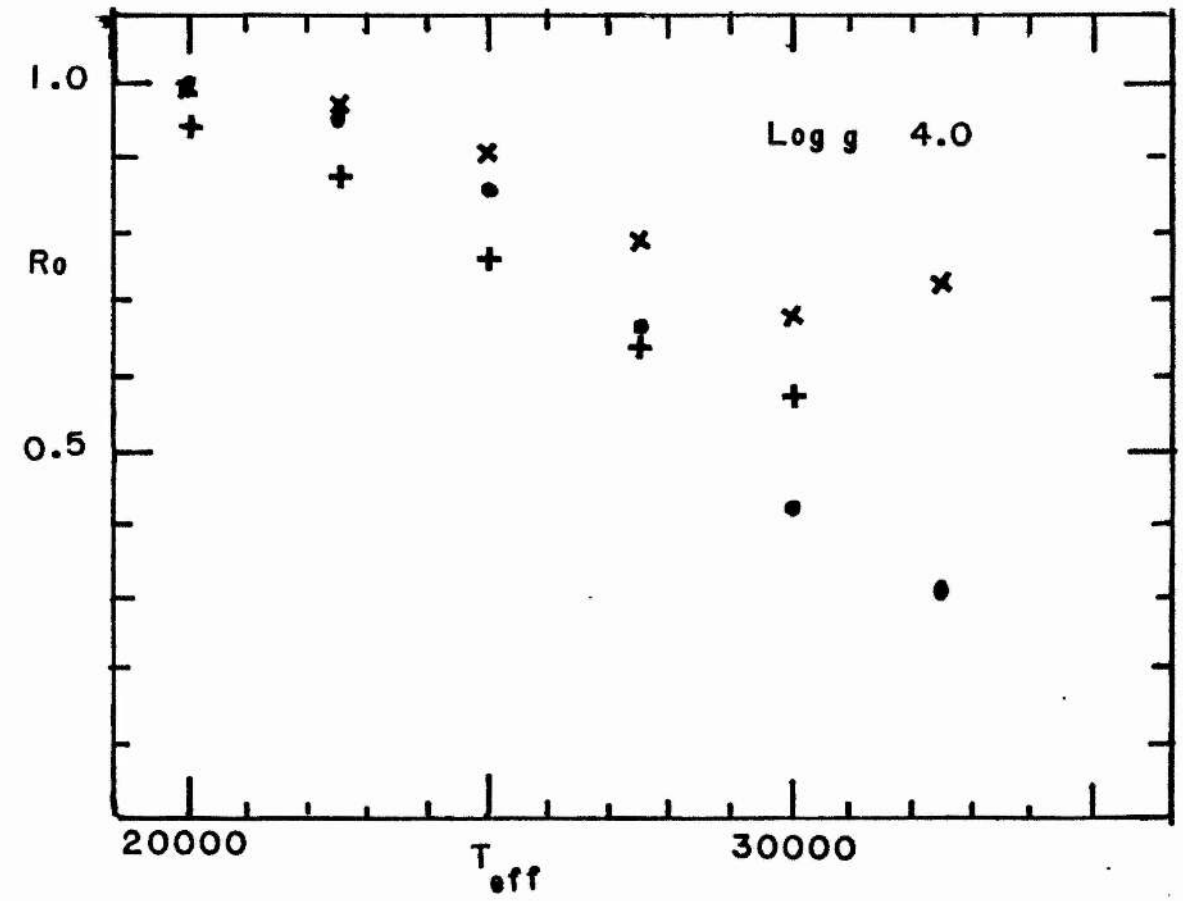

Fig. 1.6 :- As figure 1.5 for Si III 4567Å.

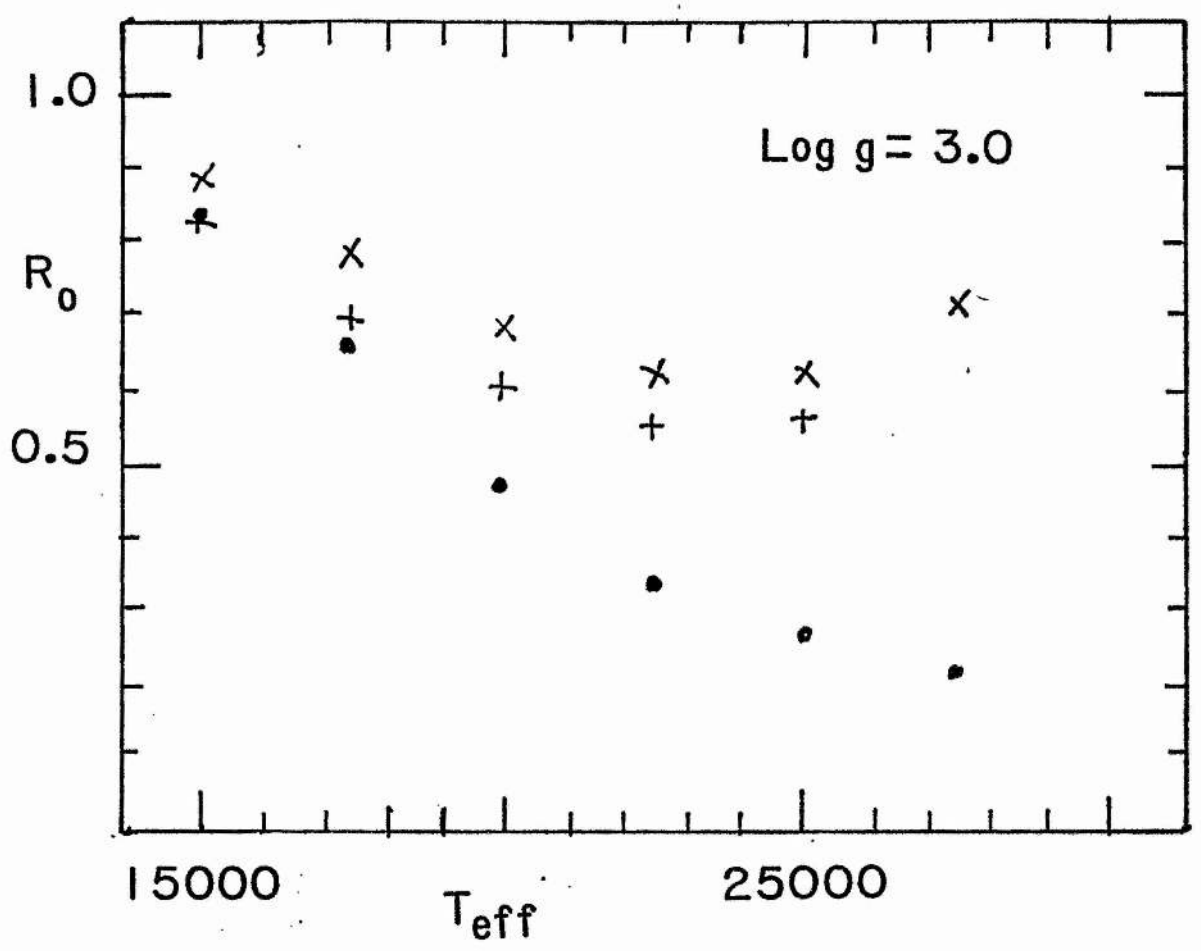

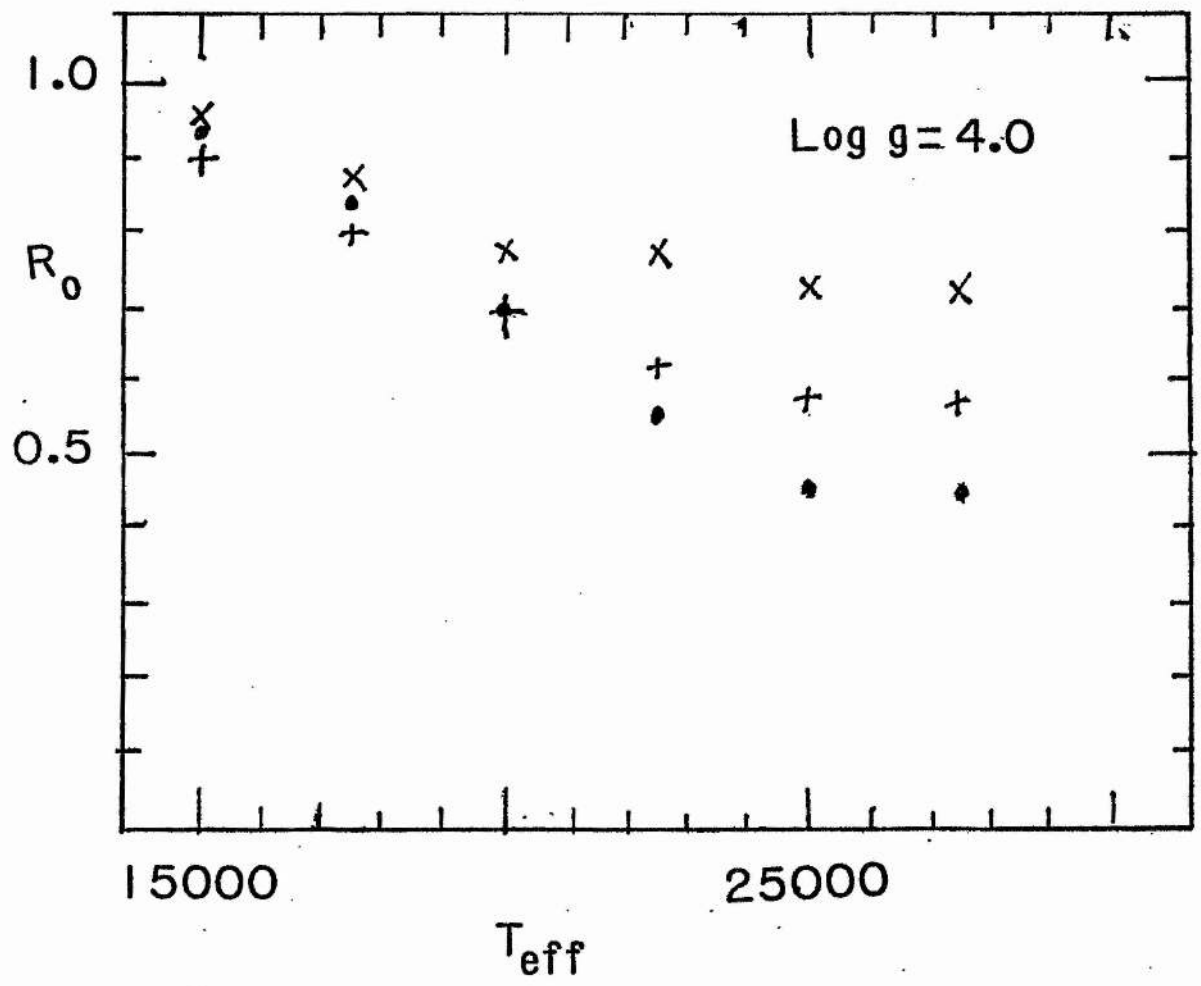

Fig. 1.7 :- As figure 1.5 for Si IV 4088Å.

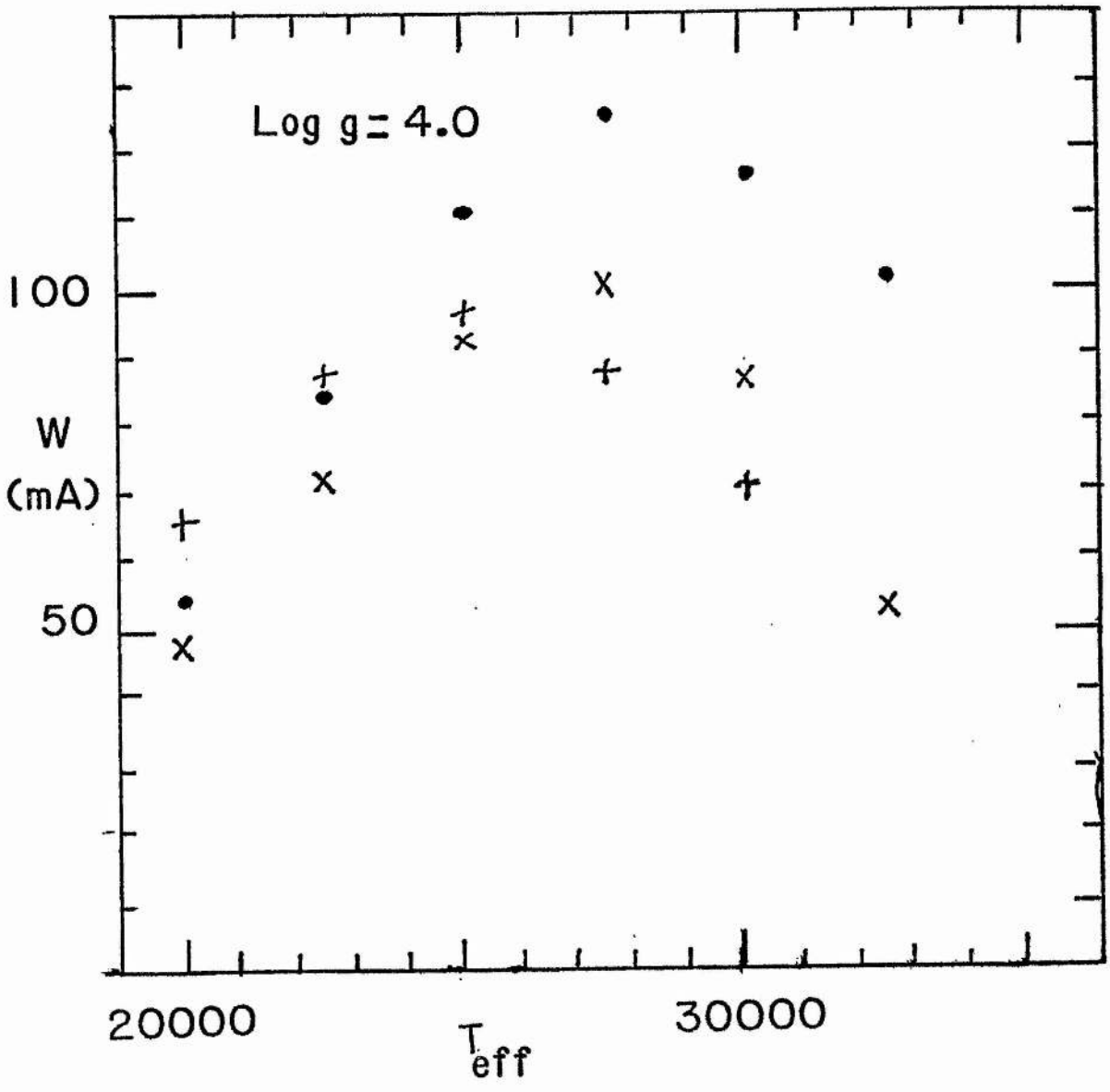

Fig. 1.8 :- As figure 1.2 for N II 3995Å.

in log g. At an effective temperature of 22500K the effect of changing log g from 4.0 to 3.0 is a variation in the equivalent width of $\approx$ 10%).

CHAPTER TWO

PHOTOGRAPHIC OBSERVATIONAL MATERIAL

2.i *Introduction*

The photographic observational material used in the principal part of this study is described in this chapter. Also described are the equipment and techniques used in the aquisition of this material. A discussion of possible sources of error due to the photographic process and the means taken to overcome these problems is given. The calibration of the plates and the aquisition of plates to determine the instrumental profile of the instrumentation used at the South African Astronomical Observatory (S.A.A.O.) are discussed.

At the time these observations were made photoelectric devices capable of measuring stellar spectra were becoming available. Photographic measurements still offered the multiplex advantage of being able to simultaneously measure a larger number of resolution elements compared to devices such as the Image Photon Counting System (I.P.C.S., Boksenburg, 1977). Another advantage of the photographic plate over the I.P.C.S. is that saturation of the I.P.C.S. reduces the data aquisition rate for bright stars to a level at which which exposure times to obtain sufficient signal to noise ratios become prohibitively long, negating the aperture advantages of large telescopes and the better inherent quantum efficiency of photoelectric devices. (For non photon counting devices such as the Reticon the latter disadvantage does not hold although the former does.) As it was hoped that the techniques of measurement developed for this project would overcome some of the problems traditionally associated with photographic spectrophotometry it was felt that the use of photographic material would be of value. In particular, it was hoped that the relatively new IIIaJ emulsions with improved resolution and noise characteristics would prove advantageous.

2.ii *Sources of the Plate Material*

Plates for the project were obtained from three sources. Dr. P. W. Hill provided a collection of plates taken with the 74" Radcliffe telescope in 1964 using the Y camera of the coudé spectrograph. This collection consisted of ≈60 plates of 15 B stars taken on IIaO and 103aF emulsions. The wavelength coverage was ≈ 3000Å – 7000Å for each of the stars. The blue plates have a reciprocal dispersion of 6.7Å mm^{-1} and the red plates 13.4Å mm^{-1}. From this collection 16 plates of 4 stars were chosen for the study on the basis of the rotational velocities of the stars as quoted in the catalogue of Uesugi and Fukuda, 1970. Details of the plates are given in Table 2.i. Photometric calibration for the plates was by means of a spot sensitometer, exposures of the spots being made on different plates of the same emulsion and developed simultaneously with the respective stellar spectrum plate.

An additional eight spectra of eight stars were supplied by Dr. R. W. Hilditch. These were taken with the coudé spectrograph of the 72" telescope at the Dominion Astrophysical Observatory. Calibration for these spectra was by means of a step wedge dispersed through the same optics as the stellar spectrum and superimposed on the same plate. Details of the spectra are given in Table 2.ii. The emulsion used was IIIaJ and the wavelength region covered was ≈ 3600Å to 4900Å at a reciprocal dispersion of ≈ 8Å mm^{-1}.

The final set of spectra used in the project were obtained by the author, assisted by Dr. C. W. Fraser, with the Y camera of the coudé spectrograph of the 74" telescope at S.A.A.O. during March 1978. The aquisition of these spectra will be described in detail below.

2.iii *Radcliffe Telescope and Spectrograph*

The telescope is situated at the Sutherland outstation of the S.A.A.O. in the Karoo region of Cape Province, having been moved there from Pretoria since the spectra provided by Dr. P. W. Hill were taken. The spectrograph camera is at the f30 coudé focus and is situated in a coudé room together with the collimator and grating. This room adjoins the dome where the telescope and slit are sited.

Spectra were taken using the B grating and Y camera, details of which are given

Table 2.i

Spectra Supplied by Dr. P.W. Hill

Star	*Plate*	*Emulsion*	*Exposure(min)*	*Dispersion*	*Wavelength*[a]
HD 15371	*DY* 1084	*IIaO*	35	6.7	1
B5 III	*DY* 1097	103*aF*	57	13.4	2
κ Eri	*DY* 1113	*IIaO*	48	6.7	3
	DY 1128	*IIaO*	40	13.4	4
HD 165024	*DY* 1075	*IIaO*	15	6.7	1
B2 Ib	*DY* 1086	103*aF*	36	13.4	2
θ Ara	*DY* 1100	*IIaO*	30	6.7	5
	DY 1115	*IIaO*	35	13.4	4
HD 169467	*DY* 1077	*IIaO*	14	6.7	1
B3 III	*DY* 1088	103*aF*	34	13.4	2
α Tel	*DY* 1102	*IIaO*	36	6.7	5
	DY 1117	*IIaO*	30	13.4	4
HD 207971	*DY* 1079	*IIaO*	8	6.7	1
B8 III	*DY* 1090	103*aF*	22	13.4	2
γ Gru	*DY* 1104	*IIaO*	24	6.7	3
	DY 1118	*IIaO*	16	6.7	1

Note: a:- approximate wavelength range of useful spectrum

1: 3300Å - 4600Å

2: 4400Å - 7000Å

3: 3700Å - 5000Å

4: 3000Å - 5000Å

5: 4000Å - 5000Å

Table 2.ii

Spectra supplied by Dr. R.W. Hilditch

Star		*MK type*
HD 147394	τ *Her*	*B5 IV*
HD 166182	102 *Her*	*B2 V*
HD 180163	η *Lyr*	*B2 IV*
HD 184171	8 *Cyg*	*B3 IV*
HD 184930	ι *Aql*	*B5 III*
HD 195810	ϵ *Del*	*B6 III*
HD 214680	10*Lac*	*O8 III*
HD 218376	ι *Cas*	*B0.5 III*

in the S.A.A.O handbook. This configuration gives second order spectra at a reciprocal dispersion of 6.7Åmm^{-1} with the grating being blazed at an angle to give maximum efficiency at 5000Å. The grating angle was chosen to give coverage of the wavelength region between 4000Å and 5300Å. This gives coverage of the principal silicon lines in the blue and green regions of the spectrum, including the Si II doublet at 5056Å for which measurements with the Michelson interferometer were also made. Spectra are recorded singly on a 10" by $\frac{23}{32}$" plate.

Both the slit width and length are continuously variable. Two moveable prisms provide control of the slit width and these are also used to project light from an iron arc discharge apparatus to give wavelength calibration.

A quartz prism field rotator is located in the optical path immediately prior to the slit. This enables the stellar image to be trailed along the length of the slit by varying the rate at which the telescope is tracked in right ascension.

Neutral density and wavelength selective filters can also be incorporated in the beam path prior to the slit assembly. Tne former were used to give reasonable observation times for Sirius and the latter to cut out ultraviolet light to prevent overlap between the third and second order spectra.

2.iv *Selection of Stars*

Prior to the observing run a list of stars with spectral types between O9 and B8 was extracted from the HD catalogue using a FORTRAN computer program written by Dr. P. W. Hill. Spectral types were taken from the catalogue of Buscombe, 1972. The stars were then grouped by spectral type and luminosity class and ordered by apparent magnitude.

Using the catalogues of Uesugi and Fukuda, 1970, and Slettebak *et al*, 1975, stars with projected rotational velocities greater than 75 $km\ s^{-1}$ were eliminated. Also eliminated were stars classified as peculiar and, in the main, spectroscopic binaries. In this context β-Cepheid variables were not considered peculiar and a number of these were retained in the observing list.

On an observing night stars were selected from this list to give the best use of observing time, subject to the constraint of covering a range of spectral type and luminosity

class. No star was observed at an hour angle of $>$ 2 hours. Brighter stars were selected in preference to faint stars of the same spectral type, unless the difference between their respective rotational values was large, in which case the star with the lower value was chosen.

In addition to the programme stars, Sirius was chosen to act as a comparison star for the Michelson interferometer observations and to be used as a measure of the internal accuracy of the reduction system.

2.v *Observational Procedure*

Prior to observing, the spectrograph was focussed by the Hartmann method, using the slit diaphragm and iron arc. Two exposures of the iron arc were taken on the same plate with the slit diaphragm in alternate positions. The displacement between the two arcs was then measured using a travelling microscope. Measurements were made for 10 lines. Adjustments to the spectrograph was then made according to an empirical scale derived by S.A.A.O. staff members. After the adjustment was made another plate was exposed and measured in the same fashion to confirm that the correct focus had been achieved.

A standard procedure was followed for each star observed. The star was acquired and centred on the slit. The image rotator was then used to align the trail direction along the slit. During this procedure the slit diaphragm was closed. The outer portions of the slit diaphragm were then opened and the iron arc struck. After $\approx$15s the outer portion of the slit was closed and then the central portion was opened to allow the starlight through.

An exposure meter, which made use of the light otherwise obscured by the plate holder, had been installed immediately prior to the the observing run, but this had not yet been calibrated or fully tested. After some initial problems and after calibration this was used to derive exposure times. After the stellar spectrum had been exposed the slit was again set to the iron arc position and the iron arc exposed for a further 15s to ensure that no movement had taken pace during the exposure of the stellar spectrum.

The non-linear photometric response of the photographic plate requires that a calibration of some form is required. The best method of calibration is the imprinting

on the same plate as the stellar spectrum of a set of sources of known relative intensity dispersed through the same optics as the stellar spectrum. Unfortunately the spectrograph design at S.A.A.O. means this is not possible. Instead a separate spectrograph had to be used for the purposes of calibration.

To reduce the possible errors caused by the use of separate plates all calibration spectra were taken on plates from the same box as the respective stellar spectrum. Plates were split into groups of 3, the outer pair being used for stellar spectra and the centre one cut to provide plates for the two calibration spectra.

An exposure time for the calibration spectrograph was calculated according to the relation

$$t_c = \frac{t_s \times L}{S}$$

where t_c and t_s are the calibration and stellar exposure times respectively, L is the slit length and S is the seeing disc. An appropriate neutral density filter was chosen and the calibration wedge spectrograph used to enable photometric calibration of the stellar spectrum. The calibration wedge spectrum was exposed at roughly the mid point of the stellar spectrum exposure and an hour was allowed to elapse after the exposure of the stellar spectrum before both plates were developed simultaneously in the manner described below.

During the exposure of the stellar spectrum the speed with which the star was trailed along the slit was set such that the slit was traversed in approximately 60s. Manual guiding and reversal of the trail direction at the end of each traverse was required.

A slit width given by a reading of 12 was chosen. This is equivalent to a slit width of 0.1 mm, which corresponds to $\approx 14\mu$ at the plate, or $\approx$ 0.1Å at the dispersion used. This was a compromise between the higher resolution possible with IIIaJ emulsion and making efficient use of the starlight. The slit width projected to the sky was $\approx$ 0".4. To give maximum signal to noise the maximum slit length of 4mm was used, giving spectra of width $\approx$ 1.1mm on the plate.

2.vi *Photographic Procedure*

Photographic spectroscopy by different observers of the same lines in the same stars has often resulted in systematic differences in the measured equivalent widths. The

causes of this problem are not fully understood. Part of the difference may be attributed to the subjective manner in which both the continuum level and line area have often been measured. Other systematic effects arise from the photographic process itself. The following techniques were employed to minimise these effects.

One of the principal problems is caused by adjacency effects. These cause a darkening of the dense region and a lightening of the other at regions of contrasting density. Mitton, 1974, has shown that the effect is more pronounced for narrow rather than broad spectral lines. The measured equivalent widths increase as the density to which the plate is exposed is increased. Plates, therefore, were exposed to a continuum density of $\approx$ 0.5, where possible, using the exposure meter provided to determine the required exposure times.

Good agitation of the developer during the development of the plate is also necessary if adjacency effects are to be minimised. To ensure this was the case a perspex bubble-burst tank was designed by the author and built by the technical staff at the University Observatory, St. Andrews. Both the stellar spectrum and the spectrum from the calibration wedge spectrograph are accomodated for simultaneous development. Bursts of gas were introduced every 15s at the base of the tank and rose through a fine mesh of holes over which the plate were set. The tank was also rocked gently during development to ensure large scale circulation of the developer.

2.vii *The Observations*

Of the seven nights of telescope allocated, bad weather rendered three unuseable for observations. An additional curtailment of the planned observing programme was caused by the necessity to use un-hypersensitised plates. This was due to problems with the plate baking system at S.A.A.O. and made longer exposure times for each star necessary.

These factors meant that, in the main, only one spectrum per star was obtained rather than the planned three. Of the 22 plates obtained only 3 proved to be of unsatisfactory quality. Two were severely underexposed during the calibration of the exposure meter and one plate broke during exposure, presumably due to the stress caused by the curved plate holder. The plates taken included 5 of Sirius. These were taken to serve a number of purposes, first to calibrate the exposure meter at the beginning of each night. A

second purpose was for a later investigation of the accuracy of the reduction and analysis system (see chapter 4) and they also allowed comparison with the data obtained with the Michelson interferometer.

A complete list of the stellar spectra obtained is given in Table 2.iii.

2.vii *Measurement of the Instrumental Profile*

In addition to the stellar plates taken three exposures were made of a cadmium low pressure lamp to determine the instrumental profile of the system. Exposure times of 30s, 2m and 8m were made. Quartz diffusers were inserted in the beam path between the lamp and the slit in a manner similar to that described by Griffin, 1968, to ensure full illumination of the slit and collimator.

It had been hoped to use a laser as the light source for this experiment but this facility was unavailable at S.A.A.O. during the observing run. The cadmium lamp, however, which was kindly lent by members of the Belfast group who were observing at S.A.A.O. at the same time, has lines with low intrinsic widths of $\approx$ 5mÅ (Dufton, 1976). It was thus felt to be an adequate substitute. Calibration wedge specra with exposure times equal to the cadmium exposures were taken and developed in the same way as the stellar spectra. The measurement of the instrumental profile is described in chapter 4.

Table 2.iii

Spectra Obtained By the Author

Plate No. DY(B)	*HD*	*Name*	*MK type*	*Exposure* min.	*Julian Date (mid − exp)* 2443220 +
4061	111123	*β Cru*	*B0 III*	55	4.48
4062	122451	*β Cen*	*B1 II*	30	4.54
4063	149438	*τ Sco*	*B0 V*	100	4.61
4064	48915	*α CMa*	*A1 V*	20	5.26
4065	81188	*κ Vel*	*B2 IV*	100	5.32
4066	109668	*α Mus*	*B3 IV*	110	5.42
4067	111123	*β Cru*	*B0 III*	40	5.49
4068	129056	*α Lup*	*B2 II*	105	5.55
4069	144217	*β Sco*	*B0.5 V*	75	5.63
4070	48915	*α CMa*	*A1 V*	20	6.24
4071	74575	*α Pyx*	*B2 II*	180	6.33
4072	106625	*γ Crv*	*B8 III*	100	6.44
4073	118716	*ε Cen*	*B1 V*	65	6.50
4074	147165	*σ Sco*	*B1 III*	135	6.59
4075	48915	*α CMa*	*A1 V*	20	7.25
4076	79351	*117 Car*	*B2 IV*	140	7.31
4077	110304	*δ Cen*	*A0 III*	70	7.39
4078	116658	*α Vir*	*B1 V*	40	7.44
4079	121263	*ς Cen*	*B2 IV*	90	7.49
4080	132200	*κ Cen*	*B2 V*	135	7.59
4081	48915	*α CMa*	*A1 V*	40	8.25
4082	48915	*α CMa*	*A1 V*	35	9.25

CHAPTER THREE

THE INTERACTIVE DATA REDUCTION AND ANALYSIS SYSTEM :- DESIGN AND IMPLEMENTATION

3.i *Introduction*

The rapid growth of electronic technology and the availability of digital computers have made possible the development of automatic plate scanning and the use of digital image processing techniques for spectral analysis. The equipment and the computer programs developed for the purposes of this project are described in this chapter. The system was developed over the period 1976 - 1979. Since then the STARLINK national facility has become available. Had such a system been available during the course of this project some changes of philosophy would have been possible.

A number of initial constraints on the organisation of the reduction package were decided upon. These were :-

(a) Spectroscopic data from a wide variety of sources and detectors should be capable of being analysed. While for this project the major source of data was from digitised photographic spectra, future analyses of material from electronic detectors such as the I.P.C.S. and data from the I.U.E. satellite were also envisaged.

(b) The system should have the ability to be used in an operator interactive mode. Interactive systems possessa number of advantages over batch processing systems. Principally these are :-

(i) the ability of the user to use his judgement and experience in dealing with complex and marginal data

(ii) batch processing algorithms can only cope with foreseen eventualities. The unforeseen may be scientifically more exciting.

(iii) while developing and utilising software immediate inspection of results can be an efficient and time saving way of debugging programs and directing further effort.

The principal disadvantage of interactive processing is that it introduces a subjective element into the analysis and the treatment of data may vary from one user to another or even within one user's analysis of different data sets. Interactive processing may also involve the the user in a larger amount of time at a computer terminal than would be the case for batch processing. On balance it was felt that the advantages of interactive processing outweighed the disadvantages. Wherever possible, however, an attempt was made to make the system sufficiently flexible for data to be batch processed as an alternative to interactive processing.

(c) Constraint (b) rendered the use of the Univerity's central computer, an IBM 360/44, impossible. This meant that the system had to operate on the NOVA 820 mini-computer within the Observatory building.

3.ii *Hardware*

The peripheral hardware available varied throughout the development of the system. The data reduction system was based on two mini-computers, a Data General NOVA 820 (NOVA) and a Honeywell 316 (H316). Transfer between the two machines could be accomplished by means of a serial link through two CAMAC crates operating at a rate of $\approx 14\ Kbs^{-1}$. The H316 has a memory capacity of 24 KBytes while the NOVA memory fluctuated in size between $\approx$ 32K and $\approx$ 64K Bytes, the variation being caused by a number of faults. (An additional problem of holes in the memory was overcome by the flexibility of FORTH, the programming language used.)

Storage for data and programs was available on either disc or magnetic tape. At the beginning of the project the NOVA supported one 2.5 MByte cartridge disc drive and the H316 a 9-track magnetic tape drive. This was later augmented by the addition of a second cartridge disc drive to the NOVA and a 7 MByte disc drive to the H316.

The data processing was carried out on the NOVA and the principal medium for interactive data processing was a Tektronix 4010 graphics terminal (T4010). Initially one of these terminals was available and this was later increased to two. Additional non-graphic VDUs and a Decwriter printing terminal were also attached to the system. The T4010 has a storage display screen with a resolution of 1024×740 pixels. It also has a cross-hair cursor which can be positioned in two orthogonal directions by the use of

thumb wheels. The T4010s were driven at an I/O rate of 9.6 Kbaud. At a later stage in the project a Hewlett-Packard flat-bed X-Y plotter became available for the production of hard-copy graphical output. Resolution approximately equivalent to that of the T4010 over an area of $\approx 40cm \times 30cm$ was given by the digital-analogue converter.

To enhance the computational speed of the NOVA a floating-point calculating module was interfaced to the NOVA via CAMAC at an intermediate stage in the project.

As well as the data processing functions the system was also used for the control of devices and the acquisition of data. Both a microdensitometer and a two-channel photometer were interfaced to either of the two computers by CAMAC modules.

A schematic representation of the hardware configuration as it was at the end of the project is shown in figure 3.1.

3.iii *Programming Language and Operating System*

The programming language used throughout this project was FORTH (Moore and Rather, 1974). This language was written primarily for the purposes of machine control by mini-computers and was originally obtained under an SRC grant to evaluate its suitability for use in the mini-computers at the Northern Hemisphere Observatory (as it was then called). FORTH proved to be extremely flexible and versatile and an extension of its use to the data reduction and analysis software showed immediate promise. FORTH is becoming more widespread amongst the astronomical community but it is not yet as familiar to most astronomers as FORTRAN. Therefore, a brief description of the language and the advantages which made it suitable for use in this project will be given here.

To perform a task using FORTH the programmer must develop a 'dictionary' of 'words'. Each word is a compound of previously defined words which perform simpler sub-tasks necessary for the execution of the main task.

This structure has several advantages when implemented on a mini-computer. Of principal importance is the efficiency with which core memory can be used. The dictionary need only contain the words necessary for the task under consideration and so redundancy can be cut down. This saving of core space enabled the NOVA to be multi-programmed. Each user is allocated some fraction of the total core space. Simple operations can be performed in a very small partition. In practice, however, the number of simultaneous

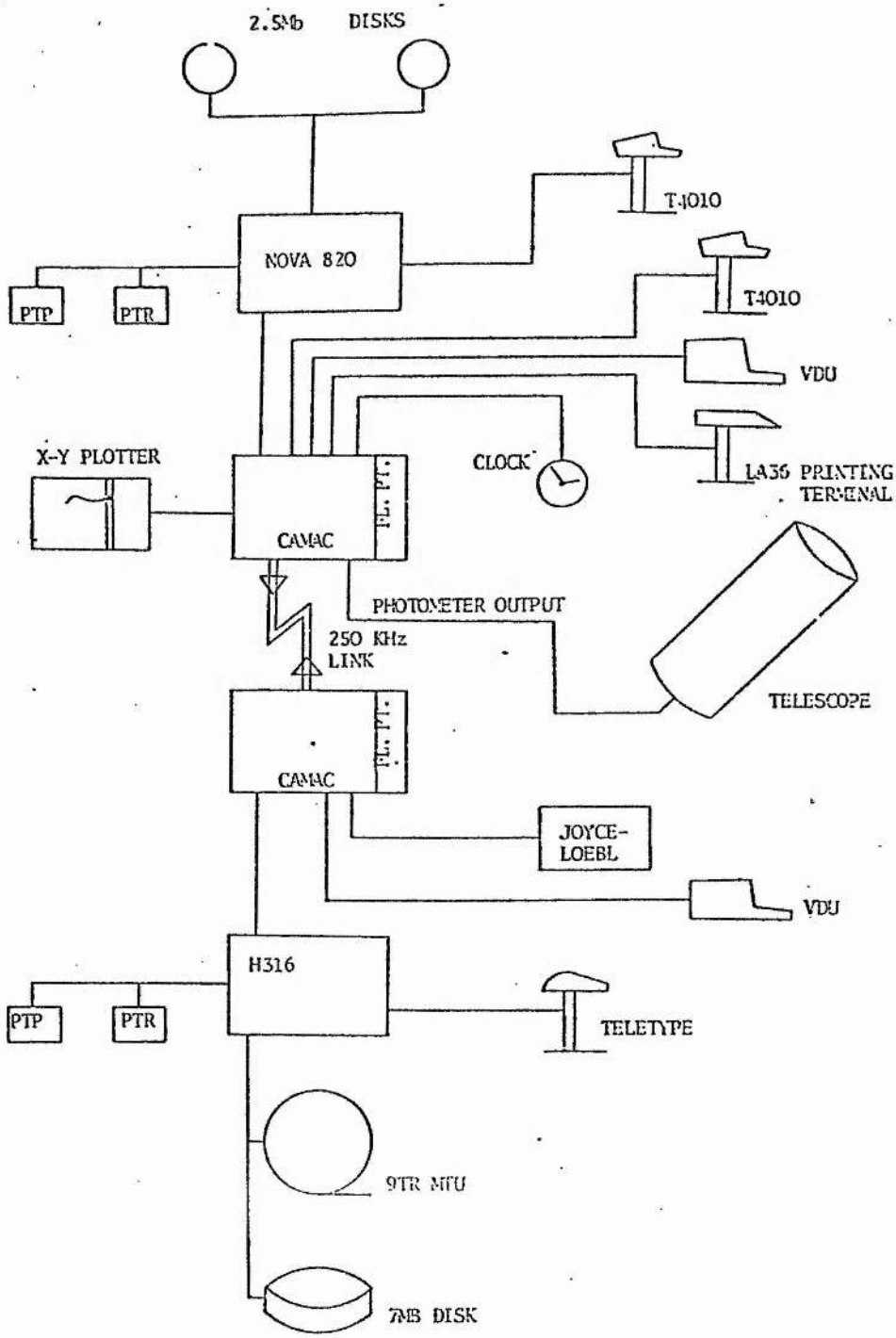

Fig. 3.1 :- Schematic illustration of the hardware configuration during the latter stages of this project.

users was limited to 4. Another advantage is gained by the self-contained nature of a word. Words can be written and tested in convenient stages, greatly decreasing the time required for program development and making the detection and correction of programming errors faster and simpler.

Interactive analysis is also enhanced by the use of FORTH. FORTH is both operating system and programming language. This means that at any time FORTH is running in the computer all words in the current dictionary are accessible and, unlike FORTRAN, the sequence of operations is not fixed. The astronomer, therefore, can be much more flexible in his approach to the analysis of his data. Communication of parameters between operations is also much simpler.

FORTH also has the advantage of a virtual memory system, a facility not then available on mini-computers with real-time operating systems and still only available in a cumbersome form with only a few operating systems. An area of core memory is used as buffer storage into which data from disc is automatically transferred when needed. This feature is another means by which efficiency in core-space is achieved.

Ease of access to the computer instruction assembler level is also a feature of FORTH. This enables the non-specialist programmer to write machine control programs without the difficulties normally associated with this type of programming.

3.iv *The Microdensitometer*

Most of the data analysed for this project was obtained by scanning photographic plates with the Joyce-Loebl mark IIIc microdensitometer interfaced to the NOVA via CAMAC. The conversion of this machine to computer control is described in Van Breda*etal*, 1974. Stepping motors have been fitted to both the X and Y movements of the carriage, giving a range of movement of $\approx 15cm \times 7cm$. The step size in the X direction can be varied from 1.5μ to 15μ by the use of different gears. During this project a unit stepsize of 5μ was used. Pulses are sent to the motors from a delayed pulse generator in CAMAC at intervals of larger than about 15ms. This time interval ensures that the motors have completed their movement prior to the arrival of the next pulse.

An initial problem was the acceptance by the motors of spurious pulses caused by electrical pick-up on the transmission lines. To alleviate this effect, the transmission

cable was shielded and the motors were disabled immediately after, and enabled only immediately before, a pulse was sent. An additional precaution was the comparison of the measured phase of the motors with their logical phases. Any discrepancy between the two phases was output to the computer terminal. Scans with such effects were rejected.

Density measurement is by a null-balancing technique. A servo-motor alters the position of a wedge with a linear density gradient. The position of the wedge is encoded to 1024 quantised steps. Repeated sampling of the wedge position at intervals of 15.4ms until two consecutive measurements are identical is undertaken to ensure the wedge has settled, before the density value is accepted by the computer and stored on disc.

3.v *Software*

Analysis of astronomical spectra by computer can be divided roughly into three phases. These phases are:-

(i) Acquisition:- the spectrum must be converted into a digital image suitable for computer analysis

(ii) Processing:- the digital image must be converted into a form in which astrophysical measurements can be made. The degradations caused by the detection and acquisition processes must be corrected to ensure the data is in a format in which photometric measurements can be made.

(iii) Analysis:- quantities required for the astrophysical analysis must be extracted from the processed data and it must be possible to input theoretical models for comparison with the observed data.

The reduction package described here incorporates computer programs to cover all three stages. In addition to the routines specifically applicable to the reduction and analysis of stellar spectra a number of contributions to the basic system software were made by the author. The basic system underwent a process of continual development during this period, principally under the auspices of Mr. R. Stapleton, the systems programmer. Mr. P. Bunclark, who was developing a surface photometry package, and Dr. P. W. Hill also made contributions. Many of the improvements were made by a process of collaboration, and I gratefully acknowledge fruitful discussions with the other FORTH users. Credit for major contributions by them is given in the relevant place and

unless otherwise stated the work described below is that of the author.

In addition to programs which perform a function specific to one of the three phases discussed above a number of routines were used throughout the package. These included plotting and interpolation routines.

The initial plotting routines provided allowed for the drawing of orthogonal axes, setting the range and size of the plot in either dimension and drawing solid or dashed vectors between points on the T4010.

A major modification made by the group was the introduction of arbitrary plotting. This allowed the plotting of any defined function or data set using the X-axis as an index. Additional improvements made by the author to the plotting routines included introducing the facility to enlarge a selected section of an already displayed plot by delineating opposite corners of a rectangle using the T4010 cursor. Automatic scaling made maximum use of the screen resolution. The introduction of a split screen facility by Mr. R. Stapleton was also found useful. This allowed the simultaneous display and comparison of two spectra in the top and bottom halves of the display.

Throughout the package some form of interpolation was often needed. Use was made of linear, polynomial, fourier and cubic spline interpolation at various points in the system. All these routines were written by the author.

(a) Linear interpolation : this is a simple routine to find $F(x)$ given x_1, x_2 and $F(x_1)$, $F(x_2)$, i.e.

$$F(x) = F(x_1) + \frac{(x - x_1)}{(x_2 - x_1)}(F(x_2) - F(x_1))$$

It was often used to interpolate between adjacent data points.

(b) Polynomial interpolation : This involved two routines. The first procedure calculates a best fitting polynomial of order n to an input array of points by the method of least squares. A maximum permitted order, N, is chosen by the user. The algorithm used was a modified version of that in the FORTRAN N.A.G. library. The second routine calculates the value of the polynomial using a recursive technique.

(c) Fourier interpolation : This was used to expand a data set by interpolating additional data points at regularly spaced intervals. The fourier transform of the data is calculated using the routine described in a later section. Additional points with an

amplitude (and phase) of zero are added to the transform at frequencies above the Nyquist frequency of the original data set and the inverse transform taken. By adding a number of new points equal to the number in the original transform one point is interpolated for each point in the data set, by making the transform 4 times as large, 3 data points are inserted and so on, in powers of two.

(d) Cubic Spline interpolation : the use of this form of interpolation for smoothly varying curves has been shown to be accurate and efficient when coded for digital computers (Birkhoff and de Boor, 1965). The cubic spline is a generalisation of Lagrange's formula of polynomial interpolation. The algorithm used was taken from a FORTRAN program in use at the D.A.O. (Hill, 1982).

A set of co-ordinate pairs (x_i, y_i) known as knots, through which the spline fit is forced are chosen. The interpolated value, $y = F(x)$ for $x_n \leq x < x_{n+1}$ is then given by

$$y = y_n\left[2\frac{(x_n - x)}{(x_n - x_{n+1})} + 1\right]\left[\frac{(x - x_{n+1})}{(x_n - x_{n+1})}\right]^2 + y_{n+1}\left[2\frac{(x - x_{n+1})}{(x_n - x_{n+1})} + 1\right]\left[\frac{(x_n - x)}{(x_n - x_{n+1})}\right]^2$$

$$+(x - x_{n+1})\left[\frac{(y_{n+2} - y_n)}{(x_{n+2} - x_n)}\right]\left[\frac{(x_n - x)}{(x_n - x_{n+1})}\right]^2 + (x - x_n)\left[\frac{(y_{n+1} - y_{n-1})}{(x_{n+1} - x_{n-1})}\right]\left[\frac{(x - x_{n+1})}{(x_n - x_{n+1})}\right]^2$$

Knots are stored in an array on disc. Interpolation between the first and last pair of knots is by the linear method. In practice the end pairs of knots were chosen to have similar x values.

Data Aquisition and Storage

The package was written primarily for the reduction and analysis of data obtained from photographic spectra scanned with the Joyce-Loebl microdensitometer. The design requirement of the system, that data from a number of sources should be capable of being analysed, was achieved by the method of data storage adopted.

A number of software interfaces were written to convert data to scaled 16-bit integers. A scale factor of 1000, giving an accuracy of 0.1% , and a dynamic range of $\pm 3.2 \times 10^4$ was found to be suitable for A.A.T., I.U.E., and Michelson interferometer data as well as the digitised photographic spectra. Data is stored on the disc in blocks of 512 points and once stored in this form data from different sources is not distinguished by

the analysis and reduction programs. The used of scaled integer format storage both saved disc storage space and allowed the use of integer arithmetic for many operations, giving a great gain in speed. If floating point arithmetic was necessary the use of conversion and scaling routines written in assembler code did not greatly increase the execution time of the programs.

Several programs to scan specific types of plate material were developed. These included programs to make a number of parallel horizontal or vertical scans at arbitrary specified separations on the plate. These could be used for scanning the stellar spectrum, iron arc spectra and clear plate levels on a single plate, or for the successive scanning of several stellar and arc spectra on the same plate. These programs were also used to scan the calibration wedge spectra at different wavelengths. A program to scan plates on which sensitometer calibration spots have been imposed was also developed.

Image Processing

Photometric Calibration

A major problem in photographic spectrophotometry is the photometric distortion of the image caused by the non-linear response of the emulsion to different intensities of incident light.

A calibration between incident intensity and photographic density is required to remove this distortion. The well known characteristic (or H.D.) curve was rejected for the purposes of this project as not being well suited to digital analysis. Some form of polynomial representation of the H.D. curve would have been required and if the variation of the curve with wavelength was also to be represented a cumbersome method of interpolating between polynomials would have had to be used.

Baker, 1925, proposed a transformation of the H.D. curve. This was subsequently ignored by photographic spectrophotometrists but readvocated for use in photographic studies of the surface brightness distribution of galaxies by De Vaucouleurs, 1968.

This transformation gives a linear relationship of the form

$$\log I = n \log \omega + \log A$$

where I is the incident intensity, and ω is the Baker density which is related to the

photographic density, D, by

$$\omega = 10^D - 1$$

Of the two constants, n and A, the latter can be set to one (effectively ignored) if the data are to be normalised to the continuum at a later stage. The calibration from density to intensity can thus be made with only one free parameter. Interpolation of the variation with wavelength is then straightforward.

The values of n were obtained interactively using scans of either the sensitometer spots or from the calibration wedge spectra. The procedure described here is that used for the latter, the determination from sensitometer spots being essentially identical.

A scan of the calibration wedge is first displayed on the T4010 screen. Using the cross-hair cursor regions of the plate background and each of the wedge steps free from any plate defect are selected (figure 3.2). The program calculates average density values for each of these regions and subtracts that for the plate background from those obtained for each of the wedge steps. Log ω values are then calculated and stored in an array on disc in which the respective values of log I have already been stored. Values of the constants n and A are then calculated using a linear least squares technique developed in collaboration with Mr. P. Bunclark. The data values and solution are displayed on the T4010 screen for appraisal. Any curvature or wedge step which deviates from the solution is apparent and the scan re-examined or that step omitted from the determination and the solution re-calculated. The entire procedure takes less than 30 seconds to complete and is repeated at each different wavelength at which the calibration wedge has been scanned.

Having calculated an array of n, λ pairs and stored them on the disc it is then necessary to convert the scan of the spectrum into relative intensity units.

The plate background is subtracted from each scan point and a value of $\log\omega$ calculated by this program. The appropriate value of n is interpolated from the stored table using spline interpolation. This is used to convert the value of ω to intensity units and the resultant value is scaled and stored in a new spectral array.

Normalisation of the spectrum to the continuum level is the next stage in the photometric correction process. Again the interactive capability of the system is useful.

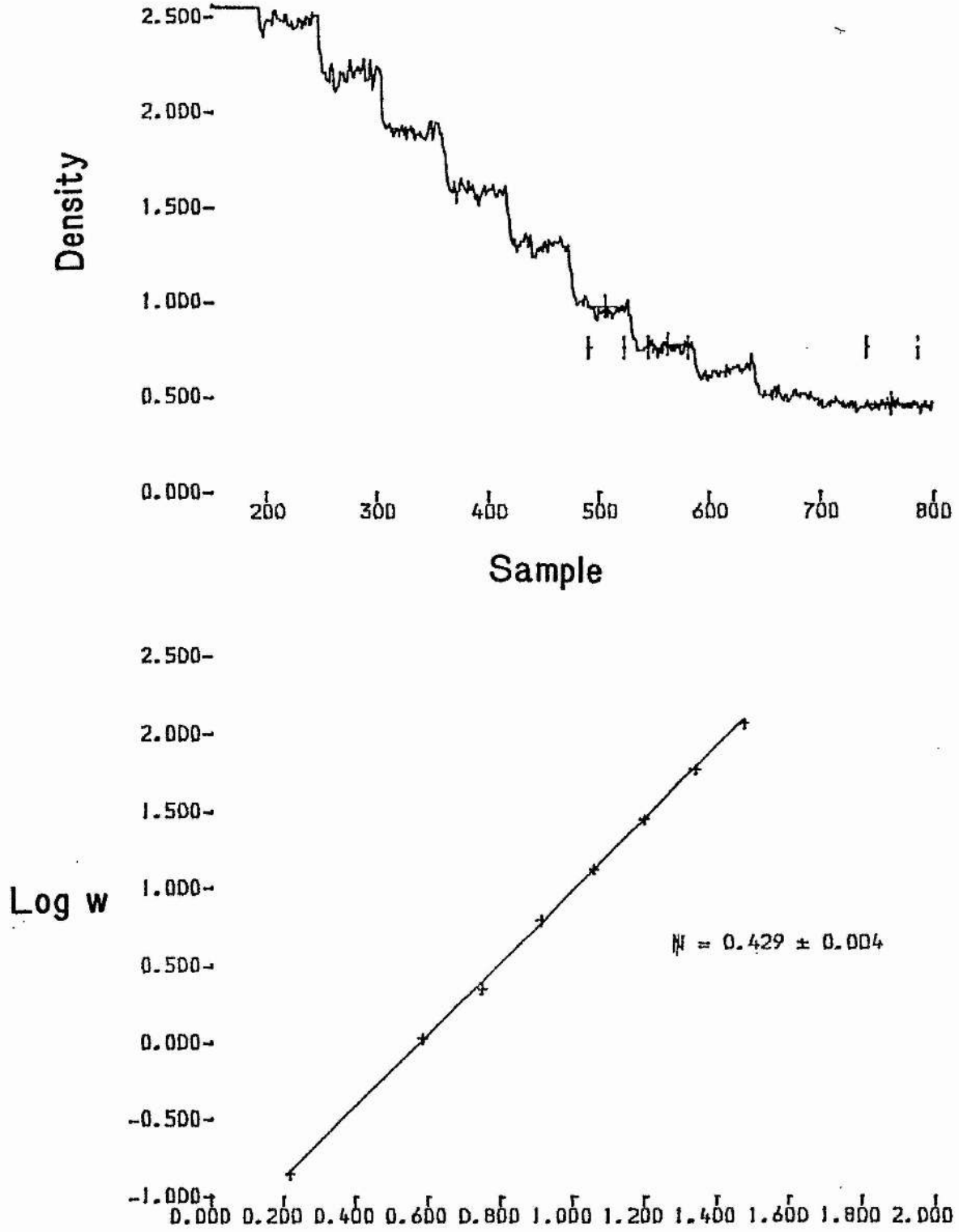

Fig. 3.2 :- **Upper: Display of a Joyce-Loebl scan of a density wedge showing averaging over steps.**

Lower: Least squares fit to find Baker density calibration constant n.

The intensity spectrum is displayed on the T4010 screen for the user to select points to represent the continuum. Two methods of selection are possible. In regions of spectrum devoid of lines the cursor is used to delimit a region over which an average intensity is calculated. Clearly this method is not suitable if the intensity is varying rapidly with wavelength. As an alternative the cursor can be used to identify a position to represent the continuum. In both cases the x position and intensity are stored in an array on the disc. For the spectra measured here the selection of points at approximately 25Å intervals gave reasonable results.

By interpolating between the selected points using the spline interpolation routine the entire continuum is generated. This is displayed superimposed on the stellar spectrum. Additional points can be inserted, or some of those previously selected rejected, until a continuum deemed satisfactory is found. Each point in the spectrum is then divided by the value of the continuum interpolated at that point, rescaled and the new normalised spectrum stored in another array on the computer disc.

Geometric Calibration

In addition to photometric distortion caused by the detector the non-linearity of the dispersive system and/or the detector means that geometric distortion may sometimes require correction.

Before the correction can be made it is necessary to calibrate the positions in the scan against wavelength. In the package provision was made for either an absolute calibration using the iron-arc comparison spectra, or a relative calibration using features in the stellar spectrum. In both cases the interactive capabilities of the system are used. Here the procedure for the use of iron-arc lines is described. That for features in the stellar spectrum is similar.

The arc spectrum is first displayed on the the T4010 screen. The cursor is used to select a region of the spectrum containing an arc line of known wavelength and not strongly affected by blending with other arc lines. The program then calculates the x position of the line centre. A number of algorithms for this procedure were experimented with. Initially simply the position of the line maximum, $x(I_m)$, was used. This proved to be rather sensitive to noise and sampling error. The next method tried involved calculating

the intensity weighted mean position, $\bar{x}$, where

$$\bar{x} = \frac{\sum_{x(I_m)-4}^{x(I_m)+4} (I_j x_j)}{\sum_{x(I_m)-4}^{x(I_m)+4} I(j)}$$

Finally an algorithm which fitted a parabola to the region $(x(I_m)-4) \leq x \leq (x(I_m)+4)$ was tried. Both of these latter methods gave results which were repeatable upon rescanning the plate and which were in agreement with each other to within $\approx \frac{1}{5}$ pixel. The intensity weighted mean position was finally selected as the method to be used throughout the analysis of the spectra because it was the faster to execute.

Corresponding wavelengths for each arc-line are entered as each line centre is measured. In practice it was found that measurements of between 20 and 25 lines roughly evenly spaced over the spectral range were required. The (x, λ) pairs are stored in an array on disc.

Two routines based on the spline interpolation routine were written to enable conversion between the two co-ordinate systems to be made. By comparing the predicted and observed positions of a number of arc lines not included in the calibration an estimate of the accuracy of the calibration could be made. Conservatively, the maximum deviation was less than a pixel and in general an accuracy of better than $\frac{1}{2}$ pixel was found.

An additional routine written for the purposes of the geometric calibration correction of spectra was based on the 'scrunch' routine of the SDRSYS package of the Anglo-Australian Observatory. This linearises the dispersion of the spectrum. It was not used in the analyses made for this project as the spectra were normalised to the continuum level and the deviations from linearity over a spectral line are negligible.

Fourier techniques

The ability to work in the Fourier frequency domain gives several advantages in the analysis of spectra. The simple convolution or deconvolution of the instrumental profile, the reduction of noise and the measurement of spectral displacement by means of the cross-correlation function are then possible. In addition it has been shown that the different line broadening mechanisms described in chapter 1 of this thesis can more readily be distinguished in the power spectrum than in the wavelength domain (e.g. Gray

and Smith, 1976). A number of routines were included in the package to perform some of these functions.

A program to calculate the numerical fourier transform

$$\sigma_k = \sum_{j=0}^{N-1} I(j) e^{\pm 2\pi i j k / N}$$

was translated into FORTH from a FORTRAN routine (Brenner, 1968) based on the Cooley-Tukey fast fourier transform (FFT) algorithm. This routine requires a data set of N equally spaced samples where N is an integer power of 2. (An alternative routine was later developed by Mr. P. Bunclark based on the Singleton algorithm. This could handle multi-dimensional data sets. The size of each dimension of the data set was limited only by the requirement that it be expressable as the product of at most 20 prime factors, the largest of which was less than 19). The computation time of the routine developed by the author varies as $3N \ln N$ and for a data set of 512 points was approximately 20 seconds.

The spectrograph and measurement techniques degrade the incident spectrum, $I(\lambda)$, by convolving it with the instrumental profile, $P(\lambda)$, to give the recorded spectrum, $D(\lambda)$, i.e.

$$D(\lambda) = I(\lambda) \otimes P(\lambda)$$

If the fourier transforms of $D(\lambda), I(\lambda)$ and $P(\lambda)$ are $d(\sigma), i(\sigma)$ and $p(\sigma)$ respectively then

$$d(\sigma) = i(\sigma) \times p(\sigma)$$

In the absence of noise the incident spectrum can be recovered if the instrumental profile is known by finding

$$i(\sigma) = \frac{d(\sigma)}{p(\sigma)}$$

and taking the fourier transform of $i(\sigma)$ to obtain $I(\lambda)$. For real data, however, noise prevents the satisfactory execution of this restoration.

At high frequencies $p(\sigma) \mapsto 0$ while in the presence of white noise $d_1(\sigma) \mapsto c$, a constant. Thus $d_1(\sigma)/p(\sigma) \mapsto \infty$ at high frequencies, where the true $i(\sigma) \mapsto 0$. To

counteract this effect a high frequency filter can be used. Brault and White, 1971, have shown that there exists a filter function which minimises the difference between the true transform, $i(\sigma)$, and the filtered deconvolved transform, $i_1(\sigma)$. This filter, which they descibe as 'the optimum filter' is given by $\phi(\sigma)$ where

$$\phi(\sigma) = \frac{1}{1 + (n(\sigma)/d(\sigma))^2} \qquad 3A$$

and $n(\sigma)$ is the fourier spectrum of the noise in the data.

As only $d_1(\sigma) = d(\sigma) + n(\sigma)$ is known, some assumptions must be made to determine $\phi(\sigma)$. Again the interactive capability of the system proved useful. By plotting $d_1(\sigma)$ and experimenting with various functional forms it was possible to derive expressions for $d(\sigma)$ and $n(\sigma)$. At high frequencies $n(\sigma)$ dominates $d_1(\sigma)$ while at low frequencies $d(\sigma)$ dominates. Examination of $d_1(\sigma)$ suggested that $n(\sigma) = \beta$, a constant, was an adequate representation of the noise spectrum, implying that only *white noise* was present in the data. In addition, experimentation showed that assuming

$$d(\sigma) = d_1(0)10^{-\alpha^2\sigma^2}$$

a convenient analytic form, gave an acceptable estimate for $d(\sigma)$.

A program was written to find values of α and β interactively. A spectrum partially corrected for the degradation of the instrumental profile could then be obtained by using a program which calculated

$$\frac{d_1(k) \times \phi(k)}{p(k)}$$

for all frequencies, k, in the fourier transform and then calculating the inverse FFT.

Figure 3.3 illustrates the processes involved in the calculation of a deconvolved and noise filtered spectrum. Clearly, the extent to which the instrumental profile can be removed is dependent upon the frequency at which the the noise filter begins to have an effect. This, in turn, depends on the signal to noise ratio in the data. From equation (3A) it can be seen that the frequency at which $\phi(\sigma) = 0.5$ is given by

$$\sigma_{\frac{1}{2}} = \sqrt{\alpha^{-2} \log\left(\frac{\beta}{d(0)}\right)}$$

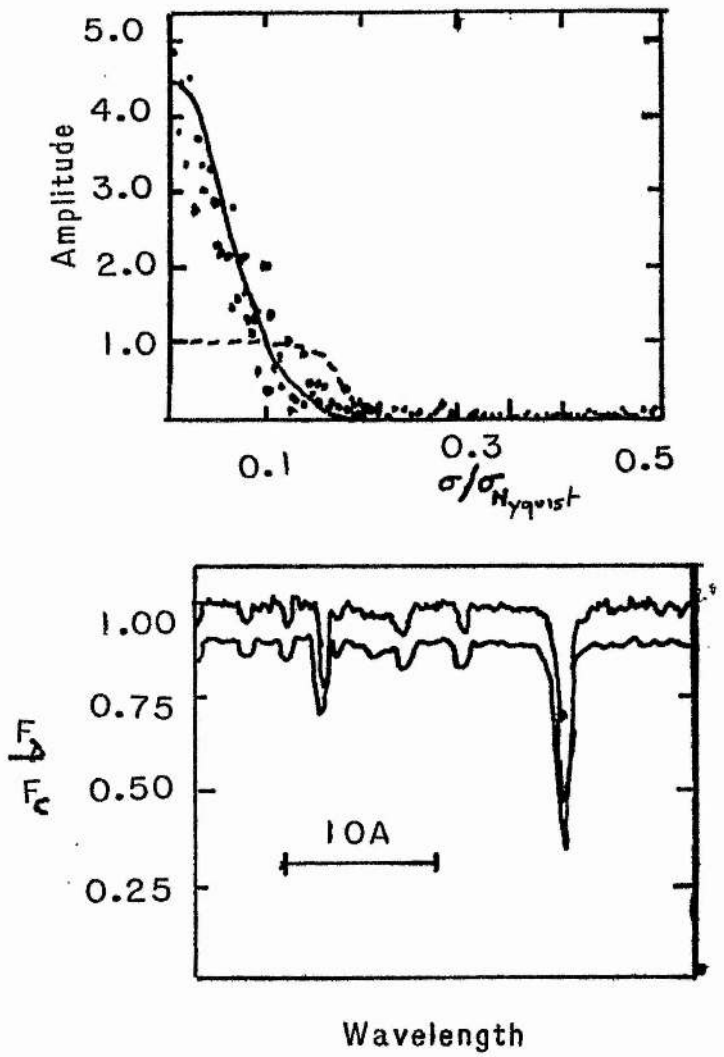

Fig. 3.3 :-

Upper: Illustration of the fitting procedure used to define the optimum filter as disussed in the text. Dots show the data, the solid line the gaussian approximation to the data and the dashed line the derived filter function.

Lower: Comparison of the data before and after application of the filter.

As $d(0)$ represents the total signal in the data and β represents the noise level, in principle an estimate of $\sigma_{\frac{1}{2}}$ can be derived *a priori* from the data. This, however, is difficult to calculate in practice. After some trials with real data sets in which problems were found in substantially removing the instrumental profile a numerical experiment was conducted. This was done in order to determine what degree of success could be achieved in removing the instrumental profile at various values of the $S : N$ ratio. The results of this experiment, which are discussed in chapter 4, were not encouraging. For this reason the modelling approach was adopted in the analyses programs. That is, rather than deconvolving the observed spectrum before a comparison with the theoretical models was made, the theoretical models were convolved with the instrumental profile and compared with the data as detected.

Another use for the fourier transform of the spectra was the calculation of the cross-correlation function. This function can be used to accurately measure relative shifts between different spectra of the same star and to measure the radial velocities of stars relative to standard stars of similar spectral types (Simkin, 1974, Da Costa *et al*, 1977).

The cross-correlation function (CCF) is defined by

$$c(\Delta) = \sum_k \tilde{s}_1(k)\tilde{s}_2(-k)e^{i2\pi k\Delta/N}$$

where $\tilde{s}_1$ and $\tilde{s}_2$ are the FFTs of spectra S_1 and S_2 respectively. The CCF has a maximum at Δ_{max} when Δ_{max} is equal to the shift between the two spectra. If the two spectra have been derived as functions of $\log\lambda$ then

$$\Delta_{max} = \log\left[1 + \frac{v}{c}\right]$$

where v is the velocity difference between the two stars and c is the velocity of light.

Routines to perform the following procedures were developed in conjunction with Mr. P. Bunclark and rationalised and improved by Mr. B. McLean.

First, sections of the arc spectra on either side of the stellar spectrum are fourier transformed and the CCF calculated. This is displayed on the T4010 screen and the region of the peak selected with the cross-hair cursor. The CCF over this region is numerically differentiated and the result plotted on the T4010 screen. The value of Δ at which the

differential equals zero is found by linear interpolation. If $\Delta y \neq 0.0$ then the plate has not been scanned parallel to the direction of dispersion or some slip between the scans has occurred. In this case the scan is rejected.

Secondly, the CCF of one comparison arc spectrum of each of the program star and the standard star is calculated. The value of Δ_{max} is found as above. From this value the zero point of the stellar spectrum scan can be found and the stellar spectrum converted into $\log\lambda$ format. The stellar spectrum is extended to twice the number of sample points by adding further points at the continuum level (=0), this having been done to the standard star spectrum before it was fourier transformed. (This procedure reduces end point problems associated with circular CCFs.) The FFT of the stellar spectrum is calculated and the CCF with that of the FFT of the standard star spectrum, which has previously been calculated and stored, is found. After finding the Δ_{max} of this CCF the radial velocity of the programme star relative to the standard star is calculated from the relationship

$$v = c\left[10^{\Delta_{max}} - 1\right]$$

Other Routines

A number of other routines were written to perform simple arithmetic operations on selected regions of spectra. Sections of two spectra could be added to, subtracted from, multiplied by or divided by each other. An arbitrary shift between the two spectra was incorporated in the routine and the two spectra could be weighted by optional amounts. For example, in the case of addition of two spectra, then if S_1 and S_2 are the two original spectra and S_3 the resultant then

$$S_3(x) = \frac{AS_1(x) + BS_2(x + \Delta x)}{A + B}$$

where A, B and Δx are set by the user. Scalar arithmetic operations on individual spectra are also possible.

These functions were incorporated to allow the comparison of spectra of the same object, and to allow the summation of these spectra to increase the $S : N$ ratio prior to analysis.

Before this is done checks should be made to ensure that no variations not attributable to noise are present in the data sets. This can be done by the subtraction or division of the data sets. A fourier transform of the residuals should then be equivalent to that of white noise if no systematic difference between the two data sets exists.

Another routine which reduces the noise level in the data, at the expense of the resolution, was also included in the package. This calculates a weighted running mean of the form

$$I^*(x) = \sum_{j=x-n}^{x+n} w(j)I(j)$$

where $\sum w(j) = 1$. The value of n is chosen by the user and the shape of the weighting function is triangular.

This is not a very satisfactory method of noise removal - a similar result can be achieved by using a larger slit on the micro-densitometer or on the spectrograph - and it is not recommended except for regions of the spectrum where only low frequency information is present, such as the continuum and wings of Balmer line profiles.

Analysis Software

After the data have been processed to a suitable form it is possible to compare the data with theoretical models. Ideally, the entire data set would be compared with the output of a spectral synthesis model and the parameters of the model adjusted until an acceptable fit to the data was achieved. This is not yet possible and an intermediate stage of extracting parameters which describe the observations and can be compared with predictions of the same parameters made by the models must be used.

For this study a number of parameters which describe absorption lines were selected. These were:-

(1) central wavelength — λ_0

(2) equivalent width — W

(3) central depth — $1 - R_0$

(4) full width at 1/4 central depth $-W_{\frac{1}{4}}$

(5) full width at 1/2 central depth $-W_{\frac{1}{2}}$

(6) full width at 3/4 central depth $-W_{\frac{3}{4}}$

These can be determined interactively for a number of lines in each spectrum in the following manner. The results are stored in a catalogue on disc for later printing, examination and comparison with the model predictions.

A section of spectrum is displayed on the T4010 screen. The user then identifies the local continuum level and the red and blue wavelength limits to an absorption line using the cross-hair cursor. The program then fits a parabola to the four central deepest samples in the line profile. From this parabolic fit the central depth and central wavelength are calculated using the previously determined wavelength calibration. Integration of the area between the wavelength limits is carried out by the program using Simpson's rule. This is subtracted from the area under the continuum and the equivalent width calculated using the dispersion at the central wavelength of the line to convert W into wavelength units. Values of $\frac{1}{4}(1-R_0)$, $\frac{1}{2}(1-R_0)$ and $\frac{3}{4}(1-R_0)$ are calculated. Linear interpolation between the data points is used to determine the wavelengths at which these intensities are attained and hence values of $W_{\frac{1}{4}}$, $W_{\frac{1}{2}}$ and $W_{\frac{3}{4}}$ are found. All the parameters are then stored in the catalogue and the counter which indexes the catalogue incremented by one. For a typical line the procedure takes a fraction of a second to execute.

An alternative procedure was introduced to extract parameters from blended lines but this could also be used for unblended lines. This procedure makes use of the function

$$F(x) = \frac{I_0}{\left[1 + \left(2^{a^2} - 1\right)\left(\frac{2(x-X_0)}{W_{\frac{1}{2}}}\right)^2\right]^{\frac{1}{a^2}}} \qquad 3B$$

where $0 < a < \sqrt{2}$, Fraser and Suzuki, 1970. This function varies between a Gaussian ($a \mapsto 0.0$) and a Lorentzian (a=1) and has some similarities to a Voigt profile.

Initial estimates for I_0, X_0, $W_{\frac{1}{2}}$ and a are made for each line in the blend. The overall intensity profile of the blend is calculated and superimposed on the display of the spectrum. The parameters are varied until the quantity $\sum (I_{calc} - I_{obs})^2$ is minimised or an acceptable fit achieved. Up to five lines can be included in the blend, although only rarely were blends of three or more lines analysed.

After a spectrum has been measured it is possible to enter other parameters for each line into the catalogue. These could be, for example, the excitation energy, $\log gf$

or simply an ion identification number. Trends of one parameter with another can be investigated using a program which accepts index numbers of the parameters to be be compared, has switches to allow the logarithms of the parameters to be used in the comparison and plots the data on the T4010 screen, having automatically selected and scaled the axes if desired.

CHAPTER FOUR

THE INTERACTIVE DATA REDUCTION AND ANALYSIS SYSTEM :- ACCURACY AND PERFORMANCE

4.i *Introduction*

In any analysis programme such as that described here it is important that the ability of the reduction system and the size of the errors involved are both well understood. Any astrophysical results can then be interpreted with a known degree of confidence. This chapter contains a discussion of several sources of error in photographic spectrophotometry and the methods used to obtain quantitative measures of their magnitudes. Digital analysis techniques such as those used in this project can provide more definitive, and possibly more accurate, results than some of the techniques used in the past. Previous studies have often presented results with only a qualitative statement about the possible errors. In the case of equivalent width measurements these can be of the order of 50%, (e.g. Wright, 1966)

Two categories of error may be delimited by their effects on line profile and equivalent width measurements: random errors and systematic errors. A systematic error in the measurement of the line profile need not give rise to an error in the derived equivalent width. For example an error arising in the correction for the instrumental profile does not influence the equivalent width obtained. Any systematic error found in the equivalent widths, however, must have arisen from a systematic error in the line profile. Systematic errors can be introduced during the detection, measurement, calibration or analysis processes. Random errors, such as noise, will, in general, only arise during detection and measurement.

4.ii *Detection Process Errors*

The major errors, apart from noise, which are introduced by the telescope and spectrograph combination are the instrumental profile (including ghosts) and scattered

light. The photographic process can also introduce the errors discussed in chapter 2.

Instrumental Profile

Using the same scanning programs and settings as those used for the stellar spectra the plates of the cadmium source taken at S.A.A.O. were measured. The scans were converted to logarithmic relative intensity units using the density-intensity calibration obtained from the wedge spectra. Profiles of individual lines were plotted on tracing paper by hand (as the graph plotter had not yet been incorporated into the system). Visual inspection of the lines showed no detectable variation with wavelength. The techniques of Griffin, 1968, were then used to superimpose the profiles of the lines from the differently exposed plates and different wavelengths. This resulted in the composite profile illustrated in figure 4.1 which extends to $\approx 0.1\%$ of the central intensity.

A full width at half maximum intensity (FWHM) of $31 \pm 1\mu$ is measured for the composite profile. This value may be compared with the values found by Blades and Powell, 1976, for a study of the same spectrograph. In their study the alternative grating was used and the light source was a red laser. Interpolation in their table to the value of slit setting used here (12) gives a FWHM of $29 \pm 1\mu$. The difference in the natural FWHMs of the two light sources at this dispersion is equivalent to $< 2\mu$ (Dufton, 1976) and the different emulsion used may also contribute.

At the dispersion used here the FWHM gives a resolution of 0.208Å which corresponds well to the value of the spectral purity of 0.211Å calculated from

$$\Delta\lambda = \cos\alpha \frac{w}{f} \frac{d}{n}$$

where w is the slit-width, d the grating line spacing, f the focal length of the collimator, α is the angle of incidence and n is the spectral order used.

Evidence for the existence of a weak ghost line was found for one grossly overexposed cadmium line. Unfortunately this line could not be fitted into the composite instrumental profile. An upper limit of 0.05% of the central intensity can be placed, however, upon the ghost intensity, in agreement with the original specification for the grating.

The shape of the instrumental profile was found to be gaussian with extended wings. Using the fitting function (equation (3B)) with $a = 0.6$ gave the excellent agreement with the observed instrumental profile shown in figure 4.2.

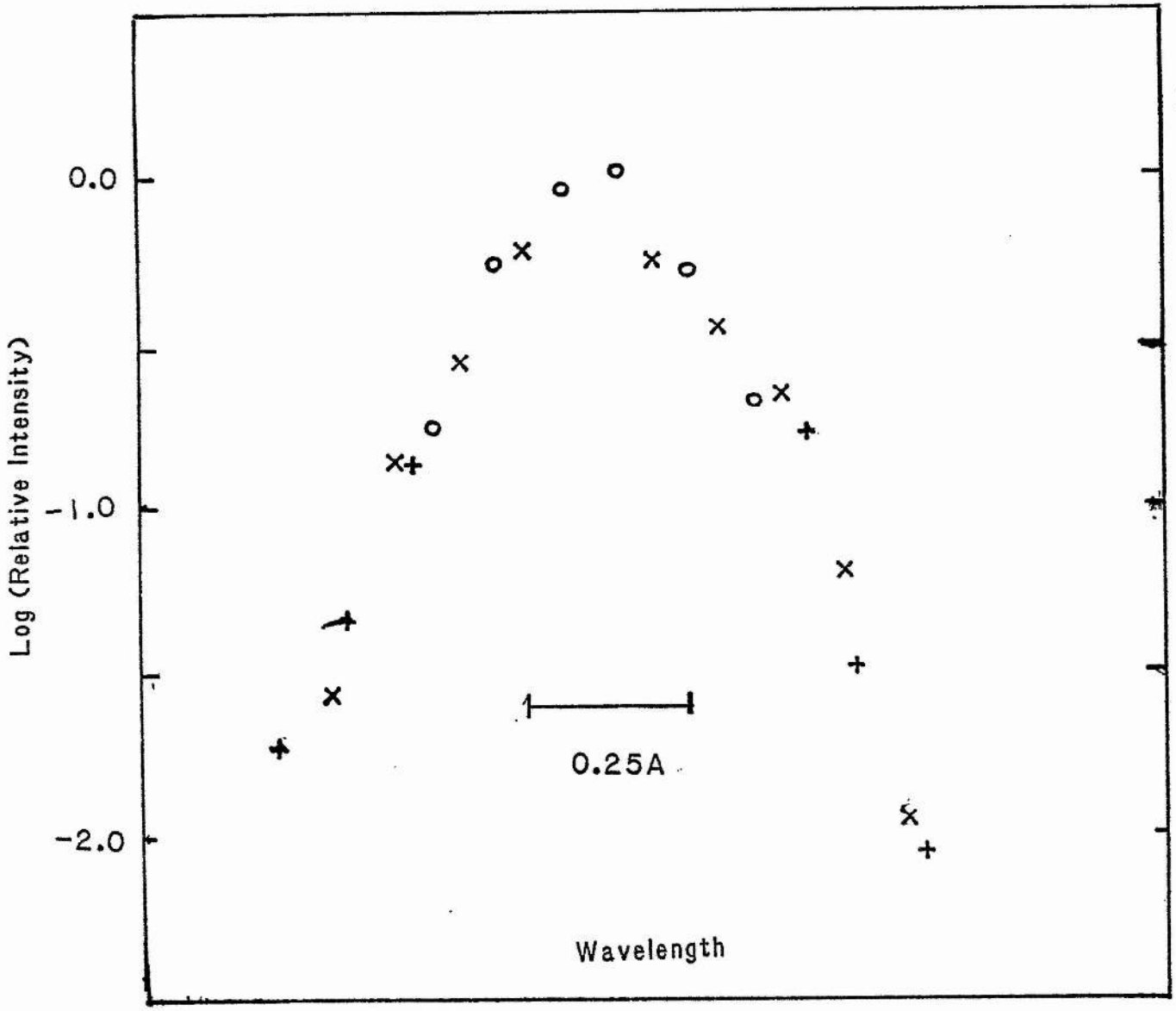

Fig. 4.1 :- **Composite instrumental profile obtained from the superposition of different Cadmium lines.**

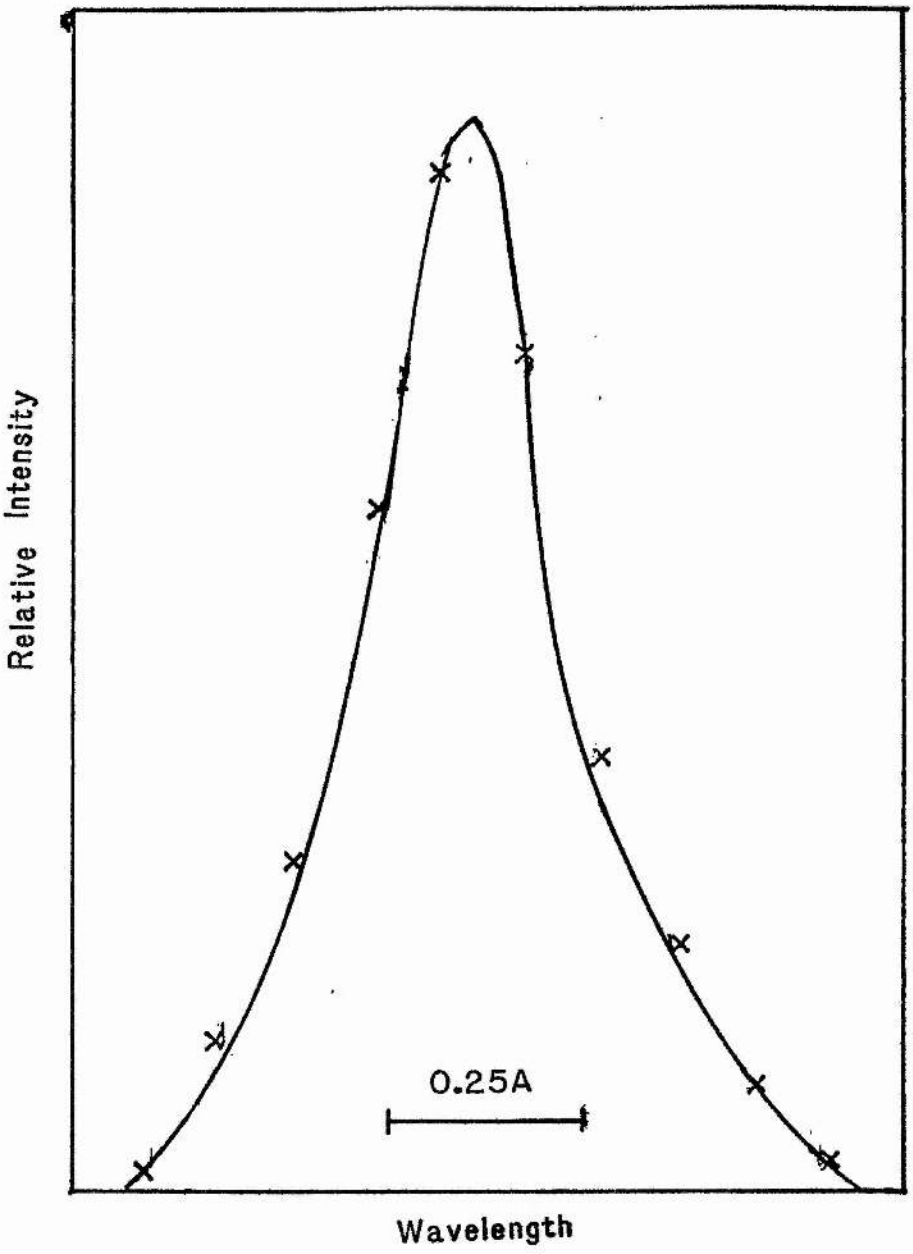

Fig. 4.2 :- Fit of analytic fitting function (equation (3B)) to the instrumental profile.

A further check on the measurement of the instrumental profile is given by the comparison of the photographic and Michelson interferometer measurements of the Si II doublet at 5056Å for Sirius. The result of convolving the Michelson interferometer data with the analytic approximation to the instrumental profile is shown in figure 4.3 together with the photographic data. Clearly,the agreement is very satisfactory.

The agreement between the line profiles and measured equivalent widths (167mÅ (photographic) and 163mÅ (Michelson)) of the two different instruments also gives an upper limit to the scattering of light in the Coudé spectrograph of $\approx \frac{1}{2}\%$ of the continuum intensity. This agreement also gives some indication of the accuracy of the intensity measurements achieved for photographic spectra with the reduction system developed for this project.

In chapter 3 a brief discussion of the difficulties found in the removal of the instrumental profile form the observed line profiles using fourier deconvolution was given. The numerical experiment discussed will be described here.

First a trial absorption line was generated using the analytic fitting function described earlier. Noise was then added to the trial data in the following pseudo-random manner. A table of random numbers in the range 0-99 was generated using the NOVA clock. The time at which a character was pressed on the keyboard was measured and the last two digits entered into the table. A few seconds were allowed to pass, the key was depressed again and the interval between the two key depressions calculated. The last two digits were entered into the table. This process was repeated 256 times, once for each point in the trial spectrum. Three new trial spectra were then generated by adding noise to the data using values of the signal to noise ratio of 10,100 and 200 and the table of random numbers :-

$$D'(i) = D(i) + \frac{(50 - R(i)) \times D(i) \times 3}{100 \times S}$$

where $D(i)$ is the original data value, $R(i)$ is the random number, S the signal to noise ratio and $D'(i)$ is the "noisy" data value. While the distribution of the noise is not gaussian the error in the following analysis caused by that effect should be small.

Fourier transforms of these three spectra were calculated. Fits to the data and noise components were made to generate the optimal noise filter as described in chapter 3. The

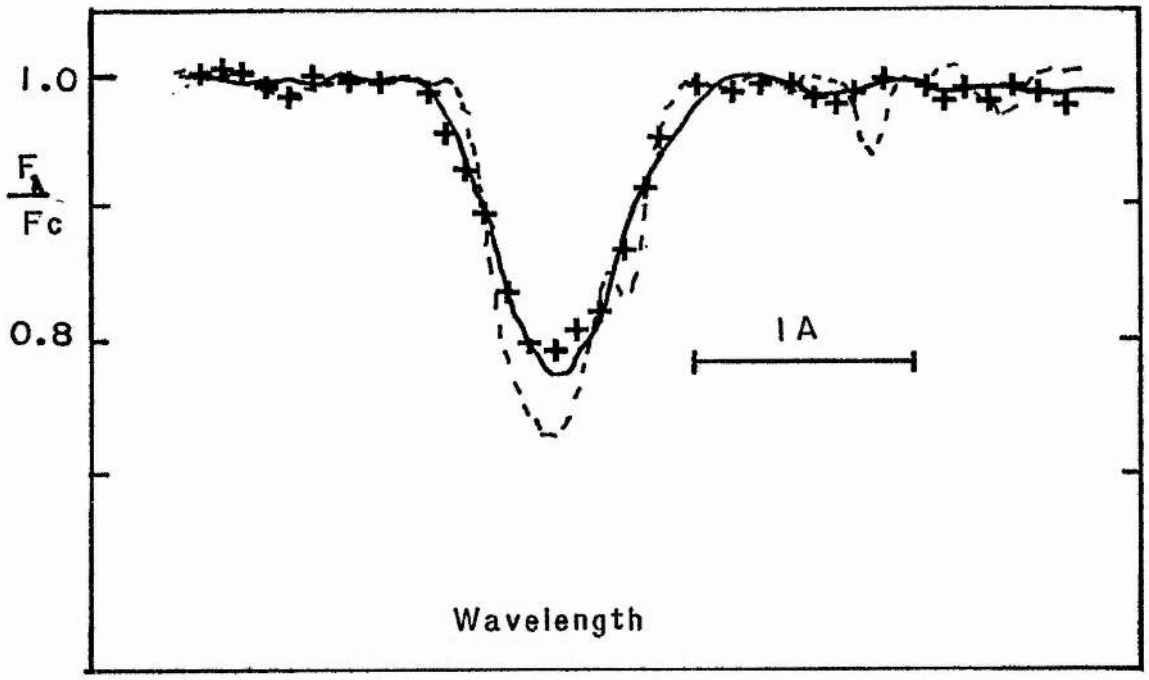

Fig. 4.3 :- **Comparison of the line profile of the Si II doublet at 5056Å obtained from the photographic spectra (+), Michelson interferometer (- - -), and the convolution of the interferometer data with the photographic instrumental profile (solid line).**

data were restored by dividing by the transform of the non-noisy data, multiplying by the noise filter and then calculating the inverse fourier transform.

For perfect removal of the instrumental profile the result would be a delta function at the central position of the line profile. The application of the filter function, however, leaves a residual in the fourier domain which is similar to a box function. The inverse transform of a box function is a sinc function. Thus after the incomplete restoration the spectrum resembles a sinc function with an effective width inversely proportional to the frequency at which the filter becomes operative.

Measuring the resultant width for the three trial spectra showed that the effective instrumental profile had been reduced to $\approx 75\%, 60\%$ and 50% of its original width for $S:N$ ratios of 10,100 and 200 respectively.

After the completion of this experiment a report was found in Code, 1973, of similar work by Miller, 1972, who found reductions to 67%, 45% and 33% for $S:N$ ratios of 10, 100 and 10^4 respectively. These results are marginally better than those reported here. However, given the rather inexact method of including noise used here the results are in reasonable agreement.

The spectra used here, typically, have $S:N$ ratios of the order of 30. Therefore little effective reduction of the instrumental profile is possible. In addition the restoration of line profiles gives a ringing effect due to the oscillations of the sinc function. Brown, 1974, has suggested redistributing the 'energy' in the 'rings' to remove this effect. This is an unsatisfactory solution as there is no physically meaningful method with which to carry out the operation.

4.iii *Measurement Errors*

Investigations were made of the photometric consistency and positional stability of the Joyce-Loebl microdensitometer and also of the noise levels at different photographic densities. In addition the error introduced by averaging photographic density over the slit rather than intensity was estimated for density gradients typical of the line profiles measured here.

Photometric Stability

Two scans were made of the same section of a plate two hours apart. A different

section of the density wedge was used, a shift of $\approx$ 200 Joyce-Loebl units, (JLU), being caused by the introduction of additional neutral density into the beam path. After subtraction of the constant density shift the standard deviation of the differences between the two scans was calculated. A value of 1.8JLU ($\approx .002D$) was found, showing the excellent stability of the Joyce-Loebl as a density measuring machine. The error corresponds to $\approx \frac{1}{2}\%$ of the continuum density of a typical plate used in this project.

Positional Accuracy

It is not necessary to know the absolute size of a Joyce-Loebl machine step to any high degree of accuracy, nor is it necessary for that step size to be constant over the entire length of the leadscrew. The wavelength calibration techniques can account for both these effects without introducing error. It is, however, important that any variations are repeatable and that they be on a scale length larger than the interval between calibration points.

As discussed in chapter 3, software and electronic checks were made to ensure that any extra pulses to the stepping motors, or pulses which did not result in movement of the stepping motors, were recorded. The software also included a routine to minimise errors caused by backlash in the leadscrew. All plates were scanned over approximately the same section of the leadscrew. The size of a unit Joyce-Loebl step has been measured and found to be within 1% of the nominal 5μ value (Bunclark, 1979). Bunclark also found no evidence for variations of the stepsize on scale lengths of $\approx$ $1mm$ over a range of $\approx$ $5cm$.

An investigation of the radial velocities of standard stars using the scanning and cross-correlation programs discussed in chapter 3 has been made by McLean, 1979. An accuracy of $\approx \pm 5kms^{-1}$ was found for these measurements. To achieve this standard of accuracy any positional error would have to be $\leq 3\mu$ over a 5cm range. Some contribution to this error will come from misalignment of the scannning direction with the direction of dispersion of the spectrum.

Photometric noise

Scans were made of grey levels using the same settings and emulsion as the stellar spectra analysed. Mean densities and standard deviations were calculated for each scan

which consisted of 512 samples. A plot of the standard deviations obtained against the mean densities is shown in figure 4.4. At these densities and slitsize the grain noise and photon statistics of the photographic process is the main source of noise. Photon statistics in the measuring machine only become important at densities of $\approx 5D$, (Ring, 1974).

The noise levels obtained here are lower than those found by Lindgren, 1974. The major part of this difference is attributable to the IIIaJ emulsion used here as opposed to the baked IIaO emulsion used in the study at Lund.

At the continuum density to which most of the plates were approximately exposed the noise level is $\approx 1 - 2\%$. The $S : N$ ratio is, however, proportional to the density. Hence the noise is relatively larger in the cores of absorption lines than in the continuum.

Fourier transforms of two of the scans confirmed the noise to be 'white noise', the power spectra being approximately constant at all frequencies.

The Joyce-Loebl averages density over the slit rather than intensity. A broad slit would therefore lead to considerable photometric errors in areas of rapidly varying density, i.e.

$$\log A + n \log \left[10^{**} \left(\frac{\int_x Dx}{\int_x x} \right) - 1 \right] \neq \log \left[\frac{\int_x Ix}{\int_x x} \right]$$

At typical density gradients encountered in this project the narrow slit width used, 5μ, introduces an error of only 0.1%.

4.iv *Calibration Errors*

The calibration of the non-linear response of the photographic emulsion to varying intensities of light is a major source of possible error in photographic spectrophotometry. The response of the emulsion is affected by many factors — the exposure time, the continuity of exposure, the wavelength of the incident light, the photographic development techniques used, the emulsion type, the particular batch of emulsion and whether any hypersensitisation has been used.

The influence on the derived line profiles and equivalent widths of the calibration constant, n, in the relationship $I = A\omega^n$, where ω is the Baker density, is large.

Consider the effect of changing the calibration constant from n_1 to n_2. The relative intensity derived for a point with density, D, normalised to a continuum with density,

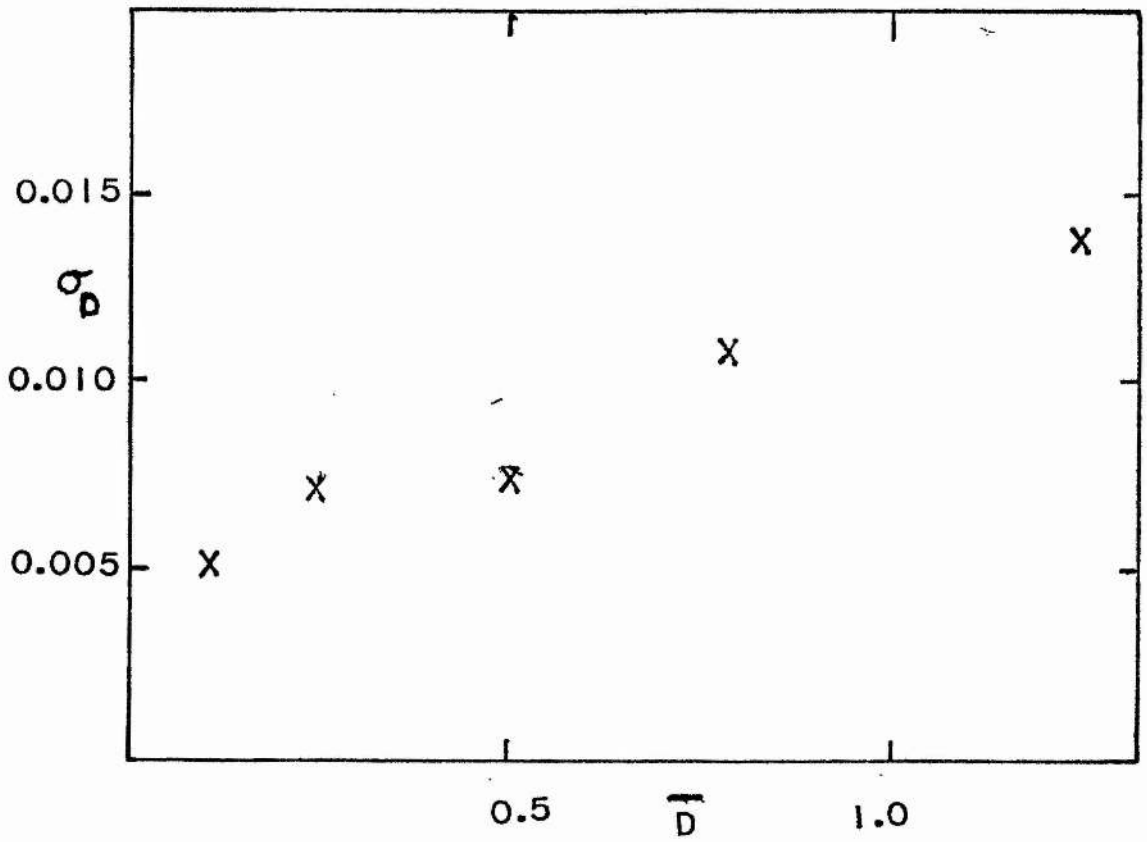

Fig. 4.4 :- **Variation of the standard deviation of the scans of different grey levels as a function of the mean density of the grey level.**

D_c, will alter from I_1 to I_2 according to the relation

$$\frac{I_1}{I_2} = \left(\frac{10^D - 1}{10^{D_c} - 1}\right)^{n_1 - n_2}$$

When $D \approx D_c$ then $I_1 \approx I_2$. As the strength of the absorption increases, however, and $D/D_C \mapsto 0$, the magnitude of the effect becomes more important.

The dependence of the derived equivalent widths on the value of n for three representative lines is shown in figure 4.5. These lines have been normalised to nominal equivalent widths of 50,200 and 1000 mÅ for $n = 0.4$ and a continuum density of 0.5. Clearly, the variation of n will also alter the shape of the measured line profiles because it has a differential effect at the different densities contained within the line profile.

The formal error of the least squares fit in any one determination of n was typically 2%, and rarely $> 4\%$. In any case where the formal error was greater than 5% the data were re-analysed after a careful examination for plate defects. These, if found, were omitted from the subsequent reduction. If after re-analysis the formal error was still $> 5\%$ that measurement was rejected and not included in the table of n, λ pair. In all only 5 out of a total of ≈ 300 measurements were rejected for this reason.

Calibration for the plates supplied by Dr. P.W. Hill was provided by sets of exposures made with a spot sensitometer contemporaneously with the stellar spectra. Two sets of spots with different exposure times are imprinted on each calibration plate. The exposure times were , usually, 2 minutes and 4 minutes for the calibration plates on IIaO emulsion and 2 minutes and 8 minutes for those exposed on 103aF emulsion.

The mean values of n found were:

IIaO (9*plates*)		103*aF* (5*plates*)	
2*min*	4*min*	2*min*	8*min*
0.61 ± 0.03	0.58 ± 0.03	0.49 ± 0.04	0.39 ± 0.03

The difference between the means found for the two 103aF exposure times is clearly significant. The difference is probably due to reciprocity failure. While the difference between the means found for the two exposure times for IIaO emulsion is not statistically significant it was noted that for each individual plate the longer exposure had a value of n which was lower than that found from the shorter exposure.

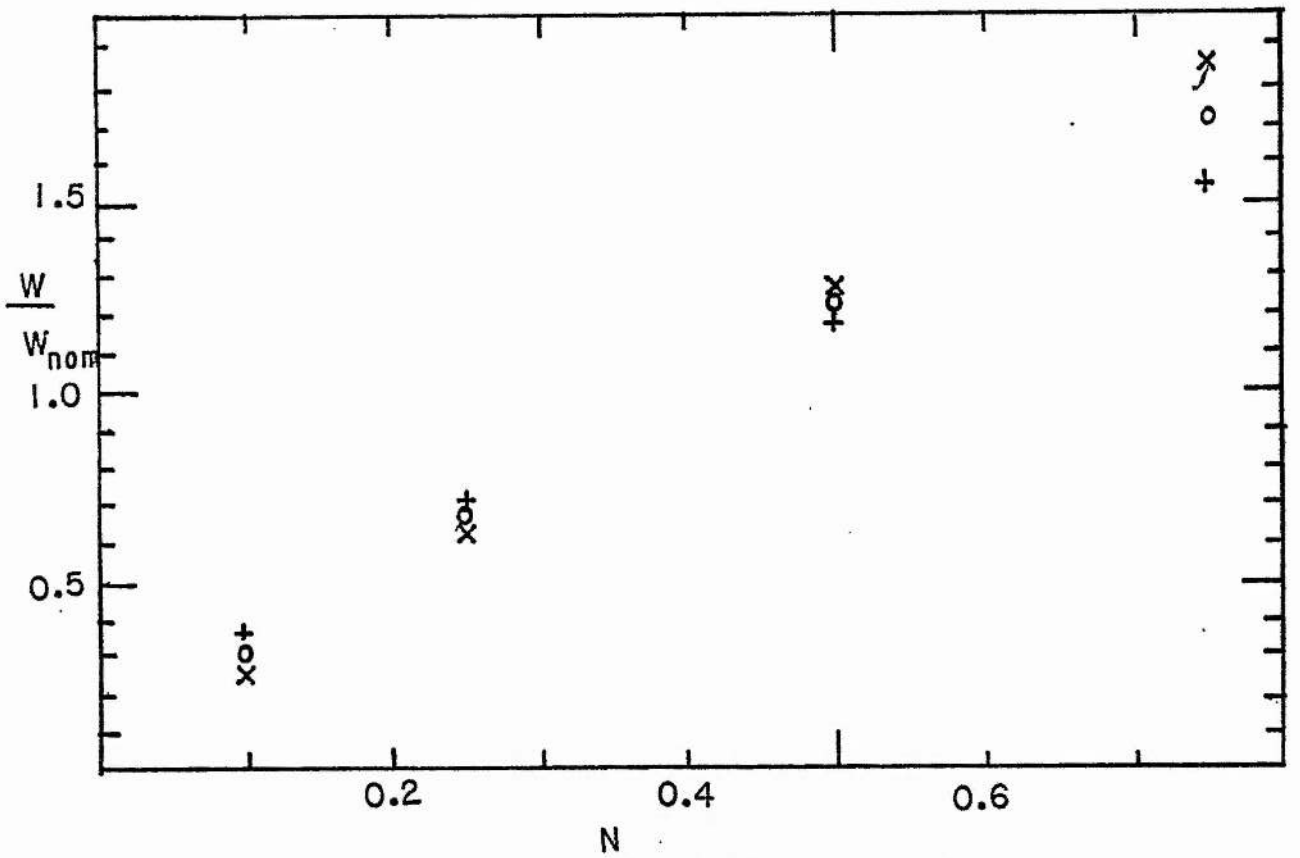

Fig. 4.5 :- Dependence of the derived equivalent width on the calibration constant n normalised to the value for $n = 0.4$. The lines have nominal equivalent widths of 50 (×), 200 (⊙), and 1000 (+) mÅ.

Given this possibility that the value of n is a function of exposure time, the range of exposure times of the stellar spectra supplied by Dr. P. W. Hill and the sensitivity of the derived line profiles to the value of n it was decided to further investigate the variation of n with exposure time.

Drs. H. J. Walker and A. E. Lynas-Grey kindly agreed to obtain the necessary exposures using the calibration wedge spectrograph at S.A.A.O. Two sets of exposures on unbaked and baked IIaO emulsion were obtained. Each set contained 1 plate with exposure times of 1 minute and 32 minutes and 2 exposures at each of 2,4,8 and 16 minutes duration. For each of the plates a suitable neutral density filter was included in the light path to ensure the density range covered by the calibration plates was appropriate to those of the stellar spectra. The pairs of plates with the same exposure were taken with different neutral density filters such that there were pairs of plates with different exposures but the same neutral density filter.

Each of the plates was scanned at a wavelength of 4500Å and reduced in the standard manner. No significant trend with exposure time was found for either emulsion when a linear least-squares fit was made to the derived values of n. Figure 4.6 illustrates the results of this survey. The shift between the IIaO and IIaOb results shows the extra contrast given by the baking process. Note that the anomalous IIaOb plate with an exposure time of 8 minutes was thought by Dr. H. J. Walker at the time of exposure to have been inserted in the plate holder with the emulsion at the wrong side. Despite the apparent absence of any effect correlated with exposure time in this investigation the procedures described in chapter 2 were followed to minimise the difference between the effective exposure times of the stellar and calibration wedge spectra obtained by the author.

Another important effect is the variation of n with wavelength. While some authors have been satisfied with the use of one HD curve at all wavelengths, the need to use a calibration curve derived within $\approx$ 100Å of the point being converted to intensity has been stressed by Wright, 1966. A quantitative examination of the importance of this effect for both IIaO and IIIaJ emulsions was possible using the reduction system developed here and the simple parameterisation of the Baker density calibration method.

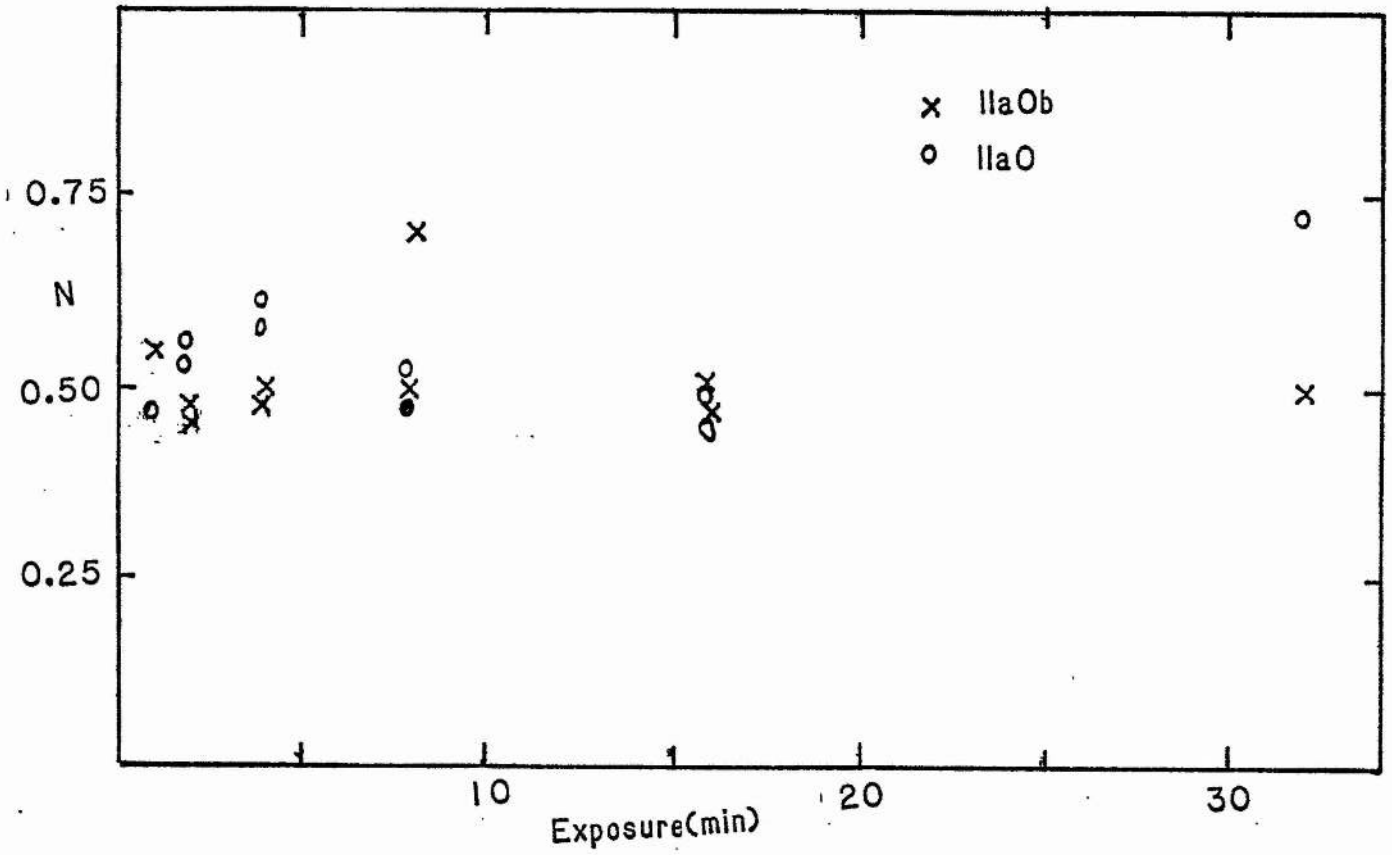

Fig. 4.6 :- **Value of n found for different exposure times.**

Figure 4.7 shows the variation of n with wavelength for representative plates with IIaO and IIIaJ emulsions. The range of values found for n is $\approx 0.36 - 0.62$ and $\approx 0.28 - 0.87$ for the respective emulsions. Less regular variations over the wavelength range are found for IIIaJ emulsion. A typical gradient of $\approx 5\%$ per 100Å is apparent for the IIaO plate while that for the IIIaJ plate is $\approx 2\%$ per 100Å.

In general, all plates of a given emulsion show trends of n with λ which have the same shape but are shifted relative to each other by roughly constant differences in n. For the IIIaJ emulsion calibration wedge spectra used in the calibration of the stellar spectra taken at S.A.A.O. the value of n measured at a wavelength of 4750Å varied between 0.26 and 0.35. It is not clear at which stage in the photographic process these differences are introduced. The differences may be caused by real plate to plate emulsion differences, by different exposure times or slight differences in the development of each plate.

For IIIaJ emulsion using values of n at 200Å intervals would introduce an error slightly greater than the typical uncertainty of a given value of n. In this investigation values of n were found for the calibration wedge spectra at intervals of 100Å. Spline interpolation was then used to derive an individual value of n for each point in the stellar spectrum. This procedure should minimise possible calibration errors.

For the IIaO plates calibrated by spot sensitometer a different procedure was adopted. The two sets of spots were reduced and a mean value of n calculated. This was used to determine the normalisation applied to a mean wavelength-dependent calibration which had been found from the plates supplied by Drs. Walker and Lynas-Grey.

4.v *Analysis Errors*

Two sources of systematic error arise in the calculation of equivalent widths from the data. The first is the setting of the continuum level. As this operation contains a subjective element it is difficult to quantify the accuracy with which it is executed. By going through the entire reduction process twice for the same plate at well separated times it is possible to estimate the consistency with which an individual user sets the continuum. This process gave an estimated error of $\approx 1 - 2\%$ except in the region of the Balmer lines where an error of $\approx 4\%$ was found. The error caused by this effect

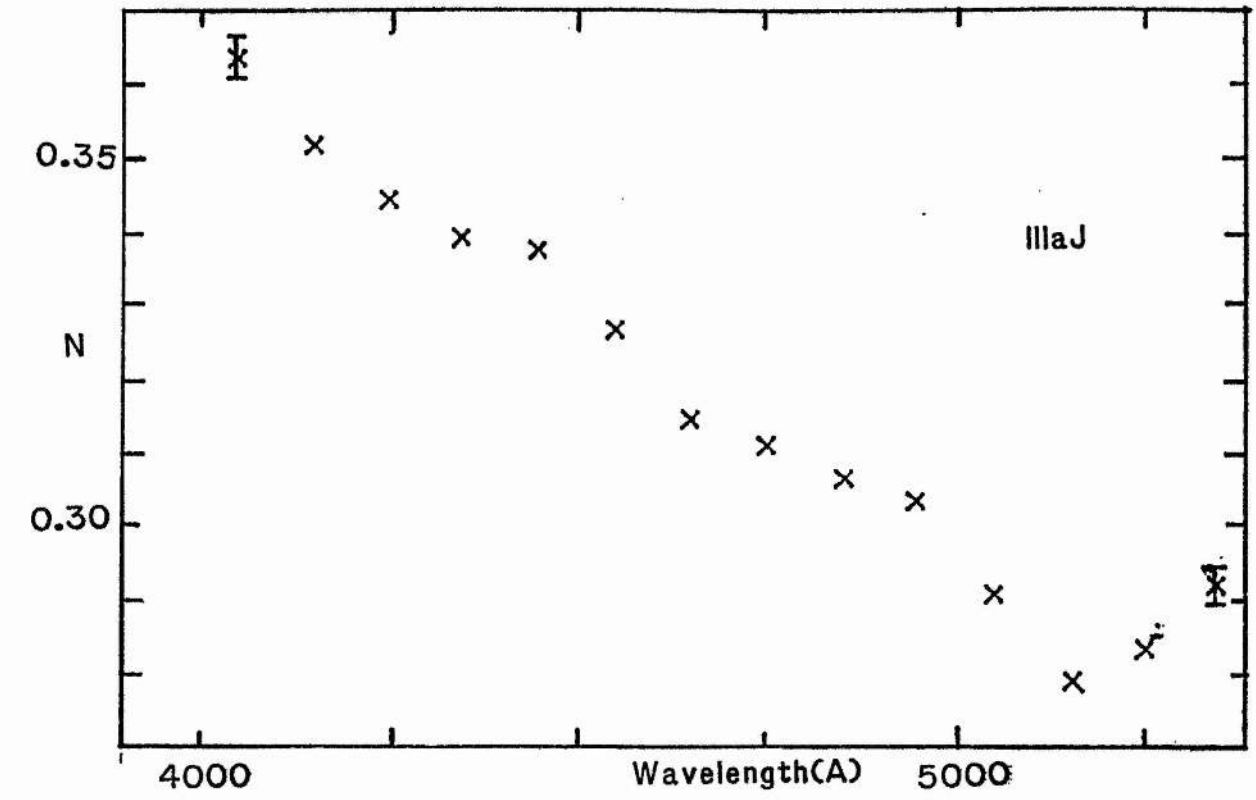

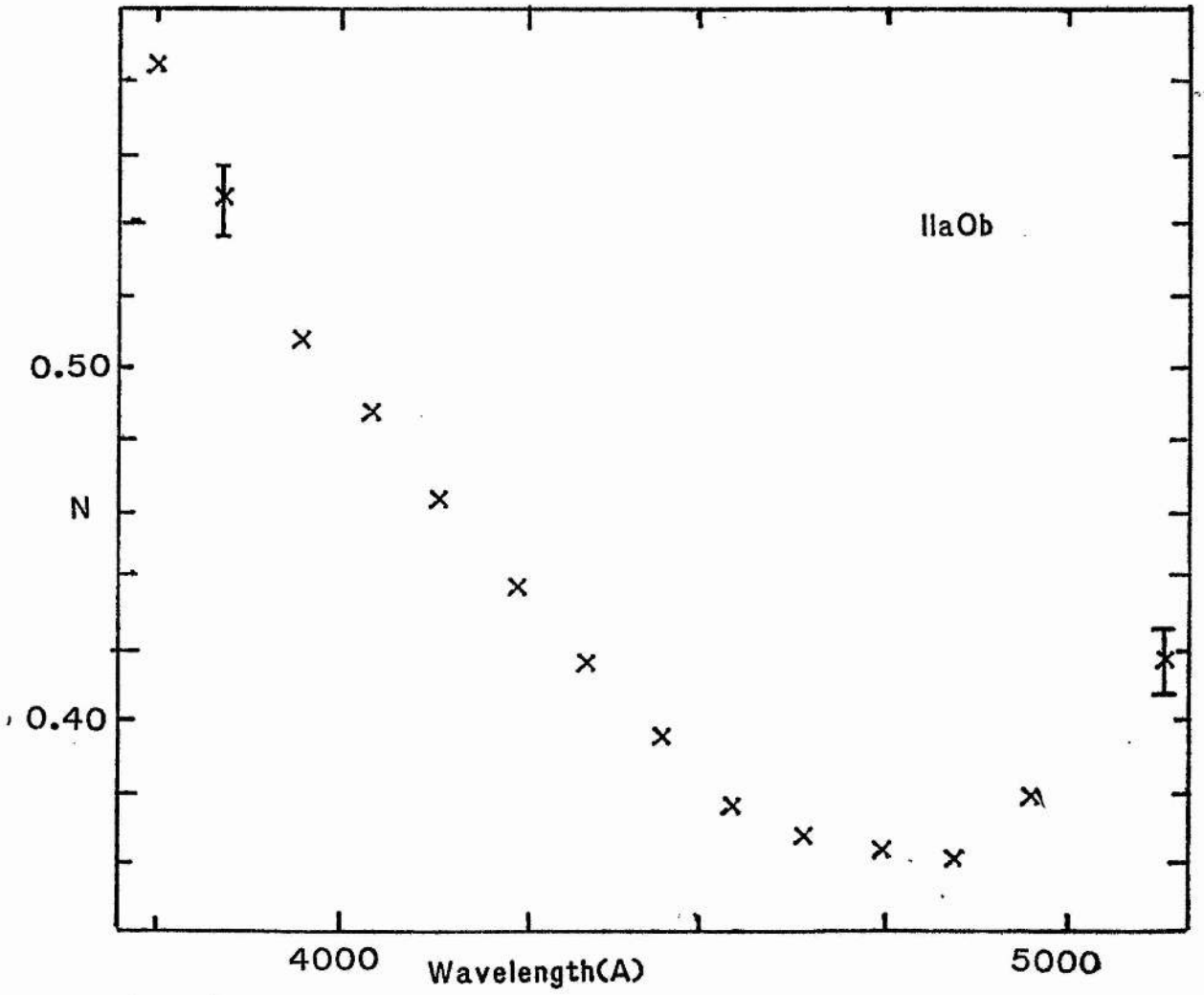

Fig. 4.7 :- Variation of n with wavelength for typical plates.

in the derived equivalent widths does, of course, vary from line to line. The method used to integrate the line area can also cause an error. The accuracy of the Simpson's rule integration used here is dependent on the number of points used, the sampling interval and the gradients present in the line profile. For a typical line in this investigation the error $\ll 0.5\%$.

4.vi *Overall Accuracy*

The only manner in which an estimate of the overall accuracy of the measurements can be made is by comparison with other measurements. This comparison can be internal, between different plates of the same star, or external, by using the previously published measurements of other authors. It is not only important that the size of the random errors be established but also that any evidence for systematic trends with wavelength or equivalent width be investigated.

In the following section comparison is made between the published results for Sirius (Kohl, 1964 quoted in Strom *et al*, 1966) and τ Her (Adelman, 1977) are compared with those found in this investigation. In addition, a comparison is made between results obtained from the different plates of Sirius. (To some extent this section anticipates the discussion of the scanning parameters, reduction procedure and results given in chapter 5 to which the reader is referred for details.)

External Comparisons (a) *Sirius*

A comparison of the equivalent widths measured from a single spectrum of Sirius with the data quoted by Strom *et al*, 1966 (hereafter *SSG*) is shown in figure 4.8. The latter values are averages obtained from measurements of 19 plates, most of which had a reciprocal dispersion of $2\,\mathring{A}\,mm^{-1}$. Approximately 120 lines are included in the comparison.

The lines were separated into three categories according to the equivalent width attributed to a particular line by *SSG*, W_s. The r.m.s. difference ϵ, between W_s and the equivalent width found in this project, W, was calculated for each group according to the formula

$$\epsilon = \left(\frac{\sum \left(\frac{W - W_s}{W_s} \right)^2}{N} \right)^{0.5}$$

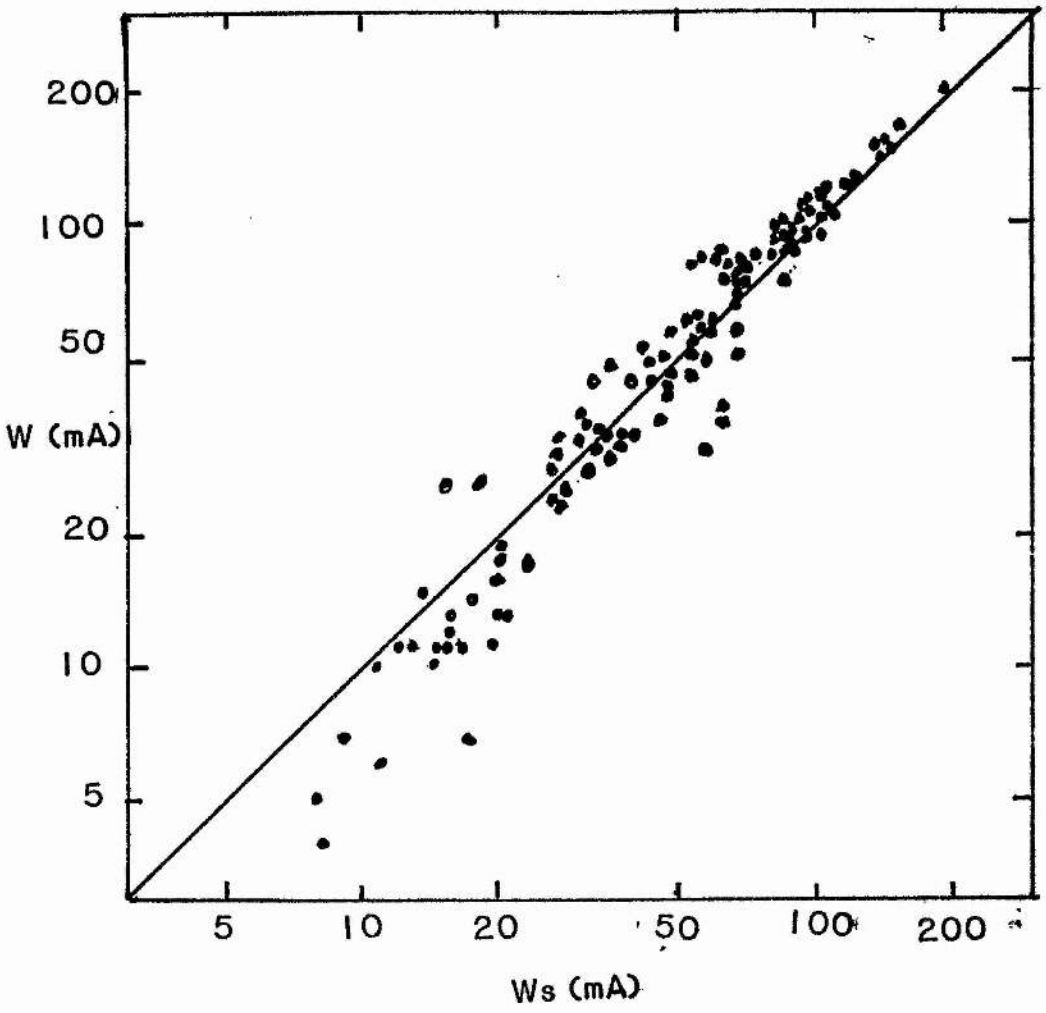

Fig. 4.8 :- Comparison of the equivalent widths of lines in the spectrum of Sirius found in this project, W, and those of Kohl quoted in SSG, W_S. The solid line shows the locus, $W = W_S$.

A polynomial (of maximum order 6) was fitted to the data in each group and the maximum relative difference, L, also noted. The results are summarised in Table 4.i.

While the scatter in the group with the smallest equivalent widths is large this is not unexpected. The lack of any systematic trend in this group is heartening. The slight systematic trends found for the other two groups are more disturbing. Neither is significant at the 1σ level, however, and so no corrections were applied in the final analysis.

When comparing results from investigations of stellar spectra made with plate material obtained at different dispersions a trend opposite to that recorded here is often noted. Usually studies at lower dispersions record equivalent widths that are increased relative to measurements of the same lines made at higher dispersions.

SSG quote an error of $\approx$ 10% for a single measurement. For the average result from 19 spectra it is reasonable to assume that the residual error in the mean values is $\frac{1}{\sqrt{19}}$ of this value or $\approx$ 2.5%. This suggests that the error for an individual measurement in this project is 12.5% for lines in group b and 6.5% for lines in group c.

An examination of the trend of relative difference with wavelength for lines with $W_\bullet > 50m\mathring{A}$ was also made. The results are plotted in figure 4.9. No trend is apparent. The least squares polynomial fitting routine gave a linear best fit with a gradient of $0.002 \pm 0.04\, m\mathring{A}/\mathring{A}$ when applied to this data.

(b) τ *Her*

Adelman, 1977, has published a study of this B5 IV star in which he uses equivalent widths averaged over the measurements from 6 plates at $8.9\mathring{A}mm^{1}$ and 3 at $4.3\mathring{A}mm^{-1}$, his final results being adjusted to the scale derived from the higher dispersion measurements.

For the 25 lines in common with this study, with equivalent widths in the range $50m\mathring{A} \leq W_a \leq 1000m\mathring{A}$, a similar comparison to that just discussed for Sirius was made. Figure 4.10 shows a plot of Adelman's measurements, W_a against those determined here, W. The best fitting polynomial is again linear (up to a 7^{th} order polynomial was allowed) and is given by:

$$W = 1.015(\pm 0.05)W_a - 3.4(\pm 2.0)m\mathring{A}$$

Table 4.i

External Comparison of Equivalent Widths: Sirius

Group	$W\,(m\mathring{A})$	*No. of Lines*	ϵ	$\lvert L\rvert$
(*a*)	$0 < W_S \leq 50$	43	0.24	0.43
(*b*)	$50 < W_S \leq 100$	47	0.13	0.21
(*c*)	$100 < W_S$	28	0.07	0.16

Least square polynomial fits:

(*a*) $W = 0.999 \pm 0.048\, W_S - 2 \pm 1 \;\; m\mathring{A}$

(*b*) $W = 0.973 \pm 0.036\, W_S - 2 \pm 2 \;\; m\mathring{A}$

(*c*) $W = 0.984 \pm 0.041\, W_S + 1 \pm 3 \;\; m\mathring{A}$

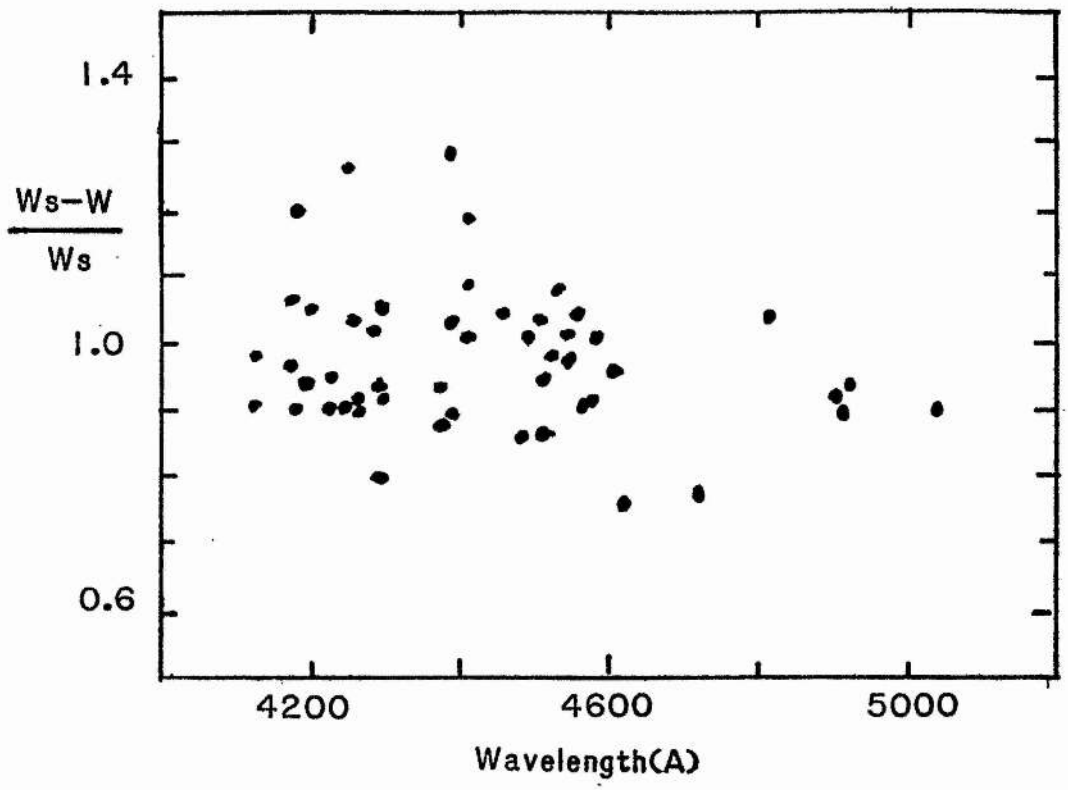

Fig. 4.9 :- Variation with wavelength of the difference, $W - W_S$, normalised to W_S

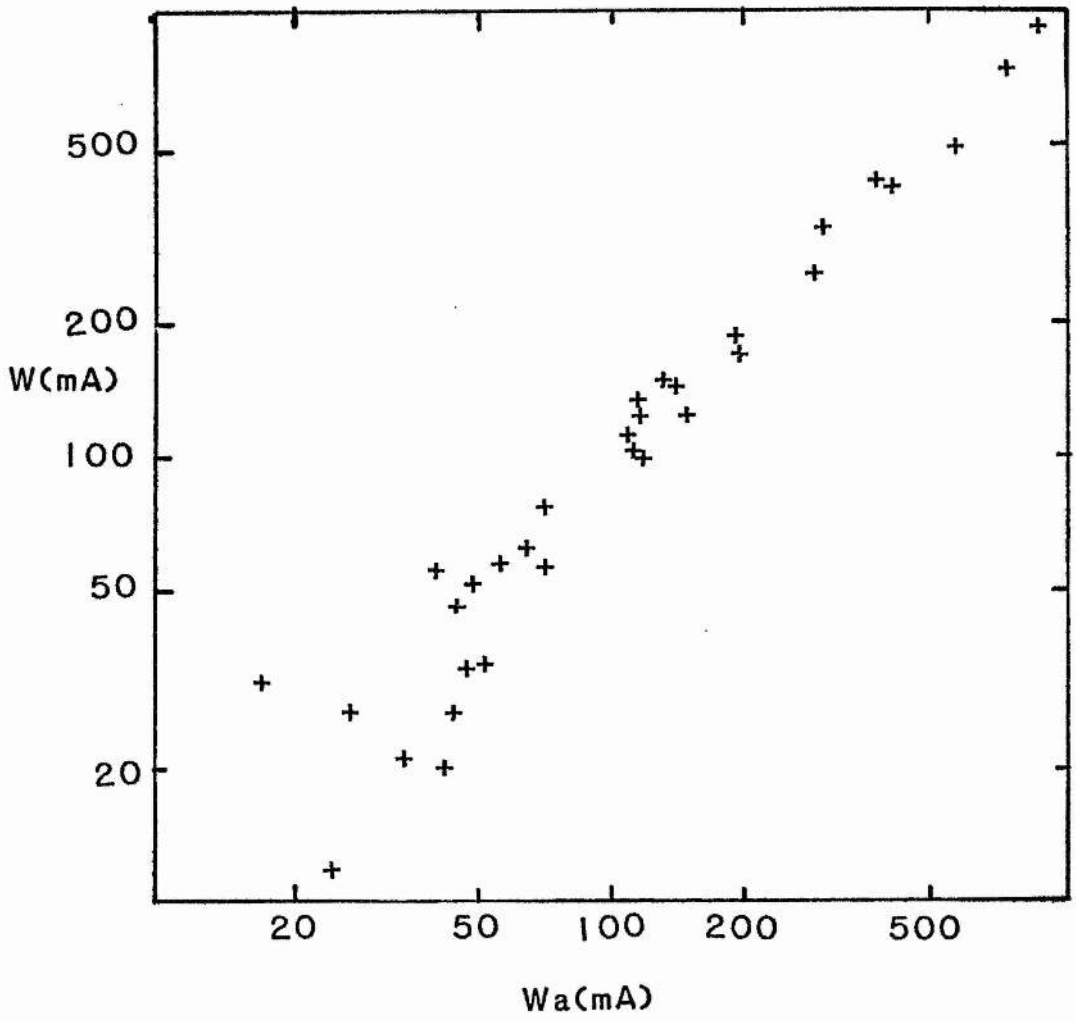

Fig. 4.10 :- Comparison of the equivalent widths of lines in the spectrum of τ Her measured in this project, W, and those of Adelman, W_A.

The value of ϵ found for these lines was 0.10 and $|L|$ had a value of 0.18. No systematic trend with wavelength was found for $(W_a - W)/W_a$.

(It was noted that for 17 lines from 5 elements the difference, $W_a - W$, was in the sense that would produce less scatter in the abundance determinations made by Adelman)

Internal comparisons

Information on the consistency and accuracy in setting the continuum level, the noise level of the spectra and the accuracy of converting from photographic density to intensity can be found from an internal comparison of two plates of the same object.

The result of subtracting one normalised spectrum of Sirius from another is shown in figure 4.11. Before the subtraction was made the wavelength origin shift was calculated using the cross-correlation routines and fourier interpolation was used to interpolate between the data points to an accuracy of $\frac{1}{8}^{th}$ of a pixel. The units used are those of the normalised continuum intensity.

A mean difference of -0.0005 and an r.m.s. difference of 0.018 were calculated from the data. Only in the region of the H_β line at 4861Å does any systematic difference over a long wavelength scale appear to exist. Over the 100Å region centred on this line the mean difference is found to be 0.03. The systematic error in setting the continuum level in the wings of hydrogen lines is well documented and is particularly important at the spectral type of Sirius. Calibration errors will also contribute to the difference found here so this result is not unsatisfactory. The mean difference is indicative of the repeatability achieved in the setting of the continuum level using the interactive techniques of the reduction system developed here.

Measurements of the equivalent widths obtained from 4 individual spectra of Sirius were also compared. The mean equivalent widths for each of thirty lines of Fe II, Cr II and Si II were calculated from the individual measurements. A comparison was then made for each individual set of measurements with the mean set of equivalent widths in the same manner as for the external comparisons of Sirius and τ Her. The values of ϵ obtained for each set were averaged and the standard deviation calculated for the group. The results are given in table 4.ii. The values obtained are consistent with the values derived from the external comparisons.

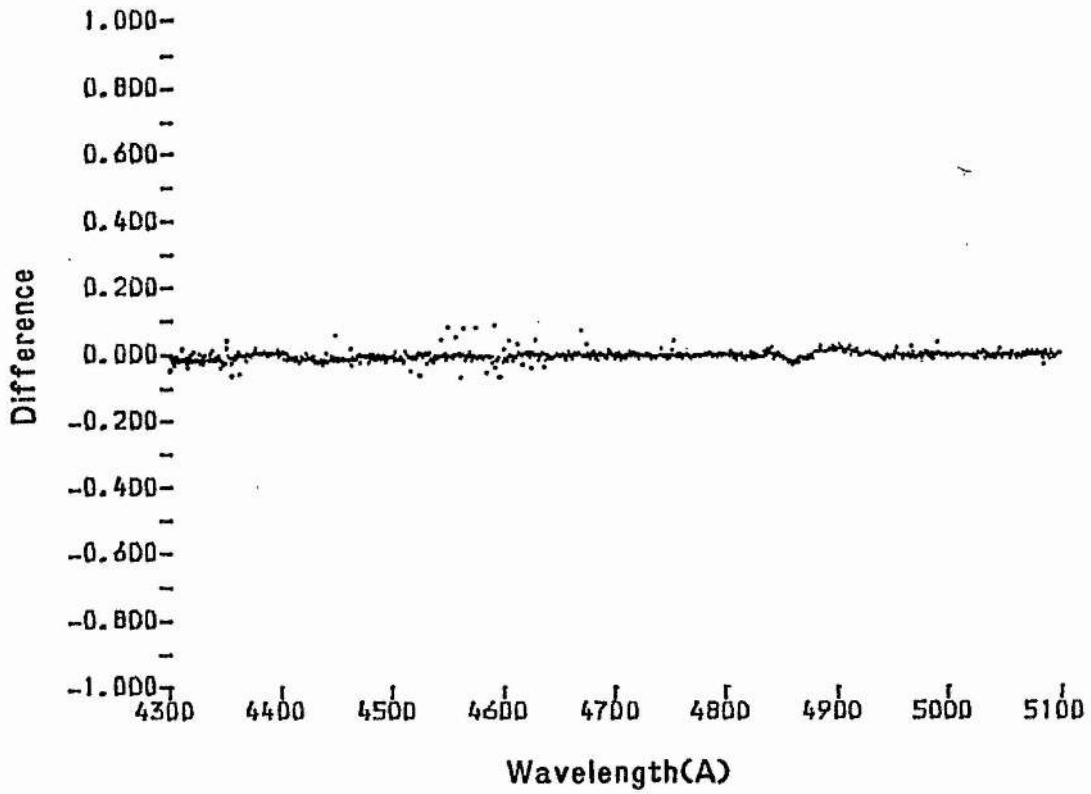

Fig. 4.11 :- **Result of the subtraction of two reduced scans of Sirius.**

Table 4.ii

Internal Comparison of Equivalent Widths: Sirius

Group	*No. of Lines*	ϵ	*S.D.*
(*a*)	6	0.17	0.03
(*b*)	13	0.11	0.02
(*c*)	11	0.08	0.01

4.vii *Profile Errors*

A comparison of metal line profiles with the results of other authors is rather more difficult to make due to the lack of published measurements and the different instrumental profiles of different measurements.

Measurements of the half-width of the He I 4471Å and Mg II 4481Å lines are given for a number of stars in Slettebak *et al*, 1975. Twenty-one of the line measurements presented there were also measured in the course of this project. A comparison between the two sets of measurements is shown in figure 4.12. A linear relationship of the form

$$W_{\frac{1}{2}} = 1.02(\pm 0.04) W_{\frac{1}{2}}^{Slettebak} + 2.3(\pm 1.5) m\mathring{A}$$

was found to give the best least-squares fit to the data. No correction for the instrumental profile was made as both sets of observations were made with approximately the same resolution.

An alternative approach to the problem of estimating the error in the line profiles is to investigate what intensity error at each point in the line profile would produce the errors found in the measured equivalent widths. The stability of the errors found in the previous section suggests the value of such an approach.

To simplify this investigation a further approximation was made. This was to assume that there exists a linear relationship between the central depths, $1\text{-}R_0$, and equivalent widths of the lines. Such a relationship,

$$W(m\mathring{A}) = \frac{1000}{1.78}(1 - R_0)$$

is shown fitted to the Sirius data in figure 4.13.

To first order the approximation is indeed reasonable. The magnitude of an error in $1\text{-}R_0$ that would correspond to a given equivalent width error can then be calculated. The results of such a calculation for an average line in each of the three equivalent width ranges used previously are given in table 4.iii. The percentage error in intensity is then the systematic error in intensity or the mean random error in intensity, (or some combination of both) at each point in the line profile. As there are typically 12-20 points in each line profile a random noise level of $\approx 2\%$ would contribute approximately 0.5% of the total

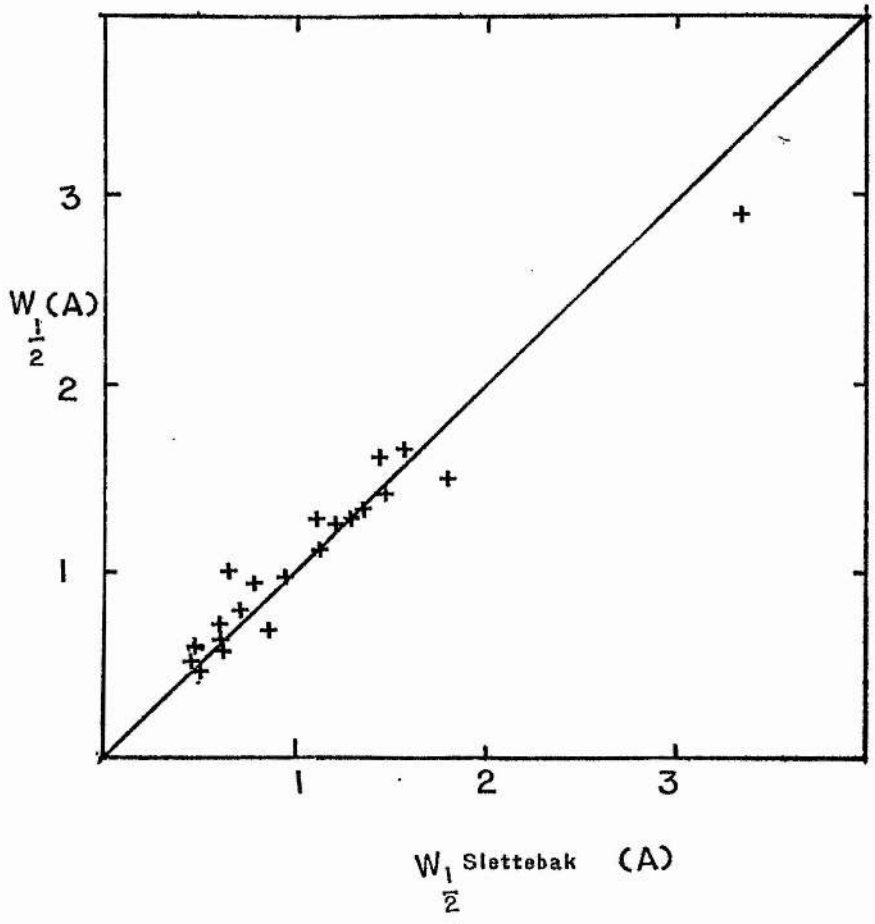

Fig. 4.12 :- **Comparison of the half-widths of the Mg II 4481Å and He I 4471Å lines obtained here, $W_{\frac{1}{2}}$, and those given by Slettebak *et al*, $W_{\frac{1}{2}}$(Slettebak).**

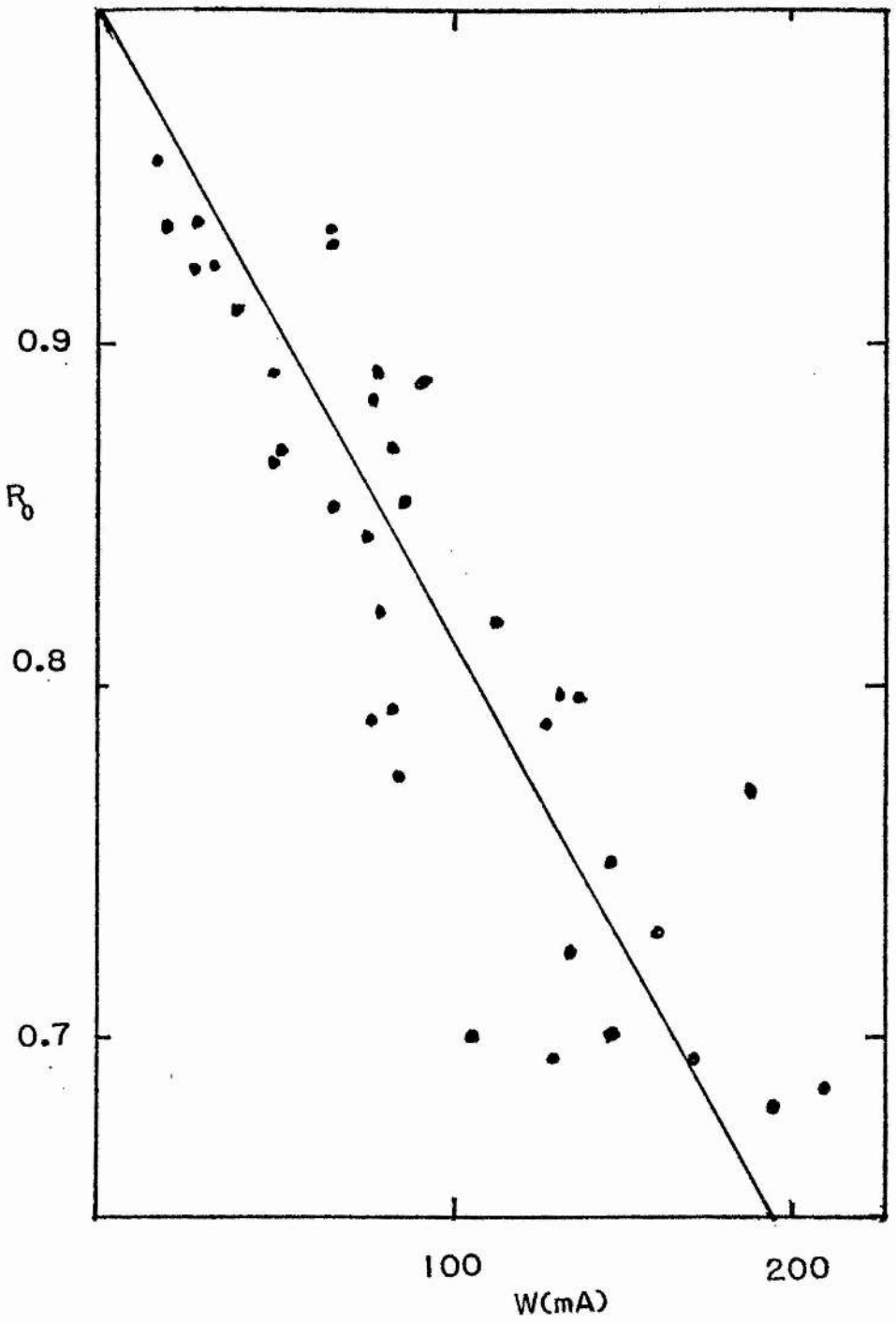

Fig. 4.13 :- **Comparison of the central depth and equivalent width measures for lines in the spectrum of Sirius. The line is the least squares fit described in the text.**

Table 4.iii

Intensity Error Required for R.M.S. Equivalent Width Error

Group	$\bar{W}(m\AA)$	R_0	ϵ	ΔR_0	$\Delta I(\%)$
(*a*)	25	0.956	0.25	0.011	1.2
(*b*)	75	0.867	0.12	0.016	1.8
(*c*)	150	0.733	0.08	0.022	2.9

error. The remaining error of 1-2% must come from the setting of the continuum level and the calibration procedure.

4.viii *Summary*

The spectra used in this investigation, when measured and reduced with the interactive computer package, give results which compare favourably with those of other authors. The repeatability of the results is good and for lines with equivalent widths larger than 50mÅ an r.m.s. error of $\approx$ 10% is found. The larger error of 20 – 25% found for weaker lines is not unreasonable at the dispersion used here. In addition the lack of any systematic shift between the measurements made for this project and those made at higher dispersions suggest that the attention given to the development and calibration procedures has been worthwhile.

CHAPTER FIVE

THE ANALYSIS OF THE PHOTOGRAPHIC SPECTRA

5.i *Introduction*

In this chapter the results obtained from the analysis of the photographic spectra using the FORTH reduction system and the subsequent interpretation of the data using LTE and non-LTE models will be discussed. A comparison of the merits of both types of model will be given and the fundamental stellar properties deduced.

5.ii *Scanning*

All the plates were scanned using the Joyce-Loebl microdensitometer and the following procedures. Plates were first aligned with the direction of dispersion parallel to the long axis (x-axis) of the plate table. This was accomplished with the aid of the table rotation screw.

A stellar scan was composed of five individual parallel scans of the same length. These were:

a) clear plate

b) comparison arc spectrum

c) stellar spectrum

d) the other comparison arc spectrum

e) clear plate

The y position of the starting points of each scan were input to the controlling computer using the push buttons on the Joyce-Loebl control panel. The slit width was set to 5μ and the slit length set to maximise the area of plate scanned. The distance between sample points was fixed at 15μ. This ensured that the sampling theorem,

$$a < \Delta(x) < \Delta(R)$$

where a is the slit width, $\Delta(x)$ is the sampling interval and $\Delta(R)$ the size of a resolution element, was satisfied.

Scans were composed of approximately 15360 samples. This meant that approximately 9" of plate was traversed which caused an intitial problem in that the focus of the Joyce-Loebl was not constant over the entire scan length. This was overcome by inserting a pause routine in the scanning program. This halted the scan until a character on the terminal keyboard was depressed, allowing the focus to be adjusted if necessary. This action was only taken if the microdensitometer was scanning a continuum region of the spectra. Halts occurred at roughly 1.5 cm intervals.

Scans of calibration wedge spectra plates were made perpendicular to the direction of dispersion at $\approx 100\mathring{A}$ intervals. The wavelength scale was obtained by measuring the positions of the arc lines superimposed on these plates. This was done using the Joyce-Loebl push button control panel. The same stepsize parameters were used as for the scans of the stellar spectra. The length of each scan was sufficient to include a region of clear plate before and after the data containing the step wedge density information.

For spot sensitometer calibration plates the centre of each spot was found using the push button controls and the positions were then input to the controlling computer. In general 12 individual scans of 512 samples were then needed, 1 per spot pair, the region between each of the spots in a pair being used to determine the local background.

5.iii *Calibration, Conversion to Intensity, and Normalisation.*

Baker density calibration constants, n, were determined as described in chapter 3. For the spectra with calibration wedge spectra tables of n, λ pairs were stored on disc. For the IIaO and IIaOb plates with spot sensitometer calibrations a mean value of n was determined from the two individual values found from the two sets of spots. This value of n was then used to normalise a mean n, λ set derived during the experiment to investigate the variation of n with exposure time. For the 103aF plates a constant value of n derived from the sensitometer spots was used at all wavelengths.

The wavelength scales of the stellar spectra were found using the comparison arc spectra. Both scans of the arc lines were first compared using the cross-correlation routines to ensure no shift had occurred between scans. A set of x, λ pairs was stored on disc as

discussed in chapter 3.

Mean values of the clear plate level were obtained by averaging the individual scans of clear plate. Where any large-scale variation of the clear plate level with x position was found the spline interpolation routine was used to define a clear plate level for each sample point in the scan of the stellar spectrum. Otherwise a constant value was assumed.

The stellar spectrum was then converted to baker density, ω, and then to log (relative intensity) units using the calibration constant. Finally the spectrum was normalised to the continuum level using the interactive routines discussed earlier.

After each stage in this reduction process a copy of the data was transferred to magnetic tape via the H316 for permanent storage.

5.iv *Measurement*

After a period of familiarisation with each spectrum, when the Fourier transform and noise filter routines were used to obtain a measure of the $S : N$ ratio and the distinction between real and spurious features, data on the absorption lines were extracted from the spectra in the following manner.

Each spectrum was displayed on the T4010 screen in overlapping consecutive sections of $\approx 50\mathring{A}$ in length. Shortward and longward wavelength limits to unblended lines were selected interactively with the cursor. Equivalent widths and the other line parameters were then calculated and stored in a catalogue on disc as described in chapter 3. For blended lines (apart from those of hydrogen and helium) the analytic fitting function (equation 3B) was used to separate the individual components of the blend, the line parameters calculated analytically and stored in the catalogue. Parameters for the hydrogen lines were obtained by first selecting points interactively to represent the unblended line profile and using the spline interpolation routine to generate an unblended line profile and to store this in a separate disc storage area. This was then measured in the same manner as for unblended metal lines. An additional parameter was also measured for the Balmer lines. This parameter was the full width of the line at a residual intensity of 75%, W_{75}.

After measuring all lines, line lists published by other authors and the tables of Moore, 1959, and Kurucz and Peytremann, 1975, were used to identify the lines. After

measuring all lines for all stars it was decided that, principally for computational reasons, it would be necessary to restrict the analysis to a subset of the data.

The following criteria were used in choosing this subset although some exceptions were made. Lines of CII,CIII,NII,NIII,OII,SII,SIII,MgII,AlIII,SiII,SiIII and SiIV were chosen to cover, where possible, a range of wavelength, a range of observed strength, and a range of excitation energy. Attempts were made to select lines free of possible blending and for which atomic data of reasonable accuracy was available.

Table 5.i lists the lines chosen together with the log gf values. It should be stressed that this list is somewhat arbitrary and with hindsight some different lines would have been selected. The set chosen did however enable the major aims of the project to be pursued.

After the selection of lines the spectra were re-measured. Only lines on the list were measured but in this analysis if no line was evident at the expected position the wavelength region around the expected position was used to determine an upper limit to the strength of a line. In general the upper limits for unmeasured lines are of the order of $\approx 10 - 15m\mathring{A}$ but for the spectra with the lowest $S : N$ ratios or the broadest lines this could rise to $\approx 25m\mathring{A}$.

A comparison of the results derived from both sets of measurements showed only very small differences ($\leq 2\%$) caused principally by the marginally different continuum level and line wavelength limits chosen.

Table 5.ii gives the mean values of equivalent widths found for the lines. The lines are identified by ion and wavelength in $\mathring{A}$ and the measurements are in $m\mathring{A}$. Also included are measurements of the Balmer discontinuity, D_β, which are in magnitudes and were taken from the literature (in particular the catalogue of Breger, 1976). Lines for which no detection was made are indicated by a *. Those outwith the wavelength region measured are given by a —. An F at the position of a line indicates that a plate flaw prevented the measurement of that line while a B means that the line could not be measured because of blending effects. A colon after a measurement implies that it is more uncertain than other measurements.

5.v *Analysis of Equivalent Width Data*

Table 5.i

Log gf values and Line Components

Ion	*Wavelength*	*Type of Computation*	*Components*	log *gf*
CII	3921	*W*	3920.68	−0.24
	4074	*P*	4074.48	0.19
			4074.54	0.39
			4074.84	0.58
	4267	*P*	4267.00	0.56
			4267.26	0.72
	4374	*W*	4374.28	0.66
	4411	*P*	4411.20	0.54
			4411.52	0.69
	5145	*W*	5145.16	0.17
	5151	*W*	5151.08	−0.21
CIII	4056	*W*	4056.06	0.40
	4647	*W*	4647.40	0.10
	4650	*W*	4650.16	−0.12
	4664	*W*	4663.53	−0.56
NII	3995	*W*	3995.00	0.30
	4176	*W*	4176.16	0.60
	4228	*W*	4227.75	−0.02
	4447	*W*	4447.03	0.28
	4530	*W*	4530.40	0.57
	4614	*W*	4613.87	−0.59
	4631	*W*	4630.54	0.23
	5005	*P*	5005.14	0.61
			5005.30	−0.90
NIII	4515	*W*	4514.89	0.29
	4524	*W*	4523.60	−0.34
	4634	*W*	4634.17	−0.07
	4641	*W*	4640.64	0.19

Table 5.i (contd.)

Ion	*Line*	*Type of Computation*	*Components*	log *gf*
OII	4072	*W*	4072.16	0.53
	4087	*W*	4087.20	0.38
	4093	*W*	4092.94	−0.25
	4317	*W*	4317.14	−0.33
	4326	*W*	4325.77	−1.06
	4415	*W*	4414.91	0.31
	4417	*W*	4416.98	0.00
	4591	*W*	4591.01	0.37
	4596	*W*	4596.20	0.22
	4649	*W*	4649.14	0.35
MgII	4385	*W*	4384.64	−0.78
	4391	*W*	4390.56	−0.53
	4434	*W*	4433.99	−0.90
	4481	*P*	4481.14	0.76
			4481.31	0.59
AlIII	4513	*W*	4512.57	0.41
	4529	*W*	4529.18	0.66
SiII	3854	*W*	3853.66	−1.61
	3856	*W*	3856.02	−0.60
	3863	*W*	3862.60	−0.85
	4128	*W*	4128.07	0.31
	4131	*W*	4130.89	0.46
	5041	*W*	5041.03	0.25
	5056	*P*	5055.99	0.50
			5056.33	−0.44
	6347	*W*	6347.10	0.31
	6371	*W*	6371.36	0.01

Table 5.i (contd.)

Ion	*Line*	*Type of Computation*	*Components*	log *gf*
SiIII	4552	*W*	4552.62	0.19
	4567	*W*	4567.82	−0.04
	4575	*W*	4574.76	−0.51
	4813	*W*	4813.33	0.85
	4820	*W*	4819.71	0.57
	4829	*W*	4828.96	1.09
SiIV	4089	*W*	4088.85	0.20
	4116	*W*	4116.10	−0.11
	4212	*W*	4212.40	0.81
	4631	*W*	4631.13	1.18
	4654	*W*	4654.31	1.49
SII	3923	*W*	3923.48	0.32
	4816	*W*	4815.52	−0.08
	4925	*W*	4925.32	−0.17
	5014	*W*	5014.00	0.16
SIII	3984	*W*	3983.77	−0.72
	4285	*W*	4284.99	0.11
	4362	*W*	4361.53	−0.33
	4365	*W*	4364.75	−0.68

Table 5.ii

Equivalent Widths in mÅ:

Carbon II

HD	3921	4074	4267	4374	4411	5145	5151
15371	35	18	58	6	*	—	—
74575	—	35	193	23	38	43	23
79351	—	23	219	19	31	32	25
81188	—	40	289	17	35	42	33
106625	—	—	52	*	*	*	*
111123	—	37	187	19	35	36	30
116658	—	*B*	222 :	*B*	*B*	*	*
118716	—	*	187	*	*	*	*
129056	—	51	260	17	49	37	29
132200	—	30	266	16	28	28	12
147165	—	*B*	128	*B*	27 :	*B*	*
147394	62	*	155	*	*	—	—
149438	—	13	73	8	14	*	*
165024	155 :	*B*	184	*B*	*	*	*
166182	85	19	208	*	16 :	—	—
169467	88	*	204	*	*	—	—
180163	58	15	199	*	12	—	—
184171	63	14	178	*	9 :	—	—
184930	30	*	88	*	7	—	—
195810	57	*	112	*	5 :	—	—
207971	14 :	*	*	*	*	—	—
214680	10	*	48	*	*	—	—
218376	58	*	149	9 :	13	—	—

Table 5.ii (contd.)
Carbon III

HD	4056	4647	4650	4664
15371	*	*	*	*
74575	*	18	*B*	*
79351	*	8	*B*	*
81188	*	*	*	*
106625	*	*	*	*
111123	—	144	*B*	*
116658	—	*B*	*B*	*B*
118716	—	56	*B*	*
129056	—	25	*B*	*
132200	—	*	*B*	*
147165	—	*B*	*B*	*B*
147394	*	*	*	*
149438	29	163	125	8
165024	*	*B*	*B*	*
166182	*	*	*	*
169467	*	*	*	*
180163	*	*	*	*
184171	*	*	*	*
184930	*	*	*	*
195810	*	*	*	*
207971	*	*	*	*
214680	33	176	60 :	*
218376	8	82	*B*	5 :

Table 5.ii(contd.)

Nitrogen II

HD	3995	4176	4228	4447	4530	4614	4631	5005
15371	10	5	5	8	*B*	—	—	—
74575	140	28	49	84	19	49	103	62
79351	—	30	10	16	20	11	23	18
81188	—	38	28	54	17	19	73	45
106625	—	*	*	*B*	*B*	*B*	*B*	*
111123	—	21	28	43	10	56	119	74
116658	—	*	*	*B*	*B*	*B*	*B*	*
118716	—	14 :	24 :	22	*B*	27	34	18 :
129056	—	27	58	70	26	52	108	89
132200	—	9	12	23	10	11	48	50
147165	—	*	*	53	*B*	*	46 :	*B*
147394	29	*	*	*	*	*	*	—
149438	—	20	16	54	19	20	28	34
165024	324	41	74	135	*B*	70	197	142 :
166182	115	12	33	41	24	*	58 :	—
169467	20 :	*	*	*	*	*	*	10 :
180163	37	*	*	*	*	*	*	—
184171	15	*	*	*	*	*	*	—
184930	14	*	*	*	*	*	*	—
195810	5 :	*	*	*	*	*	*	—
207971	*F*	*	*	*	*	*	*	—
214680	18	*	*	16	*	*	23	—
218376	111	29	5 :	54	38	65	109 :	—

Table 5.ii (contd.)

Nitrogen III

HD	4515	4524	4634	4641
15371	*	*	*	*
74575	*	*	*	*
79351	*	*	*	*
81188	*	*	*	*
106625	*	*	*	*
111123	*	*	*	*
116658	*	*	*	*
118716	*	*	*	*
129056	*	*	*	*
132200	*	*	*	*
147165	*	*	*	*
147394	*	*	*	*
149438	40	22	36	66
165024	*	*	*	*
166182	*	*	*	*
169467	*	*	*	*
180163	*	*	*	*
184171	*	*	*	*
184930	*	*	*	*
195810	*	*	*	*
207971	*	*	*	*
214680	65	20	26	56
218376	*	*	*	*

Table 5.ii (contd.)

Oxygen II

HD	4072	4087	4093	4317	4326	4415	4417	4591	4596	4649
15371	*	*	*	5	*	11	8	*	*	10
74575	105	36	43	104	29	140	124	90	71	197
79351	35	*	*	34	*	46	22	11	6	41
81188	59	*	*	51	23	66	62	43	46	60
106625	*	*	*	*	*	*	*	*	*	*
111123	226	43	56	164	93	213	195	190	188	196 :
116658	*B*	*B*	*B*	*B*	*B*	*B*	*B*	*B*	*B*	*B*
118716	157	35 :	40 :	75	*	132	159	82	90	144 :
129056	123	30	33	99	36	124	133	84	65	187
132200	64	10	*	44	13	66	53	32	36	82
147165	*B*	*B*	*	100 :	60 :	*B*	*B*	81 :	87 :	*B*
147394	*	*	*	*	*	*	*	*	*	*
149438	84	24	27	78	55	88	85	83	78	120
165024	124 :	38	*	108	*	174 :	127 :	139	126	*B*
166182	48	13	*	59	10	49	29 :	30	26	68
169467	*	*	*	*	*	*	*	*	*	*
180163	17	*	*	14	*	27	25	*	18	20
184171	11	*	*	*	*	16	10	*	*	*
184930	*	*	*	*	*	*	*	*	*	*
195810	*B*	*	*	10 :	*	8 :	*	*	*	*
207971	*	*	*	*	*	*	*	*	*	*
214680	*B*	*	*	28	*	24	42	*	*	48
218376	171	27	32 :	131	32	146	134	167	101	249 :

Table 5.ii (contd.)

Silicon II

HD	3854	3856	3863	4128	4131	5041	5056	6347	6371
15371	69	110	104	90	94	75	110	229	198
74575	—	—	—	35	40	11	8	—	—
79351	—	—	—	67	87	33	59	—	—
81188	—	—	—	59	66	27	44	—	—
106625	—	—	—	160	152	126	145	—	—
111123	—	—	—	*	*	*	*	—	—
116658	—	—	—	*	*	*	*	—	—
118716	—	—	—	*	*	*	*	—	—
129056	—	—	—	28	33	17	29	—	—
132200	—	—	—	44	50	34	50	—	—
147165	—	—	—	*	*	*	*	—	—
147394	77	133	111	100	102	—	—	—	—
149438	—	—	—	*	*	*	*	—	—
165024	*B*	*B*	41	*B*	*B*	19 :	48 :	*	*
166182	15 :	45	34	40	39	—	—	—	—
169467	41	87	74	68	83	74	106	150	89
180163	59	117	101	89	100	—	—	—	—
184171	53	94	92	73	84	—	—	—	—
184930	59	118	111	118	130	—	—	—	—
195810	82	153	135	122	144	—	—	—	—
207971	66	143	112	117	123	102	174	228	188
214680	*	*	*	*	*	—	—	—	—
218376	*	*	*	*	*	—	—	—	—

Table 5.ii (contd.)

Silicon III

HD	4552	4567	4575	4813	4820	4829
15371	19	8	*	*	*	*
74575	208	168	117	30	42	56
79351	77	57	28	9	17	6
81188	152	110	69	20	27	*
106625	*	*	*	*	*	*
111123	335	264	185	47	73	60
116658	223 :	144 :	114 :	33 :	42 :	43 :
118716	175	130	85	20	40	28
129056	285	213	137	41	54	45
132200	118	91	66	17	28	32
147165	239	187	128	28 :	32 :	35 :
147394	27	20	15	*	*	*
149438	113	93	60	15	28	18
165024	324	224	186	*B*	*B*	108 :
166182	107	60	26	—	—	—
169467	42	27	10	*	*	*
180163	61	35	21	*	*	*
184171	43	26	10	*	*	*
184930	*	*	*	*	*	*
195810	*	*	*	*	*	*
207971	*	*	*	*	*	*
214680	47	40	20	*	*	*
218376	260	198	103	15	38	24

Table 5.ii (contd.)

Silicon IV

HD	4089	4116	4212	4631	4654
15371	*	*	*	*	*
74575	64	47	*	*B*	*
79351	*	*	*	*	*
81188	26	10	*	*	*
106625	*	*	*	*	*
111123	262	178	37	*	43
116658	42 :	*	*	*	*
118716	118 :	90 :	23 :	26 :	18 :
129056	47	27	*	*	*
132200	23	*	*	*	*
147165	*B*	*B*	15	*	*
147394	*	*	*	*	*
149438	167	146	29	64	74
165024	139	78	*	*	*
166182	*	*	*	*	*
169467	*	*	*	*	*
180163	*	*	*	*	*
184171	*	*	*	*	*
184930	*	*	*	*	*
195810	*	*	*	*	*
207971	*	*	*	*	*
214680	253	157	48	31	72
218376	219 :	109	*	*B*	10 :

Table 5.ii (contd.)

	Sulphur II				Sulphur III			
HD	3923	4816	4925	5014	3984	4285	4362	4365
15371	18	26	30	22	*	*	*	*
74575	—	5	*	27	34	31	21	16
79351	—	19	29	34	—	*	*	*
81188	—	15	*B*	23	—	*B*	*	*
106625	—	*	*	14	*	*	*	*
111123	—	10 :	10 :	5 :	—	*B*	63	43
116658	—	*B*	*B*	*B*	—	*B*	*B*	*B*
118716	—	*	*B*	*	—	56	14 :	*
129056	—	12	*	*F*	—	26	27	13
132200	—	17	14	33	—	*	*	*
147165	—	*	*B*	*B*	—	*B*	*	*
147394	*	*	—	—	*	*	*	*
149438	—	*	*	*	—	30	17	10
165024	*B*	*	*B*	*B*	*B*	*B*	23 :	*B*
166182	*	—	—	—	*B*	*	*	*
169467	*	*	*	*B*	*	*	*	*
180163	23	10 :	—	—	*	*	*	*
184171	6	*	—	—	*	*	*	*
184930	*	*	—	—	*	*	*	*
195810	10	*	—	—	*	*	*	*
207971	*	*	—	—	*	*	*	*
214680	*	*	—	—	*B*	21	23	17
218376	12	16	—	—	9	*B*	36	21

Table 5.ii (contd.)

	Magnesium II				Aluminium III	
HD	4385	4391	4434	4481	4513	4529
15371	20	33	10	272	*	8
74575	*	*	*	146	34	59
79351	16	18	24	203	28	53
81188	*	5	7	172	24	47
106625	46 :	44	24	417	*	*
111123	*	*	*	165	57	88
116658	*B*	*B*	*	218 :	*	*B*
118716	*	*	*	86 :	*	28 :
129056	*	19	7 :	187	45	75
132200	*	23	*	195	*	10
147165	*	*	*	168	25 :	*B*
147394	28	58	34	272	*	*
149438	*	14	*	78	19	38
165024	*B*	*B*	*B*	210	58	*B*
166182	*	*	*	134	10	26
169467	*	*	*	185	*	*
180163	*	23	*	167	*	10 :
184171	*	*	*	220	*	*
184930	*	*	*	234	*	*
195810	31	43	*	313	*	*
207971	23	46	*	334	*	*
214680	*	*	*	68	*	*
218376	*	*	*	87	16	31

Table 5.ii (contd.)

Hydrogen, W_{75}, D_β

HD	H_γ	W_{75}	H_δ	D_β
15371	4400	6670	4700	.80
74575	2820	3190	2750	.30
79351	5950	8000	5990	—
81188	5550	8500	6010	.42
106625	8360	12600	—	.91
111123	3330	4300	3100	.22
116658	4600 :	6000 :	4740 :	.32 :
118716	3180	3800	3410	.29
129056	3620	4700	3710	.40
132200	5360	7200	5680	.36
147165	3650	5000	3950	.27
147394	7710	11500	8040	.59
149438	2840	2800	3280	.15
165024	2190	3100	2280	.30
166182	3910	3500	4240	—
169467	4960	5800	5200	.58
180163	4140	4900	4070	—
184171	4820	5200	5240	—
184930	6910	8400	7130	—
195810	8210	12200	8460	—
207971	8950	9300	8740	—
214680	2110	1600	1980	.12
218376	2690	2000	2760	—

The equivalent widths, W, were then used to determine values for the effective temperature, T_{eff}, logarithmic surface gravities, $log\ g$, microturbulent velocities, ξ_t, and elemental abundances, $[X]$, for the programme stars. (Element abundances are expressed in logarithms relative to [H]=12.0). Both LTE and non-LTE models were used independently to derive values.

LTE Analysis

A grid of stellar photosphere models was calculated using the ATLAS computer program described previously. The range of T_{eff} of these models was 12000K↦ 35000K and log g varied from 3−4.5. A full list of the models is given in Table 5.iii.

The photospheric structures output by this program were then used as input to the WIDTH6 program. This program calculated equivalent widths for the lines identified with a W in the line list in Table 5.i.

Equivalent widths for each line were predicted at intervals of 0.25dex over the range $([X]_{\odot} - 1.25 \mapsto [X]_{\odot} + 1.00)$ and at values of ξ_t of 0,5 and 10 $km\ s^{-1}$. Occasionally predictions for higher values of ξ_t had to be calculated.

For lines identified with a P in Table 5.ii it was necessary to explicitly calculate line profiles with the WIDTH6 program. These are lines which are complex blends of components insufficiently separated to be treated independently and too widely separated or of too similar strengths to be treated as a single line.

Individual components were combined to give a line profile for the blend and this profile was integrated using *Simpson's Rule* in a manner similar to that used for the observed equivalent widths.

Profiles were calculated only at intervals of 0.5 in [X] and the integration only carried out at points indicated by the results from other lines.

Having derived a grid of predicted equivalent widths for a number of lines these were used to determine the photospheric parameters in the following conventional way. Figures 5.1 - 5.23 illustrate the solutions found for each individual star.

The abundances required to reproduce the observed equivalent widths of every line of each element represented by more than one stage of ionisation were first calculated. Linear interpolation was used between the predicted values. This was done at all tabulated

Table 5.iii

Grid of LTE Models

	$\log g$				
T_{eff}	3.0	3.5	3.75	4.0	4.5
12000	+			+	
13500	+			+	
15000	+			+	
17500	+			+	
20000	+	+		+	
22500	+	+		+	
25000	+	+		+	
27500		+	+	+	
30000			+	+	+
32500			+	+	+
35000				+	+

values of ξ_t for four model photospheres. The four models were chosen so as to have two values of T_{eff} at each of two values of log g such that the sign of the difference in abundance between ions of the same element changed between models of different T_{eff}.

Mean abundances and standard deviations were then calculated for each ion. Both the variation of the standard deviation with ξ_t and the trend of [X] with W for the lines of an ion were investigated for a minimum. If necessary abundances at values of ξ_t intermediate to those calculated for the grid were interpolated linearly from those already found. In general values of the standard deviations minimised at the same value of ξ_t that showed the least trend of [X] with W. The scatter amongst different ions was usually $< 3km\,s^{-1}$. A value of ξ_t was chosen from weighting these values from individual ions according to the number and quality of lines and the atomic weight of the ions concerned.

Values of T_{eff} at which ionisation equilibrium (i.e. equal abundances from each of 2 ions) occurred were then calculated for each pair of ions of each element at both values of log g. This was done by interpolating linearly between the grid temperatures to find the temperature at which the abundance difference between ion pairs went to zero.

The locus of points linearly connecting the two (T_{eff}, log g) points was assumed to represent the range of acceptable solutions.

The equivalent width and W_{75} of H_γ were used in conjunction with the published H_γ line profiles of Kurucz, 1980, and the D_β value with the values calibrated by Underhill (Underhill and Doazan, 1982), also calculated with the ATLAS6 model photosphere programme to define similar loci.

All the loci were plotted and the values of T_{eff} and log g which gave the most acceptable solution determined. Consideration was given to the number of lines and accuracy of each defining locus in determining the solution.

Finally abundances for all the lines were interpolated to the point of solution. Mean abundances were calculated for each ion and a check was made that the ionisation equilibrium constraint was still satisfied.

Non – LTE Analysis

The non-LTE analysis was based on the grid of calculations made for lines of silicon by Kamp, 1974, 1976. This is the only work which presents results for lines of a metallic

element in more than one stage of ionisation. Use was also made of the calculations for hydrogen lines (Mihalas, 1972) and nitrogen II lines (Dufton and Hibbert, 1982). All these calculations use as their basis a programme by Mihalas which calculates a model photosphere allowing for the departures from LTE of hydrogen,helium and a mean light element. Only the silicon and hydrogen line calculations and values of D_β calculated from the Mihalas models were used in determining values of T_{eff}, log g and ξ_t (although the nitrogen lines were used to check this latter parameter).

The grid of silicon line predictions is tabulated at 2500K intervals in T_{eff} and at values of log g of 3.0 and 4.0.(Additional values of surface gravity are also sometimes tabulated). Values of 0, 5 and sometimes 15 $km\ s^{-1}$ are used for ξ_t. In the main the calculations are only made for [Si]=7.50. Kamp, 1978, however, has shown that the slope of the curve of growth for non-LTE line calculations is similar to that in the LTE case.

He shows that the slope,D, defined by

$$D = \frac{\delta(\log(W))}{\delta([Si])}$$

can be closely approximated by

$$D = 0.9167 - 0.0833\log(\tau_0) - Q \times \cos(\log(\tau_0) - 2.0)$$

where τ_0 is the central optical depth of the line and Q is a parameter determined from the model (it is ≈ 0.5).

This assumption is clearly only valid for values of [Si] close to 7.50. The results obtained will show that this is a justified assumption.

A method similar to that adopted for the LTE analysis was followed here. The abundances required to reproduce the observed strengths of the silicon lines were calculated using the formulae given above for models at two or three effective temperatures at each of two values of the surface gravity. Abundances were calculated for models with $\xi_t = 0 km s^{-1}$ and $\xi_t = 5 km s^{-1}$ (and where appropriate $\xi_t = 15 km s^{-1}$). Abundances at other values of ξ_t were interpolated or extrapolated linearly using these.

Mean abundances and standard deviations for the lines of each ion were then calculated. Again the standard deviations and the trend of [Si] with W were investigated to determine ξ_t.

Effective temperatures at which the derived abundances for each pair of ions were equal were then found as before for both surface gravities.

A similar process was undergone for the equivalent width and W_{75} of H_γ and for D_β using the tabulations of Mihalas, 1972.

All the loci of the solutions were then plotted as for the LTE analysis and the solution best satisfying all parameters chosen. Silicon and nitrogen abundances were then interpolated from the respective theoretical grids. The work of Dufton and Hibbert presents results for 6 lines of nitrogen II, of which 4 (the lines at 3995Å, 4228Å, 4447Å and 4631Å) were included in this study. The predictions are made at up to 6 values of [N] over the range $7.1 < [N] < 8.6$ and for $\xi_t = 0$ and $\xi_t = 5\ km\ s^{-1}$. Unfortunately they present results only for model photospheres with $\log g = 4.0$. This should not cause too great an error for most of the stars in this survey if the effect of varying the surface gravity on the non-LTE models is the same as that for the LTE models. Here the effect of reducing $\log g$ from 4.0 to 3.0 at effective temperatures less than about 25000K is to reduce the required nitrogen abundance by$\approx$ 0.2 dex. Abundances for each line were linearly interpolated (or extrapolated) in their tables for both$\xi_t = 0km\ s^{-1}$ and$\xi_t = 5km\ s^{-1}$. Values at the value of ξ_t indicated from the silicon lines were also calculated from these results. The mean and standard deviations were calculated as before and the trend of [N] with W investigated. The values of ξ_t derived from the silicon lines were, in general, completely compatible with the nitrogen line results.

5.vi *The Results*

Values of T_{eff}, $\log g$, and ξ_t calculated with the LTE models are given in Table 5.iv while those found using the non-LTE models are listed in Table 5.vi. Table 5.v shows the resuluts of the abundance determinations for [C],[N],[O], [Mg],[Al],[S] and [Si] from the LTE analysis while Table 5.vii gives the non-LTE values of [N] and [Si].

The graphical solutions for each star are displayed in figures 5.1↦5.23. The LTE solution is displayed in part (a) (upper) of each figure while the lower portion (part (b)) is the non-LTE solution. Each locus of solution is identified by the parameters used to define it and the chosen solution is marked with a + .

Before discussing the errors involved and comparing the results of the two analyses

Table 5.iv

LTE Solutions

HD	T_{eff}	$\log g$	ξ_t
15371	13500	3.1	3.
74575	22200	3.1	10.
79351	20600	4.1	8.
81188	23200	4.1	10.
106625	11800	3.4	3.
111123	26200	3.4	13.
116658	23500	3.9	10.
118716	26300	3.8	10.
129056	22500	3.5	15.
132200	23500	4.1	7.
147165	27100	4.1	10.
147394	16200	4.0	2.5
149438	31750	4.1	5.
165024	22800	3.1	15.
166182	20100	3.3	5.
169467	16300	3.1	3.
180163	16500	2.9	5.
184171	16600	3.1	5.
184930	14500	3.5	3.
195810	13600	3.7	4.
207971	12200	3.5	3.
214680	33000	3.9	10.
218376	26700	3.5	15.

Table 5.v

LTE Abundances

HD	*C*	*N*	*O*	*Mg*	*Al*	*S*	*Si*
15371	8.4	7.7	8.5	7.4	6.1	7.0	7.3
74575	7.9	7.7	8.6	7.2	5.9	6.7	7.2
79351	8.2	7.5	8.1	7.6	6.1	6.9	7.0
81188	8.1	7.7	8.4	7.2	5.9	7.0	7.2
106625	8.3 :	—	—	7.3	—	< 7.3	7.6
111123	8.4	7.7	8.6	7.6	6.3	7.0	7.4
116658	—	—	—	—	—	—	7.2 :
118716	8.0	7.5	8.3	7.3	5.9	6.3 :	7.1
129056	8.1	7.6	8.3	7.6	6.0	6.6	7.0
132200	7.9	7.2	8.2	7.6	5.2 :	7.0	7.1
147165	7.8	7.5	8.4	7.8	6.0	—	7.2
147394	8.2	7.9	—	7.6	—	—	7.5
149438	8.1	7.9	8.6	7.6	6.3	6.7	7.6
165024	7.7	7.9	8.3	7.4	6.0	6.4	7.3
166182	7.7	7.7	8.4	7.3	5.5	—	7.0
169467	8.2	7.2	—	7.2	—	—	7.0
180163	7.8	7.4	8.5	7.3	5.5	6.6	7.1
184171	7.9	6.9	8.1	7.8	—	6.3 :	6.9
184930	8.0	7.5	—	—	—	—	7.3
195810	8.3	7.2 :	8.9 :	7.3	—	6.9 :	7.1
207971	8.0	—	—	7.2	—	—	7.3
214680	7.6	7.5	7.9 :	7.4	—	7.0	7.1
218376	7.8	7.6	8.3	7.1	5.7	6.8	7.1
Mean	8.01	7.53	8.38	7.42	5.94	6.79	7.20
S.D.	.22	.26	.24	.21	.25	.23	.19

Table 5.vi

Non-LTE Solutions

HD	T_{eff}	$\log g$	ξ_t
15371	14800	2.9	3.
74575	24200	3.2	5.
79351	23700	4.2	5.
81188	26000	4.2	5.
106625	12700	3.4	3.
111123	28500	3.7	7.
116658	24800	3.8	5.
118716	27000	3.5	5.
129056	24500	3.5	10.
132200	25700	4.2	3.
147165	28800	4.1	8.
147394	18600	4.1	2.5
149438	33900	3.8	0.
165024	23100	2.9	10.
166182	20800	3.1	5.
169467	17500	3.1	0.
180163	17500	2.9	3.
184171	16800	3.0	0.
184930	15000	3.3	0.
195810	$<$ 15000	$<$ 3.7	3.
207971	$<$ 15000	$<$ 3.8	5.
214680	36800	3.7	5.
218376	26300	3.2	13.

Table 5.vii

Non-LTE Abundances

HD	*N*	*Si*
15371	—	7.1
74575	8.0	7.2
79351	7.3	7.0
81188	7.7	7.3
106625	—	7.3
111123	7.7	7.7
116658	—	7.5
118716	7.3	7.3
129056	8.0	7.1
132200	7.4	7.4
147165	7.4	7.4
147394	7.4	7.3
149438	7.8	7.7
165024	—	7.4
166182	8.3	6.8
169467	—	7.2
180163	—	7.3
184171	—	7.2
184930	—	7.5
195810	—	< 7.6
207971	—	< 7.7
214680	> 7.2	7.4
218376	7.6	7.0
Mean	7.66	7.29
S.D.	0.33	0.22

and the implications of these some comments relating to individual stars will be given.

HD 15371

This star has been given an MK spectral classification of B8 III, B5 III or B5 IV by various authors. The former is in better agreement with the LTE result. HD 15371 is one of the few stars for which measurements of the Si II lines at 6347Å, and 6371Å could be made. These lines are predicted by Kamp to show the strongest evidence for departures from LTE. While the measured equivalent widths of these lines are somewhat uncertain as they come from only one 103aF plate with spot sensitometer calibration this hypothesis does seem to be borne out.

The LTE calculations showed that with a ξ_t of $5 km\ s^{-1}$ these two lines required an abundance of silicon$\approx$ 1.0 dex higher than the average of the other lines. Even with $\xi_t = 10 km\ s^{-1}$ this excess was only reduced to $\approx$ 0.4 dex, although there was then a strong trend of decreasing abundance with increased equivalent width for the other lines. An abundance difference of 1.0 dex was$\approx$ 4 times the standard deviation found from the other lines. For this reason the lines were excluded from the LTE solution and abundance determination.

The situation was improved by the use of the non-LTE calculations. Even here, however, at $\xi_t = 2.5 km\ s^{-1}$ these lines required a value of [Si]$\approx$ 0.4 dex larger than the mean derived from the other lines. At $\xi_t = 5.0\ km\ s^{-1}$ the excess was reduced to $\approx$ 0.2 dex, only 1.25 times the standard deviation of the other lines. The two lines were again omitted from the solution as the other lines clearly excluded a value for ξ_t as high as $5\ km\ s^{-1}$.

The aluminium abundance derived in the LTE analysis should be treated with some caution as it results from measurements of only one line.

HD 74575

In the LTE solution the temperatures derived from the silicon ionisation eqilibria are in good agreement. The carbon and sulphur equilibria and the D_β loci are, however rather discordant. The spread amongst the silicon ionisation is somewhat greater in the non-LTE analysis but the D_β measurement comes into better aggreement.

This star has also been studied by Kane *et al*,1980, (hereafter, *KMD*) who quote

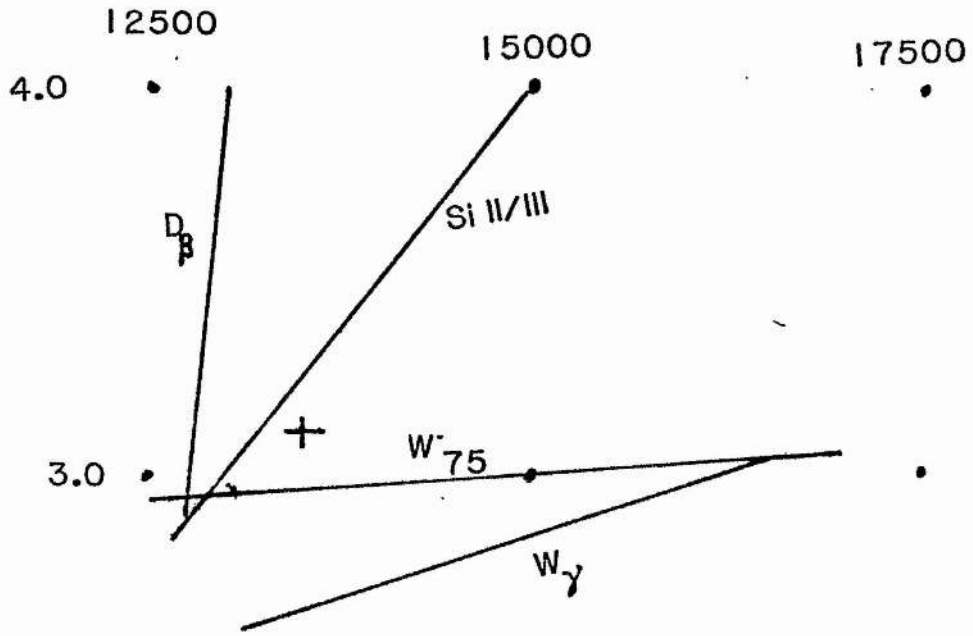

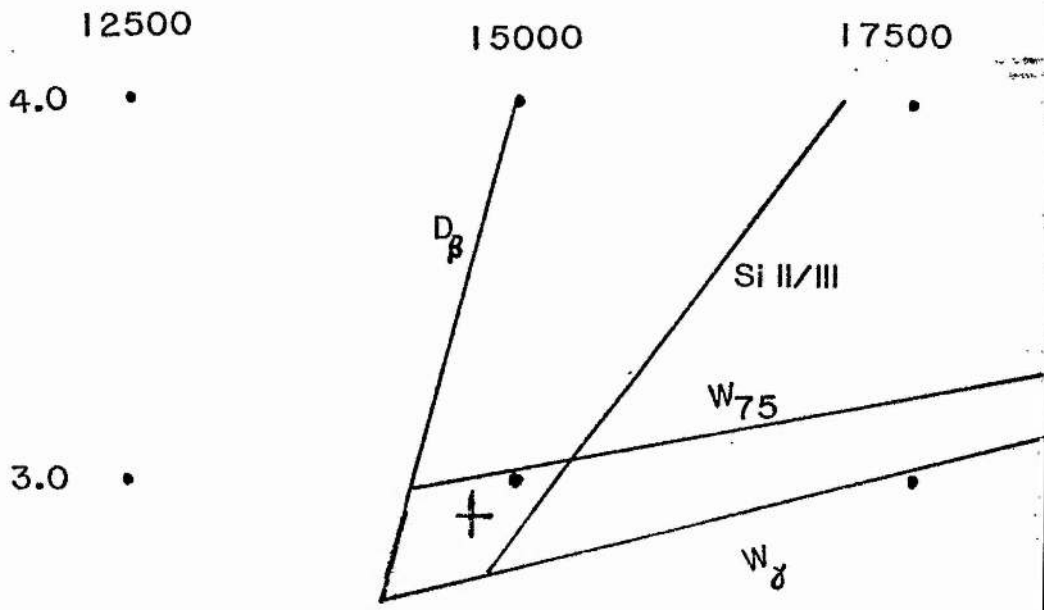

Fig. 5.1 :- LTE (upper) and non-LTE solutions for T_{eff} and $\log g$ determined graphically for HD 15371. Loci given by individual criteria are shown by solid lines labelled by that criterion and the overall solutions are indicated thus +.

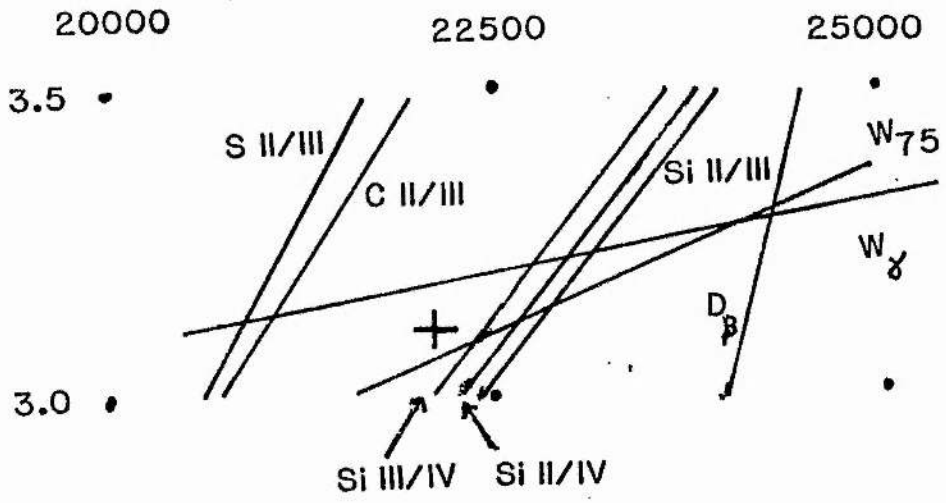

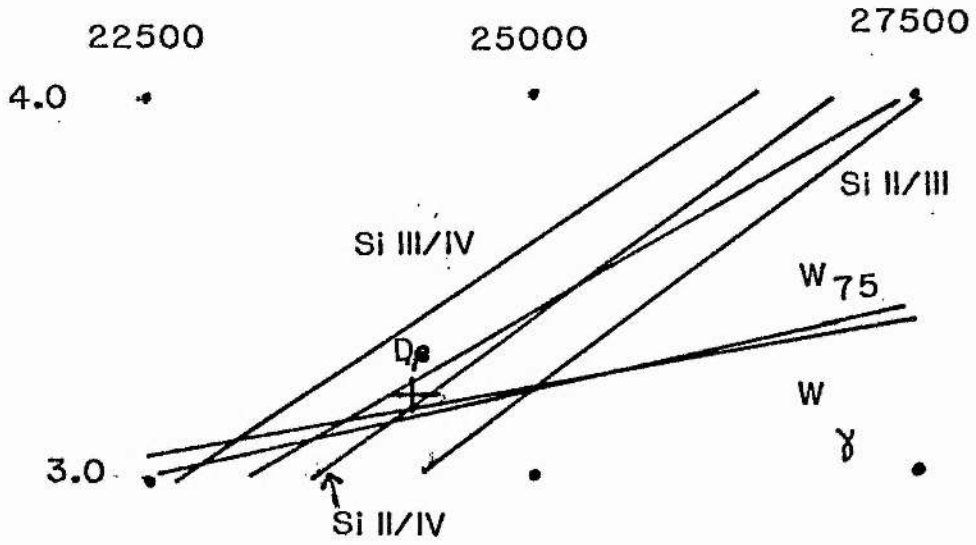

Fig. 5.2 :- As figure 5.1 for HD 74575.

a spectral type of B2 III and is included in the sample of *UDPD* who give B1.5 III. The latter derive an effective temperature of 23723K by deriving the stellar diameter from a fit to the red and infrared continuum photometry of the star using the Kurucz ATLAS6 model atmosphere programme used here and by integrating the flux at other wavelengths. They assume a *log g* of 3.5. A more detailed comparison of the results of *UDPD* with those derived here will be given later.

KMD derive values of 25700K and 3.75 for T_{eff} and log g respectively from the $[c_1]$ and β indices of HD 74575. Of the eight lines included in their study, four (CII 4267Å,NII 3995Å,4630Å and OII 4649Å) are also analysed here. Rather unsatisfactory agreement is found between the two sets of equivalent widths. Only the difference in measurements of the NII 3995Å is within the observational error of this study, the other lines being $50\% - 70\%$ larger in their analysis than in this. *KMD* found anomalous abundances for this star in comparison with other members of the Sco–Cen association. The abundances found here are, however, in better agreement with those found by Kane *et al* for the other stars. In particular the abundances of carbon and nitrogen relative to oxygen are brought more into agreement.

HD 79351

The effective temperature is better defined in the LTE analysis than in the non-LTE analysis in this case. This is both because the CII/CIII ionisation equilibrium can be used and because the slope of the SiII/SiIII equilibrium solution in the T_{eff}, log g plane is shallower in the non-LTE solution.

The nitrogen lines were very weak and gave a low value for [N], particularly in the non-LTE analysis. This underabundance is conservative because of the use of a log g = 4.0 model. The value of ξ_t used has little effect on the derived abundance and even at $T_{eff} = 20000K$ the derived abundance would be 7.7 dex.

HD 81188

The non-LTE ionisation equilibria loci are in much better agreement with each other than are those found with the LTE models. The locus defined by D_β is however not in good agreement with either set of ionisation equilibria. No reason for this discrepancy could be found and so D_β was ignored when the solutions were determined.

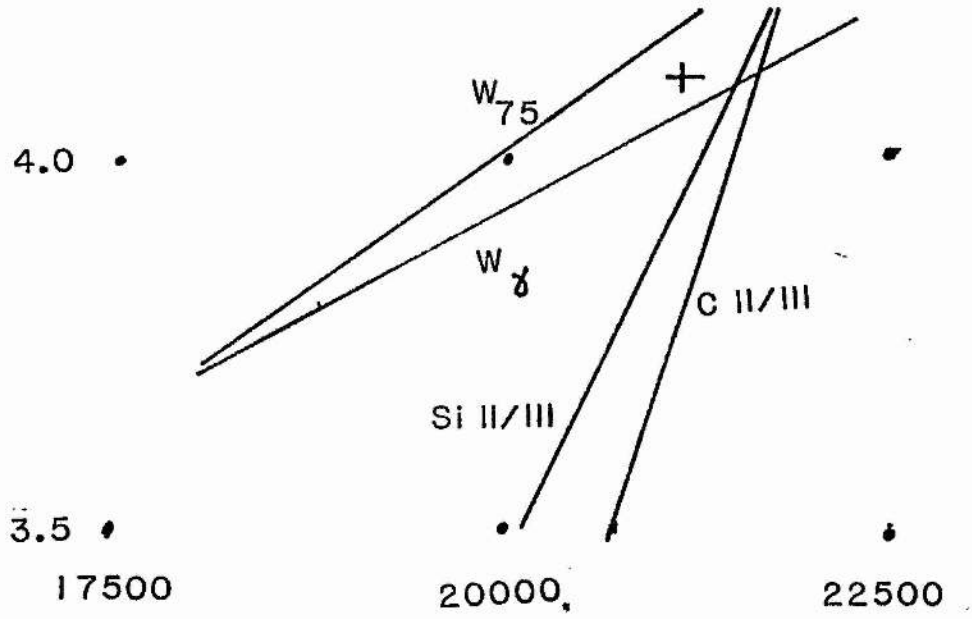

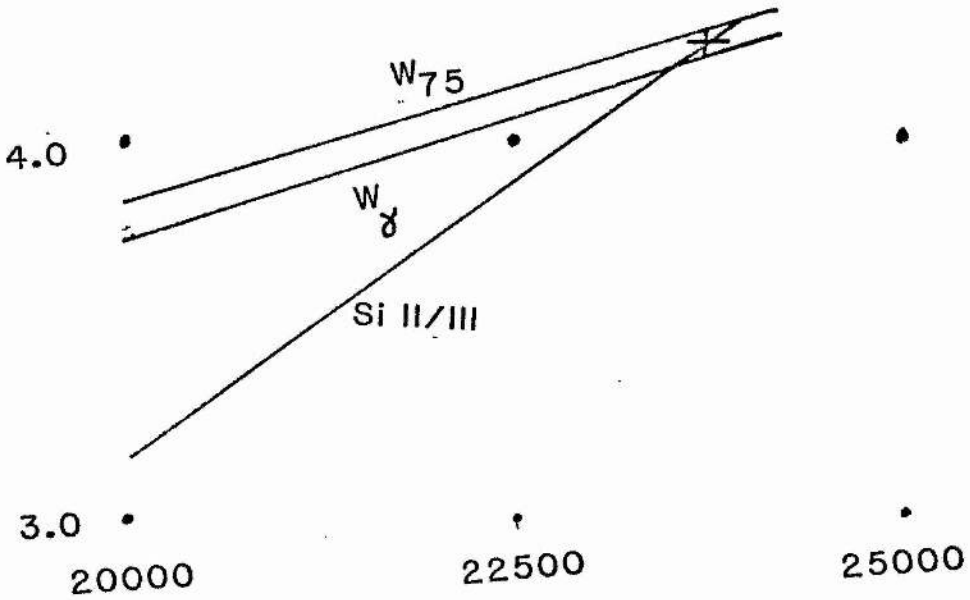

Fig. 5.3 :- As figure 5.1 for HD 79351.

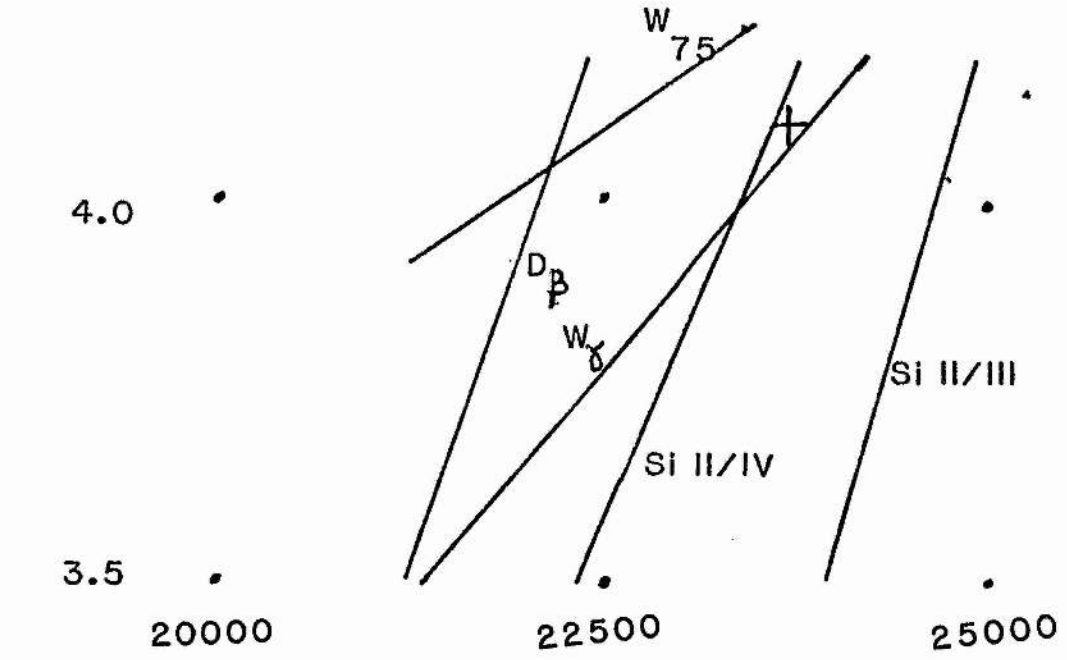

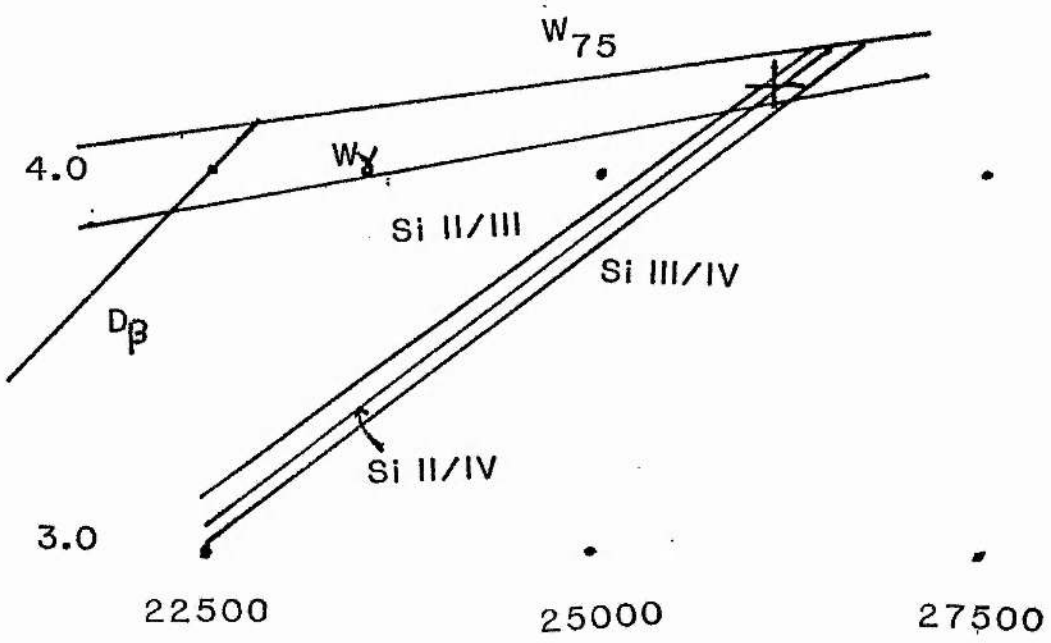

Fig. 5.4 :- As figure 5.1 for HD 81188.

This was one star where the values of ξ_t indicated by different elements were not in accord. While the silicon lines suggested a value of $12.5 km\,s^{-1}$, the nitrogen and oxygen lines had minima in their respective standard deviations at $\xi_t = 5 km\,s^{-1}$ and $7.5 km\,s^{-1}$ respectively. Rather higher weight was given to the silicon line evidence as these lines are rather more sensitive to ξ_t. The higher value of ξ_t reduces the deduced carbon and nitrogen abundances by $\approx$ 0.1 dex while to reduce the value of ξ_t to $5\,km\,s^{-1}$ would increase the required silicon abundance by $\approx$ 0.25 dex.

HD 106625

As lines of only one ion of any one element were present in the measurements the solutions could only be determined from the H_γ and D_β information. The derived non-LTE silicon abundance is rather insensitive to the assumed effective temperature and surface gravity, however, and is therefore fairly well determined despite having to be calculated by extrapolating outside the Kamp grid. Formally the standard deviation in the abundances derived from the silicon lines minimised at a T_{eff} of 15500K. The detection of very weak features which might be the NII lines at 4647 Å and 4631Å suggest that the LTE solution may underestimate the effective temperature by $\approx$ 750K.

HD 111123

The H_γ data agree rather better with the ionisation equilibria derived with the non-LTE models than with those derived using the LTE models. A rather higher value of log g is determined with the former.

A number of other authors have analysed the spectrum of this star. Watson, 1971 presents an LTE analysis in which he derives an effective temperature of 24700K and a log g of 3.85. He derives (logarithmic) abundances of C, N, Mg, Al, Si and S relative to oxygen of -0.4, -1.1 -1.6, -2.4, -0.65, and -1.7 respectively. These can be compared with values of -0.2, -0.9, -1.0, -2.3, -1.2 and -1.6 derived in this study. The discrepancies for Mg and Si are caused partly by his assumption of a value of $4\,km\,s^{-1}$ for the value of ξ_t and partly by his use of a triangular approximation to the line profiles. This latter assumption will cause large errors, particularly for the Mg II line at 4481 Å.

Balona and Feast, 1975, and Balona, 1976, from a study of the He I lines at 4144Å, 4388Å, 4026Å, and 4471Å and the H_γ line derive an effective temperature of 25600K.

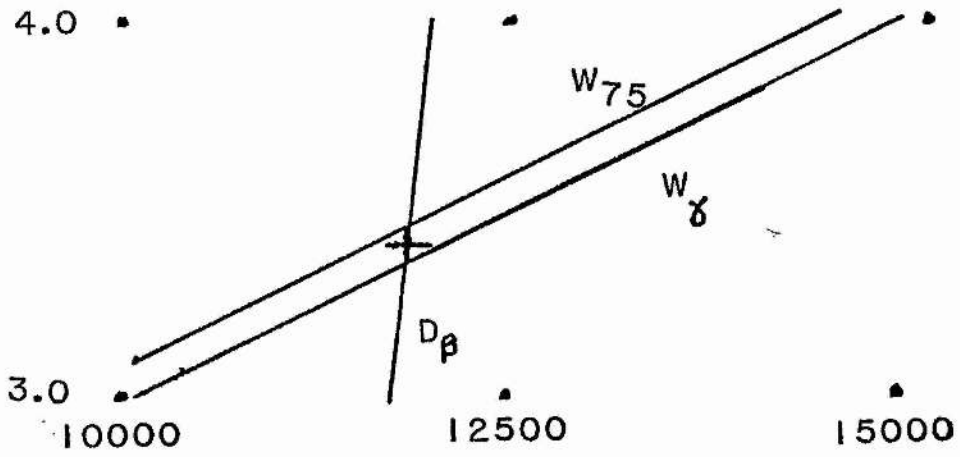

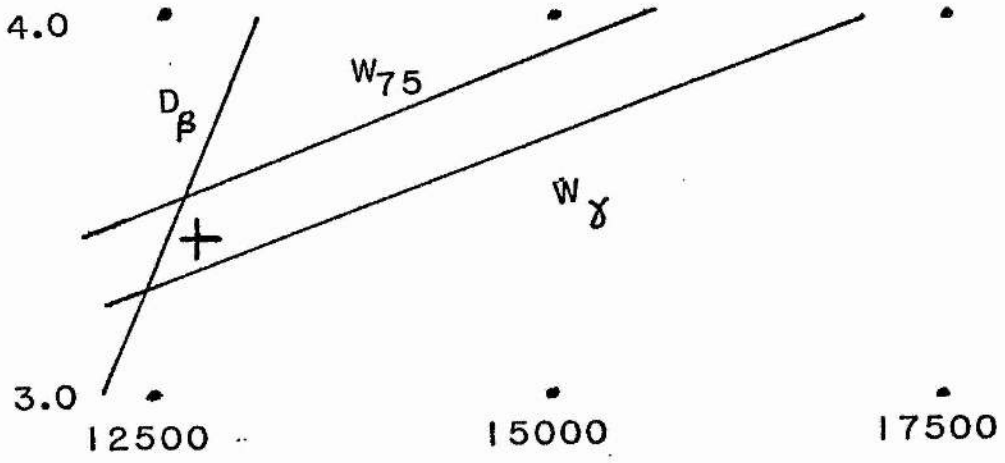

Fig. 5.5 :- As figure 5.1 for HD 106625.

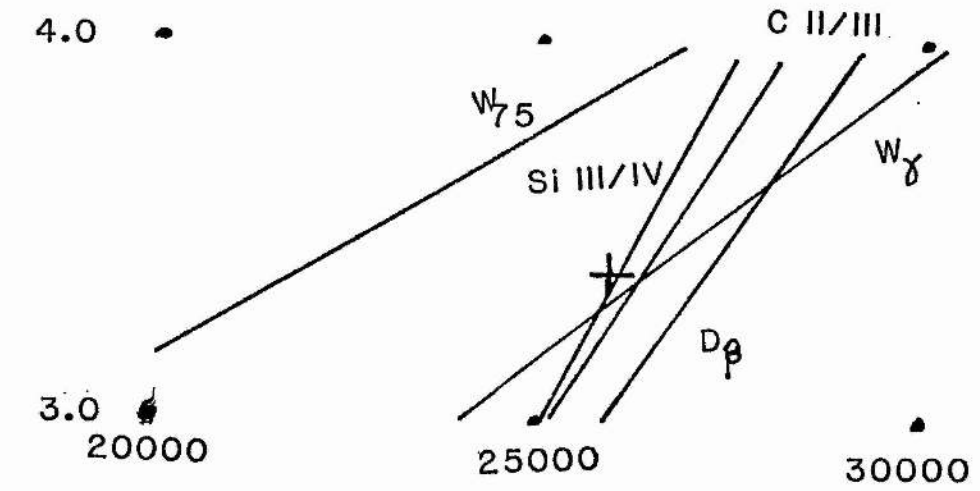

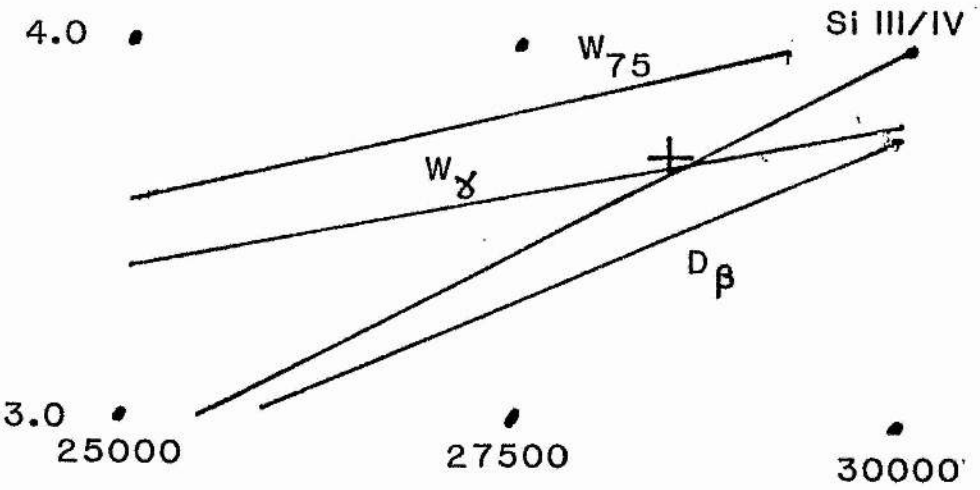

Fig. 5.6 :- As figure 5.1 for HD 111123.

The equivalent widths they find are in good agreement with those found here.

Code *et al*, 1976, find a value for T_{eff} of 26600K with an error of 1100K using data on the angular diameter obtained with an intensity interferometer (Hanbury-Brown *et al*, 1974).

HD 116658

Analysis of the spectrum of this star was complicated by the fact that the star is a binary. The primary has an MK spectral type of B1 IV (Balona and Feast, 1975) and Popper, 1980, quotes a spectal type of B4 for the secondary. The secondary contributes $\approx$ 15% to the total visual light of the system. At the time of observation the separation of the two spectral components was $\approx 100\ km\ s^{-1}$. Although the rotational broadening of the spectral lines of the primary is large, giving rise to line widths of the order of the separation of the spectral components, it was possible to measure equivalent widths for a number of the absorption lines of the primary. This was done using the analytic line fitting function described earlier and also used for blended lines. The technique of Struve, 1930, was used to correct the equivalent widths obtained in this manner for the influence of light from the secondary. While the measurements obtained should thus be reasonably accurate some uncertainty must be introduced to the analysis.

Despite these cautionary factors the LTE solution is in good agreement with the results of Code *et al*, 1976 Watson, 1971 and Kurucz, 1979, who all derive effective temperatures within 100K of 23850K and a mean log g of 3.8.

HD 118716

The LTE solution is very poorly defined.

Balona and Feast, 1975, find an effective temperature of 23000K for this star.There is, however, no evidence for the lines of Si II at the strength that would be expected at that temperature. In addition the Si III, Si IV and C III lines are much stronger than would be expected if the effective temperature was as low as 23000K.

The values derived by *KMD*, 1980, of $T_{eff} = 26500K$ and $\log g = 3.85$ are in better agreeement with the solution derived here, although there is again some discrepancy between the measured equivalent widths in common with those used here.

The spectral lines of this star show a marked assymetry(figure 5.8 (c)). This could

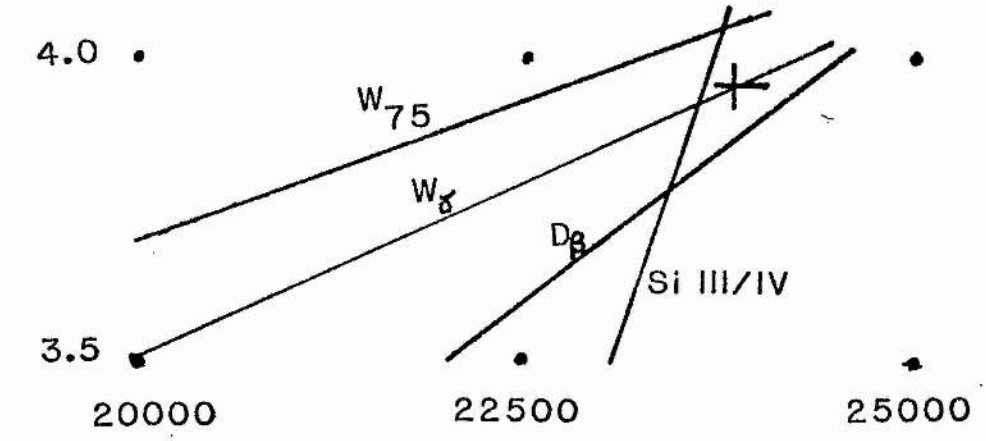

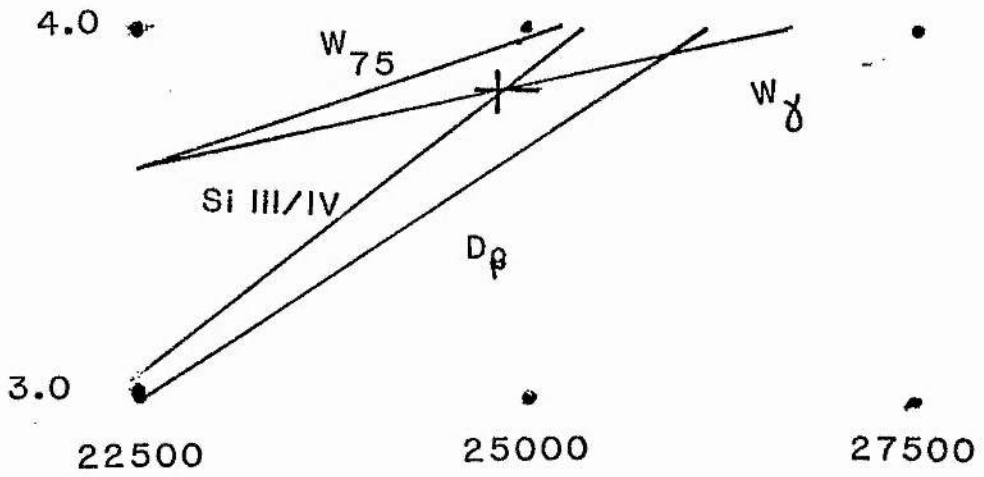

Fig. 5.7 :- As figure 5.1 for HD 116658.

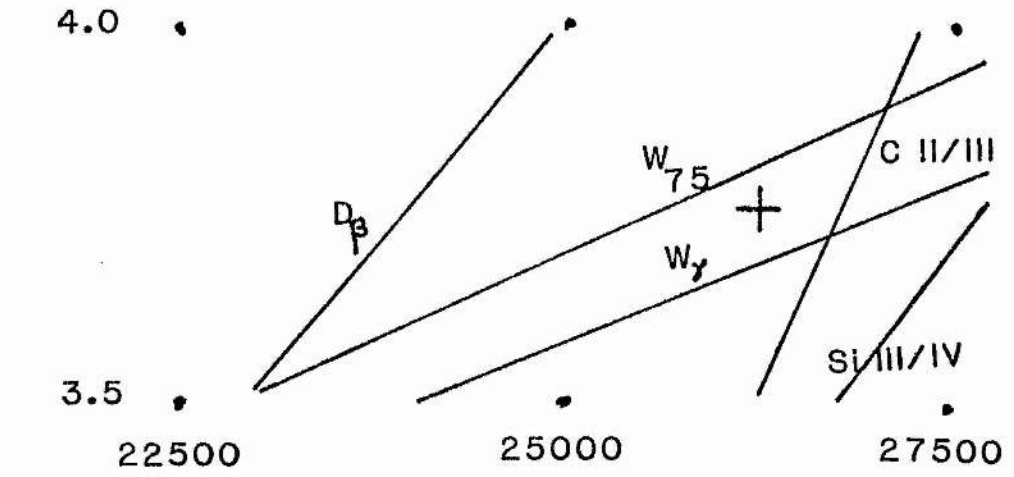

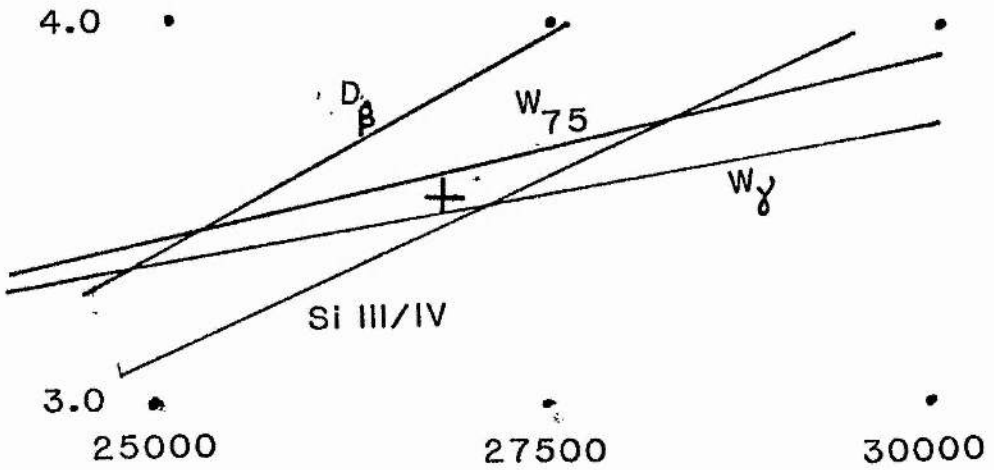

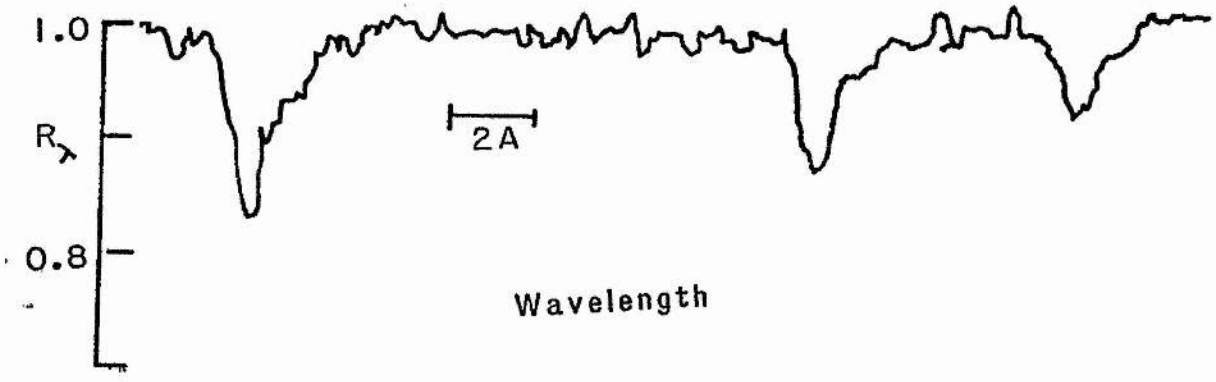

Fig. 5.8 :- As figure 5.1 for HD 118716.

be due to a binary companion or to the Beta Cepheid nature of the star.

HD 129056

Both the non-LTE and LTE solutions for this star are rather poorly determined, the spread in effective temperaures given by all parameters being $\approx \pm 1500K$ in both cases. The surface gravity, however, is rather better determined.

Previous studies of this star have found effective temperatures of 22000K (Balona and Feast, 1975), 20650K (Watson, 1971) and 23000K (Walborn, 1971). The former and latter results are in rather better agreement than that found by Watson with the LTE solution derived here. The difference in T_{eff} between this study and that of Watson probably accounts for the small differences ($\leq 2\sigma$) in the abundances of C and N relative to O as the equivalent width measurements of lines in common between the two studies are in good agreement.

HD 132200

Both solutions are quite well defined apart from the locus defined by the Balmer discontuity measurement in the LTE determination. This locus was omitted from the derivation of the LTE solution.

Nandy and Schmidt, 1975, find 19900±900K for T_{eff} from a fit to the continuum flux with a line-blanketed LTE model. This is in good agreement with the value derived by Kane *et al* (1980) who find an effective temperature of 20800K and a log g of 3.85. The study of *UDPD*, however, finds $T_{eff} = 22893K$, in better agreement with the solution found here.

The use of a T_{eff} of 20800K and the assumption that $\xi_t = 5\, kms^{-1}$ explains the difference in the nitrogen and oxygen abundances found in this study and that of *KMD*.

HD 147165

The solution for this star is quite uncertain as the Si III/Si IV ionisation balance is derived from measurements of only one weak Si IV line. Most lines are badly blended by the high rotational broadening of the star.

Other analyses of this star have also been uncertain, as evidenced by the wide spread in derived effective temperatures. Watson, 1971, finds 22800K, Balona and Feast, 1975, 24300K, Walborn, 1971, 25100K and *UDPD* 29035K.

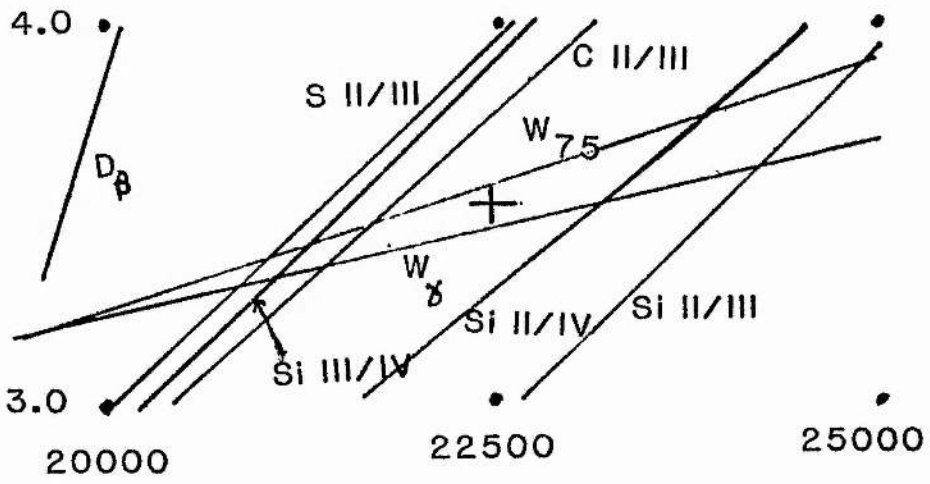

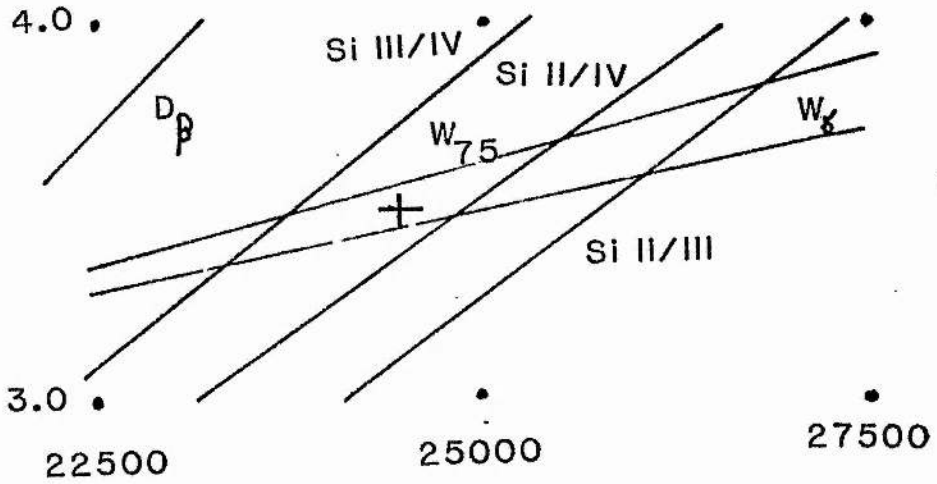

Fig. 5.9 :- As figure 5.1 for HD 129056.

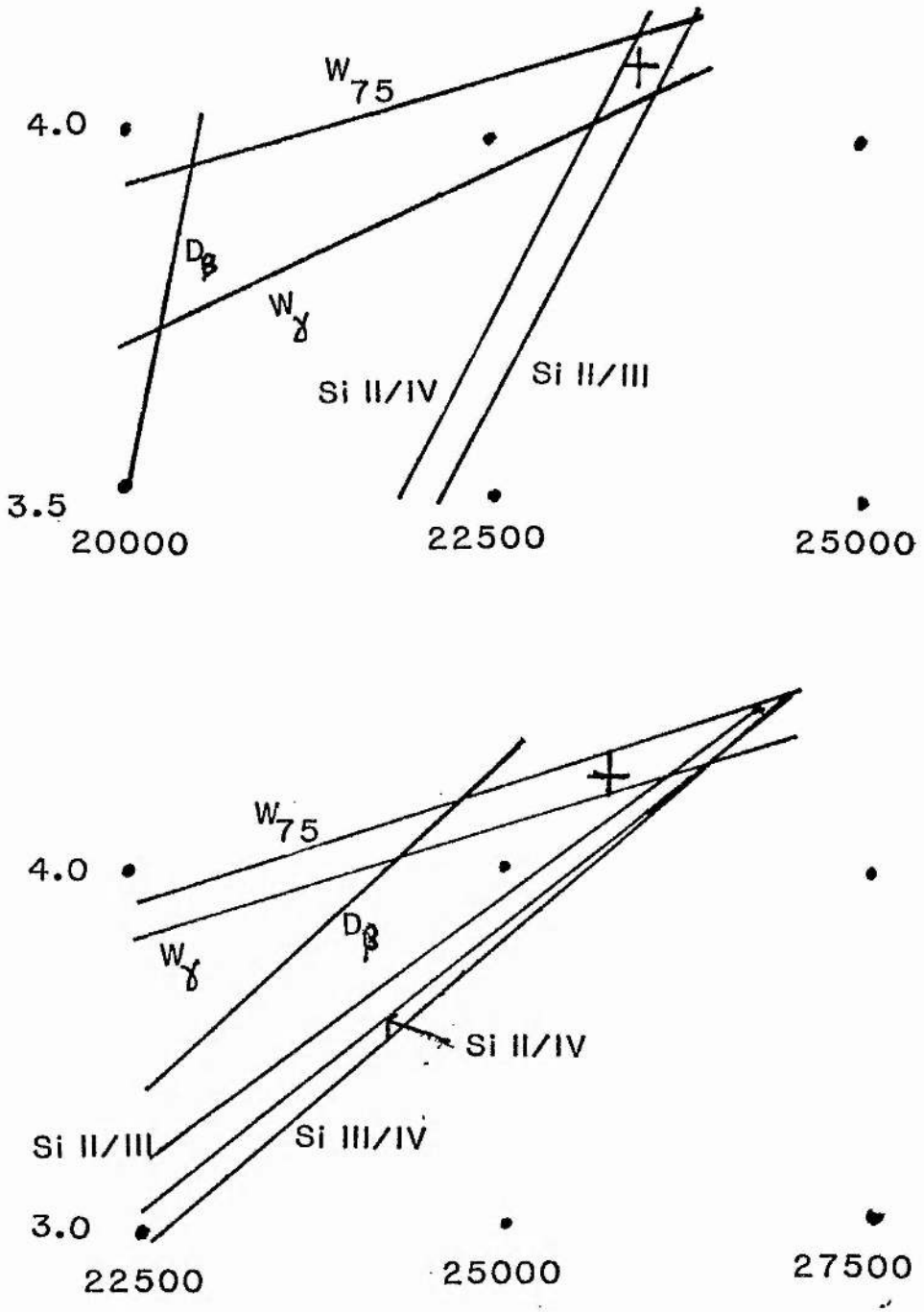

Fig. 5.10 :- As figure 5.1 for HD 132200.

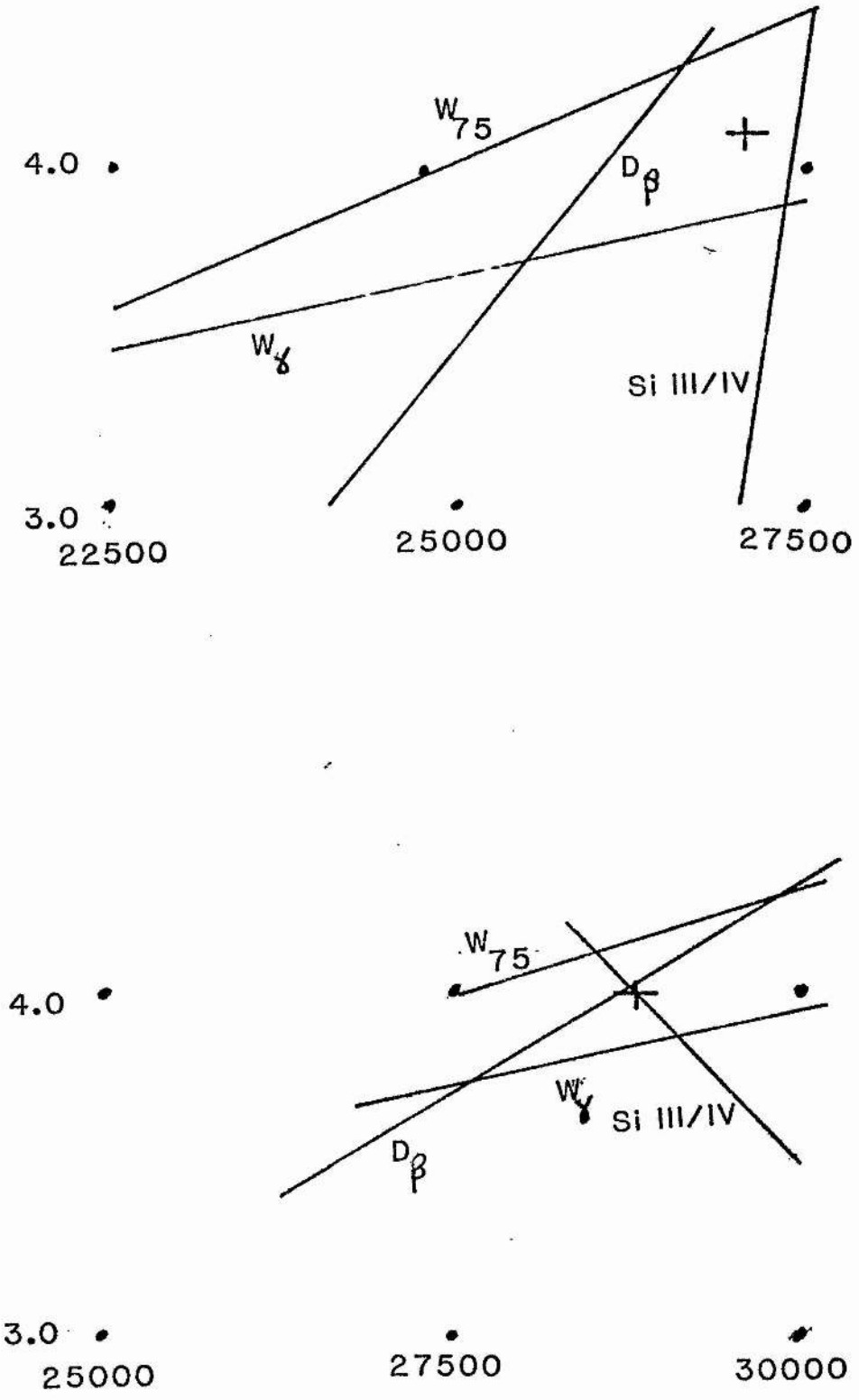

Fig. 5.11 :- As figure 5.1 for HD 147165.

HD 147394

As discussed in chapter 4 this star has been analysed in detail, using earlier versions of the line-blanketed LTE ATLAS and WIDTH programmes used here, by Adelman,1977. The LTE solution derived here is rather hotter than that derived by Adelman of 15500K. This discrepancy is not significant at the 2σ level, however. Similar abundances are found for carbon, magnesium and silicon in the two studies.

HD 147394 is also included in the sample of *UDPD* who find an effective temperature of 15012K.

It was noted that the non-LTE solution is better defined than the LTE solution. The abundance of nitrogen derived with the non-LTE models should be treated with caution as it required extrapolation outside the grid of Dufton and Hibbert and was determined using a measurement of only one line.

HD 149438

This is one of the most often studied early-type stars, principally because the spectral lines are very sharp. Traving in 1955 made one of the first detailed analyses of the spectrum of an early-type main-sequence star and found a T_{eff} of 32800K and a log g of 4.5.

Later studies employing LTE analyses of the metallic line spectrum have included those of Aller, Elste and Jugaku, 1957 who found (35000K, 4.3), Scholz, 1967, (32800K, 4.2), Hardorp and Scholz, 1970, (32000K, 4.1) and Dufton, 1972 (30300K, 3.95). Kamp, 1978, in a non-LTE study of the silicon lines, found values of 33000K for the effective temperature and 4.5 for the surface gravity. Analyses based on observations of the continuum flux have included those of Heintze, 1969, who found (27000K, 4.0) and *UDPD* who derive 30050K for the effective temperature.

Hardorp and Scholz found it impossible to explain all the features they observed with one unblanketed LTE model. In particular, while the Balmer lines indicated an effective tenperature <28000K the metallic line spectrum required a much hotter model. Hardorp and Scholz predicted that an improvement would be found when the spectrum was analysed with the aid of either line-blanketed LTE or non-LTE models.

This prediction is only partly borne out by this study.

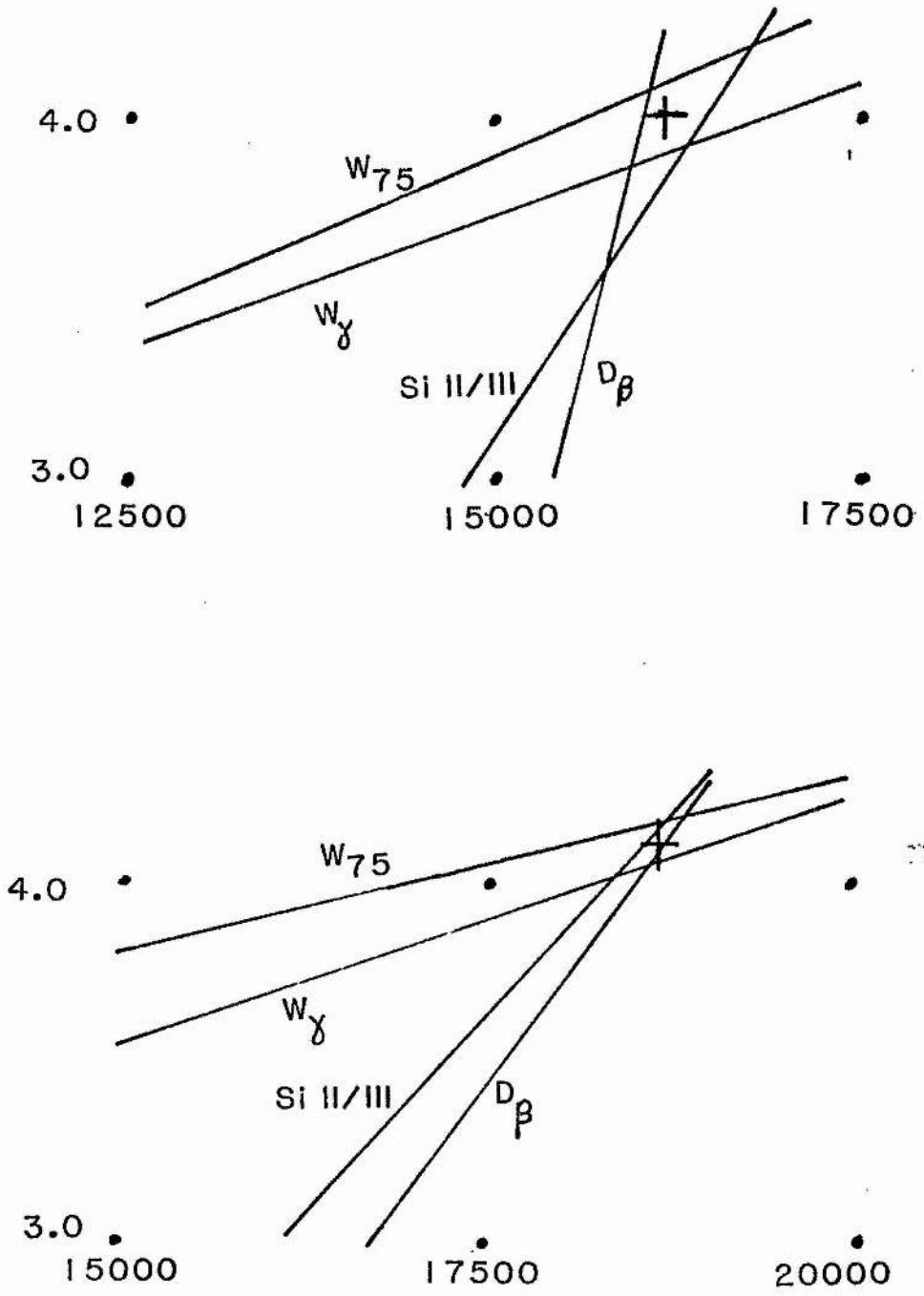

Fig. 5.12 :- As figure 5.1 for HD 147394.

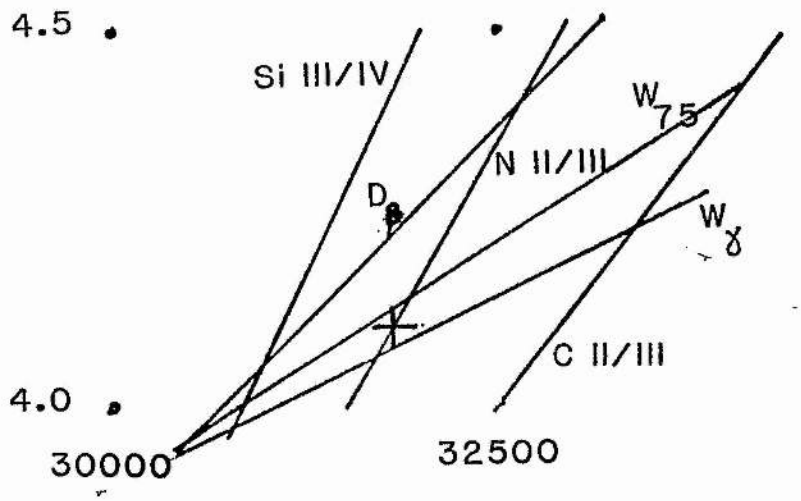

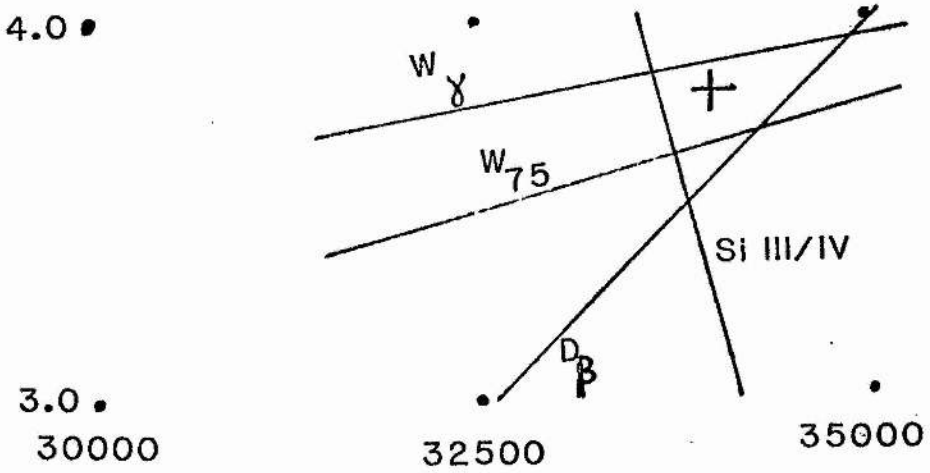

Fig. 5.13 :- As figure 5.1 for HD 149438.

In the LTE analysis while both the silicon lines and Balmer measurements would be well explained at an effective temperature of $\approx$ 30800K and a log g of $\approx$ 4.0 the carbon and nitrogen lines require a higher effective temperature. There is an overall spread of $\approx$ 2000K between all the temperature defining criteria.

A somewhat poorer agreement between the silicon line locus and the D_β locus is found in the non-LTE analysis, the spread in T_{eff} being approximately 1000K.

The abundances derived with the LTE model are very similar to those found by Hardorp and Scholz apart from the values of [N] and [S] which are discordant by $\approx$0.4 dex. The different surface gravity found here comapred to that used by Kamp results in a (non-LTE) Si abundance which is lower by $\approx$0.2 dex.

HD 165024

This is the only star in this survey for which a supergiant classification has been given.*UDPD* give a classification of B2 Ib, Dufton,1979, gives B1 Ib although the catalogue of Buscombe gives a number of references to a classification of B0.5 II.

The neglect of curvature in the extended envelope of a supergiant may introduce some uncertainty to the results found for this star. Another source of uncertainty is the fact that the measurements are made from plates supplied by Dr. P.W. Hill calibrated by use of spot sensitometer plates.

Both analyses, however, in paticular that using the non-LTE models, produce well defined solutions.

Dufton also made analyses of this star using both LTE and non-LTE models. His LTE solution with a log g of 3.92 and an effective temperature of 26000K on the line-blanketed scale of Morton and Adams, 1968, is quite different from that derived here although the same value of ξ_t (15 $km\ s^{-1}$) was deduced. In his non-LTE analysis he finds an effective temperature of 23500K in better agreement with the value found here although the surface gravity of 3.4 dex is still quite different.

UDPD also derive an effective temperature for this star. Their value of 17250K is very different from the values found here. This discrepancy will be discussed in more detail in a later section of this chapter.

(No non-LTE abundance of nitrogen was derived for HD 165024 as the required

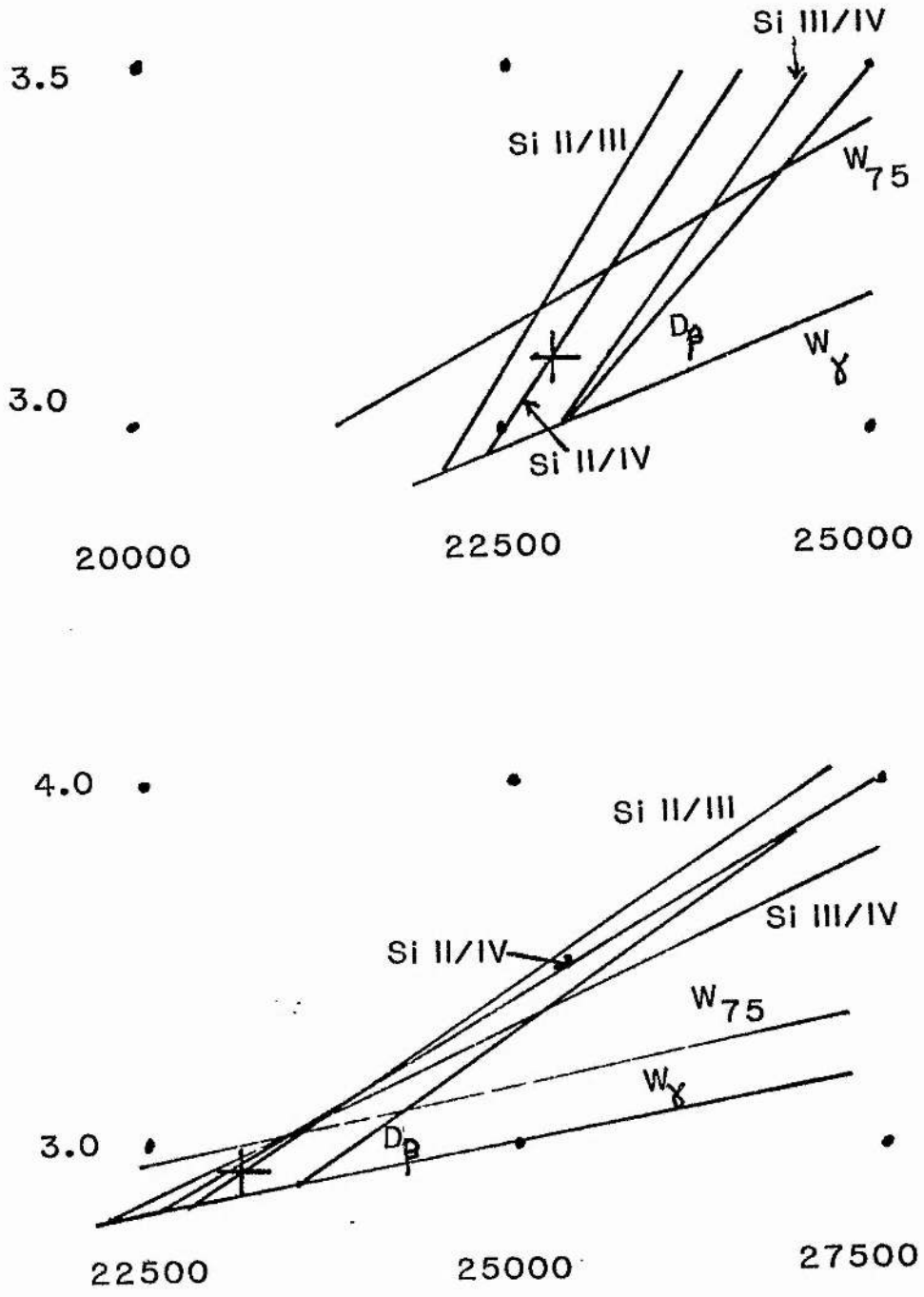

Fig. 5.14 :- As figure 5.1 for HD 165024.

extrapolations to values of log g and ξ_t well outside the tabulations of Dufton and Hibbert were felt to be unreasonable).

HD 166182

No measurement of D_β for this star could be found in the literature. The only strong constraint on the effective temperature, therefore, comes from the ionisation balance of Si II/ Si III. While the LTE solution is rather poorly defined it is in good agreement with the results of *UDPD* who find an effective temperature of 20320K.

In both the LTE and non-LTE reductions the value of ξ_t was poorly defined as different ions showed a minimum in the respective abundance determinations over the range 0–10 $km\,s^{-1}$.

HD 169467

Both the LTE and non-LTE solutions are well defined. The temperature found with the LTE models is much cooler than that determined by *UDPD* assuming $\log g = 4.0$ of 19025K. This value of $\log g$ is much larger than that found here. In this study at $\log g = 4.0$ the silicon lines would indicate a T_{eff} of $\approx$ 18000K but D_β would give only 16500K.

This was another star for which measurements of the Si II lines at 6347Å and 6371Å were made. Using the LTE model these could only be made consistent with the other silicon lines if a value of 10 $km\,s^{-1}$ was adopted for ξ_t. The non-LTE analysis however adequately explained the observed equivalent widths of these lines in a model with $\xi_t = 0 km\,s^{-1}$. (The lines were omitted from the determination of the LTE solution and are not the cause of the discrepancy discussed above).

HD 180163

While both solutions are well defined the suface gravity determined is lower than would be expected for a star of MK luminosity class IV. The H_γ profile gives essentially similar results, however, so this discrepancy is either real and suggests an alternative classification or some systematic error in the calibration of this star has occurred. No significant change in the results was obtained when the plate material was subjected to a re-measurement and reduction.

HD 184171

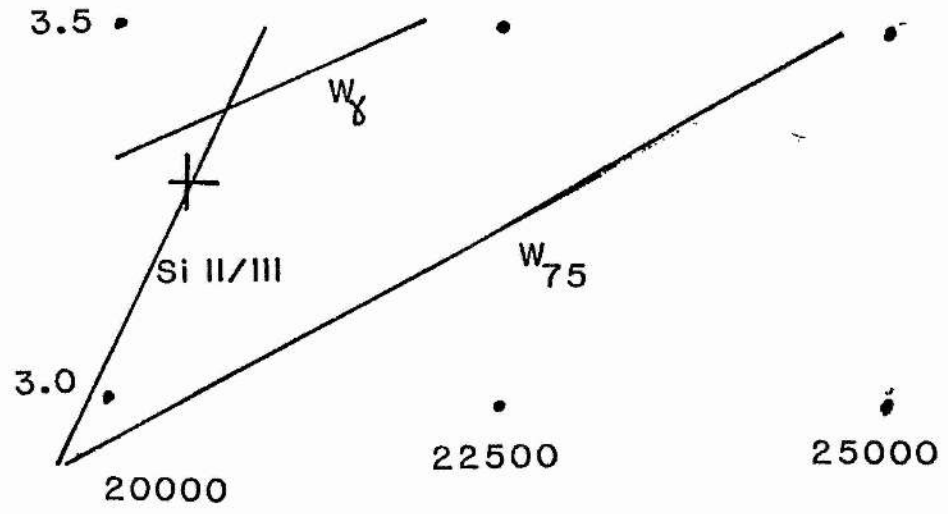

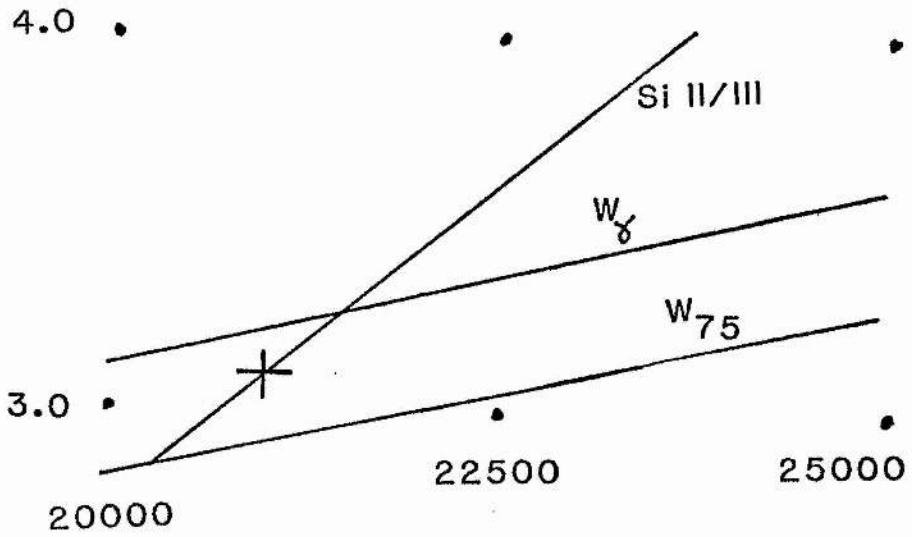

Fig. 5.15 :- As figure 5.1 for HD 166182.

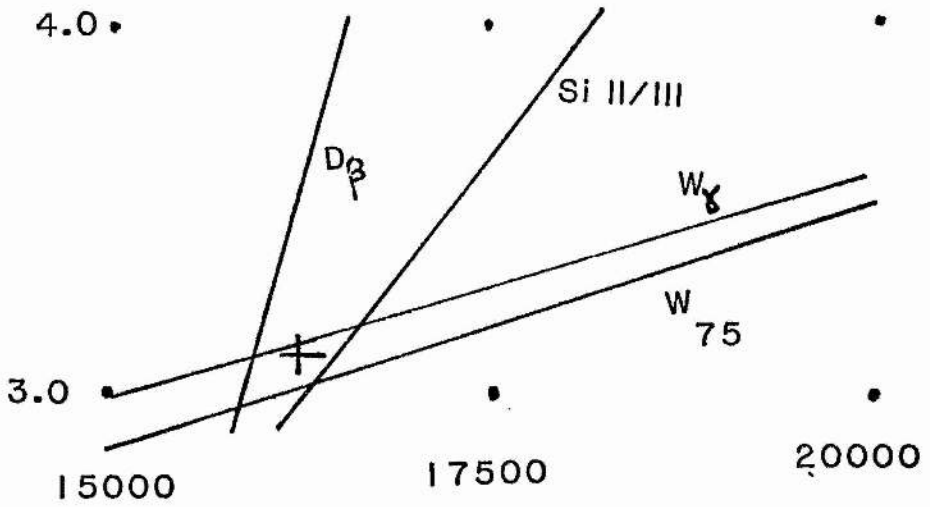

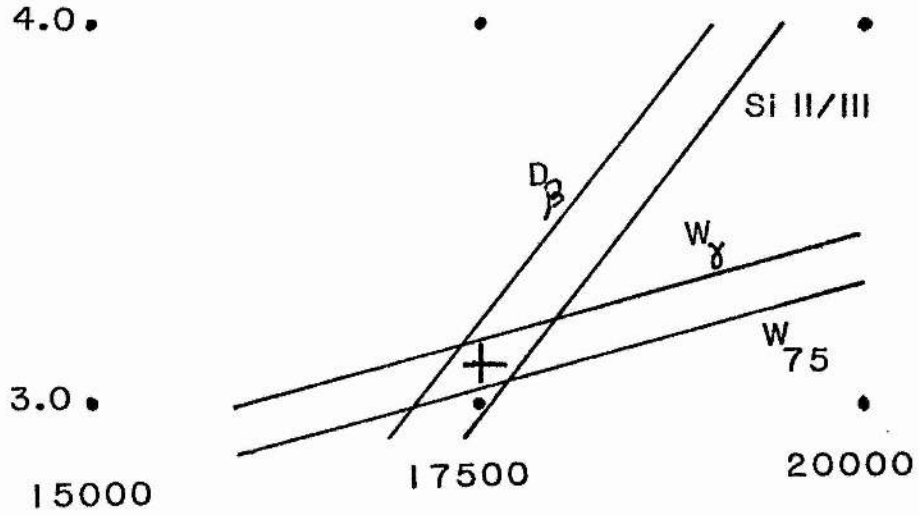

Fig. 5.16 :- As figure 5.1 for HD 169467.

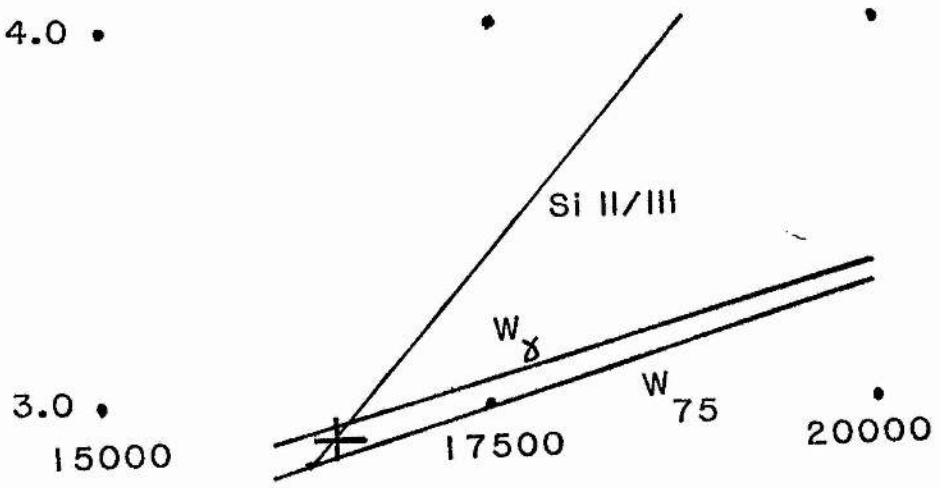

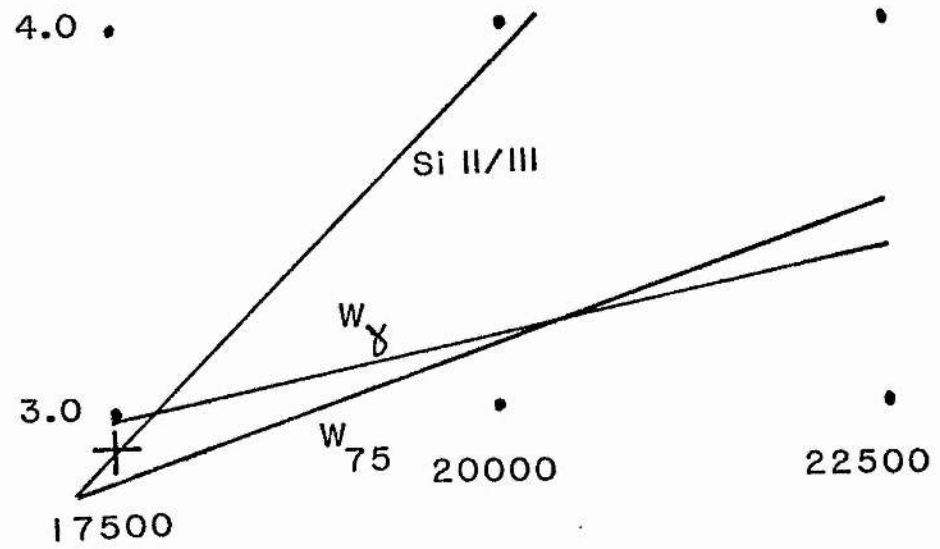

Fig. 5.17 :- As figure 5.1 for HD 180163.

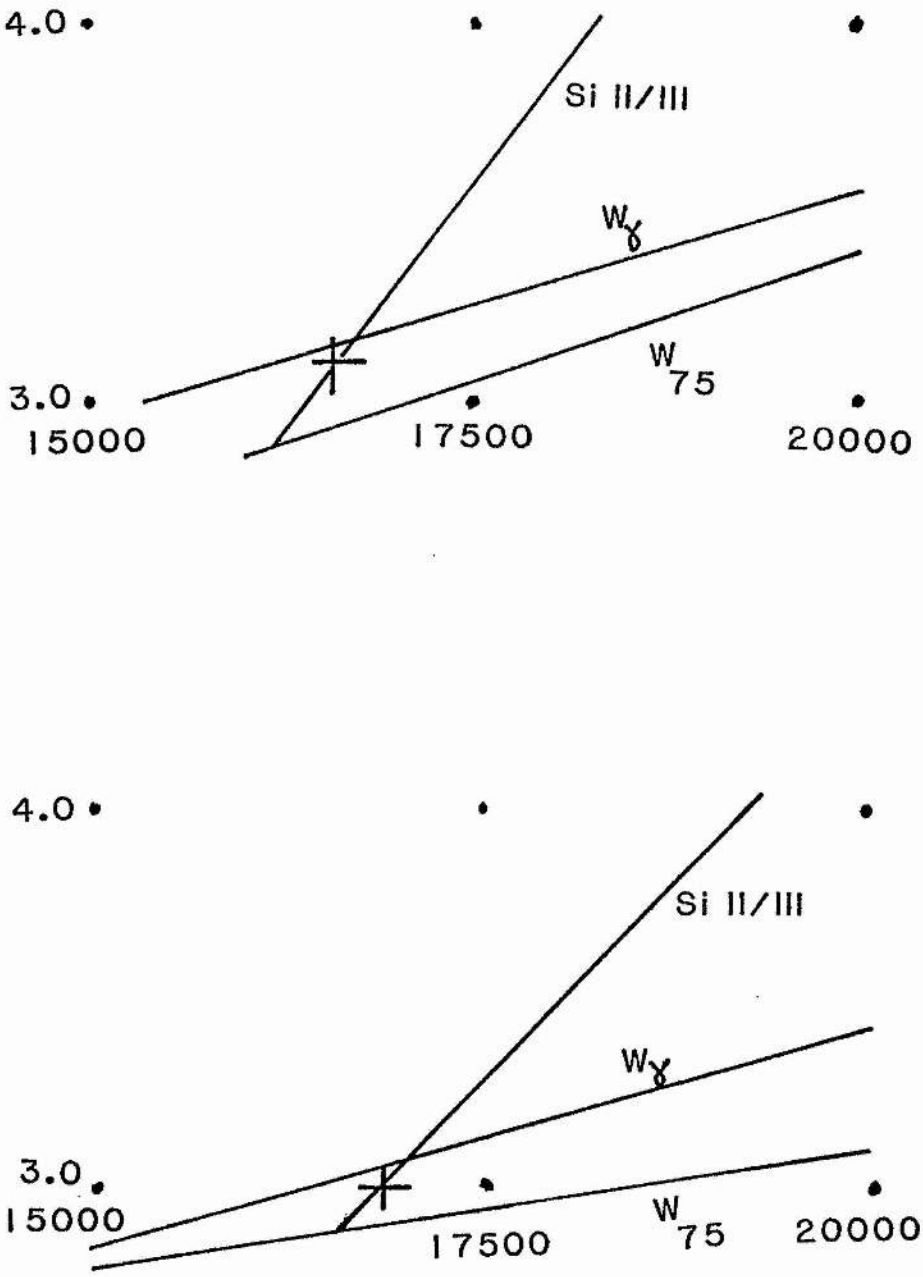

Fig. 5.18 :- As figure 5.1 for HD 184171.

The solutions are again well defined although the surface gravity determined is low. The effective temperature is lower than that found by *UDPD* of 18855K for a $\log g = 4.0$. At this value of the surface gravity the locus of the Si II/ Si III ionisation balance would give an effective temperature of $\approx$ 18300K.

HD 184930, *HD* 195810 *and HD* 207971

As there were no elements represented by lines of two ions nor measurements of D_β in the literature for any of these stars a different approach was adopted to determine their effective temperatures and surface gravities.

First the H_γ profile and equivalent width measurements were used to define a locus in the ($\log g$, T_{eff}) plane. Abundances for each of the observed lines were then calculated at 1000K intervals along this line using various trial values of ξ_t. Mean abundances and standard deviations were then calculated for each element. The solution chosen was the model where the r.m.s. of all the standard deviations was minimised. (While LTE solutions were found for all 3 stars in this manner only the solution for HD 184930 was close enough to the grid of Kamp for a non-LTE solution to be derived).

Despite the uncertainties involved the agreement of the LTE solution for HD 207971 with that found by *UDPD* suggests that this method of finding a solution is satisfactory.

Although no non-LTE solution for HD 207971 could be found the Si II lines at 6347Å and 6371Å were better predicted with a non-LTE model with an effective temperature of 15000K than with the final LTE solution (from which determination they were omitted).

HD 214680

Both solutions are quite well defined. The LTE solution is marginally cooler than the 35401K derived by *UDPD*. The non-LTE solution is in reasonable agreement with the values determined in non-LTE studies of this star by Auer and Mihalas, 1972, and by Kamp, 1973, of $\approx$ 37000K and $\approx$ 35000K respectively.

HD 218376

High values of ξ_t were required in both the LTE and non-LTE models. The former is rather better determined. Because of the difference in the temperatures indicated by the carbon and silicon ionisation balances in the LTE analysis the non-LTE effective temperature may be over estimated relative to the LTE value due to the use of only the

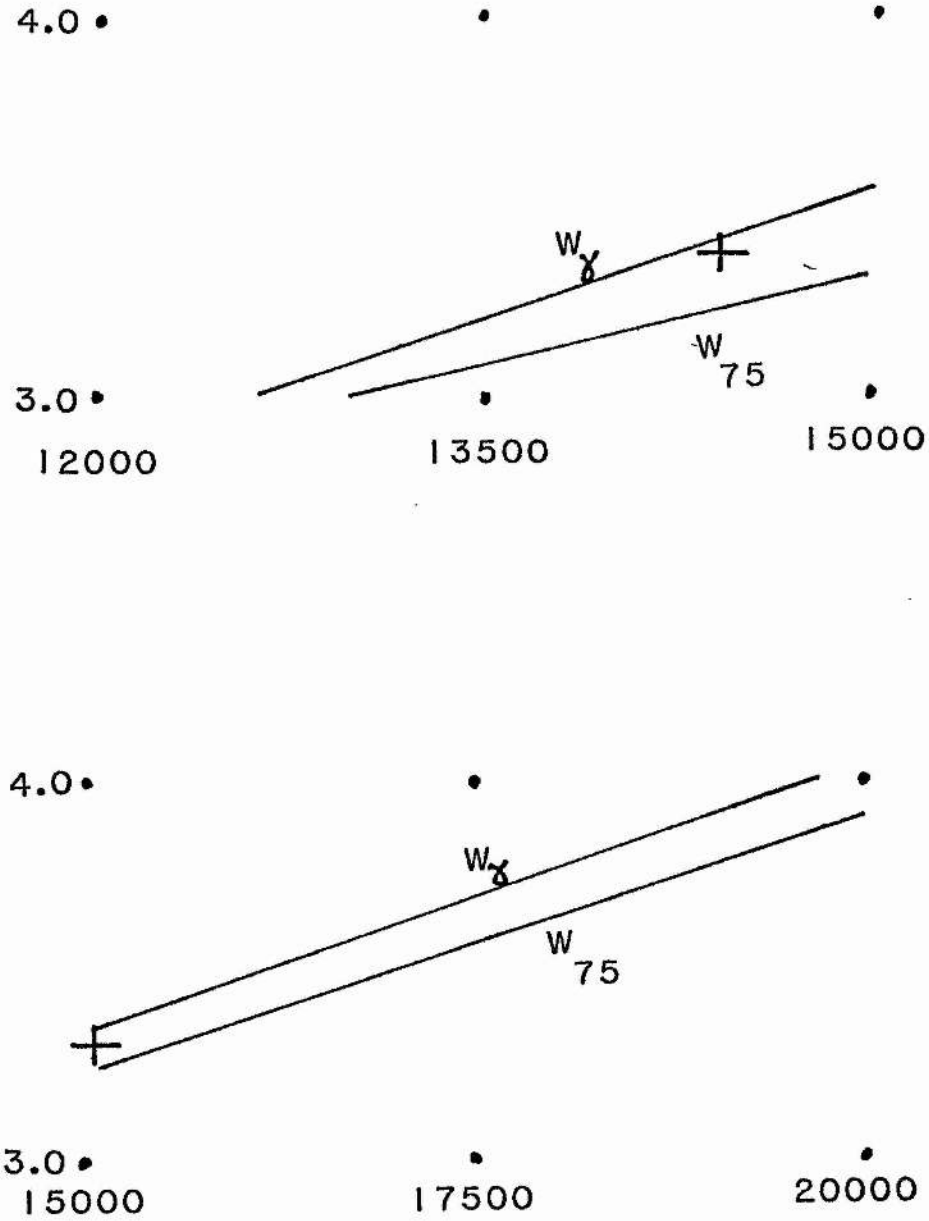

Fig. 5.19 :- As figure 5.1 for HD 184930.

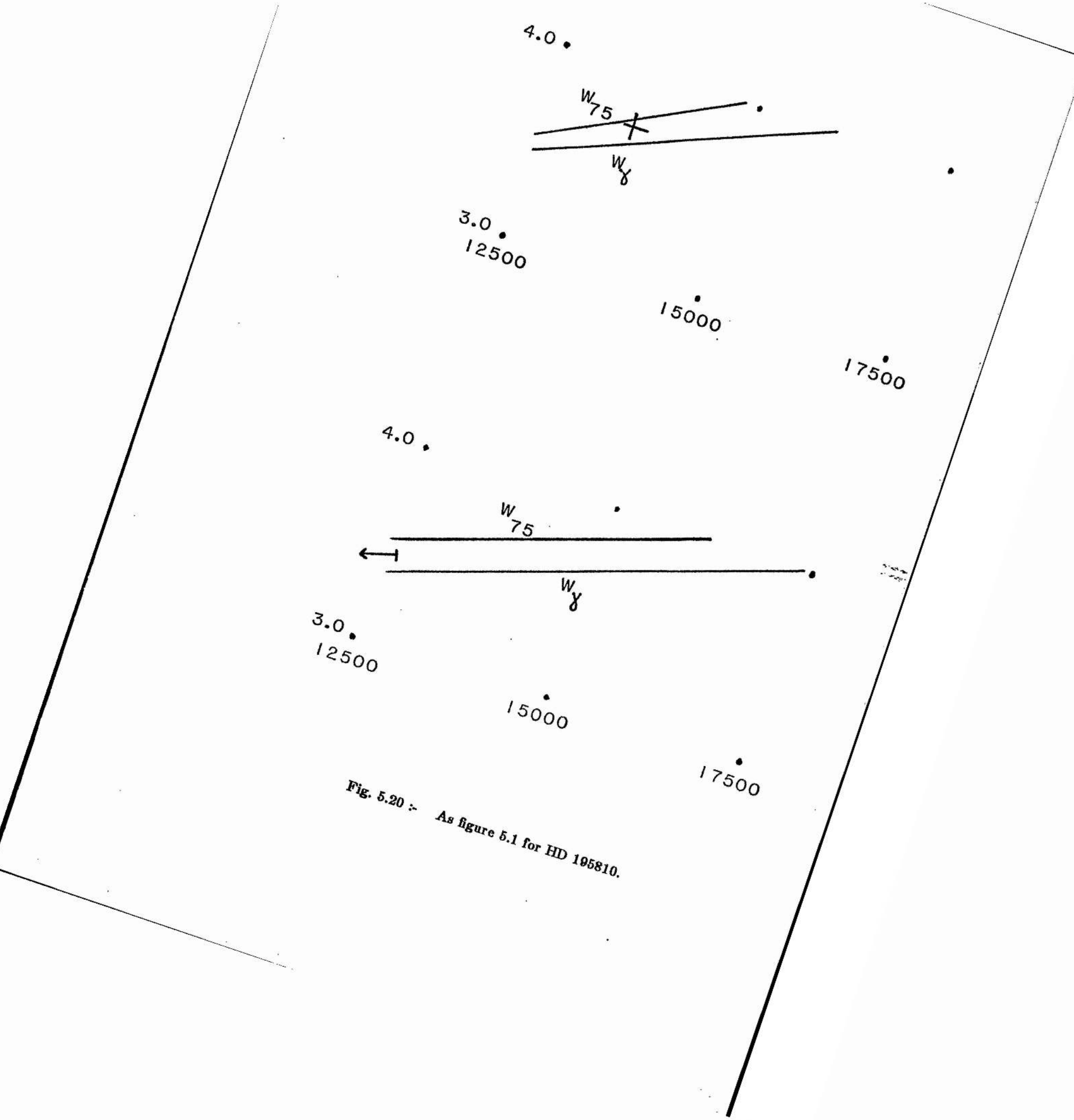

Fig. 5.20 :- As figure 5.1 for HD 195810.

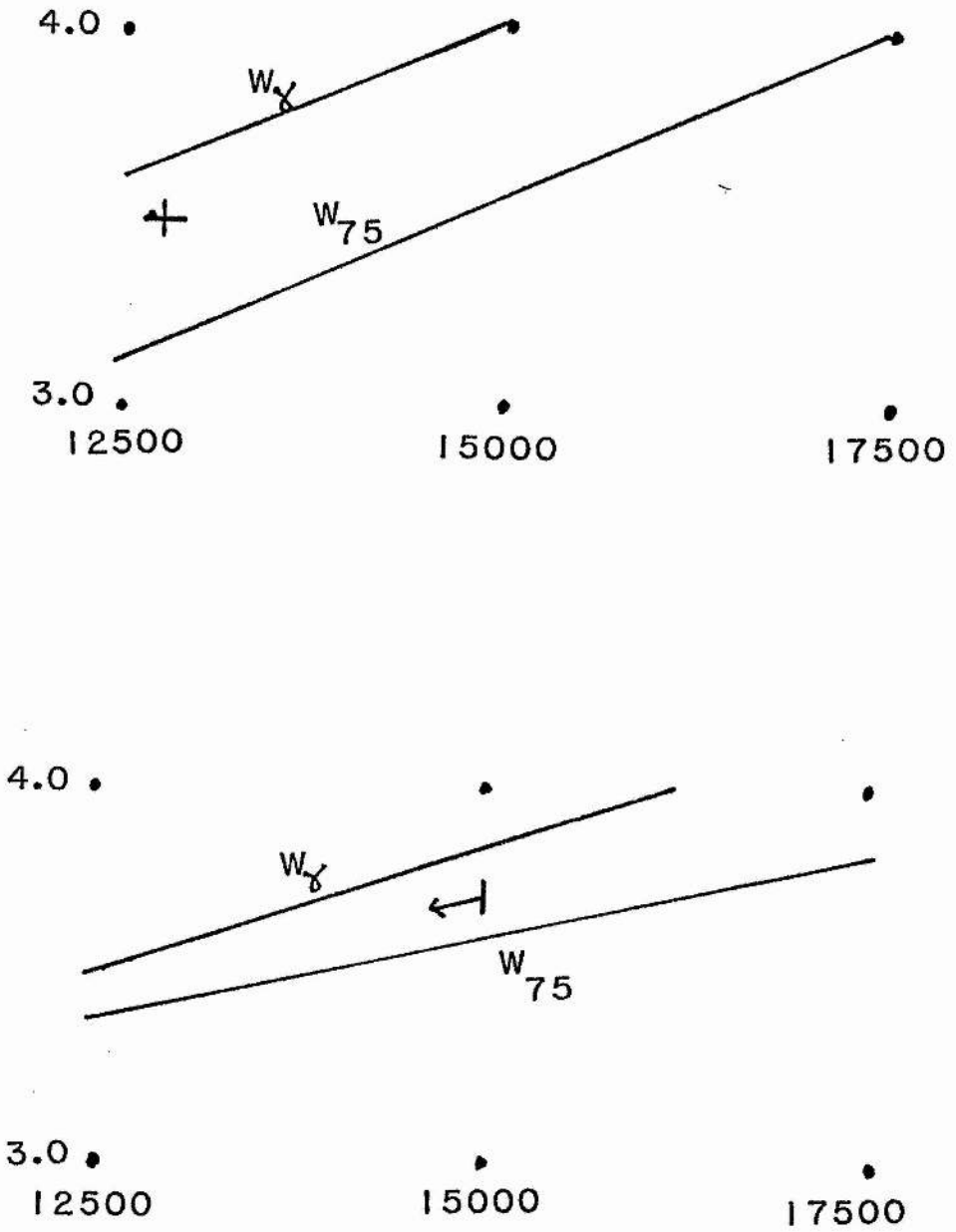

Fig. 5.21 :- As figure 5.1 for HD 207971.

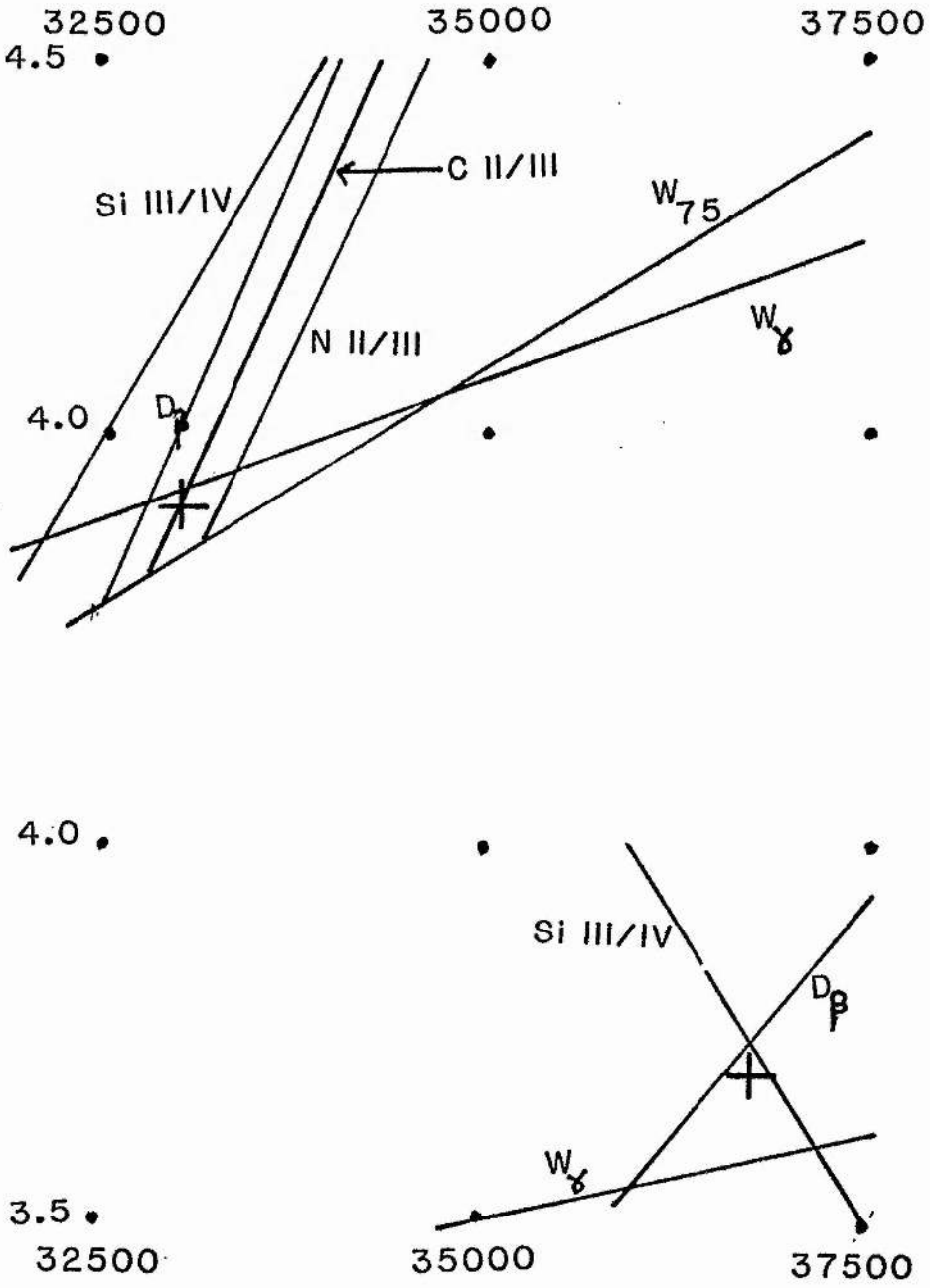

Fig. 5.22 :- As figure 5.1 for HD 214680.

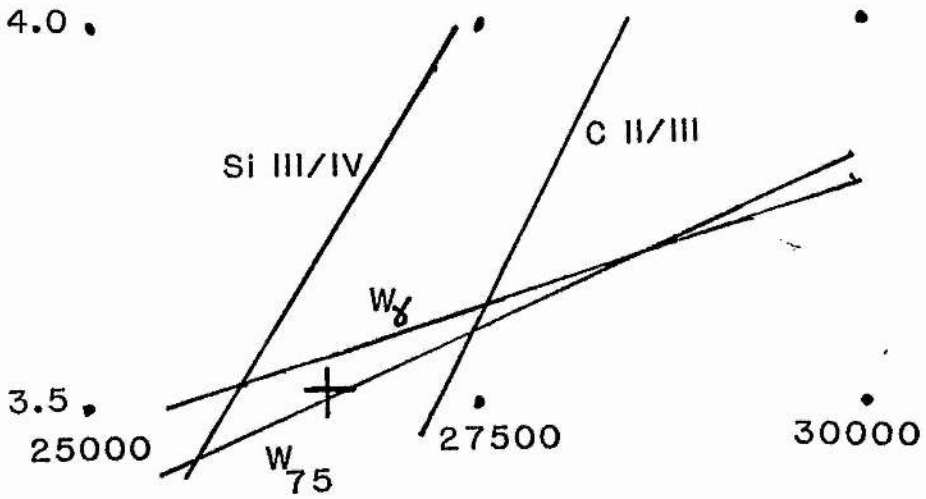

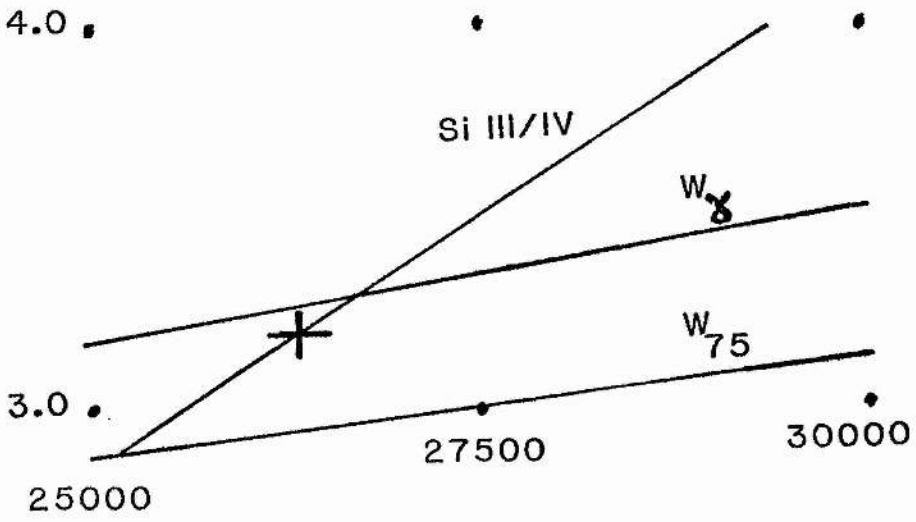

Fig. 5.23 :- As figure 5.1 for HD 218376.

silicon line data.

5.vii *General Comments*

In generating the solutions described above a number of general points were noted.

The first of these concerns the CII line at 4267Å. In all the stars for which measurements of more then two carbon lines were available this line systematically required a much lower abundance of carbon than the other lines. The mean difference between the 4267Å line and the other lines was found to be $\approx$ 0.45 dex. A similar discrepancy for this line has also been noted by *KMD*, 1980. Dufton, 1983, has shown that the problem is not due to non-LTE effects (at least for a simple model of the CII ion)

For this reason where more than two measurements of carbon lines were available the 4267Å line was ignored in the derivation of a value for [C]. In other cases the abundance determined from the 4267Å line was artificially increased by 0.45 dex before determining the mean carbon abundance. Some care must therefore be exercised in interpreting carbon abundances for stars for which this correction had to be adopted. It is unfortunate that this line should pose such a problem as it is one of the most readily observable lines of CII in the spectra of early-type stars.

It was also noted that the temperatures indicated by the value of D_β were in the main lower than those indicated by the ionisation balances. This was true for both the LTE and non-LTE analyses. No action was taken on this matter as usually the effect on the derived solution is small, $\leq 500K$.

The values of the stellar parameters derived in the analyses are not totally independent. The effect of systematic errors and their influence on the other derived parameters was, therefore, investigated and requires some comment here.

In general, ξ_t was determined to an accuracy of $\approx \pm 3\ km\ s^{-1}$. Such an error has little effect on the positions of the ionisation balance loci in the $(T_{eff}, \log g)$ plane. An investigation of a number of stars showed that the effect of a change of $\pm 5\ km\ s^{-1}$ was a shift in T_{eff} with a maximum magnitude of $\approx 400K$. The direction of the shift varied from star to star and depended on which ionic lines were most sensitive to ξ_t. Almost no difference is made to the derived value of log g by such an error. A change of $5\ km\ s^{-1}$ in the value of ξ_t also has a first order effect on the derived abundances. This

effect varies in size according to the strength of the lines and the ion under investigation. For carbon, nitrogen, oxygen and silicon the maximum variations were $\approx$ 0.15, 0.2, 0.25 and 0.35 dex respectively.

The range in effective temperature of the various criteria can be seen from figures 5.1 – 5.23 to be less than $\approx \pm$ 1250K, and is usually better than $\approx \pm$750K. The corresponding error in the derived abundances is $\leq$ 0.15 dex. Where more than one ion of an element is present this error will be reduced by the opposite directions of the change for each ion.

Values of the equivalent width of H_γ and W_{75} usually gave values of log g consistent to within $\approx$ 0.1 dex. Checks made using the H_δ line and estimates of the random error in the equivalent width and W_{75} of H_γ suggest that log g is determined to better than $\approx$ 0.25 dex.

It was noted that for most stars the derived values of log g and T_{eff} were connected in that a lower value of effective temperature would imply a lower value of log g.

Given the random errors in the equivalent width measurements and the precision with which T_{eff}, log g, ξ_t solutions are determined it is felt that the error in an abundance determination is, conservatively, 0.3 dex.

Before comparing the results obtained with the LTE and non-LTE models with each other or with the results of other authors and before examining the astrophysical implications of the stellar parameters determined with the models the *goodness of fit* of the models to the data should be examined.

Ideally the models should be tested against the data using some statistical test. With random errors of a known size a test such as the χ^2 test would provide a measure of the goodness of fit of each model. The difference in, and size of, the χ^2 statistics given by the two types of model would distinguish which of the models was the better approximation to the real physical state of a stellar photosphere and, indeed, whether the use of either model was justified.

A cursory examination of the figures illustrating the solutions for each star shows that neither type of model is entirely satisfactory. The individual loci defining each solution do not converge to a single point as would be expected in the absence of

observational error if the models were an exact representation of a stellar photosphere.

Calculations were in fact made of χ^2 for two of the stars in the survey, HD 79351 and HD 129056. (The selection of these two stars was arbitrary). Predicted line strengths for all lines of C(except 4267Å), N, O and Si lines were calculated for the model solution using the ATLAS6 and WIDTH6 programmes as before. A similar calculation was made for the silicon and nitrogen lines of HD 79351 and for the silicon lines of HD 129056 using the Kamp, and Dufton and Hibbert theoretical grids.

An observational error was calculated for each line using the formula

$$E = 5.4 + 0.05W \quad m\mathring{A}$$

where E and W are the error and observed equivalent widths in mÅ respectively. This expression gives a good fit to the results obtained in chapter 4. The sum of χ^2 could then be calculated from

$$\sum\left(\frac{W-C}{E}\right)^2$$

where C is the equivalent width of the line predicted using the model solution and derived abundance.

Values of the reduced χ^2 (χ^2 per degree of freedom) were then calculated. The number of degrees of freedom (dof) was taken to be the number of lines in the summation less three more than the number of atomic species involved (i.e. allowing for the number of abundances, T_{eff}, log g and ξ_t calculated with the data).

This calculation was made three times for each star :-

1) for all lines and the LTE model

2) a subset of the NII and Si lines and a non-LTE model

3) the same lines as 2) and the LTE model

The results were disappointing in that the values of χ^2/dof found were in the range 1.5-3. For both stars calculations 1,2 and 3 gave systematically increasing values of χ^2/dof. This suggests that there is some improvement in the fit to the nitrogen and silicon lines using non-LTE calculations. Formally, however, neither model can be fully accepted.

An alternative course of action to the rejection of the models is to postulate that the errors obtained in chapter 4 are not the correct values to use here. It would only require the errors to have been under-estimated by a factor of $\approx$ two to make the χ^2 values acceptable. Two possibilities arise. Firstly the results in chapter 4 could have over-estimated the accuracy of the reduction and measurement system. Alternatively there is another source of random error which is contributing. A likely candidate for this second source of error is the atomic data used. As was discussed in chapter 1, f-values are still rather poorly known.

An alternative approach to comparing the applicability of the models was therefore adopted. This used the following rather more qualitative arguments.

The standard deviation of the logarithmic abundances derived for all silicon lines in common between the LTE and non-LTE analyses was calculated for each star. The results are shown in Table 5.viii. The mean standard deviation is lower in the non-LTE analyses than in the LTE analyses. For only 3 out of the 23 stars does the LTE analysis provide abundances which have a smaller standard deviation than the non-LTE analysis of the same star.

This suggests that, at least for the silicon lines, the use of non-LTE models is a more accurate approximation to the stellar photosphere. Some care must be made in attaching significance to this statement however. The non-LTE solutions were derived using only the silicon and hydrogen line data. For some stars the LTE analysis also made use of information from the ionisation balances of other elements. However, an examination of the results of table 5.viii for stars for which only the silicon ionisation balances were used in the LTE analysis shows the same general trend of improvement when non-LTE models are used.

Another possibility, of course, is that the abundances derived with the non-LTE models are not as sensitive to errors in the equivalent width measurements. While this cannot be entirely ruled out, as the curves of growth used in the non-LTE analysis closely approximate the LTE curves of growth, this should not cause too strong an effect.

It is noted that the mean standard deviation in the non-LTE analyses still represents an error of $\approx$ 30% in the abundance determination (as compared to $\approx$ 50% in the

Table 5.viii

Standard Deviations of Silicon Abundance Calculations

HD	*LTE*	*non − LTE*	*No. of Lines*
15371	0.27	0.16	7
74575	.11	.08	7
79351	.12	.10	7
81188	.13	.12	9
106625	—	—	—
111123	.12	.17	7
116658	.19	.18	3
118716	.30	.22	8
129056	.06	.08	7
132200	.06	.07	7
147165	—	—	—
147394	.18	.15	7
149438	.21	.11	8
165024	.19	.15	8
166182	.24	.14	7
169467	.16	.12	9
180163	.17	.09	7
184171	.15	.12	7
184930	.08	.02	4
195810	—	—	—
207971	—	—	—
214680	.31	.20	8
218376	.32	.26	6
Mean	0.18	0.13	
S.D.	.08	.06	

LTE analysis) while the worst case represents an error of $\approx 80\%$.

A subjective analysis of figures 5.1-5.23 also suggests that the non-LTE solutions for different criteria are more self consistent than the LTE solutions. An additional argument in support of the non-LTE models is the behaviour of the 6347Å and 6371Å lines of silicon II. While neither type of model is entirely satisfactory in explaining the behaviour of these lines, the non-LTE models do bring these lines into much better agreement with the others.

5.viii *LTE vs non − LTE : Comparison of Results*

Effective Temperatures

Figure 5.24 shows the temperatures derived with the LTE models plotted against those derived using non-LTE models. For all but one star the non-LTE temperature is higher than the LTE temperature. The mean difference in the sense $T_{eff}(non-LTE) - T_{eff}(LTE)$ is 1430K with a standard deviation of 1025K. A linear fit to the data points excluding the two non-LTE upper limits gives

$$T_{eff}(non-LTE) = 1.07 \times (T_{eff}(LTE)) + 10K$$

This solution is shown as a solid line on the figure.

This is similar to the results found by comparing line-blanketed LTE models with unblanketed models for early-type stars (e.g. Morton and Adams, 1968, Philips, 1977). This suggests that the inclusion of non-LTE effects both on the model photosphere and on the absorption lines has little effect on the derivation of temperatures from absorption line data.

Surface Gravities

Figure 5.25 shows a comparison of the $\log g$ values found using both types of model. The mean difference in the sense $\log g(non-LTE) - \log g(LTE)$ is 0.06 with an r.m.s. scatter of 0.17. Clearly within the errors there is no systematic difference between the values found using either model. A linear fit to the data values, however finds a formal solution of

$$\log g(non-LTE) = 1.03 \log g(LTE) - 0.17$$

Microturbulent Velocities

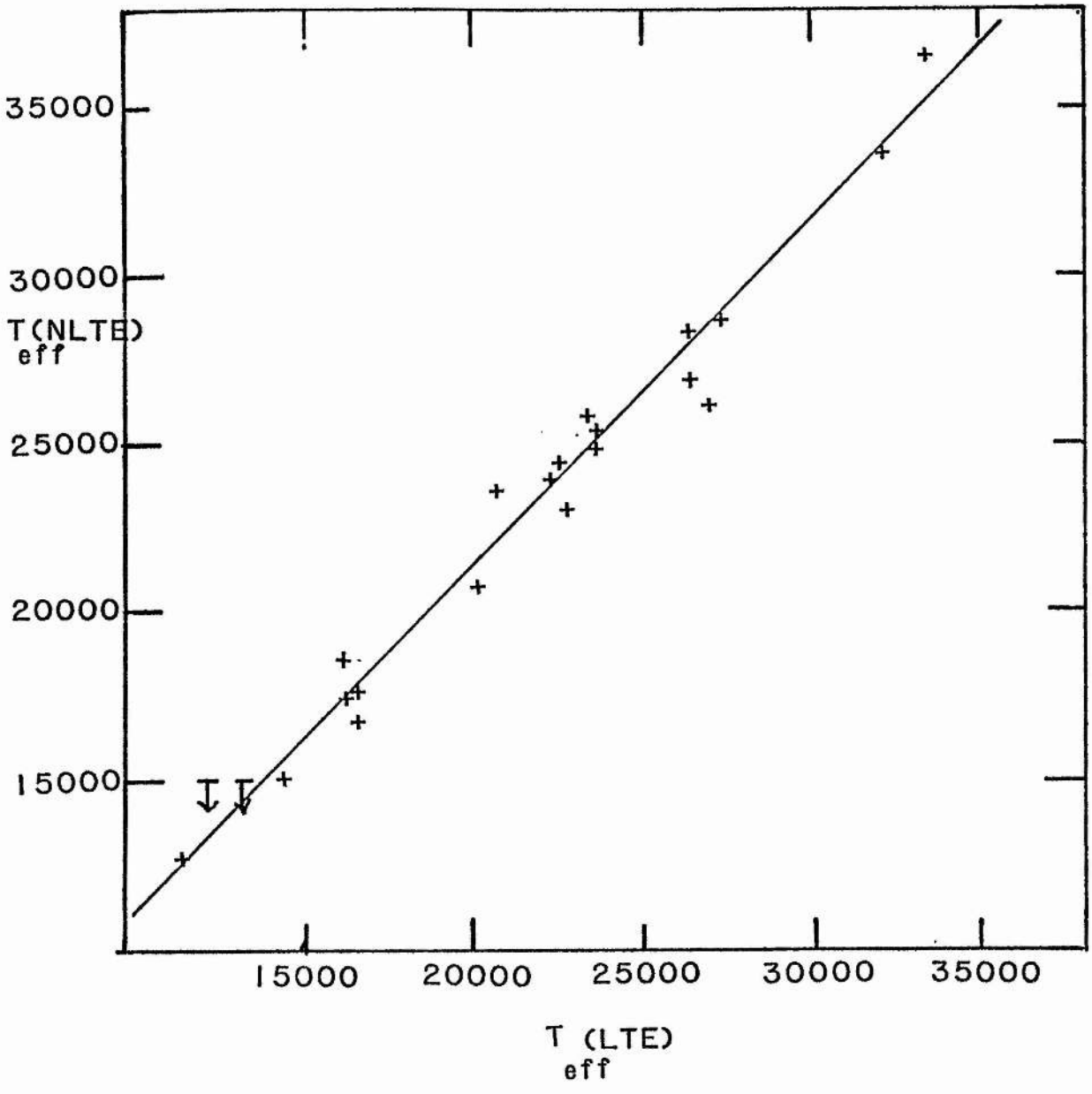

Fig. 5.24 :- **Comparison of effective temperatures derived using the LTE and non-LTE models. The solid line is the least squares fit to the data discussed in the text.**

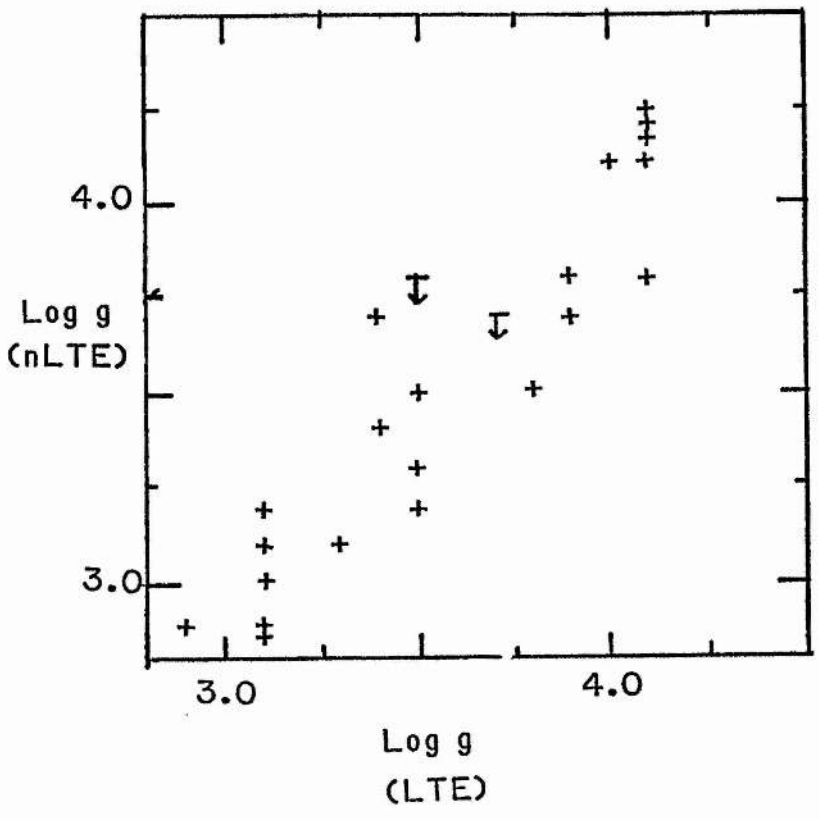

Fig. 5.25 :- **Comparison of the values of $\log g$ found with LTE and non-LTE models.**

In only one case was the value of ξ_t derived in the non-LTE analyses higher than the respective value found with LTE models. Four other stars had ξ_t values which were the same in both analyses. The mean difference between the two sets values was $3 km\ s^{-1}$ with a standard deviation of $2.2 km\ s^{-1}$. A linear fit to the data gives the solution (figure 5.26) of

$$\xi_t(non-LTE) = 0.67\xi_t(LTE) - 0.5\ km\ s^{-1}$$

That the use of non-LTE models would reduce the derived microturbulent velocities was suggested by the manner in which non-LTE line effects strengthened strong lines relative to weaker lines, the effect which microturbulence was introduced to explain. The magnitude of the reduction found here is rather smaller than that found by Kamp,1978. His solutions implied that a value of $\xi_t = 0\ km\ s^{-1}$ would explain the observations of most B stars. However, his observational material consisted of an inhomogeneous set of measurements and his techniques for finding a solution biased his results towards finding low values for the microtubulent velocity.

The implications of the remaining necessity to incorporate microturbulence will be discussed later in this chapter.

Abundances

Comparison of the abundances determined could only be made for silicon and nitrogen. As the nitogen abundances from non-LTE models were determined only for log g=4.0 this comparison should be treated with some caution.

A rather counter-intuitive result was found for both elements. This was that the abundances derived with the non-LTE models were higher for both elements than using LTE models. Neither increase is particularly significant, however. It was expected that the increased line strengths predicted by the non-LTE models would reduce the deduced abundances. This has been more than offset, however, by the reduction in microturbulent velocity. That the reduction in ξ_t is the cause of the effect is confirmed by an examination of the results for the four stars for which the same microturbulence was deduced in both analyses. Here the mean silicon abundance required has indeed decreased, by ≈ 0.25 dex.

5.ix *Comparison with the Results of other Studies*

The Effective Temperature Scale

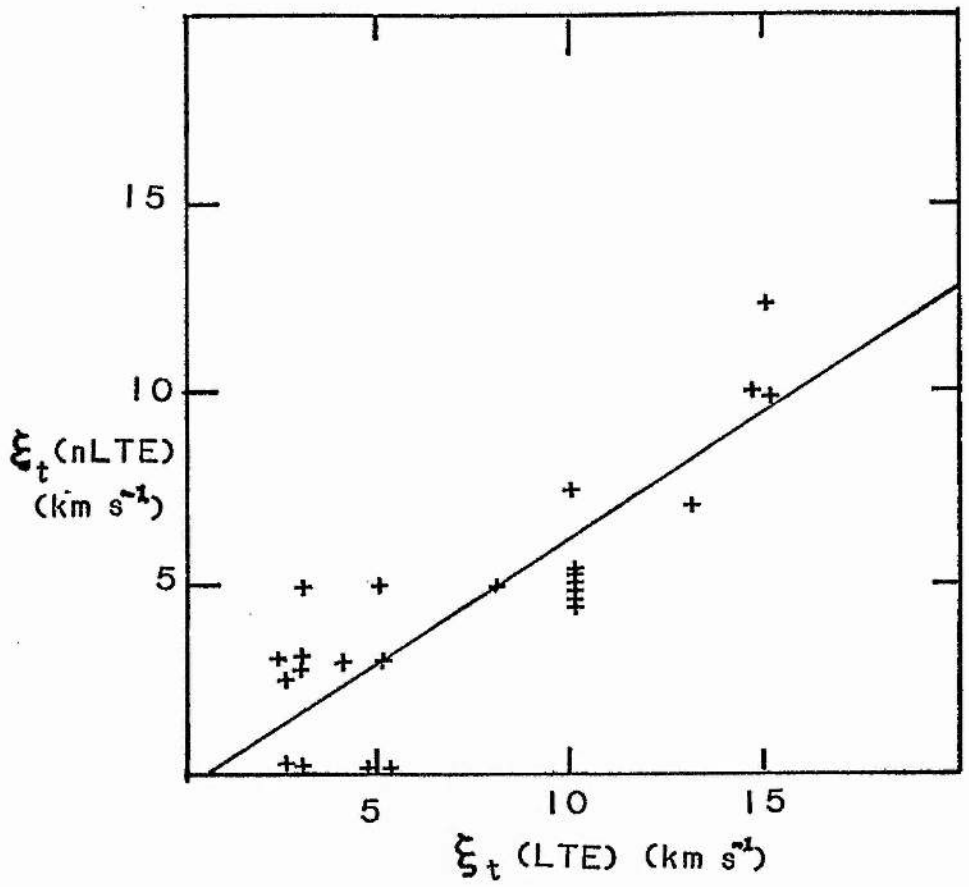

Fig. 5.26 :- **Comparison of the values of ξ_t found using LTE and non-LTE models. The solid line is the least squares fit to the data described in the text.**

The most extensive determinations of the effective temperatures of early-type stars in recent years is that of *UDPD*. They use multi-waveband measurements of the stellar fluxes, including satellite observations of the U.V. spectra. They correct for reddening and adopt a distance to the stars using previously published data. Using the same Kurucz line-blanketed LTE model photosphere computer program used in this project they determine angular diameters and effective temperatures for the stars using the iterative method of Blackwell and Shallis,1977, from

$$\sigma_R T_{eff}{}^4 = 4\theta^{-2} \int_0^\infty f_\lambda \, d\lambda$$

where σ_R is the Stefan-Boltzmann constant and θ is the angular diameter of the star. Corrections for the flux from unobserved parts of the spectrum are taken from the model. The major uncertainties in this method are the corrections for the interstellar reddening and the assumption that the angular diameter for the star determined from the red and infrared portions of the spectrum are appropriate to other wavelengths.

As the method is based on the definition of T_{eff} and is to some extent model-independent it is, in principle, the best method of determining effective temperatures. The method does still, however, rely on the use of model photospheres and, clearly, if the physics of these models is correct the same models should accurately predict the observed absorption lines. Effective temperatures derived from absorption line spectra should then be the same as those derived from the integrated flux method. Underhill and Doazan,1982, however, collect data on effective temperatures of B stars determined in more than one way. They find that effective temperatures determined from the line spectrum are systematically 1200-3100K higher than those found from integrated flux and allied measurements. None of the line studies, however, utilised the same line blanketed LTE models used by *UDPD*.

Figure 5.27 shows a comparison of the *UDPD* determined temperatures with those determined in this study with LTE models for the eleven stars in common between the two projects. The dashed line represents equality between the two sets of measurements. Apart from the results for HD 165024, the only supergiant in the comparison, the agreement between the two is satisfactory. The mean difference in temperatures derived by the two

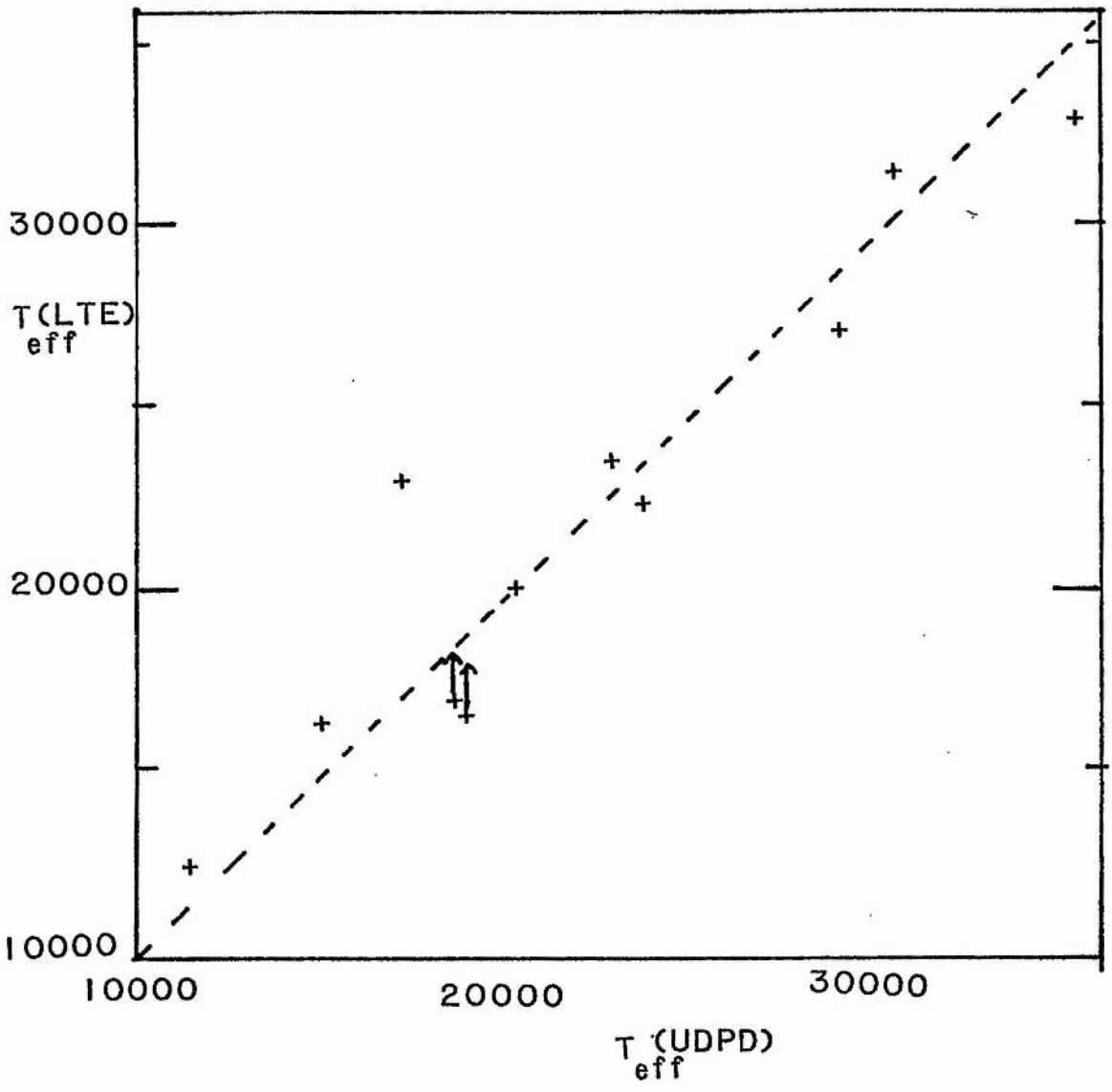

Fig. 5.27 :- **Comparison of the LTE effective temperatures found here with those found by *UDPD* using the integrated flux method. The dashed line shows $T_{eff}(LTE) = T_{eff}(UDPD)$. Arrows for two stars show the effective temperatures which would have been derived for $\log g = 4$.**

methods (in the sense $UDPD - Stewart$) is 719K. The r.m.s. scatter in this quantity is 1640K. By the criterion of Underhill and Doazan this result means that the two methods derive identical effective temperatures.

The agreement is improved still further by the elimination of HD 169467 and HD 180163 from the comparison. This reduces the mean temperature difference to 276K. These two stars were commented upon as having surface gravities much lower than those asssumed by $UDPD$. Arrowed lines in figure 5.27 connect the solutions for these stars to the solutions that would have been found for log g=4.0, the value assumed by $UDPD$.

To investigate any systematic trend between the two temperature scales linear fits were made to the data excluding HD 165024 both with, (a), and without, (b), HD 169467 and HD 180163 with the following results.

$$T_{eff}(UDPD) = 1.006 T_{eff}(Stewart) + 590K \qquad a$$

$$T_{eff}(UDPD) = 1.070 T_{eff}(Stewart) - 1431K \qquad b$$

The maximum temperature difference between the two scales is $\approx$ 1500K at 32500K (Stewart) in solution b so clearly there is no strong evidence for a systematic change in slope between them.

The discrepancy for HD165024 is difficult to explain. This is the only supergiant in the sample. $UDPD$ suggest that the effective temperatures of supergiants are much less than for other stars of the same spectal type. They claim that 'mantle' effects cause temperatures derived from the line spectrum to be systematically too high. The $UDPD$ method is also more subject to error when applied to supergiants. Corrections for extinction are larger, and possible emission effects from the Balmer and Paschen continua and red and infrared emission from the stellar winds observed in supergiants may cause errors in the derivation of angular diameters of these stars. HD 165024 is an observed X-ray source (Cash and Snow,1982) showing that non-thermal effects *are* important in this star and the high value of ξ_t found in both the LTE and non-LTE analyses of this star may also be indicative of large non-thermal effects. Other errors in the model photospheres, such as the assumption of hydrostatic equilibrium and the neglect of curvature, may be important for stars with such extended atmospheres.

A mean temperature scale with spectral type has been obtained by grouping stars of luminosity classes IV and V and classes II and III together. This is listed in Table 5.ix and is similar to that derived by *UDPD* Apart from the supergiant discrepancy the only other major difference occurs at B1 IV/V. This bin contains only HD 116658 in this sample however and consequently may be in error.

The similarity between the two scales again suggests that careful analysis of the line spectrum is as accurate and useful a method of determining effective temperatures of early-type stars as integrated flux measurements.

Abundances

The B stars present an opportunity of investigating the composition of the interstellar medium (ISM) at the time the B stars were formed. As this is relatively recent in cosmological terms (see next section) models of the enrichment of the ISM could, in principle, could be tested with this information.

Unfortunately the size of the errors in these abundance determinations is still rather high for this purpose. In this project the r.m.s scatter in the determination of an abundance of any one element in any one star was usually better than ≈ 0.20 dex. In addition to this error there is also a maximum possible systematic error caused by the selection ot the wrong $(T_{eff}, \log g, \xi_t)$ solution of ≈ 0.3 dex.

Clearly abundance differences of factors of 2 between stars cannot be considered significant. However, the t-test shows that the variation of the abundances about the means *is* significant at the 98% level. This suggests that there *are real* abundance variations amongst the stars in this sample.

Discussion here, however, will concentrate on the mean abundances of the B stars as a group. Comparison will be made with other observations of samples of B stars and of other types of object. Table 5.x summarises the results found here and also lists recent alternative abundances from large samples of B stars. Included for comparison are the solar abundances and abundances determined from emission lines in HII regions.

The mean C,N and O abundances found in this project are, at first glance, controversial. They are $\approx 2\sigma$ less than the corresponding solar values and are also quite different from other analyses of B stars whose authors have claimed that the abundances

Table 5.ix

Temperature Scale

	III/IV	*II/III*	*I*
O9	33000	—	—
B0	31750	26450	—
B0.5	—	26700	—
B1	23500	22350	—
B1.5	—	—	—
B2	21850	—	22800
B2.5	16500	—	—
B3	16450	—	—
B5	14850	14500	—
B6	—	13600	—
B8	—	12000	—

Table 5.x

Mean Abundances

(a)	X/H							
objects	*Reference*	[C]	[N]	[O]	[Mg]	[Si]	[S]	[Al]
B stars	1	8.01	7.53	8.38	7.42	7.20	6.79	5.94
	2		7.66			7.29		
	3	7.76	7.93	8.92				
	4		7.90					
	5		7.60					
HII regions	6		7.57	8.70			7.06	
Solar	7	8.52	7.96	8.82	7.42	7.55	7.20	6.20

(b)	X/O		
B stars	1	−0.37	−0.85
β − Ceph	8	−0.33	−0.68
B stars	3	−1.16	−0.99
HII regions	6		−1.13
Solar	7	−0.30	−0.86

References:

1: This project, LTE

2: This project, non-LTE

3: KMD LTE, $\xi_t = 5.\ km\ s^{-1}$

4: DKM non-LTE, $\xi_t = 0.\ km\ s^{-1}$

5: DKM non-LTE, $\xi_t = 5.\ km\ s^{-1}$

6: Shaver *et al*,1983

7: Shaver *et al*, 1983, and references therein

8: Watson 1971, LTE, $\xi_t = 4.\ km\ s^{-1}$

found are close to solar.

At first it was thought that some error had occurred in the analysis presented here. The data were examined for systematic trends with T_{eff} or with log g. When no such trend was found, however, a more critical comparison of the results was made. This raised the following points.

The largest sample of B stars analysed recently to find abundances using LTE models is that of *KMD*, 1981. They assume a value of $5 km\ s^{-1}$ for ξ_t and find abundances close to the solar values for both nitrogen and oxygen. A deficiency of ≈ 0.7 dex was found for the mean carbon abundance.

Only the line at 4267Å was used to determine the carbon abundance, however. This study, and other authors, have commented that this line gives anomalous abundances. A correction of the same magnitude used here would bring the carbon abundance found by *KMD* into agreement with that found here.

Using much the same data sample as *KMD*, Dufton *et al*, 1981, (herafter *DKM*) made a non-LTE abundance analysis of a number of nitrogen lines. They found that the line strengths could be explained with a combination of either solar abundance and $\xi_t = 5\ km\ s^{-1}$ or [N]= 7.6 dex and $\xi_t = 5\ km\ s^{-1}$. They preferred the former combination on the grounds that there was no theoretical mechanism for a depletion of nitrogen in the photospheres of early-type stars.

In the analysis of *KMD* a value of 5 $km\ s^{-1}$ was also assumed, before the abundances were derived. This study has shown that this is an underestimate of the microturbulent velocity required for most stars in an LTE analysis of near main-sequence stars. An examination of the trend of the required abundance with equivalent width for the results of *KMD* also suggests that this is true. Even with the use of non-LTE line calculations a value of 0 $km\ s^{-1}$ is too low to explain the observed lines. A value of 5 $km\ s^{-1}$ would be a better approximation here. When the use of different values of ξ_t is accounted for the results of *KMD* are in reasonable agreement with those found in this LTE study while those found in the non-LTE analysis are in good agreement with those found by *DKM*.

A further point to note is that the nitrogen abundance found here is similar to that

found from studies of HII regions in the solar neighbourhood. As HII regions are also tracers of the abundances in the ISM at sites of recent massive star formation there may be real evidence for a depletion of nitrogen by a factor of ≈ 2 since the solar system abundances were frozen in.

The oxygen discrepancy is more puzzling. The use of higher values of ξ_t by KMD would have resulted in their finding a value of $\approx$ 8.75 dex for [O], while the oxygen abundance found from HII regions is 8.70 dex. The result in this study is still 1.5σ below these values. It is possible that the use of non-LTE calculations for oxygen here would have resulted in the finding of a higher value of [O], as was found for [N] and [C], more in agreement with the value found for HII regions.

(It was noted that the method of averaging logarithmic abundances for several lines to determine the mean element abundance gives results systematically lower than would have been found if the averaging had been made in number space. The effect of this may be to reduce the derived abundance by $\approx$ 0.08 dex for lines with a spread in abundance typical of those found in this project.)

Is the evidence for deficiencies of carbon, nitrogen and oxygen real or are the low abundances derived for these elements some artefact of the reduction and analysis system? The only evidence that they might not be real comes from an observation that there is evidence of a trend of derived oxygen abundance with ξ_t. The mean abundance found for stars with $\xi_t > 5\ km\ s^{-1}$ was 8.32±0.20 dex while that for stars with $\xi_t \leq 5\ km\ s^{-1}$ was 8.53±0.23 dex. While the difference between the two subsets is not particularly significant it does suggest that it may be possible that microturbulent velocities are not real entities and are only some parameter which makes allowance for deffects in the model photospheres used. With $\xi_t = 0\ km\ s^{-1}$ abundances close to the solar or HII values would have been found for all three elements.

Apart from the individual absolute abundances of carbon, nitrogen and oxygen the relative abundances of these elements is also of interest. While carbon and oxygen are both thought to be primary products of nucleosynthesis, nitrogen is thought to be secondary in origin. A variation in the relative abundances of these elements would therefore provide constraints on late nucleosynthesis and primeval abundances. Clearly relative abundance

measurements are also less likely to be subject to difficulties in interpretation as errors in microturbulent velocities, effective temperatures, etc. affect lines of all these elements by roughly the same amount.

Table 5.x shows the mean carbon and nitrogen abundances relative to that of oxygen. Similar quantities derived by *KMD* and Watson, 1971, in a study of β-Cepheid variables are also listed along with the solar values and the nitrogen:oxygen ratio from HII regions. The results here are in excellent agreement with the solar values and with those found by Watson while the difference between the [N]:[O] ratios of this study and those of HII regions is only $\approx 1\sigma$.

While analysing the results it was noted that the scatter of the [N]:[O] ratios among the stars was only half that of the [C]:[O] or [C]:[N] ratios.

Of the other elements for which abundances were determined only magnesium was found to have the same value as solar. The other elements were again underabundant with respect to solar and the same arguments about a reduced value of ξ_t apply as for carbon, nitrogen and oxygen. Also the use of non-LTE calculations for silicon resulted in a derived abundance closer to solar than the LTE analysis.

The silicon to sulphur ratio is about three times solar. This is different to the ratios found from measurements of the X-ray spectra of young supernova remnants (e.g. Becker *et al*, 1981) who find that the inverse is true. Abundance derivations from X-ray spectra of supernova remnants are subject to error, however, due to the neglect of possible non ionisation-equilibrium effects.

5.x *Masses and Ages*

The age and masses of stars can be inferred from a comparison of their position in the HR diagram with theoretical predictions of the evolutionary tracks of stars of different masses.

Ideally the comparison should be made in the same $(T_{eff}, \log g)$ plane as these are the directly observable quantities. Unfortunately the calculations are rarely presented in this format. The most common format for the presentation of such calculations is the (T_{eff}, M_{Bol}) plane.

To compare the results found here with evolutionary calculations it was necessary to

obtain bolometric luminosities for the stars. This was done in two stages. Absolute visual magnitudes were taken from the compilations of Lesh, 1968, 1972. Bolometric corrections were interpolated using the calibration of the ATLAS6 programme made by Buser and Kurucz, 1978, and the LTE effective temperatures found in the course of this project. Table 5.xi lists these quantities and also gives an identification number for each star. These identification numbers can be used to locate individual stars plotted in figure 5.28.

Also shown in the figure are the evolutionary tracks of stars of 7,10,15 and 30 $M_{\odot}$ as calculated by Stothers and Chin, 1977. (These calculations were made using the Carson opacities.) Also shown are the zero-age main sequence positions of stars of 3 and 5 $M_{\odot}$.

Also shown in the figure is the size of a typical error bar. This assumes an error of $\approx$ 5% in the value of T_{eff} while the error in M_{bol} is taken as 0.5 magnitudes. This incorporates the error estimate of 0.4 mag given by Lesh *et al*, possible errors in the bolometric correction and systematic errors in the determination of M_v.

The masses determined for the stars and estimated ages for those stars with masses greater than $\approx 5M_{\odot}$ are given in table 5.xi. The masses range from $\approx 3M_{\odot}$ to $\approx 25M_{\odot}$ in agreement with the canonical values for B stars.

The only star in the sample for which a mass has been determined, other than from spectroscopic or photometric modelling, is HD 116658 for which a dynamical mass has been determined. Popper, 1974 found $10.9 \pm 1.3\ M_{\odot}$ as compared to the value of $13.5 \pm 2.0\ M_{\odot}$ found here. These are only marginally in agreement. The evolutionary calculations, however, ignore possible effects of mass loss and mass transfer in a binary system while the analysis here is also more subject to error because of the binary nature of the star.

Most of the stars are still probably at the stage of core hydrogen burning although a number may, within the possible errors, have entered the core contraction and hydrogen shell burning phase of evolution For stars with masses $> 5M_{\odot}$ the star which is most likely to have reached this phase according to its position in the HR diagram is HD 165024, as might have been predicted from its supergiant classification. Indeed if the effective temperature determined by *UDPD* had been used this would have been even more certain.

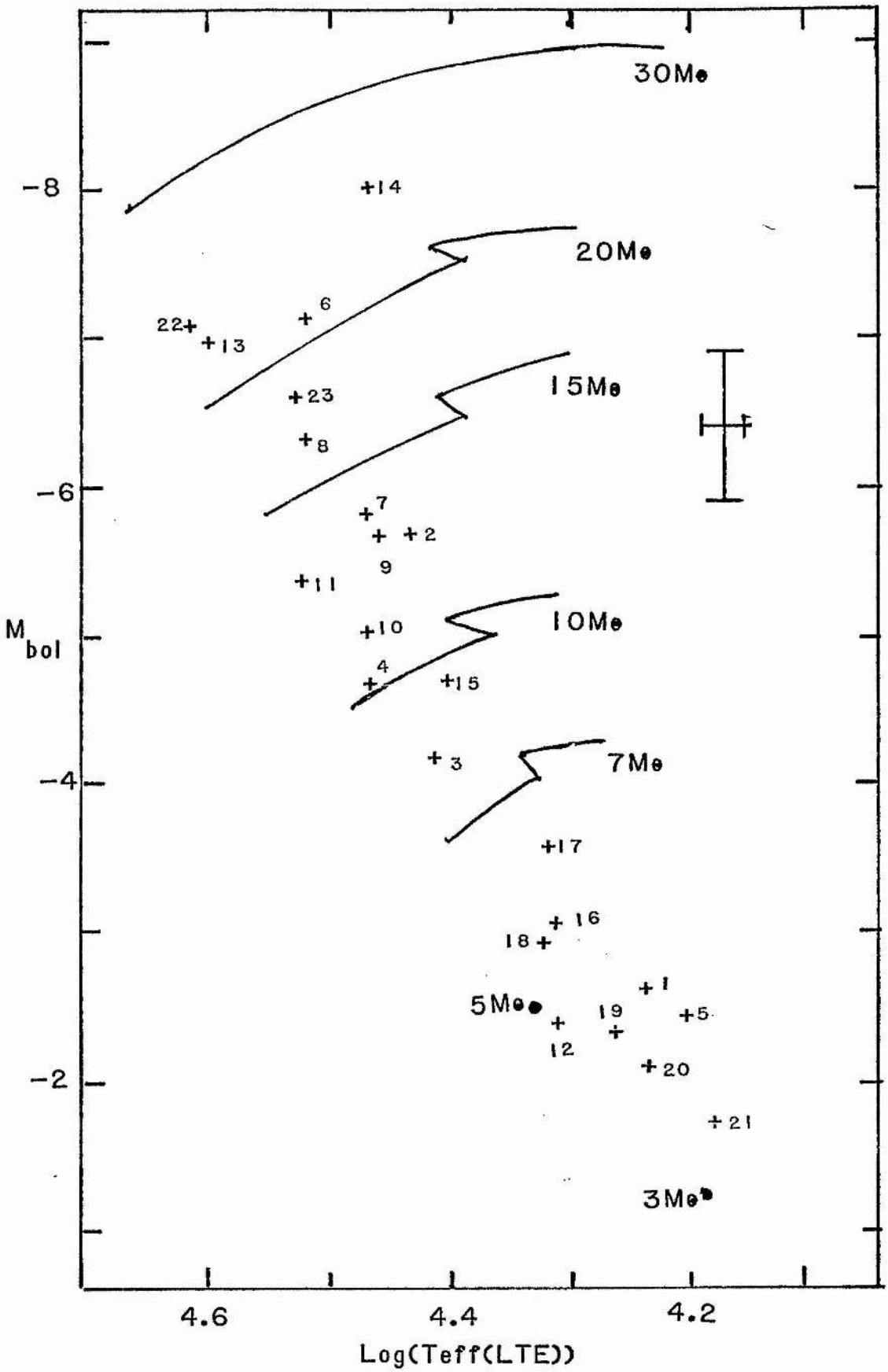

Fig. 5.28 :- **HR diagram for stars studied in this project. The evolutionary tracks calculated by Stothers and Chin are also shown.**

Table 5.xi

HD	*Id.No.*	M_v	*BC*	M_{bol}	*Mass*	*Age*
		mag.	*mag*	*mag*	$M_\odot$	$10^6 yrs$
15371	1	−1.8	−1.0	−2.8	4.6	—
74575	2	−3.5	−2.2	−5.7	12.5	10
79351	3	−2.3	−1.9	−4.2	8.3	20
81188	4	−2.3	−2.3	−4.6	10.0	10
106625	5	−1.8	−1.0	−2.8	4.3	—
111123	6	−4.7	−2.4	−7.1	21.0	6
116658	7	−3.7	−2.1	−5.8	13.5	9
118716	8	−3.9	−2.4	−6.3	16.5	7
129056	9	−3.6	−2.1	−5.7	13.0	9
132200	10	−2.9	−2.1	−5.0	11.0	13
147165	11	−2.8	−2.5	−5.3	13.0	< 2 :
147394	12	−1.0	−1.4	−2.4	4.6	—
149438	13	−4.1	−2.8	−6.9	22.0	4
165024	14	−5.8	−2.2	−7.9	24.0	6
166182	15	−2.8	−1.9	−4.7	9.5	17
169467	16	−1.6	−1.4	−3.0	5.3	—
180163	17	−2.3	−1.3	−3.6	6.0	35
184171	18	−1.6	−1.3	−2.9	5.3	—
184930	19	−1.4	−1.0	−2.4	4.3	—
195810	20	−1.4	−0.7	−2.1	4.0	—
207971	21	−1.1	−0.6	−1.7	3.5	—
214680	22	−4.0	−3.0	−7.0	23.0	3
218376	23	−4.1	−2.4	−6.5	17.0	6

5.xi *The β Cepheid Stars*

Four confirmed β-Cepheid type stars were included in the sample of stars which were observed. β-Cepheid stars show small amplitude (≤ 0.1 magnitude) photometric variations, and $\leq 100\ kms^{-1}$ radial velocity variations on periods of the order of 5 hours. Some also show evidence of line profile variations. (A number of other B stars outside the spectral range considered to be the domain of β-Cepheids stars have recently been shown to exhibit line profile variations but they have longer and less coherent periods and so are a distinct phenomenon (e.g. Smith, 1976, Smith *et al*, 1977)).

The four stars included in this survey – HD 111123, HD 116658, HD 129056 and HD 147165 – were found to have similar abundances and other properties to other B stars of similar spectral types apart from one factor.

The intriguing suggestion from the data is that the values of ξ_t found for these stars may be systematically higher than for other stars with similar effective temperatures.

Figure 5.29 shows the distribution of the derived non-LTE values of ξ_t for all stars with 20000K $< T_{eff} <$ 30000K. The locations of the β-Cepheid stars within this distribution are shaded. Only two of the five stars with values of $\xi_t > 5\ kms^{-1}$ are not β-Cepheids and one of these is the supergiant HD 165024.

No evidence could be found that HD 218376 had been photometrically investigated as a possible candidate β-Cepheid and so it is possible that all the 'high' ξ_t stars are β-Cepheids. Unfortunately the sample here is too small to come to a definite conclusion about the difference in distributions of the microtubulent velocities but it is possible that the pulsations in these stars provide a driving mechanism for microturbulence.

5.xii *Line Profiles*

It had been hoped that it would be possible to use the information in the line profiles to discriminate between the LTE and non-LTE models. For the same equivalent width the predicted LTE profiles are broader and shallower than those computed with the non-LTE models.

Unfortunately at the resolution and $S : N$ ratio available here the information on the rotational velocity given by the Fourier transform sidelobes was suppressed. This meant that it was impossible to distinguish between a non-LTE line profile with a higher

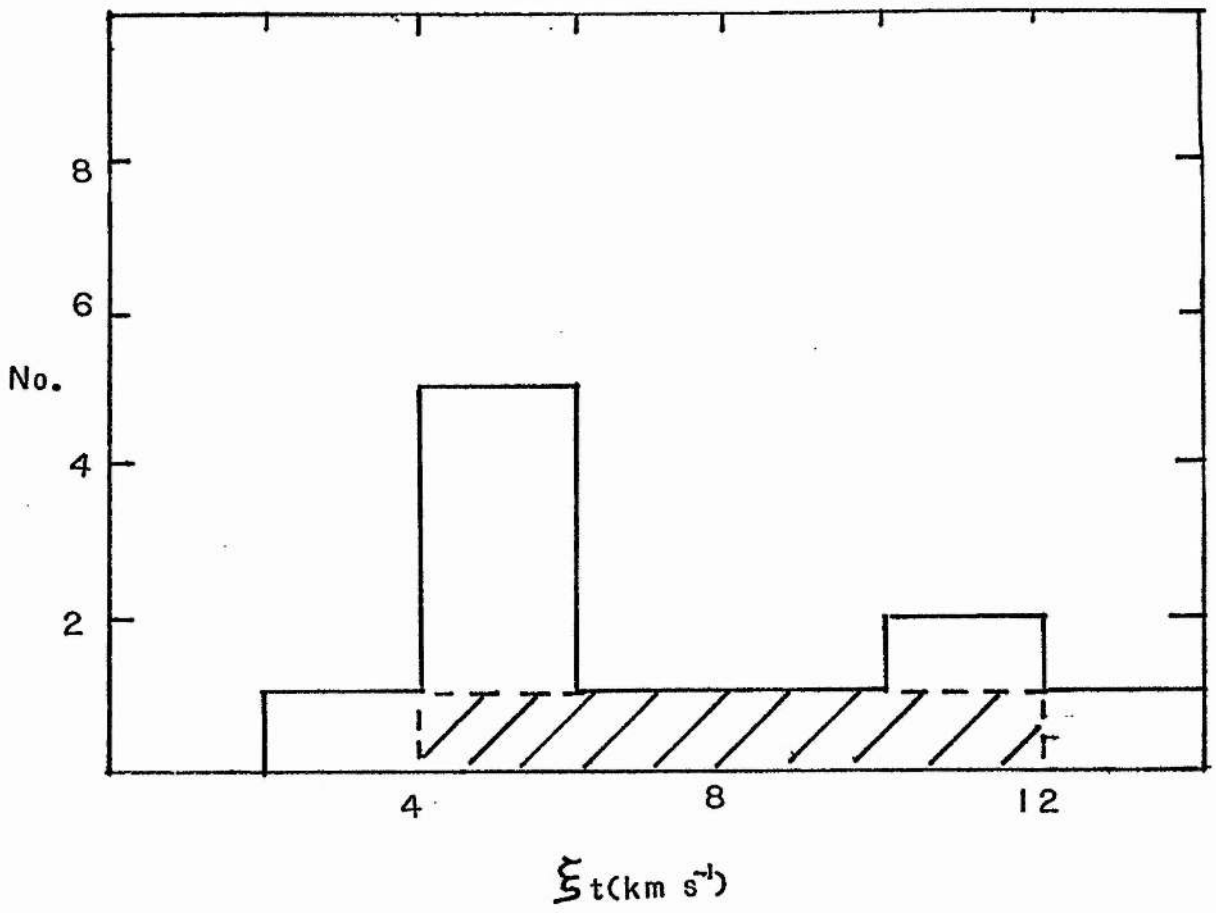

Fig. 5.29 :- Distribution of ξ_t values found for stars with $T_{eff} > 20000K$ using non-LTE models. The shaded area represents the positions of known β –Cepheids.

value of the projected rotational velocity, $V_{rot} \sin i$, and an LTE profile convolved with a lower value of $V_{rot} \sin i$. An improvement of a factor of $\approx$ 3 in either the signal to noise or the resolution would have been sufficient for this analysis to have been carried out for almost all the stars. For HD 149438 the observed line profiles were only just consistent with an LTE model and no rotational velocity.

Values of $V_{rot} sini$ were determined from the Fourier transforms of the silicon line profiles using the observed instrumental profiles and the respective non-LTE model profiles using the techiques described by Gray, 1976. For the plates obtained at S.A.A.O the instrumental profile obtained with the Cadmium source and determined as described in Chapter 4 was used. For the plates obtained at D.A.O. the mean profile of seven comparison arc lines was used. Values obtained from these plates are, therefore, more uncertain than the others and are indicated by an asterisk in Table 5.xii. The half-widths of the He I 4471 and Mg II 4481 lines were also used in conjunction with the predictions of Slettebak *et al* to determine values of $V_{rot} \sin i$. The results listed in table 5.xii are the mean values obtained by the two methods. In general the standard deviation of the values obtained from different lines was $\approx$ 20%.

The values obtained for a number of the stars by Slettebak *et al* (SEA) and those in the catalogue of Uesugi and Fukuda, 1970, (U&F) are also given in the table. The agreement between the different results is good.

5.xiii *Summary*

The principle conclusions drawn from the analyses just discussed are briefly summarised here.

The use of non-LTE models does result in greater self-consistency between the effective temperature and log g values indicated by the ionisation balances of different silicon ions, measurements of the Balmer discontinuity and the profile of H_γ than the use of LTE models. The improvement, while noticeable, does not entirely remove discrepancies between values obtained from different indicators. It may be that there exists a real variation of effective temperature across the stellar disc, in which case attempts to ascribe a unique effective temperature to the photosphere will fail. The use of integrated flux methods throws away any information about such variations and may

Table 5.xii

Rotational Velocities

HD	*Stewart*	*SEA*	*U&F*
15371	9	< 10	0
74575	10	15	1
79351	7	< 10	0
81188	28	—	31
106625	26	—	41
111123	36	35	35
116658	—	—	196
118716	80	110	—
129056	8	15	0
132200	18	10	30
147165	68	—	47
147394	35	30	27
149438	10	< 10	20
165024	140	—	139
166182	45 :	—	35
169467	19 :	20	0
180163	35 :	—	20
184171	25 :	—	10
184930	75 :	—	105
195810	45 :	—	52
207971	48 :	55	57
214680	28 :	—	23
218376	55 :	—	74

therefore require caution in its application. For both silicon and nitrogen lines, when non-LTE models are used the standard deviation amongst abundances for lines of one star is reduced relative to that found for the same lines using LTE models.

The temperature scale derived with the non-LTE models is little different from that which would have been deduced with the use of unblanketed LTE models. The use of line-blanketed LTE models gives a temperature scale derived from absorption line measurements in good agreement with that determined from measurements of the integrated flux.

Microturbulent velocities found with non-LTE models are smaller than those found with LTE models. They are not reduced to zero, however. The reality of microturbulence as a physical phenomenon is still unclear. While it remains necessary to incorporate microturbulence as a fitting parameter, its use may disguise other errors in the adopted models and may not imply the existence of small scale extra-thermal motions. There are arguments both for and against the existence of possible real microturbulence. The low abundances found would be increased were it not for the inclusion of microturbulence in the models and would then not require any physical explanation of the depletion of heavy elements in B stars. The existence of X-ray emission from B stars and the pulsations of the β-Cepheids is strong evidence of ' non-thermal ' activity in the atmospheres of these stars, as is the existence of stellar winds outflowing from the atmospheres. Both coronae and winds require the deposition of $\approx 10^{35}\ ergs\ s^{-1}$ of mechanical energy at the surface of the photosphere. It is possible that microturbulence may be the means of communicating this energy through the photosphere to the stellar 'mantle'.

The abundances derived are heavily dependent on the value of ξ_t assumed in the models. As the interpretation of the required microturbulence is unclear so are the derived abundances. Contrary to expectations the use of non-LTE models increases the required abundances, this effect being due to the reduction in ξ_t discussed above.

Clearly further observations are required to use the line profile information to investigate the reality of the microturbulence phenomenon in early-type stars.

CHAPTER SIX

MICHELSON INTERFEROMETER OBSERVATIONS

6.i *Introduction*

In chapter one of this thesis it was shown that, with certain assumptions, the effects of different line broadening mechanisms on emergent absorption line profiles could be represented by convolutions. Further, the fourier transforms of the convolving functions for rotational broadening and the broadening caused by macroturbulence can be represented by fairly straightforward analytic functions. This has led other authors to suggest the use of the power spectra of line profiles to discriminate between the different line broadening mechanisms.

Two practical difficulties occur in the application of this method to power spectra generated by fourier transforming line profiles measured with conventional dispersive spectrometers. These are the signal to noise ratio and the instrumental profile. White noise present in the original line profile transforms to a level that is constant with frequency in the fourier domain. As the signal level present in the power spectrum decreases with frequency the S:N worsens at the higher fourier frequencies where the useful sidelobe information is to be found. The instrumental profile further reduces the signal level at the higher frequencies and, as discussed earlier, without accurate measurement of the instrumental profile and high S:N values in the data, the removal of its effect is difficult.

Clearly, an instrument with almost constant signal to noise in the the frequency domain which did not suffer from the problems of an ill-determined instrumental profile would have great potential in the application of the power spectrum decomposition analysis technique. The Michelson interferometer is an instrument with these properties.

During the course of this project a Michelson interferometer developed by Dr. R. Wayte of Imperial College, London, became available for use on an experimental basis at

the coudé focus of the Isaac Newton Telescope (INT) at the Royal Greenwich Observatory (RGO), Herstmonceux.

A number of observations were made with this instrument as a pilot study to examine the potential of the analysis techniques for early-type star line profiles. These observations and their subsequent analysis are described here.

6.ii *The Interferometer*

The principles and construction of the Michelson interferometer are fully described elsewhere (Wayte and Ring, 1977) but a brief review of the principal features will be given here.

The design is not of the classical type with one fixed and one moveable mirror. Instead the two mirrors are 'catseye' constructions fixed back to back in one moveable assembly. The assembly is controlled by D.C. linear motors which drive it in an oil film through a honed tube, position measurement being made accurately using a reference laser. The maximum path difference possible, 1.5m, corresponds to a maximum sampling frequency of $200c\,\mathring{A}^{-1}$ at 5000Å or a resolving power, R, of 10^6.

At the time of use the interfered beam required monochromation prior to the detection of the two channels. This was accomplished by using a diffraction grating. The position of the grating, and hence the wavelength of the passband, is altered by means of a stepping motor. After this dispersion the beams pass through lenses and output slits to the two photomultipliers. A planned improvement to the instrument was the addition of a multi-element detector, thus enabling the simultaneous observation of a number of different wavelengths.

An INTERDATA 70 mini-computer controls the sampling electronics and mechanical movement of the interferometer. The operating programs also allow real-time viewing of the accumulating interferogram and, at intervals, the resultant spectrum.

6.iii *The Observations*

It was originally intended to investigate the Si II lines at 6347Å and 6371Å for a number of mid-late B stars which have been predicted by Kamp, 1976, to exhibit strong non-LTE effects. It proved impossible, however, to observe these particular lines as their wavelengths lay too close to that of the servo-laser. For this reason a study of the Si II

doublet at 5056Å was made.

Of the two periods, each of 4 nights, allocated by PATT to this project 5 nights proved totally unuseable due to rain. Partial cloud cover for the remaining 3 nights further limited the observations to only very bright stars. The number of reflections inherent in the construction of the Michelson interferometer make it a slow instrument. When combined with large amounts of cloud the required observing times limit observations to only the very brightest stars. This factor is reflected in the chosen observational programme which consisted of a comparative study of the silicon doublet in stars of early A spectral type. (A further consideration in the choice of this observing program was the use of Sirius as a comparison star for the photographic spectroscopy discussed earlier). The secondary criterion for inclusion in the observing programme was that the projected stellar rotational velocity quoted in the catalogue of Uesugi and Fukuda, 1970, (U+F) was low.

The observations, which were made in collaboration with Dr. R. Wayte, are summarised in Table 6.i.

6.iv *The Observational Procedure*

A passband of halfwidth $\approx$ 5Å centred at 5056.52Å was selected using a program written by Dr. R. Wayte which optimises the passband and sampling interval for a given wavelength and resolution. The step-size chosen for the movement of the catseye assembly was equivalent to 0.08114 cÅ and for all stars except α Cyg 128 samples were taken. This is equivalent to a resolution, $\frac{\lambda}{\Delta\lambda}$ of $\approx$ 100000 in the wavelength domain. For α Cyg only 64 samples were taken as the lack of high frequency information became apparent early in the observation.

Prior to, and immediately after, each night of observation scans of a white light source and of a source of line emission of known wavelength were made to ensure the alignment of the system was maintained.

Each star was observed a number of times (5-10) for short periods rather than for one long period and the individual observations were then combined to produce the final observation. This procedure was followed for two reasons. The weather made it preferable to have completed a number of short scans rather than to be midway through a long scan

Table 6.i

Michelson Interferometer Observations

HD	*Name*	*MK*	*W* ($m\text{Å}$)	$V_{rot} \sin i$ ($km s^{-1}$)
47105	γ *Gem*	*A0 IV*	145.8	21.2 ± 1.3
172167	α *Lyr*	*A0 V*	63.3	21.4 ± 0.9
95418	β *UMa*	*A1 V*	155.7	37.9 ± 2.3
48915	α *CMa*	*A1 V*	163.4	26.0 ± 1.2
97633	θ *Leo*	*A2 V*	139.6	21.9 ± 1.1
197345	α *Cyg*	*A2 Ia*	265.2	30.4 ± 2.6

when an observation was curtailed. (The Michelson can be stopped and started during an observation but only for moderately short periods.) A comparison of the results from the individual observations was made to investigate any short period variability in the line profiles. None was found.

During the scans the star was kept centred on the the entrance aperture by use of an autoguiding device affixed to the INT television monitor. After completing the observations of a program star a low resolution scan of a comparison star with no spectral line in the passband was made and used to remove the passband shape from the line profile. The $\frac{\sin x}{x}$ instrumental profile of the interferometer was also removed at this stage.

The taking of an individual sample of the interferogram was stopped when the number of counts in the channel with the lowest count rate was 100000. The noise level in the power spectrum is proportional to

$$\sqrt{\frac{I_r - I_t}{I_r + I_t}}$$

where I_r and I_t are the counts in the two interferometer channels. The $S : N$ ratio is the square root of the signal and is for a typical sample $\approx$ 150.

In figures 6.1-6.6 the resultant power spectra and line profiles are shown. The units of power are 11.74mÅ. The line profiles have been normalised to a continuum intensity of 1.0.

6.v *The Analysis*

The equivalent widths of the lines are obtained simply from the amplitudes of the zero-points of the power spectra. The statistical errors on these values are small ($< 1\%$) but possible systematic errors in the normalisation of the units of power increase the error to $\approx$ 5%. Table 6.i gives the results obtained.

An analysis of the line profiles was made using the fourier decomposition technique. A comparison of figures 6.1-6.6 with power spectra obtained from the fourier transforms of dispersive spectra (e.g. Gray, 1976) shows the high quality of the transforms to be analysed. Usually analysis of the power spectra are limited to, at best, the first and second sidelobes and frequently only the main lobe of the power spectrum is obtained above the noise level. Here, however, higher order sidelobes are available for analysis.

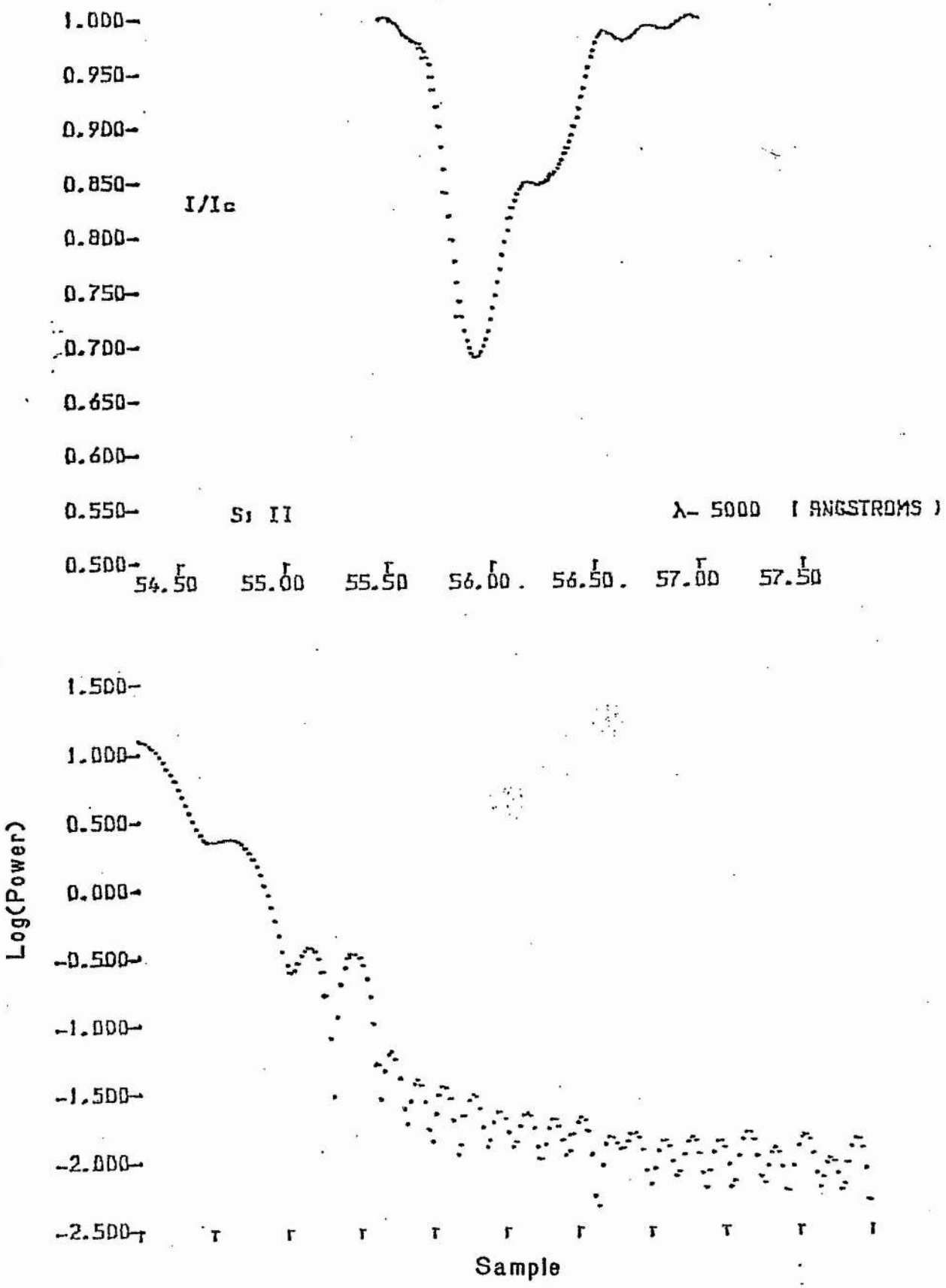

Fig. 6.1 :- **Line profile (upper) and power spectrum of the Si II doublet at 5056Å in the spectrum of γ Gem obtained with the Michelson interferometer.**

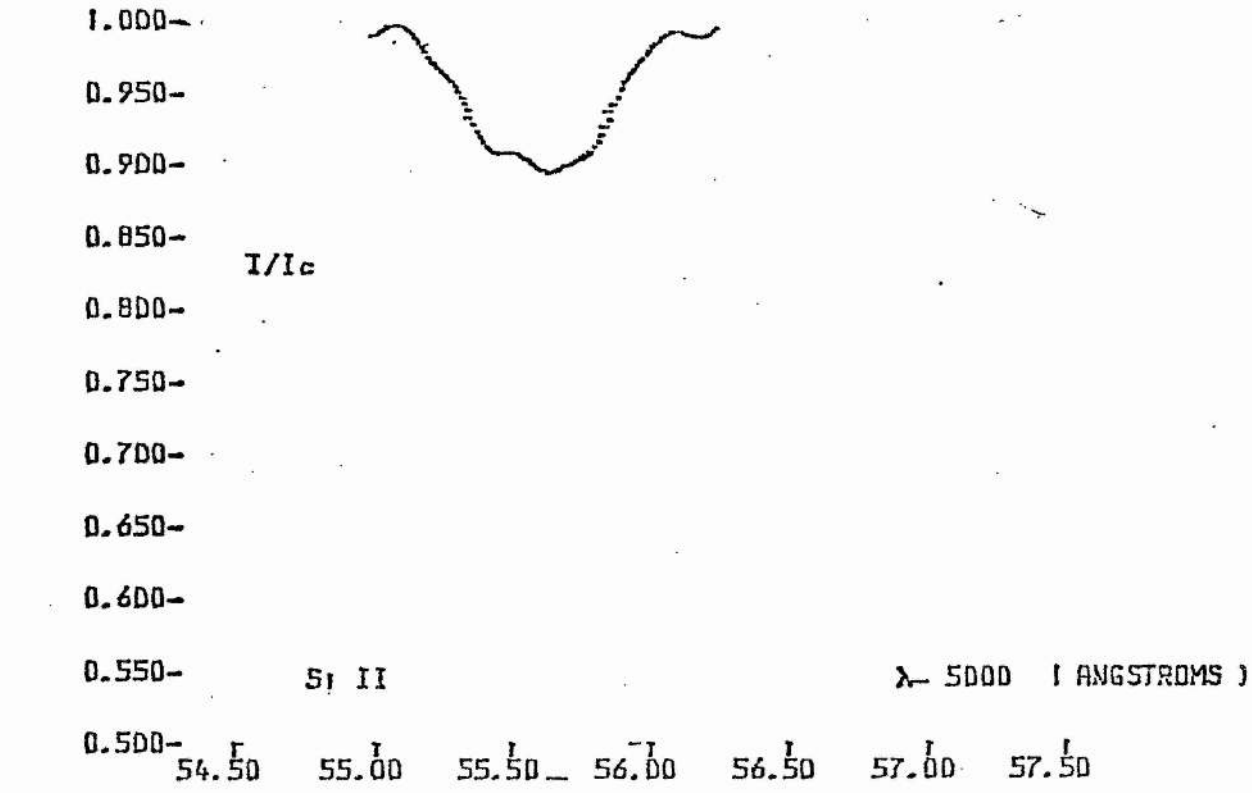

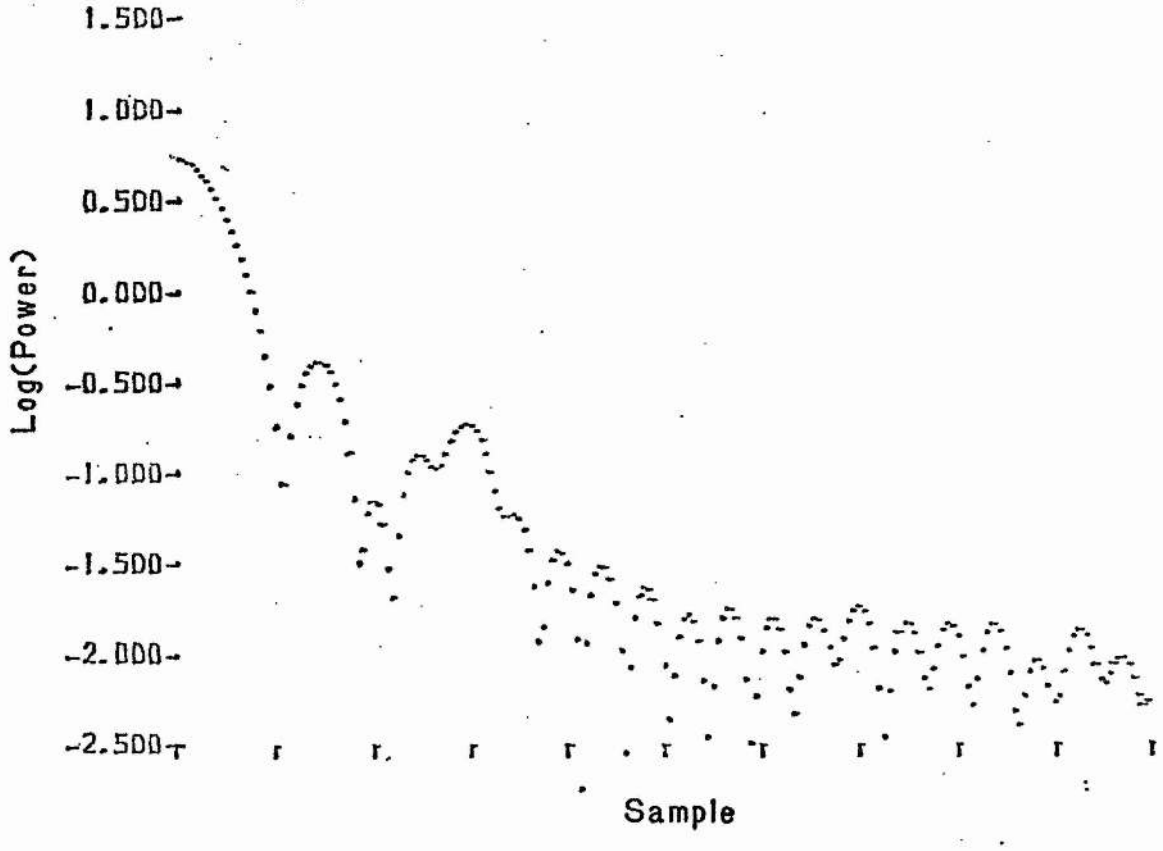

Fig. 6.2 :- As figure 6.1 for α Lyr.

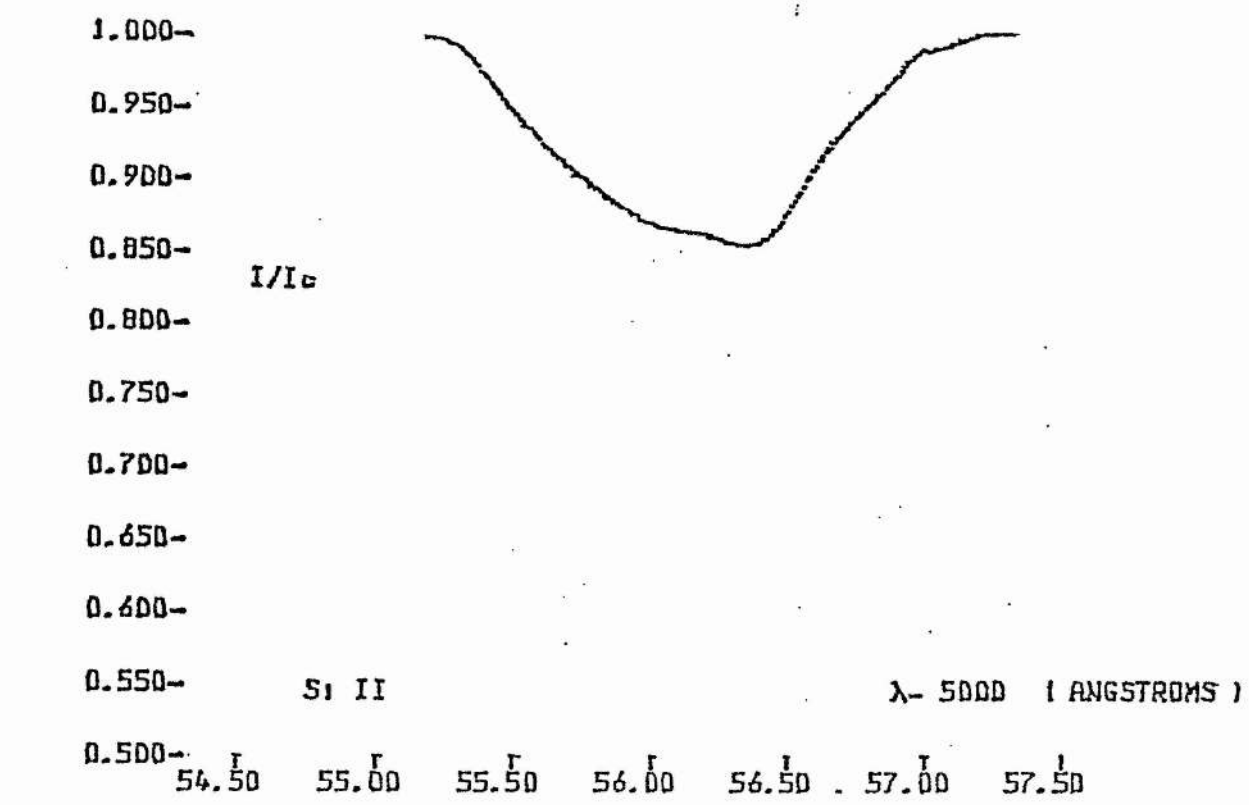

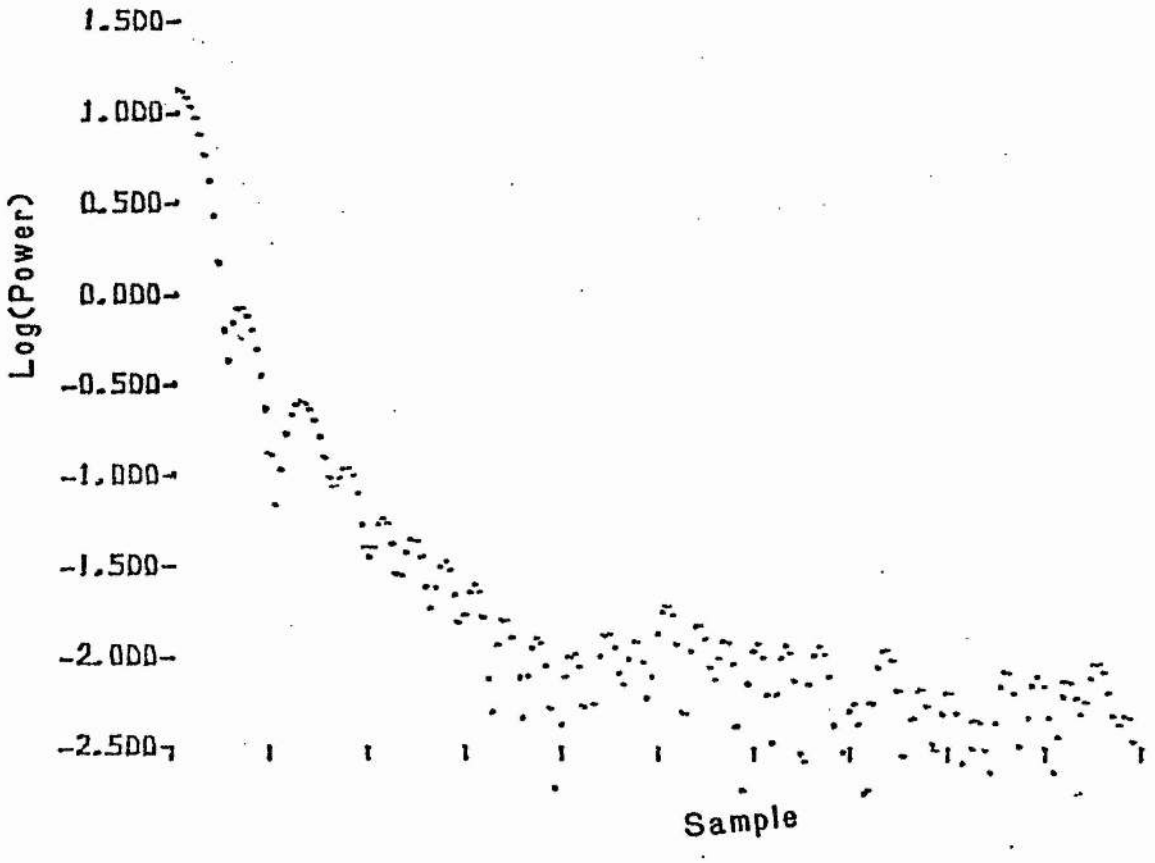

Fig. 6.3 :- As figure 6.1 for β UMa.

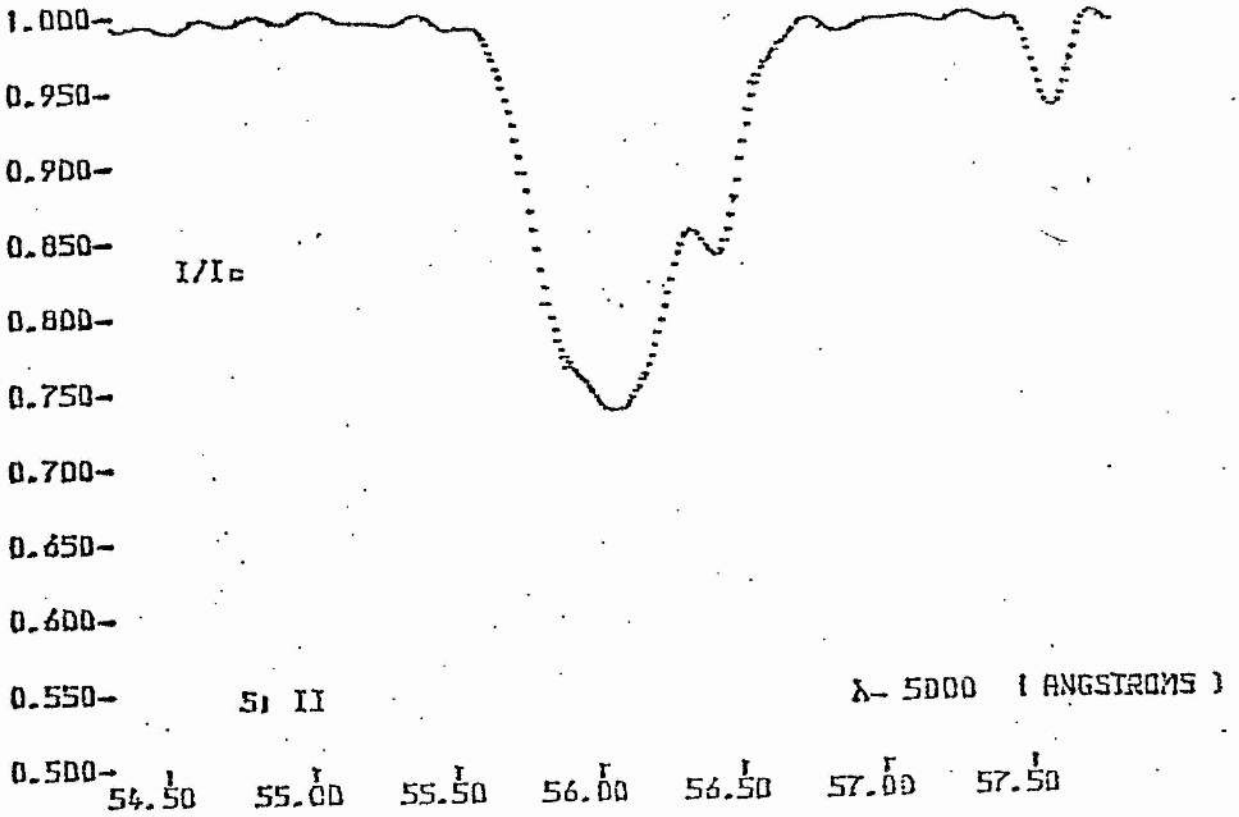

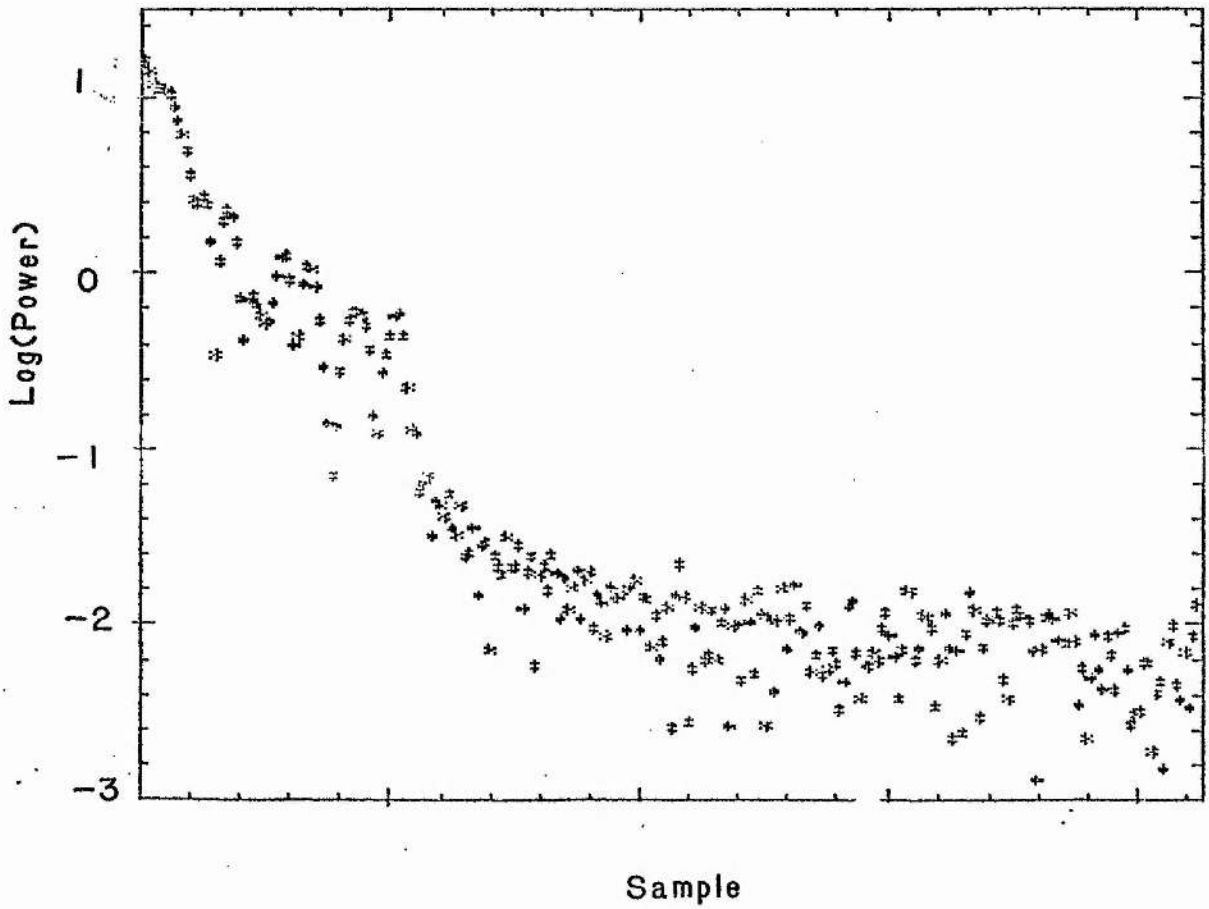

Fig. 6.4 :- As figure 6.1 for α CMa.

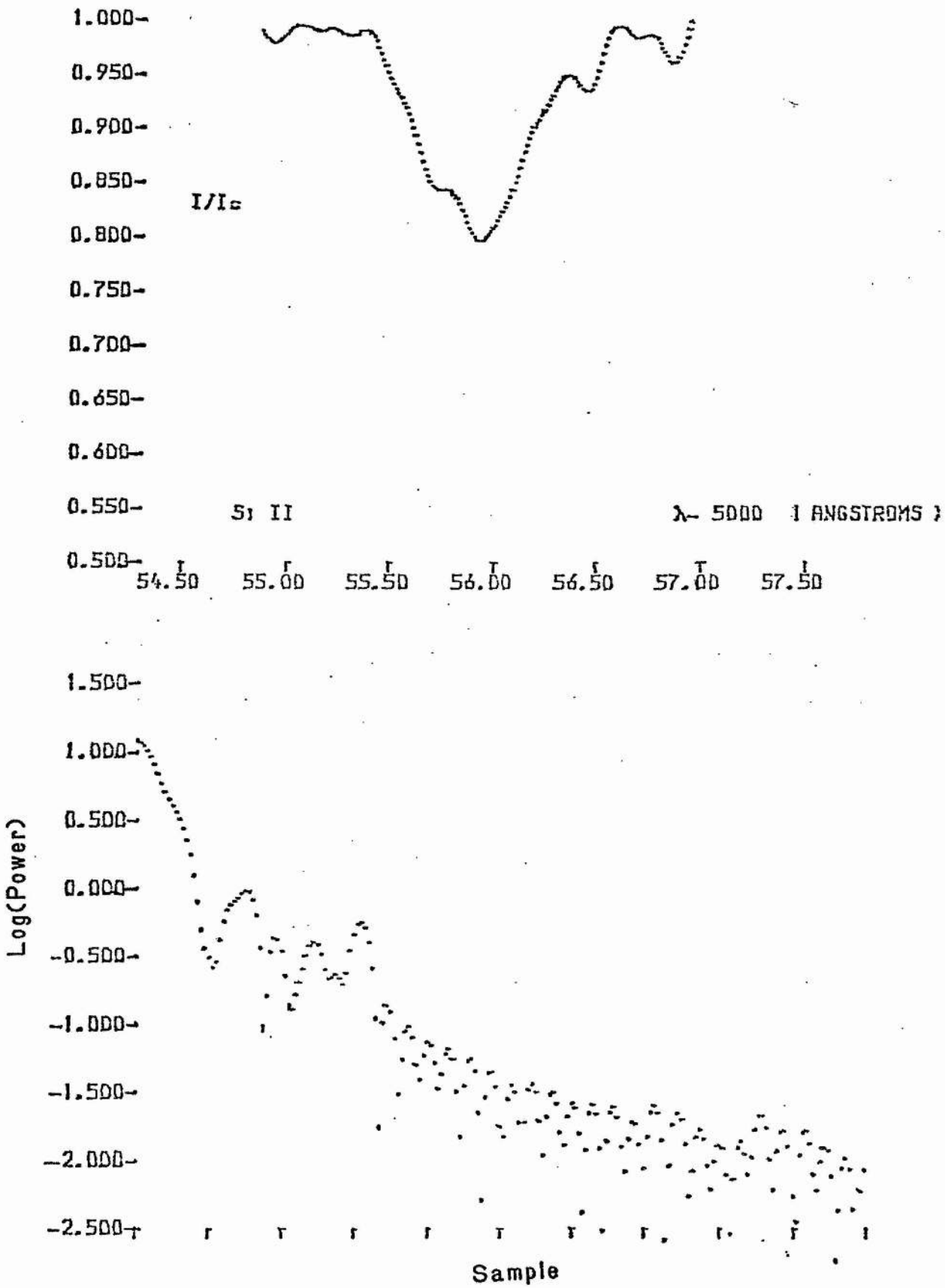

Fig. 6.5 :- As figure 6.1 for θ Leo.

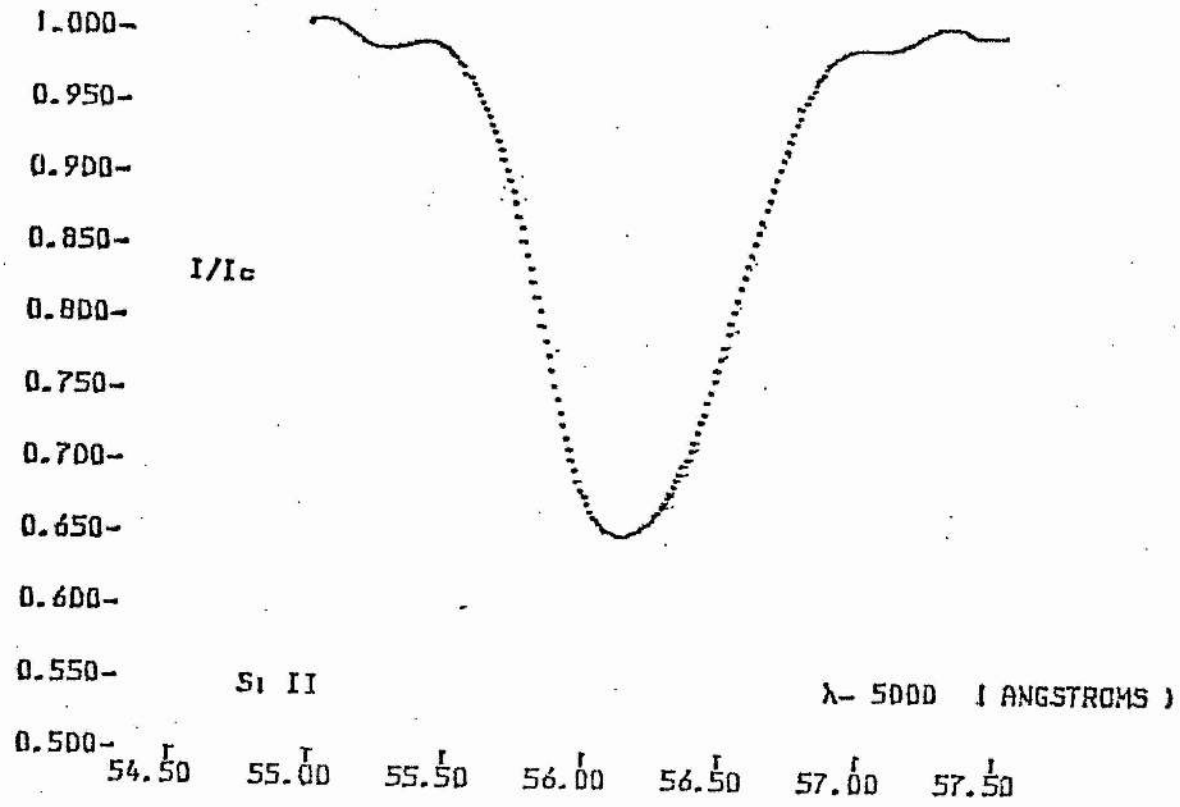

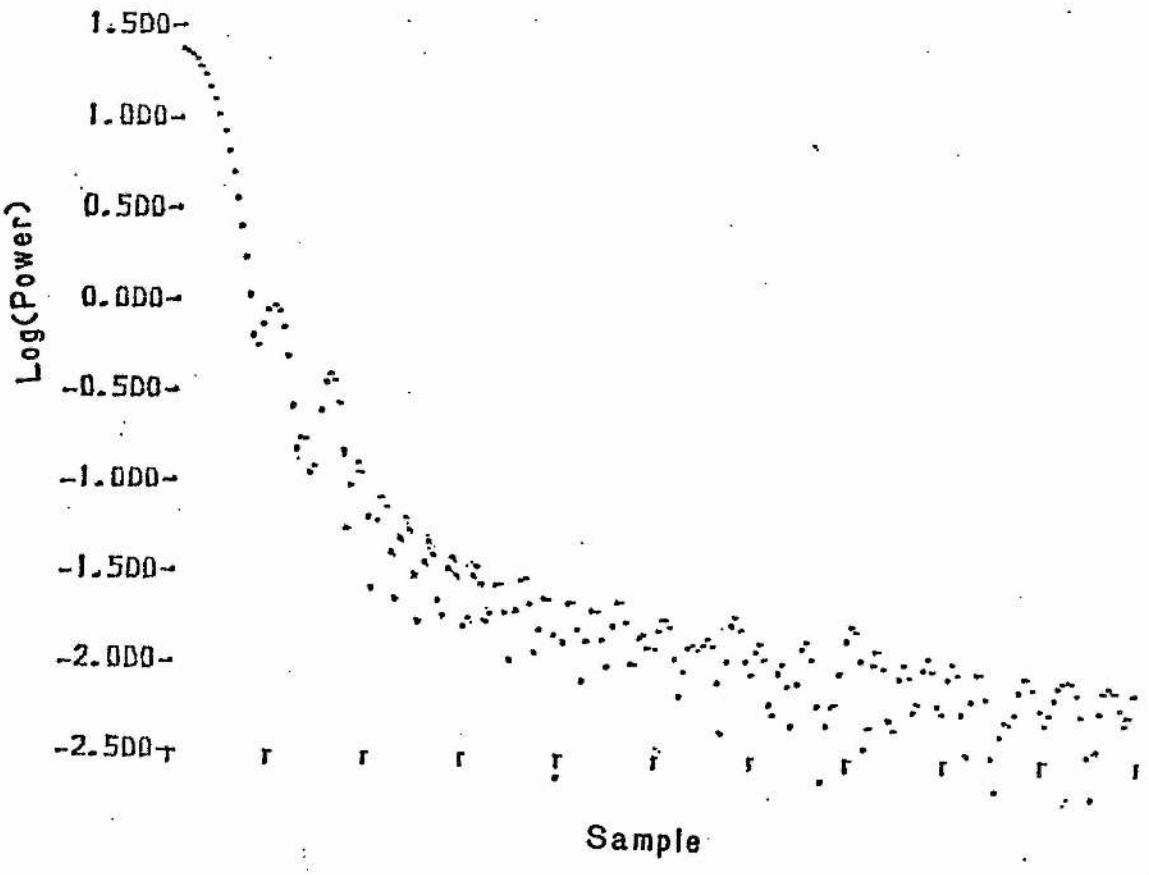

Fig. 6.6 :- As figure 6.1 for α Cyg.

As the principal broadening agent was expected to be rotation the method of analysis relied on first obtaining a value for $V_{rot} \sin i$. This was done in the following manner. The position of the first zero-point was obtained interactively using the cursor on the Tektronix T4010 terminal to select the appropriate value of frequency from a display of the power spectrum. Using the analytic rotational transform (equation 1A) and assuming a linear limb-darkening constant $\epsilon = 0.4$ a first approximation $V_{rot} \sin i$ was calculated.

The rotational transform using this value for the rotation velocity was then superimposed on the plot of the power transform and the second, third and fourth zero-points corresponding to the rotational profile were identified and their frequencies determined using the cursor. (The cursor was able to interpolate to $1/10^{th}$ of a frequency sample).

Values of $V_{rot} \sin i$ for each zero point were then calculated over a grid of ϵ between 0.3 and 0.5 and at intervals in ϵ of 0.025. Mean projected rotational velocities and standard deviations were calculated for each value of ϵ. The value of ϵ was found to have little effect on the resulting standard deviation and the mean values of $V_{rot} \sin i$ varied by only $\approx 3 km\, s^{-1}$ between $\epsilon = 0.3$ and $\epsilon = 0.4$. While this variation is larger than a typical standard deviation a value of $\epsilon = 0.4$ was used for all stars in the final analysis. This value is similar to that predicted from models of the stellar photospheres for early A stars (e.g. Carbon and Gingerich, 1969). The values of the projected rotational velocities thus found are given in table 6.i as are the standard deviations.

The next stage in the analysis programme was to determine whether the broadening of the intrinsic line profile by rotation alone was sufficient to reproduce the observed power spectra, and, if any other mechanism was needed, to attempt to identify that mechanism.

As insufficient data were available to generate an accurate model photosphere and then derive an intrinsic line profile for each star the following, rather *ad hoc*, approach was adopted.

Initially the intrinsic line-profiles were represented by a Gaussian with a half-width given by thermal broadening at a temperature of 9500K and normalised to the observed equivalent widths. A Gaussian was chosen in preference to a Voigt function or a Lorentz profile principally for ease of computation and because the contribution from the line

wings was not expected to be large for these stars.

The product of the fourier transform of this Gaussian with the rotational broadening function was compared interactively with the observed power spectrum. For nearly all the stars in the sample this was not an adequate representation of the observed power spectra. The observed high frequency components were suppressed relative to those predicted by the simple model and in some stars additional zero-points were clearly present in the data.

Two further alternatives were investigated.

(*i*) the half-width of the thermal profile was increased interactively until the best fit, determined by eye, to the observed power spectrum was obtained.

(*ii*) a second rotational broadening function was introduced. The appropriate value for rotation was again selected manually until the best fit by eye to the observed power spectrum was obtained.

The results obtained and the interpretation of the additional required broadening are discussed below for each star in the observing programme individually.

HD 47105 γ *Gem*

The rotational velocity found is rather lower than that given by $U+F$ of $37 kms^{-1}$ but rather higher than that found by Slettebak *et al* (hereafter SEA) of $< 10 kms^{-1}$.

While the power spectrum is not at all consistent with simply a thermally and rotationally broadened profile both the inclusion of an extra rotational component and the excess broadening of the Gaussian component give qualitatively acceptable representations of the power spectrum (Fig 6.7).

The excess broadening required for the gaussian component is equivalent to an additional broadening of $2.2 km s^{-1}$. This value might be associated with a microturbulence velocity or alternatively a macroturbulent velocity. Discrimination between the two possibilities is not possible as the resultant power spectra are indistinguishable at frequencies below $\approx 5c\mathring{A}^{-1}$.

At a quantitative level the fits are rather poor. The observed first and third sidelobes are stronger than those predicted by a factor of two.

HD 172167 α *Lyr*

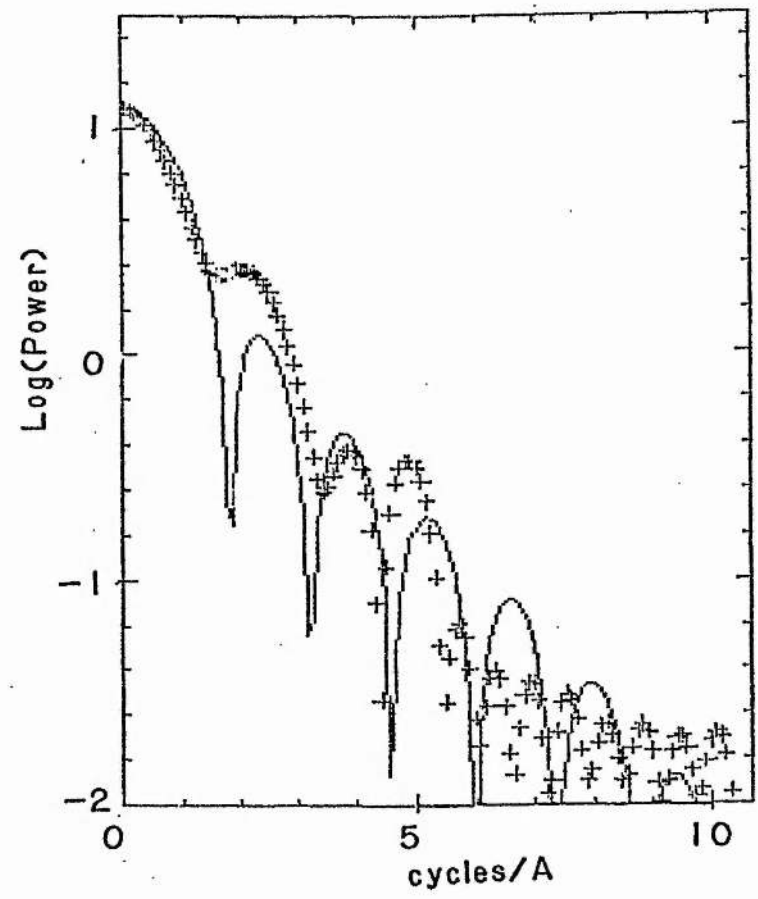

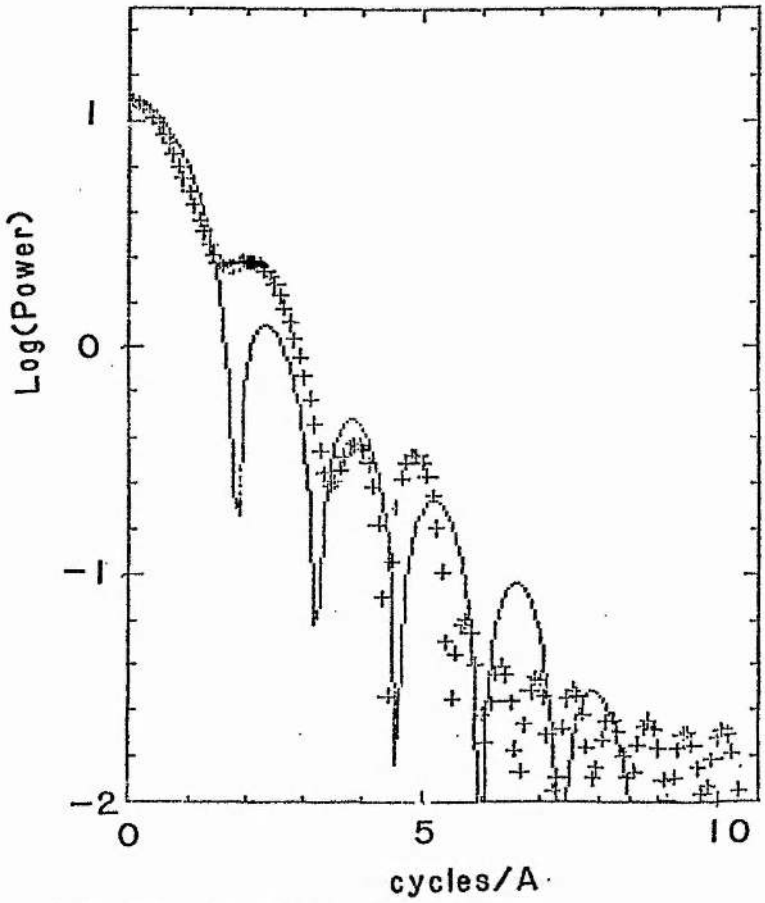

Fig. 6.7 :- **Fits obtained to the power spectrum of γ Gem using :**
(upper):- thermal, rotational velocity and additional gaussian components
(lower):- thermal and 2 rotational velocity components.

The equivalent width obtained for this star is much lower than those obtained for the others. It is, however, in reasonable agreement with that obtained by Strom *et al*, 1966, who give a value of 73mÅ.

The rotational zero-points were identified with the first, second and fourth local minima in the power spectrum. The derived projected rotational velocity of $21.4 \pm 0.9 km\,s^{-1}$ is higher than the values of $U+F$ and SEA.

The third local minimum, which cannot be identified with a zero-point of the rotational broadening function, and the increased amplitude of the third and fourth sidelobes are strongly suggestive of microturbulent broadening with a value of ξ_t insufficient to cause line de-saturation. To accurately model this broadening requires the calculation of the intrinsic line profile including microturbulence. Typically, however, the effect is to produce a strong first sidelobe (Gray, 1976, pp436). A value of $\xi_t = 4.5 km\,s^{-1}$ would produce a zero-point at the third minimum in the transform and would also produce a main and first sidelobe similar to that produced by thermal broadening with the increased thermal width. Figure 6.8 shows that the increased thermal width does produce a good fit to the power spectrum to a frequency of $\approx 3c\mathring{A}^{-1}$

Strom *et al* used a value of $\xi_t = 0 km\,s^{-1}$ in their analysis of this star and found a silicon abundance of twice solar. The inclusion of the microturbulence found here would reduce their derived abundance to $\approx$ solar.

HD 95418 β *UMa*

The rotational velocity found for this star of $37.9 km\,s^{-1}$ is in good agreement with the values of SEA and $U+F$ of $35 km\,s^{-1}$ and $43 km\,s^{-1}$ respectively.

The lack of additional zero-points combined with the strong filtering needed for a purely rotational broadening of the intrinsic thermal profile makes the overall power spectrum rather difficult to fit. The best fit is achieved by broadening the intrinsic profile by $7 km\,s^{-1}$. (Figure 6.9). There is no evidence for the increased sidelobe that would be caused if this were microturbulent broadening. The most plausible explanation is therefore gaussian macroturbulence.

HD 48915 α *CMa*

This star shows the most complex of the power spectra observed, and because of

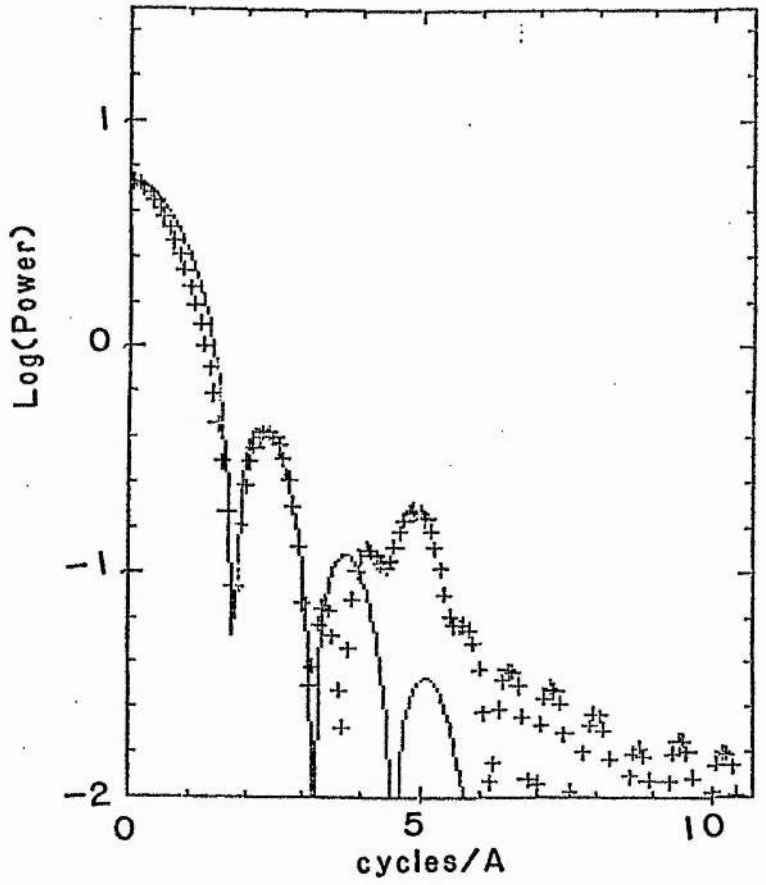

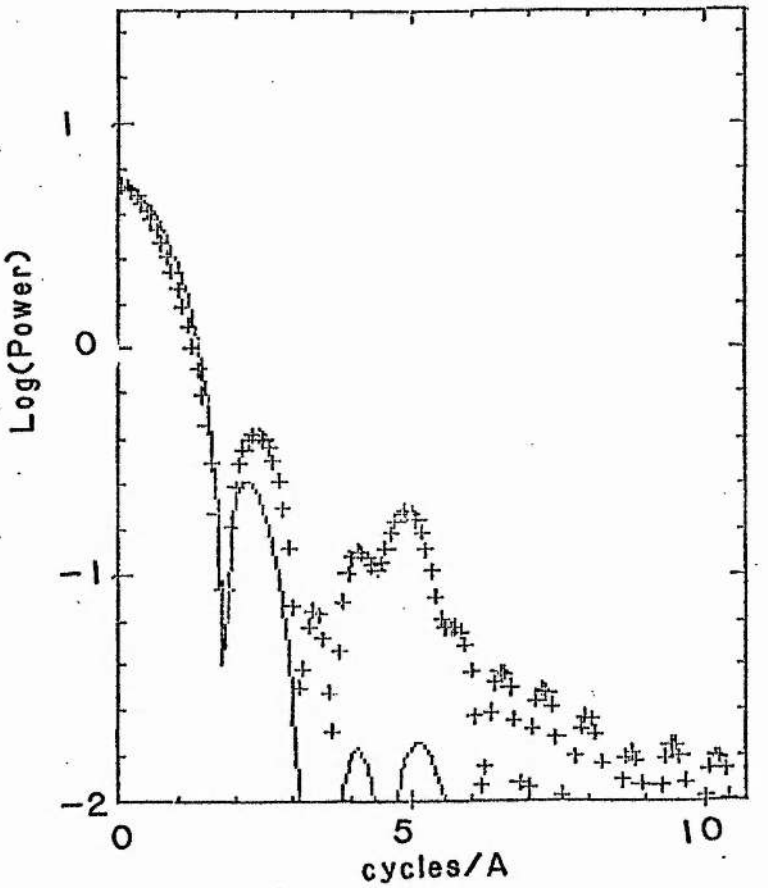

Fig. 6.8 :- As figure 6.7 for α Lyr.

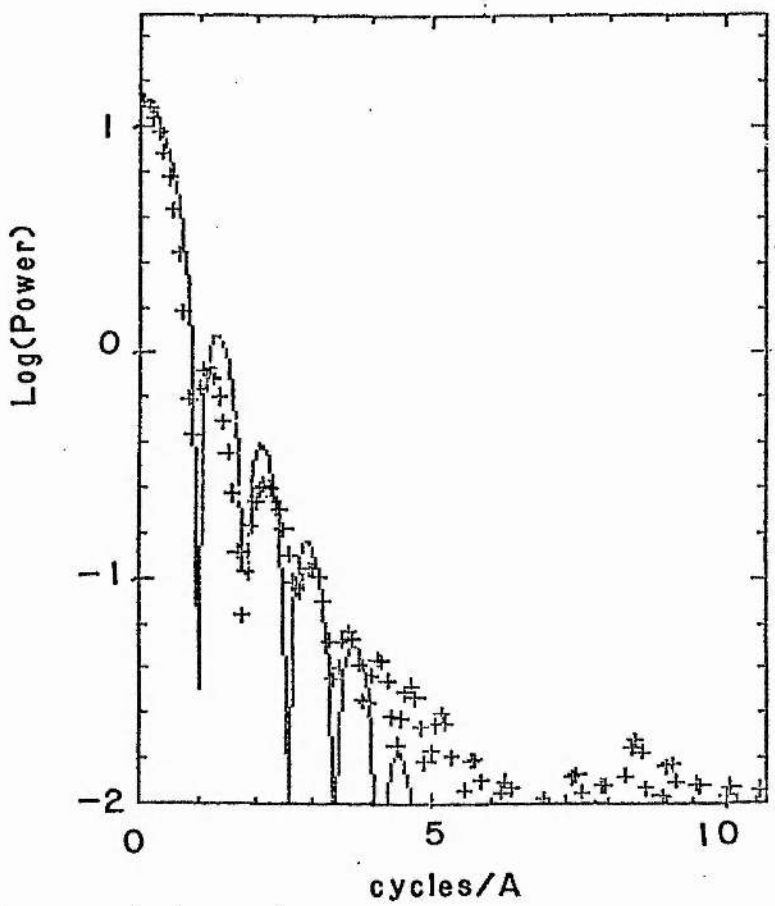

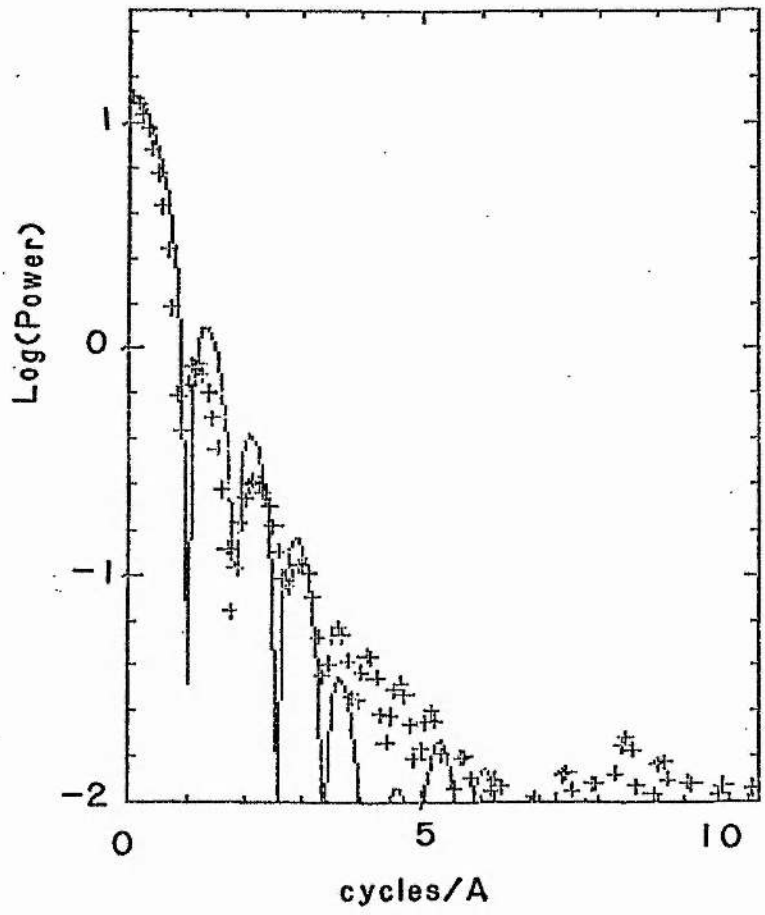

Fig. 6.9 :- As figure 6.7 for β UMa.

the desired comparison with the photographic data it is also the best observed power spectrum. As has been discussed earlier the observed line profile and equivalent width agree well with that obtained from the photographic observations and also with the equivalent width quoted by Strom *et al*,1966.

The best qualitative fit to the power spectrum was obtained with a projected rotational velocity of $26.0 km\ s^{-1}$. This was the only star for which the qualitative agreement between the thermal profile broadened with rotation is acceptable although even here the fit is not perfect (Figure 6.10).

This value of $V_{rot} \sin i$ is higher than the value of $0 km s^{-1}$ quoted by $U+F$ and that of $10 km s^{-1}$ given by *SEA*. Kurucz and Furenlid, 1979, use a value of $16 km s^{-1}$ in their spectral atlas of Sirius. A comparison of these latter authors' data and predicted spectra suggests that they have slightly underestimated the required rotational broadening. In addition they have assumed a $2 km s^{-1}$ microturbulent broadening which is not required in the Michelson interferometer data, but is not ruled out. The silicon doublet is not included in the spectral atlas. Dr R. Kurucz, however, kindly provided the author with the observational data for this wavelength region from material not published in the atlas. Figure 6.11 shows a comparison of the data supplied by Kurucz obtained at an original dispersion of 1.1 $\AA\, mm^{-1}$ and a resolution of $\approx 45 m\AA$ with the line profile obtained here. The superiority of the Michelson data is evident.

HD 97633 *θ Leo*

Again there appears to be some evidence for a contribution to the power spectrum from a broadening agent with the characteristics of microturbulence. The rotational broadening function has zero-points which can be identified with the first, second and fourth minima in the power spectrum. The third minimum and subsequent strengthening of the next sidelobe is similar to that found for α Lyr. In this case, if microturbulence is the broadening agent, a value of 3.2 $km\ s^{-1}$ is found. Figure 6.12 shows the observed power spectrum fitted with rotational broadening and a gaussian with half-width equivalent to the thermal and nicroturbulent velocities.

HD 197345 *α Cyg*

This supergiant has the largest equivalent width of any of the stars in the sample.

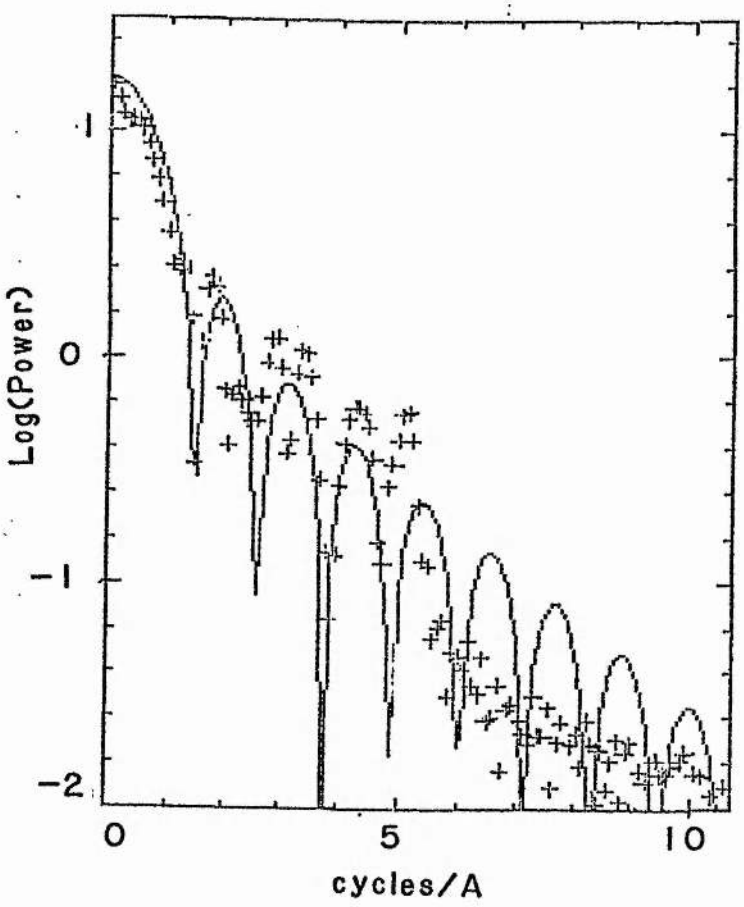

Fig. 6.10 :- As figure 6.7 for α Cma with only thermal and rotational broadening.

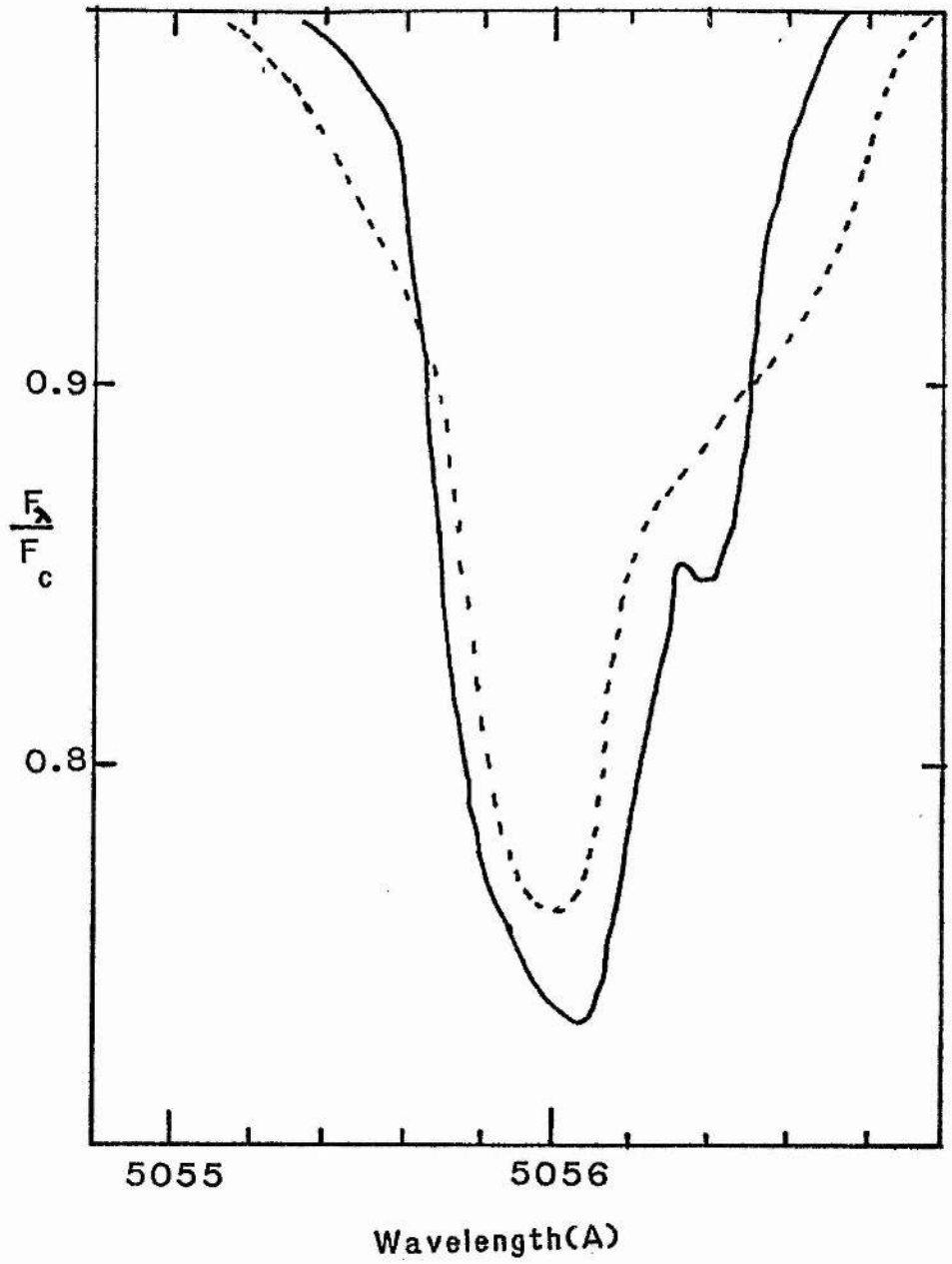

Fig. 6.11:- Comparison of the interferometer line profile (——) for Sirius with the photographic data of Kurucz and Furenlid. (- - -)

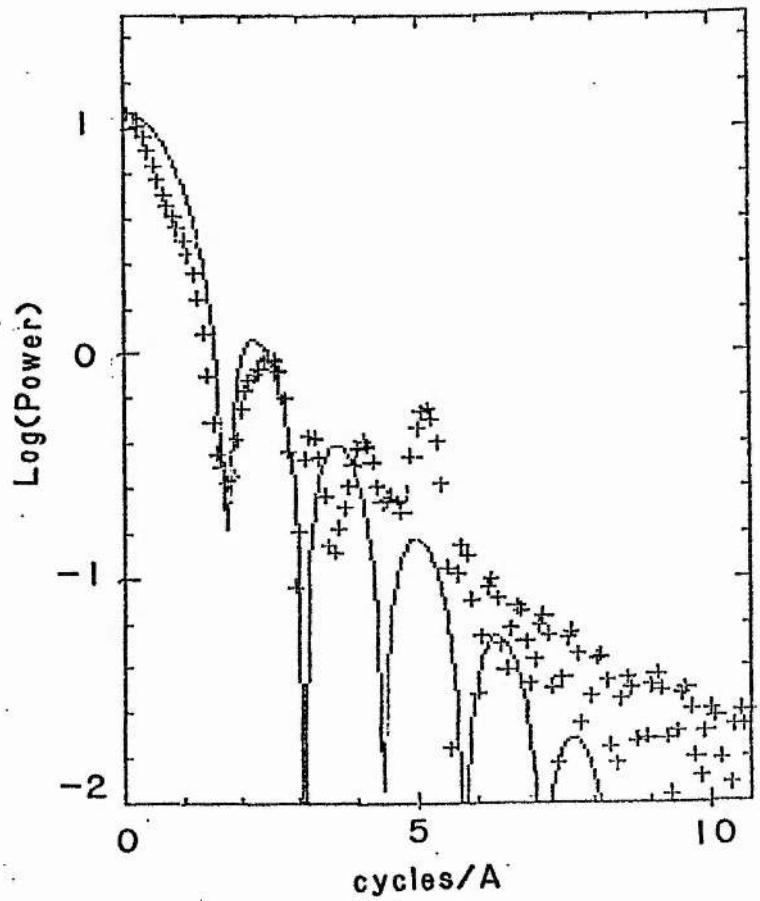

Fig. 6.12 :- As figure 6.10 for θ Leo.

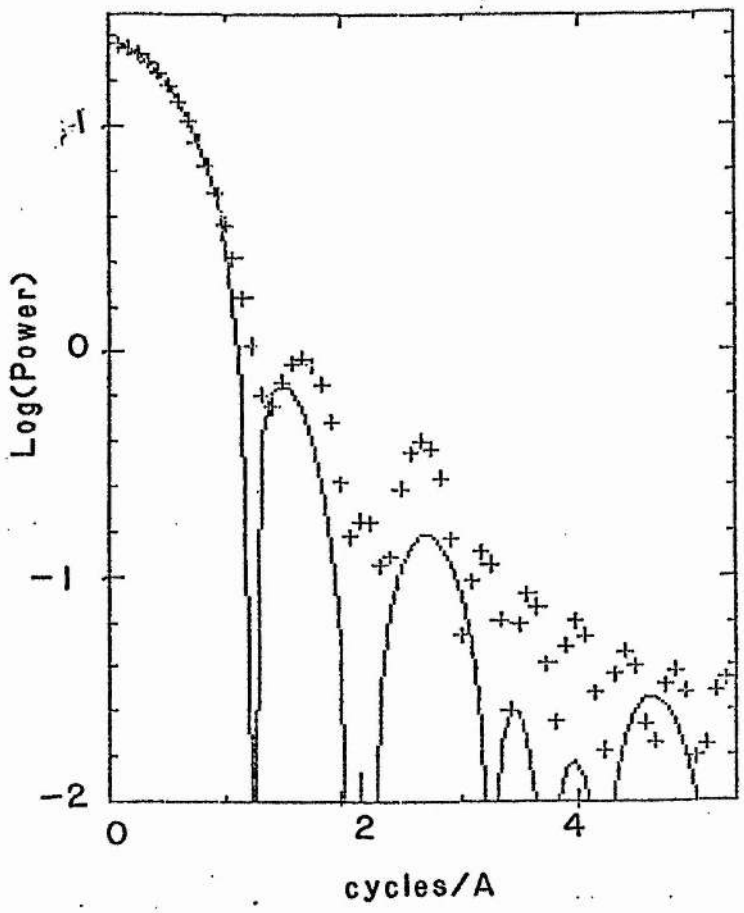

Fig. 6.13 :- As figure 6.7 for α Cyg for only thermal and 2 component rotational broadening.

It also has the most broadening. The rotational broadening was found to be $30\ km\ s^{-1}$, in reasonable agreement with that given by $U+F$ who quote $21\ km\ s^{-1}$. The power spectrum of this star required a further broadening which was best fit with a velocity of $18\ km\ s^{-1}$, (figure 6.13).

A previous analysis of an absorption line profile of this star using fourier decomposition techniques has been made by Gray, 1975. He used photoelectric scanner observations of the 4481Å line of MgII. His power spectrum was of insufficient quality to show sidelobes, however, and he came to the conclusion that the principal broadening agent was a radial-tangential macroturbulence with a velocity of $42\ km\ s^{-1}$. Reasonable agreement is found between the total broadening of his study and that here although the interpretation is different.

It is unclear whether the $18\ km\ s^{-1}$ component can be identified with micro- or macro-turbulence. Groth, 1972, and Rosendahl, 1970, have both made studies of the depth dependence of the microturbulence in the photosphere of this star using equivalent width data. The former found that ξ_t varied between $2\ km\ s^{-1}$ at the base of the photosphere to $20\ km\ s^{-1}$ at the top while the latter found values of $12\ km\ s^{-1}$ and $6\ km\ s^{-1}$ at the base and surface respectively. As was discussed in the previous chapter, however, classical model photospheres may not be particularly applicable to supergiants, so some caution must be given to attributing the broadening to a physical microturbulence.

6.vii *Summary*

This pilot study has shown the quality of the power spectra obtained by a michelson interferometer. The quality of the data surpasses the analysis techniques used here and more detailed modelling is required.

The diversity of the line profiles obtained over a small spectral range suggests a variety of line broadening mechanisms are in operation in addition to rotational and thermal broadening. Rather poorer fits are obtained than have been reported for some stars by other authors. This may be due to the better data or to the breakdown of the assumptions in the analysis technique for early-type stars. It is interesting to note that Gray, 1977, in an analysis of power spectra of A stars with higher projected rotational velocities also found stars which were not well fit with this technique.

Clearly, more detailed analysis is required to resolve some of these uncertainties. The use of detailed profiles generated using model photospheres and the integration of the flux over the disc rather than the convolution techniques used here may help. Observations of more then one line in a star would also aid in discriminating between different mechanisms. While the rotational broadening would be the same in each case the influence of microturbulence would depend on the line-strength.

The addition of multi-band detectors to the Michelson interferometer would therefore be of great value. This would also improve the speed of the instrument and make it more competitive with other instruments in terms of observing time required. Some further improvements to the optical system reducing the light lost and the use of a larger telescope at a better observing site would also be of value. An additional improvement would be the addition of a second reference laser with a different wavelength to overcome the 'blind-spot' problem which prevented observations of the 6347Å and 6371Å lines.

CHAPTER SEVEN

CONCLUSIONS AND SUGGESTIONS

7.i *Introduction*

The analysis of stellar spectra must procede in an iterative fashion. This is true of any study which relies on the process of developing models to fit observed data. Predictions made by one generation of models are compared with the best observations then available. Improvements in the models may then be suggested by the inconsistencies found between the observations and the predictions. Models which seem adequate may later be shown to be deficient by improved observational material. A new generation of the models must then be developed. This generation will be more capable of explaining all the observations and will thus be a better representation of the physics of the situation being modelled.

The sophistication of the developed models at the end of this iterative process should depend on the physical information which is required. In practice, additional constraints on the development of models also come from the quality of the basic atomic data and the observations.

It is important that each new generation of models should be tested against data similar to that which originally suggested the modifications. This ensures that the modifications have had the expected results. This, however, is not always done. There exists a tendency amongst astronomers to test each successive generation of models against successively more "exotic" objects which have been discovered with the improved observing techniques and equipment developed simultaneously with the models. A further problem is the tendency to concentrate on one improvement suggested by the discrepancies between the observations and models and to neglect the other possibilities when that improvement has been incorporated.

To some extent these failings have occurred in the study of the spectra of B stars. In

the mid-1960's failure of the models was commonly ascribed to the breakdown of the LTE approximation or to the neglect of line-blanketing, although the quality of the atomic data and the possible influence of velocity fields was also of concern.

The success of non-LTE models in explaining the observations of O stars led to the assumption that the discrepancies found in analyses of main-sequence B stars would also be removed by the use of non-LTE models.

At the same time as the non-LTE models became available ultraviolet observations became possible with the use of rocket and satellite borne telescopes. The subsequent discovery that stellar winds are a common phenomenon in early-type stars has led to a large theoretical effort in solving the radiation transfer problem in a moving medium. Recent observational work has tended to concentrate on the UV spectrum and on abnormal or supergiant stars. Little work has been done to examine how much better non-LTE models are for the interpretation of the visual spectra of main-sequence B-type stars than the earlier LTE models.

This project was begun for that reason. During the course of the project line-blanketed LTE models also became available. This has allowed the comparison of the two types of model. In this chapter the results of this study are summarised, the implications of the derived properties of the stellar photospheres for the broader study of astrophysics are examined, some remaining problems for the analysis of the visual spectra of B-type stars are discussed and some suggestions as to the best method of tackling these problems are made.

7.ii *Discussion*

Neither the non-LTE or the line-blanketed LTE models used in this project gave fits to the observed equivalent widths which, in a statistical sense, could be described as entirely satisfactory. The most probable cause of these inadequacies is the inaccuracy of the atomic data available. (The possibility that the cause of the remaining errors is the inhomogeneity of the stellar photospheres and that models with one set of parameters cannot adequately represent the real physical situation cannot be ruled out.) The non-LTE models gave results for the silicon and nitrogen lines which were more internally consistent than those given by the LTE models. However, for studies in which the primary

photospheric parameters of interest are the effective temperature and surface gravity the use of the line-blanketed LTE models is recommended. It has been shown here that the effective temperatures determined from the metallic absorption line spectra of B stars near the main sequence with the LTE models are in good agreement with those determined from the use of the integrated flux method. Systematic errors caused by the correction for interstellar reddening are avoided and the need for space observations of the UV in addition to flux calibrated photometry in other regions of spectrum are removed if the line spectrum is used in preference to the integrated flux method. While the reddening correction error is not large for nearby stars, it will become more important for more distant, more reddened stars especially if the reddening law varies with location in the galaxy. The absorption line technique is thus more accurately extendable to fainter stars. Unblanketed non-LTE models give systematically high effective temperatures. While this could be corrected by a calibration of the two temperature scales, the non-LTE models are more computationally expensive and so there is little benefit to be gained from their use for effective temperature determinations until line-blanketed non-LTE models become available.

For abundance calculations the non-LTE models are preferred, particularly if lines in the red and near-infrared are to be used. There are significant line non-LTE affects for these lines which significantly affect the derived abundances as the results for the Si II lines at 6347Å and 6371Å show.

For both types of model the derived abundances are sensitive to the microturbulent velocity in the photosphere. The use of non-LTE models, while reducing the required microturbulence, does not eliminate the need to incorporate microturbulent broadening for most B stars. Empirical corrections for LTE abundances cannot therefore be made in the straightforward manner used by some authors because of the inter-relation between abundance and microturbulence.

One area of future research in the atmospheres of B stars will be the non-thermal processes which give rise to the X-ray emitting coronal region and the initial acceleration of the stellar wind. While the line-driven wind theory (e.g. Castor, Abbott and Klein, 1975) is the accepted explanation of the acceleration of a supersonic wind there is as yet no

satisfactory theory for the acceleration of the wind material from subsonic to supersonic velocities. The existence of stellar coronae around B stars requires the deposition of mechanical energy above the photosphere. Some mechanism for the transport of this energy through the photosphere is required.

Underhill and Doazan, 1982, esimate energy budgets for various regions of typical B star atmospheres. Energy losses for the mantle are dominated by the X-ray luminosity, L_x, and the the kinetic energy of the stellar wind, L_w. For a typical main-sequence B0 star observed values of L_x are $\approx 10^{32}\ ergs\ s^{-1}$. Stewart and Fabian, 1981, show that the observed X-ray luminosity is only $\approx$ 10% of that emitted by the corona, the remainder being absorbed by the material in the stellar wind. The kinetic energy of the wind is given by

$$L_w \approx 3 \times 10^{31}\ \dot{M}_6 v_{10}^2\ ergs\ s^{-1}$$

where $\dot{M}_6$ is the stellar mass loss in units of $10^{-6} M_\odot yr^{-1}$ and v_{10} is the wind velocity in units of $10\ km\ s^{-1}$. The total energy removed by a wind in a typical B0 star is $\approx 10^{35}\ ergs\ s^{-1}$. Most of this energy is gained by the wind at some distance from the stellar *surface*. At the base of the wind the total kinetic energy in the wind is comparable to the X-ray luminosity of the corona.

Both the wind and X-ray luminosities are small in comparison to the bolometric luminosity of the star, which is $\approx 10^{39} ergs s^{-1}$. The internal energy of the mantle, $\frac{3}{2}NkT$, is, however, only $10^{37}\ ergs\ s^{-1}$ (Underhill and Doazan, 1982) or $\approx$ 20% of the internal energy of the photosphere. If the typical microturbulent velocity is the $5\ km\ s^{-1}$ found here, this too represents approximately 20% of the internal energy of the photosphere. Clearly, an understanding of the microturbulence phenomenon must play an important part in future studies of B stars.

The existence of coronae around B stars implies the existence of magnetic fields. Pulsations have been observed in both β –Cepheids and other B stars. The interaction of both a microturbulent medium and a pulsating medium with a magnetic field requires study.

The microturbulence phenomenon requires study, not only for an understanding of the dynamical state of a stellar photosphere, but also in order that accurate abundance

measurements, free from possible systematic errors, can be made. Accurate abundances from B stars are important. While studies of HII regions, planetary nebulae, supernova remnants and other objects also give information on the present composition and rate of enrichment of the interstellar medium, the heavy element abundances of young stars are required to draw definite conclusions on nucleosynthesis and recycling models.

There is some evidence that low and high mass stars are formed preferentially in different enviroments (Lequeux, 1980, Fabian, Nulsen and Canizares, 1982). Regions of high pressure, high dust density and associated with molecular clouds may favour the formation of high mass stars. The preferential removal of heavy elements by grains may influence the abundances in newly forming B stars. HII regions may have enhanced metal abundances if stellar winds preferentially accelerate heavy elements or the heavy elements trapped in grains are released by the radiation of the high mass stars.

Before progress can be made in these areas a further detailed study of the spectra of early-type stars is required to improve upon some of the deficiencies of this study. Here only equivalent widths could be used. A study of line profiles is required in order to separate the broadening caused by rotation and macroturbulence from the other line broadening mechanisms. Studies with a resolution of $\approx 3 \times 10^5$ are required to give a velocity resolution of $\approx 1\ km\ s^{-1}$, and signal to noise ratios of better than 100 are required if fourier decomposition techniques are to be used.

As an alternative to high dispersion coudé spectroscopy over the full wavelength region, observations of a limited number of profiles of well-selected lines using the Michelson interferometer coupled with moderate dispersion spectroscopy to determine equivalent widths of a greater number of lines might prove a more efficient use of telescope time. (For high-dispersion spectroscopy the exposure times required are proportional to the resolution cubed.) If a multi-element detector could be used to enable simultaneous observations of a number of spectral lines with the Michelson interferometer this would be beneficial.

While most of the flux of a B star is emitted in the UV the use of visual spectra is still an important part of the study of these stars. The visual spectrum is not so strongly affected by the complications caused by the existence of a mantle as the UV spectrum. If the visual spectrum can be used to determine the basic properties of the

stellar photosphere this enables the UV spectrum to be used to investigate the mantle in more detail.

Other deficiencies which require work are the use of static model photospheres to represent the photospheres of pulsating stars. Whether the best approach is to use high time resolution spectroscopy and line profiles from static models modified to include the distorting effects of pulsations, as Smith and co-workers have done, or to develop dynamical models of these atmospheres is not clear.

Before these studies are made, however, it is important that the quality of the basic atomic data, such as log gf values and damping constants is improved. Without good atomic data little faith can be put in the derived results. Until this data is available the recommended approach would be to develop a system of standard B stars which could be analysed in detail with the best available models. The technique of differential analysis, which has long been recommended, could then be used in studies of other stars.

The advent of STARLINK and the collaborative computer projects, such as the astronomical spectra and basic atomic data projects, offer an opportunity for these studies to be made. Fast, good interactive data reduction and analysis systems for stellar spectra on STARLINK in combination with the modelling programs provided by CCP7 should enable the principal photospheric parameters to be determined rapidly especially if computer communication between the two systems is improved. The spectral synthesis programs which are now becoming available could then be used to refine the derived parameters in almost real time until satisfactory fits to complete spectra are achieved.

REFERENCES

Adelman, S. J., 1973, Astrophys. J.,**182**, 531.

Adelman, S. J., 1977, Mon. Not. R. astr. Soc.,**181**, 667.

Aller,L.H., Elste,G. & Jugaku,J., 1957, Astrophys. J.,**144**, 1073.

Aller,L.H. & Jugaku,J., 1959, Astrophys. J. Suppl.,**4**, 109.

Aller,L.H., 1960, In 'Stars and Stellar Systems VI' (Ed: Greenstein, J.L.,), Chicago.

Auer,L.H., Heasley,J.N. & Mikey,R.W., 1972, Kitt Peak Nat. Obs. Contr. **55**.

Auer,L.H. & Mihalas,D., 1969, Astrophys. J.,**158**, 641.

Auer,L.H. & Mihalas,D., 1970, Mon. Not. R. astr. Soc.,**149**, 65.

Auer,L.H. & Mihalas,D., 1972, Astrophys. J. Suppl.,**24**, 193.

Auer,L.H. & Mihalas,D., 1973, Astrophys. J.,**184**, 151.

Baker,E.A., 1925, Proc. R. Soc. Edinburgh, **45**, 166.

Balona,L.A., 1976, Mem. R. astr. Soc., **78**, 51.

Balona,L.A., & Feast, M.W., 1975, Mon. Not. R. astr. Soc.,**172**, 191.

Becker,R.H., Holt,S.S., Smith,B.W., White,N.E., Boldt,E.A., Mushotzky,R.F. & Serlemitsos,P.J., 1981, Astrophys. J.,**235**, L5.

Blackwell,D.E. & Shallis,M.J., 1979, Mon. Not. R. astr. Soc.,**186**, 669.

Blades,J.C. &Powell,A.L.T., 1976, Mon. Not. astr Soc. South Africa, **35**, 30.

Boksenburg, A., 1977, I.A.U. Colloqium No. **40**, 131.

Bradley, P.T. & Morton, T.C., 1969, Astrophys. J., **156**, 687.

Brault, J.W. & White, O.R., 1971, Astron. &Astrophys., **13**, 169.

Breda, I.G. van, Hill, P.W., Campbell, R.J., Lynas-Grey, A.E. & Carr, D.M., 1974, Proc. 1st Camac Symposium (Suppl. to Camac Bulletin No. **9**, 157.

Breger, M., 1976, Astrophys. J. Suppl., **32**, 1.

Brenner, N., 1968, IBM Contributed Programs Library No. 360D-13.4.002.

Bunclark, P.S., 1979, Private communication.

Buscombe, W., 1972, MK Spectral Classification (Evanston).

Carroll, J.A., 1933, Mon. Not. R. astr. Soc., **93**, 478,680.

Cash,W. & Snow,T.P., 1982, Preprint.

Cayrel, R., 1958, Ann. d'Ap. Suppl., **6**, 125.

Code, A.D., 1973, Ann. Rev. Ast. and Astrophys., **11**, 239.

Code, A.D., Davis, J., Bless, R.C. &Hanbury-Brown, R., 1976, Astrophys. J.,**203**, 417.

Corliss, C.H., & Bozmann, W.R., 1962, Nat. Bur. Stand. Monograph No. **53**.

Costa, G.S. Da, Freeman, K.C., Kalnajs, A.J., Rogers, A.W. & Stapinski, I.E., 1977, Astron. J., **82**, 810.

Dufton, P.L., 1972, Ph.D. Thesis, Cambridge.

Dufton, P.L., 1976, Private communication.

Dufton, P.L., 1979, Astron. &Astrophys., **78**, 203.

Dufton, P.L., 1983, in CCP7 Newletter **6**.

Dufton, P.L. & Hibbert, A., 1981, Astron. &Astrophys., **95**, 24.

Dufton, P.L., Kane, L., M^{c}Keith, C.D., 1981, (DKM) Mon. Not. R. astr. Soc., **194**, 85.

Elvey, C.T., 1930, Astrophys. J., **71**, 221.

Fraser, R.D.B. & Susuki, E., 1970 Spectral Analysis: Methods and Techniques (Ed: Blackburn, J.A.), 171.

Fraunhofer, J., 1815, Denkschriften der Akademie Munchen Band v, 206.

Gray, D.F., 1975, Astrophys. J., **202**, 148.

Gray, D.F., 1976, The Observation and Analysis of Stellar Photospheres, (Wiley).

Griffin, R.F., 1968, A Photometric Atlas of the Spectrum of Arcturus, (Cambridge Philosophical Society).

Groth, H.-G., 1972, Astron. &Astrophys., **31**, 415.

Gustaffson, B., Bell, R.A., Eriksson, K., Nordlund, A., 1975, Astron. &Astrophys., **42**, 407.

Hanbury-Brown, R., Davis, J. & L.R., 1974, Mon. Not. R. astr. Soc., **167**, 475.

Hardorp, J., 1966, Zs. f. Ap., **63**, 137.

Hardorp, J. & Scholz, M., 1970, Astrophys. J. Suppl., **19**, 193.

Heintze, J.R.W., 1969, B.A.N., **20**, 1.

Hejlesen, D.M., 1980, Astron. and Astrophys., **39**, 347.

Hill, G., 1982, Publ. Dom. Ast. Obs., xvi, 67.

Huang, S.S., 1953, Astrophys. J., **118**, 285.

Huang, S.S. & Struve, O., 1953, Astrophys. J., **118**, 463.

Huggins & Miller, 1863, Philosophical Magazine, **26**, 319.

Kamp, L.W., 1973, Astrophys. J., **180**, 447.

Kamp, L.W., 1976, N.A.S.A. TR **R-455**.

Kamp, L.W., 1978, Astrophys. J. Suppl., **36**, 143.

Kane, L., M^{c}Keith, C.D. & Dufton, P.L., 1980, (KMD), Astron. &Astrophys., **84**, 115.

Karp, A.H. & Fillmore, J.A., 1980, Astrophys. J., **236**, 294.

Kennedy, P.M. & Buscombe, W., 1974, MK Spectral Classification (Evanston).

Kodaira, K. & Scholz, M., 1970, Astron. &Astrophys., **6**, 93.

Kohl, K., 1964, Z. f. Ap., **60**, 115.

Kurucz, R.L., 1970, S.A.O. Special Report No. **309**.

Kurucz, R.L., 1979, Astrophys. J. Suppl., **40**, 1.

Kurucz, R.L. & Furenlid, I., 1979, S.A.O. Special Report No. **387**.

Lesh, J.R., 1968, Astrophys. J. Suppl., **17**, 371.

Lesh, J.R., 1972, Astron. and Astrophys. Suppl. **5**, 129.

Lesh, J.R. & Aizenman, M.L., 1978, Ann. Rev. Astron. and Astrophys., **16**, 215.

Lindemann, E. & Hauck, B., 1973, Astron. and Astrophys. Suppl., **11**, 119.

Lindgren., H., 1974, Lund Obs. Rep., **6**, 15.

McLean, B., 1979, Private communication

Mihalas, D., 1970, Stellar Atmospheres (Freeman).

Mihalas, D., 1972, Astrophys. J., **177**, 155.

Mihalas, D., 1972b, NCAR-TN/STR-76.

Mihalas, D., Heasley, J.N. & Auer, L.H., 1975, NCAR-TN/STR-104.

Mihalas, D., 1978, Stellar Atmospheres, 2nd ed. (Freeman).

Mitton, J., 1974, Ph.D. Thesis, Univ. of Cambridge.

Miller, R.H., 1972, Quart. Rep. No. 32, Inst. of Comp. Res., University of Chicago.

Moffat, A.F.J., Schmidt-Kaler, T. & Vogt, N., 1973, IAU Symposium, **54**, 114.

Moore, C.H. & Rather, E.D., 1974, Astron. &Astrophys., **15**, 529.

Morton, D.C. & Adams, T.F., 1968, Astrophys. J., **151**, 611.

Nandy, K. & Schmidt, E.G., 1975, Astrophys. J., **198**, 119.

Nelson, G.D., 1980, Stellar Turbulence, (Eds Gray, D.F. & Linsky, J.L.).

Pagel, B.E.J., 1956, Mon. Not. R. astr. Soc., **173**, 709.

Peterson, D.M. & Shipman H.L., 1973, Astrophys. J., **180**, 635.

Philips, A.P., 1977, Mon. Not. R. astr. Soc., **181**, 777.

Popper, D.M., 1974, Astrophys. J., **188**, 559.

Popper, D.M., 1980, Ann. Rev. Ast. and Astrophys., **18**, 115.

Ring, J. & Worswick, S.P., 1975, Image Proceesing Techniques in Astronomy, (Eds. Jager C.D. & Nieuwenhuijzen, H.), 117.

Rosendahl, J., 1970, Astrophys. J., **160**, 627.

Scholz, M., 1967, Zs. f. Ap., **65**, 1.

Scholz, M., 1972, Vistas in Astronomy, **14**, 53.

Simkin, S.M., 1974, Astron. &Astrophys., **31**, 126.

Sletttebak, A., Collins, G.W., Boyce, P.B., White, N.M. & Parkinson, T.D., 1975, (SEA), Astrophys. J. Suppl., **29**, 137.

Smith, M.A., 1971, Astron. &Astrophys., **11**, 325.

Smith, M.A., 1976, Astrophys. J., **208**, 487.

Smith, M.A., 1977, Astrophys. J., **215**, 574.

Smith, M.A. & McCall, M.L., 1977, Astrophys. J., **223**, 221.

Snijders, M.A.J. & Lamers, H.J.G.L.M., 1975, Astron. &Astrophys., **41**, 245.

Snow, T.P. & Morton, D.C., 1976, Astrophys. J. Suppl., **33**, 269.

Stewart, G.C. & Fabian, A.C., 1981, Mon. Not. R. astr. Soc., **197**, 713.

Stoeckley, T.R. & Mihalas, D., 1973, NCAR-TN/STR-84.

Stothers, R. & Chin, C.-W., 1977, Astrophys. J., **211**, 189.

Strom, S.E., Gingerich, O. & Strom, K.M., 1966, Astrophys. J., **146**, 880.

Struve, O. & Elvey, C.T., 1934, Astrophys. J., **79**, 409.

Traving, G., 1955, Zs. f. Ap., **36**, 11.

Traving, G., 1957, Zs. f. Ap., **41**, 215.

Treffitz, E. & Zare, R.N., 1969, J.Q.S.R.T., **9**, 643.

Uesugi, A. & Fukuda, I., 1970, (U+F), Contr. Inst. Ap. and Kwasan Obs., Univ. of Kyoto No. **189**.

Underhill, A.B., 1966, The Early Type Stars, (Reidel).

Underhill, A.B., 1973,Astron. &Astrophys., **25**, 161.

Underhill, A.B., Divan, L., Prévot-Burnichon, M.-L. & Doazan, V., 1979, (UDPD), Mon. Not. R. astr. Soc., **189**, 601.

Underhill, A.B. & Doazan, V. (Eds.), 1982, B Stars With and Without Emission Lines, N.A.S.A. SP-456.

Unsold, A., 1942, Zs. f. Ap., **21**, 22.

Vaucouleurs, G. de., 1968, Applied Optics, **7**, 1513.

Walborn, N.R., 1971, Astrophys. J. Suppl., **23**, 257.

Watson, R.D., 1971, Astrophys. J., **169**, 343.

Wiese, W.L., Smith, M.W. & Glennon, B.M., 1969, Atomic Transition Probabilities, **2**, (N.B.S).

Westgate, C., 1933, Astrophys. J., **77**, 141.

Wright, K.O., 1966, IAU Symposium, **26**, 15.

Wright, S.L., 1975, Comm. univ. London. Obs., **74**.

Wright, S.L. & Argyros, J.D., 1975, Comm. Univ. London Obs., **75**.

Acknowledgements

It is a pleasure to acknowledge here the help given to me by a number of people over the course of this project. I should like to thank the Directors and staff of the University Observatory, St. Andrews and the South African Astronomical Observatory. In particular I should like to thank Drs. P.W. Hill and T.R. Carson who at various times supervised this project and Dr. C.W. Fraser for his assistance during the observing run at S.A.A.O. The development of the FORTH system owes much to discussions with Peter Bunclark and Roger Stapleton. I am indebted to Dr. R. Wayte, w ithout whom the Michelson interferometer observations would have been impossible, to Drs. H.J. Walker and A.E. Lynas-Grey for obtaining the series of calibration plates to Dr. Lynas-Grey for his guidance through CCP7 software, and to Drs. P.W. Hill and R.W. Hilditch for the provision of some of the spectra.

I am obliged to the Panel for the allocation of telescope time for the allocation of observing time at S.A.A.O. and the I.N.T. and to the S.R.C. for travel and subsistence awards to cover these observing trips. I am also grateful to the S.R.C. for the award of a Research Studentship for the academic years 1977-78 and 1978-79.

Finally, I should like to thank my wife, Sharon, and my parents for their patience and encouragement throughout.